PHOTOGRAPHIC STUDIES OF QUASI-STELLAR OBJECTS AND OTHER ACTIVE RADIO SOURCES

By

ROGER LEONARD SCOTT

A DISSERTATION PRESENTED TO THE GRADUATE COUNCIL OF
THE UNIVERSITY OF FLORIDA
IN PARTIAL FULFILLMENT OF THE REQUIREMENTS FOR THE
DEGREE OF DOCTOR OF PHILOSOPHY

UNIVERSITY OF FLORIDA

1975

ACKNOWLEDGMENTS

The author is extremely grateful to his advisor and Graduate Committee chairman, Dr. Alex G. Smith, for guidance and help throughout the course of his graduate studies, and for the intriguing photographic research that Dr. Smith and he have performed together. The contributions made by Drs. G. R. Lebo, C. N. Olsson, F. B. Wood, and T. L. Bailey as members of his Graduate Committee are acknowledged and appreciated. Drs. N. F. Six and S. S. Ballard are thanked for help received at various times during the author's graduate career.

The photographic studies of quasars in this dissertation would not have been possible without the help of A. G. Smith, R. J. Leacock, K. R. Hackney, R. L. Hackney, G. H. Folsom, B. Q. McGimsey, and P. L. Edwards in the acquisition and reduction of the data. Special thanks are extended to G. H. Folsom and H. R. Miller for their help in the BL Lac and PKS 0735+17 campaigns, and for kindly allowing data taken at the Bradley Observatory of Agnes Scott College to be included in this study.

E. E. Graves, H. W. Schrader, and W. W. Richardson constructed and maintained much of the equipment at Rosemary Hill, and donated much time and effort to helping the author with various problems during his graduate work. Special

recognition is given to E. E. Graves for the careful construction of the Cassegrain camera and the cold emulsion cassette used in the author's studies. The recently installed Rosemary Hill Ritchey-Chrétien 18-inch telescope was acquired and refurbished largely through the efforts of J. P. Oliver, A. G. Smith, and E. W. Ludington. The final adjustments necessary to allow the telescope to become photographically operational were performed by R. L. Hackney and K. R. Hackney, assisted by a special grant from the National Science Foundation. P. L. Coleman and R. B. Warren are thanked for helpful advice pertinent to the cold emulsion investigations.

Special gratitude is extended to M. A. Lynch, R. L. Hackney, S. S. Prasad, and P. L. Edwards for the many hours of help given in the photographic study of Jupiter. Thanks are given to A. E. S. Green and to R. D. McPeters for the use of their microdensitometer to scan the Jovian images. The proper operation of the densitometer was assured by the installation of parts by J. P. Oliver, borrowed from a similar instrument loaned to the department by the National Aeronautics and Space Administration.

The author was supported during his studies by graduate assistantships from the Department of Physics and Astronomy, the Graduate School, the National Science Foundation, and the College of Arts and Sciences. The quasar research program at Rosemary Hill is partially supported by the National Science Foundation through its grant NSG 23456. The careful preparation of the final manuscript by Mrs. Elizabeth Godey is most appreciated. Gratitude is expressed to Mrs. C. J. Kerrick, the department secretary, for her friendship, help, and encouragement.

The author is especially grateful to Karen R. Hackney and Richard L. Hackney for their help and friendship during the course of this study. Their companionship and encouragement have been much appreciated. The author's most profound gratitude is to his father, Mr. Sankey Scott. During the author's long graduate career his father's support and encouragement have never faltered, and have been a major factor in its successful completion. It is to his father that the author dedicates this work.

TABLE OF CONTENTS

Page

ACKNOWLEDGMENTS ii

LIST OF TABLES ix

LIST OF FIGURES xi

ABSTRACT xvi

CHAPTER

I INTRODUCTION 1

Quasars: An Astronomical Enigma 1

Variability of Quasars 2
The Redshift-Luminosity Paradox 5
Quasars and Related Objects 11

Models 19

Supernova Theory 19
Spinar Theory 20
Irtron Model 21
Gravitational Lens Hypothesis 22

The Florida Program 22

Jupiter, Another Active Radio Source 23

II RESEARCH TECHNIQUES AND INSTRUMENTATION 29

Photographic Studies of Quasars 29

Program Techniques 36
Magnitude Systems 37

A Photographic Attempt to Detect the
Jovian "Hotspot" 41

The Cassegrain Camera 41
Plates and Filters 48
Choosing Observation Times 51
Observing Techniques 56

TABLE OF CONTENTS - Continued

CHAPTER Page

III NITROGEN BAKING AND EMULSION COOLING AS METHODS OF HYPERSENSITIZATION 59

Introduction 59

Hypersensitization of Kodak 103a-0 Plates by Nitrogen Baking 62

Experimental Procedure 63
Results 64
Photometric Tests 72
Summary 73

Hypersensitization by Emulsion Cooling . . . 74

Experimental Procedure 75
Results 81
Summary 89

IV A STUDY OF THE OPTICAL VARIABILITY OF A SAMPLE OF QUASARS AND RELATED OBJECTS 91

Introduction 91

Photometric History and Discussion 94

PKS 0048-09 94
PKS 0420-01 95
PKS 0725+14 98
PKS 0735+17 98
PKS 0736+01 101
PKS 0906+01 104
PKS 1004+13 109
PKS 1055+20 112
PKS 1116+12 112
4C 09.42 119
PKS 1510-08 119
PKS 1645+17 126
PKS 2145+06 126
PKS 2349-01 131

Summary 131

V COLOR STUDIES OF QUASARS AND RELATED OBJECTS . . 137

Introduction 137

The Recent Photometric History of the Florida Objects 138

3C 120 143
3C 390.3 149

TABLE OF CONTENTS - Continued

CHAPTER Page

V (Continued)

BL Lac 150
OJ 287 158
3C 273 170
3C 345 170
3C 454.3 178
PKS 2134+004 179
4C 05.34 182

Color Variations of the Florida Objects . . . 186

The Short-Term Color Trends of OJ 287 and 3C 345 192

Possible Relationships Between Classes of Objects 205

The Color-Redshift Relation for Quasi-Stellar Objects 210

VI A STUDY OF THE SHORT-TERM OPTICAL ACTIVITY OF FIVE LACERTIDS 215

Introduction 215

The Optical Activity of PKS 1514-24, ON 231 and ON 325 216

PKS 1514-24 216
ON 231 222
ON 325 228

A Search for Intraday Optical Activity in BL Lac and PKS 0735+17 234

BL Lac 234
PKS 0735+17 248

Summary 262

VII A PHOTOGRAPHIC SEARCH FOR AN IO-RELATED JOVIAN HOTSPOT 265

Introduction 265

The Estimated Brightness of the Spot 265

The Jovacentric Coordinates of the Spot . . . 267

Digitizing the Jovian Images 277

The Computer Programs 286

Examination of the Computer Output 293

TABLE OF CONTENTS - Continued

Page

CHAPTER

VIII CONCLUSIONS 295

APPENDIX

I LIBRARY OF JUPITER IMAGES 309

II THE SUPERIMPOSED ARRAYS FROM JSUPER 319

Index 320

BIBLIOGRAPHY 349

BIOGRAPHICAL SKETCH 356

LIST OF TABLES

Table Page

1 Observational Similarities Between Quasars, and Seyfert and N-Type Galaxies 18

2 Speed Gains Relative to Unbaked 1L1 for Five Emulsion Batches Baked at 65°C 64

3 The Effect of Cooling on Emulsion Speed 83

4 Effect of Cooling on Baked IIIa-J 89

5 A Sample of Objects from the Florida Program . . 93

6 The Photographic Comparison Star Magnitudes for PKS 0048-09 94

7 The Objects Used for the Color Studies 140

8 The Rosemary Hill U, B, and V Observations of 3C 390.3, 3C 273, 3C 454.3, PKS 2134+004, and 4C 05.34 141

9 The Comparison Stars for 3C 120 148

10 The Comparison Stars for 3C 390.3 150

11 The Comparison Stars for BL Lac 158

12 The Comparison Stars for OJ 287 167

13 The Comparison Stars for 3C 273 173

14 The Comparison Stars for 3C 454.3 179

15 The Comparison Stars for PKS 2134+004 182

16 The Comparison Stars for 4C 05.34 186

17 The Observed Short-Term Ranges in Magnitude and Color of the Florida Objects 190

18 The Comparison Stars for ON 231 225

19 The Comparison Stars for ON 325 234

LIST OF TABLES - Continued

Table Page

20 Intraday Observations of BL Lac 238

21 Intraday Observations of PKS 0735+17 259

22 A Comparison of the Expected Brightness of the Auroral Hotspot and the Jovian Limb 269

LIST OF FIGURES

Figure Page

1 Observed correlation on the redshifts of quasars and radio galaxies, with angular size 10

2 The continuum spectra of three Seyfert galaxies, NGC 1275, NGC 1068, and 3C 120, and the quasar 3C 273 14

3 Color-color diagram for quasars, Seyfert galaxies, and N-type galaxies 17

4 A polar diagram of Jupiter's decametric radio sources 25

5 Current sheets in the Io flux tube 27

6 The Rosemary Hill Observatory 30-inch Newtonian/Cassegrain Tinsley reflector, with both Newtonian and Cassegrain cameras mounted 31

7 Comet Kohoutek in the brilliant zodical light, as seen from Rosemary Hill Observatory on the evening of January 10, 1974, at 2030 EDT 33

8 The Rosemary Hill Observatory 18-inch Ritchey-Chrétien telescope showing offset guiding telescope and camera 35

9 The infrared system response function used in the QSO studies, obtained by combining the Kodak type I-N emulsion with a Schott RG-8 infrared filter 40

10 The Cassegrain camera mounted on the guidebox of the 30-inch reflector showing offset guider, counterweights, base tube, rotation clamps, eyepiece projection tube, filter holder, shutter, with cable release, and camera bed, with dark slide 43

11 Tricolor separation print of Jupiter from negatives taken on July 29, 1972 47

LIST OF FIGURES - Continued

Figure		Page
12	Spectral reflectivity of Jupiter	50
13	The ultraviolet response function used in the Jupiter studies, obtained by combining the Kodak type 103a-0 emulsion with a Kodak #18 A filter	53
14	The infrared system response functions used in the Jupiter studies, obtained by combining the Kodak type I-Z emulsion with a Schott RG-8 filter for broad band coverage, and a Corning 7-56 filter for narrow band coverage	55
15	Speed and fog curves for emulsion batches 1L1 and 1K2, baked in nitrogen at 65°C	66
16	Speed and fog curves for batch 1E2 baked at 65°C in air and in dry nitrogen	69
17	Speed and fog curves for batches 1L3 and 1K2 baked in dry nitrogen at 72.5°C	71
18	Schematic diagram of the cold cassette	78
19	Photograph of the cold cassette	80
20	Speed and fog curves obtained by cooling Kodak Tri-X Pan and Kodak Contrast Process Pan	85
21	Speed and fog curves obtained by cooling Kodak 103a-0 and Kodak IIIa-J	88
22	The Florida light curves of PKS 0048-09, PKS 0420-01, and PKS 0725+14	97
23	The sequence finder for PKS 0725+14	100
24	The Florida light curves of PKS 0735+17 and PKS 0736+01	103
25	The sequence finder for PKS 0736+01	106
26	The Florida light curve of PKS 0906+01	108
27	The Florida light curves of PKS 1004+13, PKS 1055+20 and PKS 1116+12	111
28	The sequence finder for PKS 1004+13	114

LIST OF FIGURES - Continued

Figure Page

29 The sequence finder for PKS 1055+20 116

30 The sequence finder for PKS 1116+12 118

31 The Florida light curves of 4C 09.42, PKS 1510-08 and PKS 1645+17 121

32 The sequence finder for 4C 09.42 123

33 The sequence finder for PKS 1510-08 125

34 The sequence finder for PKS 1645+17 128

35 The Florida light curves of PKS 2145+06 and PKS 2349-01 130

36 The sequence finder for PKS 2145+06 133

37 The sequence finder for PKS 2349-01 135

38 The Florida four-color light curve of 3C 120 . . 145

39 Apparent variations in the color indices of 3C 120 147

40 The sequence finder for the N galaxy 3C 390.3 152

41 The Florida four-color light curve of BL Lac . . 154

42 The color indices of BL Lac corresponding to the light curves shown in Figure 41 157

43 The Florida four-color light curve of OJ 287 . . 160

44 The color indices of OJ 287 corresponding to the light curves of Figure 43 163

45 The Rosemary Hill Observatory light curve of OJ 287 from early 1970 to the present, showing an increase in the long-term component before the long decline shown in the color observations 166

46 The sequence finder for the lacertid OJ 287 . . 169

47 The sequence finder for the quasar 3C 273 . . . 172

LIST OF FIGURES - Continued

Figure Page

48 The Florida three-color light curve of 3C 345. . 175

49 The color indices of 3C 345 corresponding to the light curves of Figure 48 177

50 The sequence finder for the quasar 3C 454.3 . . 181

51 The sequence finder for the quasar PKS 2134+004 184

52 The sequence finder for the quasar 4C 05.34 . . 188

53 The normalized color regression plots of OJ 287; the long-term decline in intensity has been removed 195

54 The normalized color regression plots of 3C 345; the long-term declines in intensity has been removed 197

55 A model to explain the color trends suggested by OJ 287 and 3C 345 202

56 The positions of the objects used in the color study on a color-color diagram 208

57 The observed correlations between the color indices of quasars and their redshifts 214

58 The Florida light curve of PKS 1514-24 219

59 The sequence finder for PKS 1514-24 221

60 The Florida B and V light curves of ON 231 . . . 224

61 The sequence finder for ON 231 227

62 The Florida B and V light curves of ON 325 . . . 230

63 The sequence finder for ON 325 233

64 Light curves of BL Lac intraday campaigns held on August 9 and October 2 at Rosemary Hill Observatory 240

65 Light curves of the joint Florida-Georgia BL Lac intraday campaign held on October 4, 1973 242

LIST OF FIGURES - Continued

Figure Page

66 Light curves of BL Lac intraday campaigns held at Rosemary Hill on June 23 and July 16 of 1974 using the 30-inch and 18-inch reflectors 244

67 Light curve of PKS 0735+17 intraday campaign held at Rosemary Hill on January 24, 1974 251

68 Light curves of PKS 0735+17 intraday campaigns held at Bradley Observatory on January 31, February 1, and February 12 of 1974 253

69 Light curves of PKS 0735+17 intraday campaigns held at Bradley Observatory on February 18, February 27, and March 15 of 1974 255

70 Light curves of joint Florida-Georgia PKS 0735+17 intraday campaigns held on February 25 and March 18 of 1974 257

71 The projected Jovacentric coordinates X and Y of the hotspot 272

72 A polar view of the flux tube projected positional geometry 274

73 The model MK III C Joyce-Loebl scanning microdensitometer 279

74 The analog-to-digital converter designed and built by Dr. M. A. Lynch 281

75 The 10-level pixel array of infrared image no. 72 generated by JSCAN, compared with a standard print of image no. 72 290

76 The 35-level centered pixel array of image no. 72 generated by JSUPER compared with a standard print of image no. 72 292

Abstract of Dissertation Presented to the Graduate Council
of the University of Florida in Partial Fulfillment of the
Requirements for the Degree of Doctor of Philosophy

PHOTOGRAPHIC STUDIES OF QUASI-STELLAR OBJECTS AND OTHER ACTIVE RADIO SOURCES

by

Roger Leonard Scott

March, 1975

Chairman: Dr. Alex G. Smith
Major Department: Astronony

Nitrogen baking of the Kodak type 103a-0 spectroscopic emulsion has proved to be an effective means of hypersensitization, yielding speed gains of from 2 to 3 over an untreated plate. The preliminary results of this process were reported by R. L. Scott, A. G. Smith, R. J. Leacock, B. Q. McGimsey, P. L. Edwards, K. R. Hackney, and R. L. Hackney in "Response of 103a-0 Spectroscopic Emulsion to Controlled Baking and Its Advantages for Photographic Monitoring of Quasi-Stellar Objects," presented at the 40th Meeting of the Southeastern Section of the American Physical Society, 1973 November 8-10, in Winston-Salem, North Carolina. After further experimentation, the final results were reported by R. L. Scott and A. G. Smith in "Hypersensitization of Kodak type 103a-0 Plates by Nitrogen Baking," Astronomical Journal, 79, 656 (1974).

Studies of the optical variability of a sample of 14 quasars and similar objects at Rosemary Hill Observatory

detected statistically significant fluctuations in the light curves of PKS 0048-09, PKS 0420-01, PKS 0735+17, PKS 0736+01, PKS 0906+01, PKS 1510-08, and PKS 2349-01. The preliminary results of this study were partially communicated by R. L. Scott, A. G. Smith, R. J. Leacock, B. Q. McGimsey, P. L. Edwards, K. R. Hackney, R. L. Hackney, and G. H. Folsom in "Optical Variations of a Sample of Quasars and Related Objects," presented at the 41st Meeting of the American Astronomical Society, 1973 December 2-6, in Tucson, Arizona.

Apparent color variations observed in a sample of QSO's at Rosemary Hill appear to be generally compatible with the expanding source model. However, OJ 287 and 3C 345 appear to be exceptions, as variations in their color indices suggest that changes in the slope of the optical spectrum may not be simply correlated with brightness. A spectral model composed of thermal and non-thermal components is offered as a possible explanation for the color variations observed in the objects studied. The optical variations of OJ 287 are discussed by A. G. Smith, R. L. Scott, R. J. Leacock, B. Q. McGimsey, P. L. Edwards, R. L. Hackney, and K. R. Hackney in "Four-Color Photometry of OJ 287 During Its Recent Three-Magnitude Decline," Publications of the Astronomical Society of the Pacific, in press (1975).

Studies of the lacertids PKS 1514-24, ON 231, and ON 325 suggest that the optical behavior of PKS 1514-24 and ON 231 is similar to that of the prototype lacertid BL Lac, while ON 325 shows more moderate short-term optical behavior superimposed on long-term fluctuations of several months' duration.

A search for intraday activity in BL Lac detected statistically significant variations on two nights; the largest such variation was a decline of $0^{m}.6$ in 33 minutes. Observations of PKS 0735+17 suggested that intraday activity may have been marginally detected. The preliminary results of this study were partially communicated by R. L. Scott, A. G. Smith, R. J. Leacock, B. Q. McGimsey, P. L. Edwards, and K. R. Hackney in "Recent Observations of the Lacertids BL Lac and OJ 287, and a Possible Lacertid, PKS 0735+17," presented at the 38th Annual Meeting of the Florida Academy of Sciences, 1974 March 21-23, in Orlando, Florida.

A search for an Io-related Jovian auroral hotspot has ended with essentially negative results. During the 1973 Jovian apparition, a total of 160 Jovian images were taken at Rosemary Hill in low-albedo ultraviolet and infrared regions. Visual examination and computer reductions revealed no trace of the hotspot. The results were presented by R. L. Scott, A. G. Smith, M. A. Lynch, S. S. Prasad, P. L. Edwards, R. L. Hackney, and K. R. Hackney in "A Search for an Io-Related Jovian Hotspot," 144th Meeting of the American Astronomical Society, 1974 December 10-13, in Gainesville, Florida.

CHAPTER I

INTRODUCTION

Quasars: An Astronomical Enigma

More than a decade has passed since Thomas Matthews and Allan Sandage discovered the first quasi-stellar radio source, but perhaps no event has had as great an impact upon modern astronomy. In 1960, using plates taken with the 200-inch telescope, they identified the radio source 3C 48 with a 16th-magnitude stellar object, completely starlike except for traces of surrounding nebulosity. The pecularity of 3C 48 was immediately evident, for no star other than the sun had ever been found to be a radio source. In addition, its spectrum was very different from that of a normal star; it contained a large ultraviolet excess and several broad unknown emission lines. Several more such objects were soon discovered, but their true significance was not realized until 1963, when Maartin Schmidt recognized that the lines in the optical spectrum of 3C 273 were the ordinary Balmer lines of hydrogen, greatly redshifted. Schmidt's discovery enabled lines in the spectra of the four other such objects then known to be likewise identified as familiar lines greatly displaced toward longer wavelengths.

At present, more than two hundred such objects have been identified with known radio sources; they are often called "quasars," short for quasi-stellar radio sources, or simply QSO's (quasi-stellar objects). Many radio-quiet QSO's have also been discovered, on the basis of their colors and redshifts. Quasars have confronted astronomers with a most perplexing problem, for placing them at the cosmological distances implied by their redshifts necessitates intrinsic luminosities considerably in excess of that of an entire galaxy. Their observed variability implies source sizes of a few light days or years in diameter, and creates severe luminosity requirements for source emission mechanisms. There are advocates of non-cosmological redshifts, such as large Doppler shifts due to ejection from relatively nearby objects, and redshifts of a gravitational nature. But the consensus of opinion favors a cosmological interpretation, and current source models must satisfy cosmological luminosity requirements.

Variability of Quasars

The optical variability of the quasar prototype 3C 48 was firmly established by Matthews and Sandage (1963), whose observations showed a $0\overset{m}{.}4$ change within thirteen months. Subsequent observations of the other known quasars have shown that the majority of them are variable at optical and radio wavelengths. Due to the difficulty in establishing their identification, little work has been done with radio-quiet objects. However, those that have been monitored regularly show the same type of variability as radio-emitting quasars.

The nature and time scale of observed fluctuations vary widely from object to object. Many quasars exhibit moderate variations of a few tenths of a magnitude over a time of weeks or months, then suddenly undergo changes of a magnitude or more in a few days. Such objects are known as optically violent variables (OVV's). A classic example is NRAO 512. In June of 1970, Folsom observed this object to flare $1^{\mathrm{m}}.2$ with a rise time of only two days, and then decline even more rapidly (Folsom _et al_. 1970).

Other objects appear to undergo quiescent periods, where activity ceases for an extended period of time. The optical counterpart of PKS 1004+13 dropped $0^{\mathrm{m}}.3$ between 1967 and 1969 according to Hunter and Lü (1969). Lü (1972) reports a decline of a magnitude between March of 1969 and May of 1970. However, no statistically significant variations were observed from March of 1972 to May of 1973 (Scott _et al_. 1973).

An apparent periodicity may have been observed in the activity of the OVV 3C 345. Kinman _et al_. (1968) reported flares in the light curve of this object which appeared to occur in a phase-locked pattern of four, with an average interval of 80 days between individual outbursts, and a period of about 320 days for recurrence of the group. However, observations of Lü (1972) and Hackney (1973) suggest that these outbursts were not permanent features of the object's light curve.

The optical counterpart of 4C 05.34, which until recently had the largest known redshift, does not exhibit any activity of a violent nature, but appears to undergo long-term amplitude variations of approximately $0\overset{m}{.}1$ per year (Hackney *et al.* 1972a).

The peculiar object BL Lac is characterized by variability of an extremely violent nature. BL Lac is the protytype of a class of objects now called lacertids, which resemble quasars but have featureless optical spectra. Day to day fluctuations on the order of a magnitude were observed by DuPuy *et al.* (1969), and other observers have reported similar activity. Intraday variations greater than $0\overset{m}{.}5$ in a few hours were reported by Bertaud *et al.* (1969), and Weistrop (1973) reports a decline of $1\overset{m}{.}2$ in 23 minutes. While observations by Hackney (1973) and Scott *et al.* (1973) show intraday variations of a less extreme nature, the object apparently spends a large portion of its time in violent activity. BL Lac is also variable at radio wavelengths, and Hackney *et al.* (1972b) report that radio outbursts seem to lag optical events by several months. Recently, Oke and Gunn (1974) have succeeded in obtaining a redshift of 0.07 for the faint envelope of this object whose spectrum resembles that of a compact galaxy. The envelope is very faint and is visible only in long exposures with large instruments.

Studies of the optical variations of quasars provide many clues as to the nature of these objects. Assuming quasar redshifts are distance indicators, the implied luminosities combined with the observed rapid fluctuations create an intriguing paradox for astronomers.

The Redshift-Luminosity Paradox

The known range of quasar redshifts runs from 0.06 for B 234 to the enormous value of 3.53 for the recently measured OQ 172 (Wampler et al. 1973). Most galaxies have redshifts greater than 0.001 but less than 0.01, with 3C 295 having the largest known galaxian redshift of 0.46 (Morrison 1973). While the quasar and galaxian redshift ranges do overlap, many quasars have redshifts greater than 1, and the implied cosmological distances place them far beyond the most distant galaxy. The resulting intrinsic luminosities, as high as 10^{47} ergs/sec (Colgate 1969), are more than 100 times those of the giant elliptical galaxies at optical wavelengths. According to Terrell (1964,1967), the time required for significant variations to occur sets an upper limit to the size of the active region, assuming non-relativistic motion in the source. Since many quasars have been observed to undergo significant fluctuations on a time scale of hours or days, a cosmological interpretation of their redshifts confronts astronomers with an object of solar system size which has a luminosity much greater than that of an entire galaxy.

Terrell (1964) attempted to overcome these difficulties by suggesting that quasars were local objects, being ejected from the central part of our galaxy at relativistic speeds. This idea found little acceptance, due to the problems in imagining such an object being accelerated to relativistic velocities while retaining a compact form. Another argument against the ejection theory is the absence of blue shifts. Objects moving toward the observer should appear brighter than those moving away, and in a survey down to a given apparent magnitude, the blue-shifted objects should predominate.

While no quasars have as yet been found to have blue shifts, there are certain objects, according to Chiu and Morrison (1973), which are likely candidates. These objects are the half-dozen or so lacertids; their flat line free spectra could well represent a region ordinarily seen in the infrared. However, this theory remains an interesting speculation at the present, and Oke's measurement of a redshift for the envelope of BL Lac seems to discourage this hypothesis (Oke 1974).

Attempts to explain the redshifts as due to the effects of an intense gravitational field on escaping photons, as predicted by general relativity theory, have also faced difficulties. Greenstein and Schmidt (1964) have shown that in conventional models the potential gradient should broaden spectral lines more than observations show. These models assume the lines arise from a thin shell surrounding a highly compact object. Hoyle and Fowler (1967) overcame this difficulty by constructing a model where the emitting gas is concentrated well in the center of a massive object, which could consist of a cluster of neutron stars or white dwarfs in order to be transparent to the line radiation. However, there are objections to this model on theoretical grounds, and at present no satisfactory model of this type has been constructed.

Observational evidence against cosmological distances for quasars and related objects has been put forward by Halton Arp and the Burbidges. Arp (1971) reports the discovery of a luminous filament connecting the nucleus of the spiral galaxy NGC 4319 with the quasar Makarian 205, two objects with quite different redshifts. Burbidge _et_ _al_. (1971) report the apparent proximities of four quasars to small-redshift galaxies, and the existence of a physical connection between the comparatively nearly galaxy IC 1746 and the radio-quiet QSO PHL 1226. Burbidge _et_ _al_. (1972) claim that the blue stellar object Weedman 2, a possible lacertid, appears to be associated with the galaxy NGC 2992. In all these cases the QSO and associated galaxy have different redshifts except for Weedman 2, whose redshift has never been measured due to its featureless optical spectrum. This would rule out cosmological redshifts for the involved QSOs if the physical connections are real.

While these apparent associations between galaxies and quasars are extremely interesting, they are seen in only a small sample of the entire quasar population. In addition, Sanitt (1972) warns against a literal interpretation of filaments connecting adjacent images on a photographic plate, as peculiar photographic effects sometimes occur which give the appearance of a physical connecting bridge. If these apparent physical relationships could be proven, it would show that at least some quasars have non-cosmological redshifts, but widespread acceptance awaits more convincing evidence.

Perhaps the most convincing evidence in favor of a cosmological interpretation is the "redshift-angular size" relationship (Miley 1971). Figure 1 shows the angular separation at a wavelength of 11.1 centimeters of the double radio components of quasars (open circles) and radio galaxies (closed circles) plotted versus redshift. Because the data represent the component separation of three-dimensional radio sources projected on the sky, the solid line is an upper envelope. As Figure 1 shows, a definite decrease in the angular size of radio components occurs with increasing redshift. This, together with the apparent continuity between the angular size properties of radio galaxies and quasars, suggests that the origin of the redshifts of the two classes of objects is not appreciably different, and that the redshifts are actual distance indicators.

Additional support for a cosmological interpretation is supplied by the investigation of the "magnitude-redshift relation" for quasars which are most luminous optically in the redshift range from 0.2 to beyond 2.0 (Bahcall and Hills 1973). Bahcall and Hills have found that the distribution of

Figure 1. Observed correlation of the redshifts of quasars and radio galaxies, with angular size. On this log scale plot, the solid line is a best fit to the envelope of all the points. The quasars are represented by open circles; the radio galaxies by closed circles. After Miley (1971).

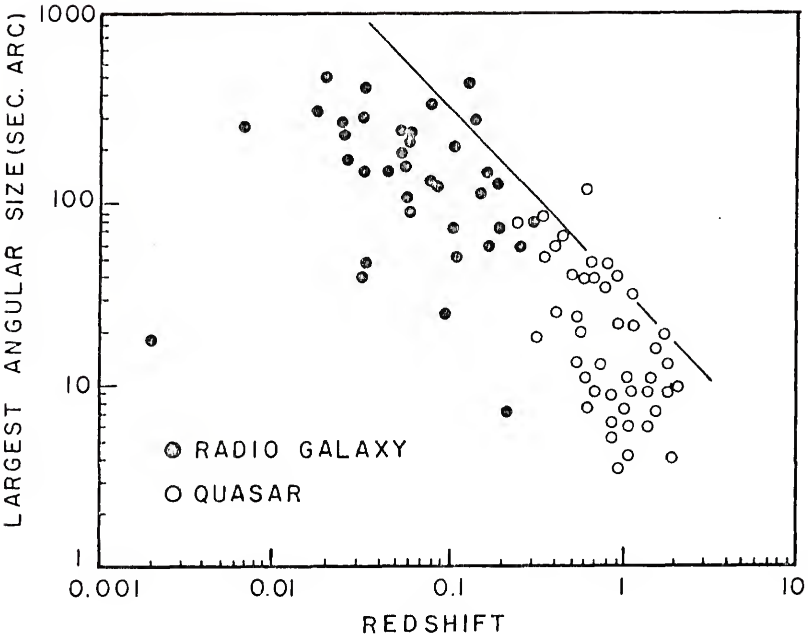
LARGEST ANGULAR SIZE (SEC. ARC)
1000
100
10
1
0.001
0.01
0.1
1
10
REDSHIFT
● RADIO GALAXY
○ QUASAR

redshifts relative to magnitudes is consistent with quasars being at the cosmological distances implied by their redshifts.

The nature of quasar redshifts is still unresolved, but the preponderance of opinion favors a cosmological interpretation. Even if a few quasars do prove to be associated with galaxies, and have redshifts of a non-cosmological origin, the majority of these objects appear to be very distant, and participating in the general expansion of the universe.

Quasars and Related Objects

Seyfert galaxies, named for Carl Seyfert, who first studied them in 1943, are compact spirals with a bright starlike nucleus which is far more luminous than the nucleus of an average galaxy. They represent about 1 percent of the total galaxy population. Both quasars and the nuclei of Seyfert galaxies have a large ultraviolet excess, and appear very blue in photographs. Seyfert galaxies are the most luminous of the spiral galaxies, and many of them have radio power outputs in the range of average radio galaxies, while others emit no detectable radio emissions. Like quasars, they emit the largest portion of their energy in the infrared.

The most luminous galaxies at optical wavelengths are N-type galaxies, which appear similar to Seyferts, except that their envelopes are smaller and more amorphous with no well-defined spiral structure. The ultraviolet excess and infrared emissions of their nuclei are even greater than those of Seyfert galaxies, and they are among the most powerful radio emitters.

Except for their surrounding galactic envelopes, Seyfert and N-type nuclei appear strikingly similar to quasars. All three classes of objects produce starlike images on a photographic plate, and have spectra characterized by broad emission lines up to 100 Å in width, superimposed on a blue continuum. While the spectra of Seyfert and N-type galaxies are identical, there are two minor differences between their spectra and those of quasars. The O II emission line at 3727 Å is faint or missing in quasar spectra (Burbidge 1968), and the spectra of some quasars contain narrow absorption lines, especially around $z = 1.95$.

Predominantly, the typical quasar is a non-thermal source whose emission-line intensity corresponds to 10 percent of the total optical intensity. The optical energy distribution of quasars may be described by a typical synchrotron electron continuum, strongly polarized, with a power law intensity shape described by

$$I \propto \nu^{-n} \tag{1.1}$$

where I is the observed spectral intensity, ν is the frequency, and n is the spectral index (Morrison 1973). This form of spectral energy distribution also describes the optical continuum spectra of Seyfert and N-type galaxies. Figure 2 shows the spectra of the Seyfert galaxies NGC 1275, NGC 1068, and 3C 120, compared with the quasar 3C 273 (Colgate

Figure 2. The continuum spectra of three Seyfert galaxies, NGC 1275, NGC 1068, and 3C 120, and the quasar 3C 273. Large variations are known to exist in the frequency range 10^9 to 10^{11} Hz, so little weight should be placed upon this portion of the curves. After Colgate (1969). Reproduced by permission of Physics Today.

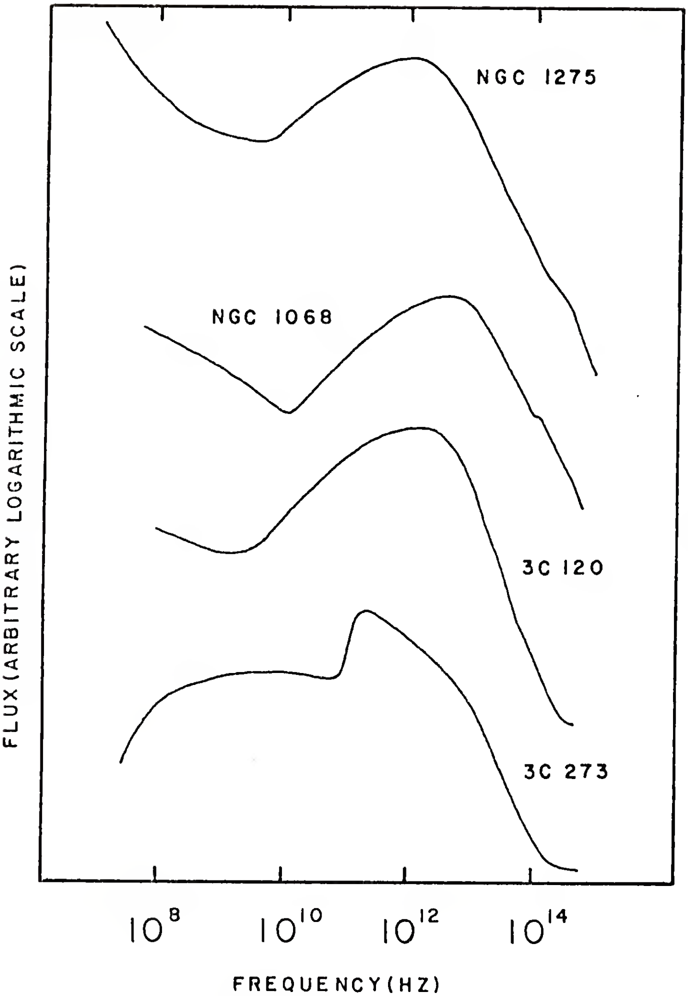
NGC 1275
NGC 1068
3C 120
3C 273
FLUX (ARBITRARY LOGARITHMIC SCALE)
10^8
10^{10}
10^{12}
10^{14}
FREQUENCY (HZ)

1969). At optical wavelengths all resemble a typical single peaked synchrotron spectrum.

The optical variability observed for the nuclei of Seyfert and N-type galaxies is similar in character to that of quasars though in general of lesser amplitude. An exception is the Seyfert galaxy 3C 120, which was observed by Folsom et al. (1971) to undergo fluctuations of a magnitude or more on a time scale of days or weeks. The Florida observations of this object also show considerable activity at infrared wavelengths as discussed in Chapter V.

On a color-color diagram, all three classes of objects lie well above the main sequence, with the region occupied by quasars and Seyfert galaxies overlapping to some extent. This is shown in Figure 3. Color studies by Hackney (1973) and others show that in general these objects all become progressively bluer as they brighten optically, and redder as they decline. Such observations, together with the observed similarities in spectral energy distribution and variability, suggest that quasars and the nuclei of Seyfert and N-type galaxies have similar mechanisms for the release of energy, the process being less violent in the latter objects.

Table 1 is a list of observational similarities between quasars, Seyfert galaxies, and N-type galaxies, compiled by Colgate (1969). These observations, and those previously mentioned, suggest a relationship between classes of objects. If the redshifts of quasars are indeed cosmological, then the majority of them are seen at a very early epoch in the age of

Figure 3. Color-color diagram for quasars (Q), Seyfert galaxies (S), and N-type galaxies (N). The curved line represents the main sequence (MS). After Burbidge and Hoyle (1966) and Hackney (1973).

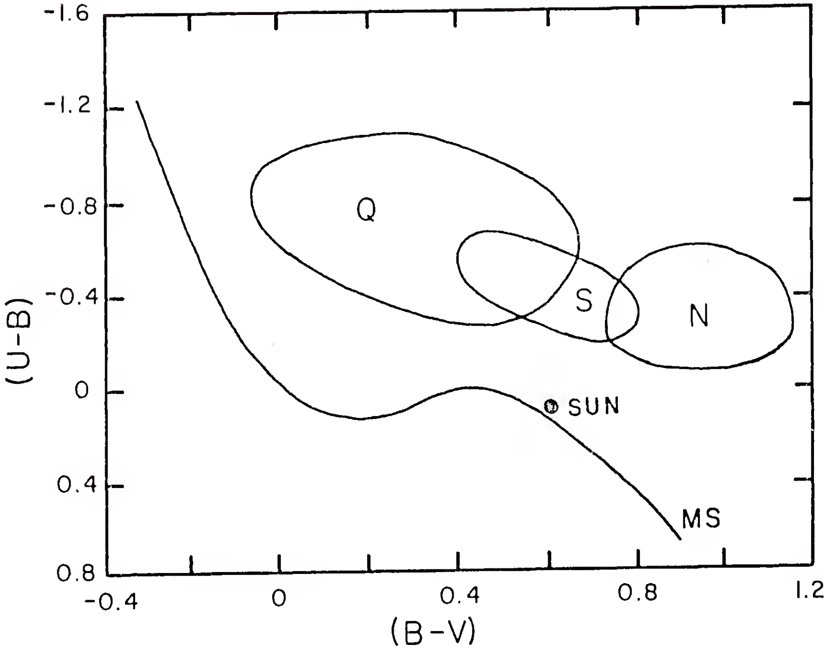
-1.6
-1.2
-0.8
-0.4
0
0.4
0.8
(U-B)
-0.4
0
0.4
0.8
1.2
(B-V)
Q
S
N
SUN
MS

Table 1

Observational Similarities Between Quasars, and Seyfert and N-Type Galaxies

Observation	Seyfert and N-type Galaxies	Quasi-stellar Objects
Infrared luminosity	10^{45}-10^{46} ergs/sec	10^{46}-10^{47} ergs/sec
Optical luminosity	10^{44}-10^{45} ergs/sec	10^{45}-10^{46} ergs/sec
Radio spectrum, wavelength less than one meter	flat	flat
Radio spectrum, wavelength greater than one meter	synchrotron power law	synchrotron power law
Infrared fluctuations	?	possible
Optical continuum fluctuations	0.5 magnitude/year	1.0 magnitude/year
Optical line fluctuations	none	none
Radio fluctuations, wavelengths less than one meter	0.5 magnitude/year	1.0 magnitude/year
Radio fluctuations, wavelengths greater than one meter	none	none
Optical polarization	small	small
Radio polarization	large	large
Radius	30-50 parsec	less than 15 parsec
Absorption lines	?	strong
Absorption-line redshift		half and half

Reference: After Colgate (1969). Reproduced by permission of *Physics Today*.

the universe. This implication, together with the apparent similarities between classes of objects, suggests an evolutionary relationship, starting with quasars and ending with galaxies such as our own. Seyferts and N-types are interpreted as intermediate stages. Such a relationship would imply a gradation of average properties relative to distance and retarded time. Kleinmann and Low (1970) suggest that the spectral energy distribution for all galaxies is very similar, excluding variability, lending further weight to the evolutionary hypothesis.

Models

Observations of quasars, Seyfert galaxies, and N-type galaxies have suggested various source models. Since evidence favors cosmological distances for most quasars, models must not only explain the similarities between classes of objects, but also must conform to cosmological luminosity requirements. While no current quasar model completely satisfies all observational requirements, a few of the more interesting are now briefly outlined.

Supernova Theory

Colgate (1969) has proposed that the observed characteristics of quasars may be explained by a model in which a dense cluster of stars coalesces to form stars of 50 $M_\odot$, which rapidly proceed to the supernova state. A supernova rate of 5 per year yields a peak luminosity of 10^{47} ergs/sec, in good agreement with that calculated for quasars. Collisional excitation of expanding supernovae envelopes gives rise to the rapid fluctuations of the continuum radiation. The optical lines, arising from the excitation of the whole gas cloud, would not be subject to these fluctuations, in agreement with observations. Colgate argues that the large infrared flux observed for quasars could be due to the excitation of a surrounding dust cloud by intense ultraviolet radiation. Since this does not explain the rapid variations observed at infrared and millimeter wavelengths, he proposes an alternate to the dust cloud theory, in which the high-energy fraction of the supernovae ejecta excites a weak two-stream instability in the ionized gas cloud, the infrared and millimeter emissions being due to plasma oscillations. A scaled-down version of this model is used by Colgate to explain the energy released in the nuclei of Seyfert galaxies.

Spinar Theory

This theory, proposed by Cavaliere et al. (1970) and Morrison (1973), imagines a pulsar-like mechanism operating in quasars, consisting of a rapidly rotating central "spinar" having a mass of 10^8 $M_{\odot}$, with an attached coherent magnetic field. The rotating central body, well under one-tenth of a light year in size, has an extermely high peripheral speed of perhaps 0.01 to 0.1 of the velocity of light. Using the pulsar mechanism, such an object can efficiently eject particles at relativistic velocities. The high infrared flux is explained as synchrotron emission, occurring when the particles interact with the innermost portion of the magnetic field. The optical and x-ray continua arise from Compton-recoil emission, due to curvature of the magnetic field lines, as the particles progress outward. Moving outward, clouds of expanding particles give rise to the radio frequency emission. Hot and cool gas filaments give rise to the optical lines.

Irtron Model

Low (1970) envisions clusters of identical infrared sources called irtrons to be characteristic of the central regions of quasars and the nuclei of all galaxies. Continuous creation of matter and antimatter within the irtrons, and the subsequent annihilation, convert a large portion of the created mass directly into relativistic particles, which radiate by the synchrotron process when interacting with a magnetic field of about 100 gauss. Such a process creates a peak in the flux distribution for 100 MeV electrons at approximately 75 microns, which agrees well with observations. Luminosity fluctuations are explained as interactions between irtrons, or between irtrons and stars, which affect the injection of particles into the magnetic field. As an object ages, the number of irtrons diminishes and activity decreases. Low suggests an evolutionary chain, starting with quasars and ending with galaxies similar to our own.

Gravitational Lens Hypothesis

A somewhat different approach is presented by Barnothy and Barnothy (1968). They theorize that quasars and N-type galaxies may not be real objects, but rather the images of Seyfert galaxy nuclei, amplified by gravitational lenses in the form of intervening galaxies. In the case of a quasar, the deflector galaxy is very distant and invisible, but in N-type galaxies it is close enough so that part of it can be seen surrounding the brilliant nucleus, which is the image of the Seyfert galaxy behind it. The observed emission lines could originate either in the object or the deflector, or both. Variability is explained as a combination of intrinsic brightness fluctuations of the object, combined with the changing aspect between the object and lens, due to their differential velocity across the line of sight. This somewhat novel theory has received little support, the majority of opinion being that quasars are indeed a distinct class of extragalactic objects.

The Florida Program

In 1968 a program for photographic monitoring of the optical variability of quasars was initiated by A. G. Smith and G. H. Folsom, using the University of Florida's newly installed 30-inch Tinsley reflector. K. R. Hackney and R. L. Hackney have contributed extensively to the expansion and continuation of this program. At present, observations and data reduction are carried out by A. G. Smith, R. J. Leacock, B. Q. McGimsey, P. L. Edwards, and the author. Through the efforts of these observers, and through cooperation with other observatories, the Florida program has amassed considerable knowledge about the nature of quasar variability. Over 160 objects are now being monitored; the majority are quasars, but Seyfert and N-type galaxies, and lacertids are also included.

The author has selectively monitored several of the more active sources in an attempt to learn more about these particular objects. In addition, to study apparent similarities between classes of objects and possible evolutionary relationships, the average properties of representative classes of objects have been compared, and the observed properties of several quasars have been compared with their redshifts. Various photographic techniques which are directly or indirectly related to the author's studies have been investigated.

Jupiter, Another Active Radio Source

While the majority of the author's research is concerned with extragalactic radio sources, as a further exercise in photographic techniques a study was made of another active radio source, the planet Jupiter.

Since its discovery in 1955 by Kenneth Franklin and Bernard Burke, the decametric radio emission of Jupiter has intrigued astronomers with the problem of understanding the origin of these energetic radio bursts. Histograms plotting the probability of receiving emissions as a function of central meridian longitude show three well-defined peaks or "sources," which are illustrated in Figure 4 (Smith 1969).

In 1964 the Australian statistician E. K. Bigg showed that the position of the satellite Io in its orbit had a definite effect on the probability of reception (Bigg 1964). Bigg found that when Io was at 90° and 240° from superior geocentric conjunction, the probability of reception was definitely enhanced. When Io is at 90°, source B is activated, and when Io reaches 240°, sources A and C are activated. In addition, source A emits some radiation which is apparently unrelated to Io.

Thus far, no theory has been able to account for all the observed phenomena. One of the most interesting theories proposed to explain the role of Io is that of Goldreich and Lynden-Bell (1969). There have been several variations of this theory put forth in recent years, but the general idea remains approximately the same. Goldreich and Lynden-Bell theorize that Io may be considered a unipolar generator which develops an emf of 7×10^5 volts across its radial diameter, as seen from a frame of reference rotating with Jupiter. It is assumed that Io's orbit is circular, that the Jovian magnetic field has permeated Io, and that Io always keeps the same side toward Jupiter. Assuming further that Io is a fairly good conductor, at least as good as the upper mantle

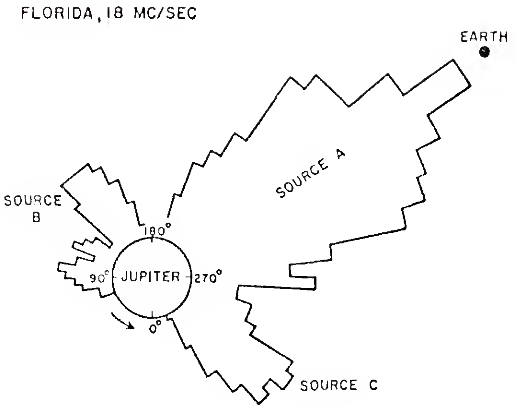

Figure 4. A polar diagram of Jupiter's decametric radio sources. The radial coordinate is the probability of receiving Jovian emissions. After Smith (1969).

of the earth, the electric field will have to vanish inside the tube of flux enclosing the satellite. Any plasma enclosed by the flux tube will be frozen to Io, and as Jupiter rotates the "feet" or intersections of the flux tube with the Jovian ionosphere will slip. This induces a voltage of approximately 700,000 volts, which drives a current of a million amperes across each foot of the flux tube. The current is assumed to flow up one side of the tube, cross the magnetic field in Io, and then flow back down the other side of the tube. This current circuit is illustrated in Figure 5. Instabilities in these current sheets are theorized as being responsible for the Io-induced decametric bursts. The geometry of the beaming of the bursts suggests coherent cyclotron radiation as the emission mechanism, the coherence being produced by bunching of the electrons in the current sheets.

When energetic charged particles from the sun stream along the earth's magnetic lines of force into the earth's ionosphere, they often cause intense auroral emissions. Similar emissions may radiate from the feet of the proposed Jovian flux tube, and if observed could provide substantial support for the Goldreich and Lynden-Bell theory. Photographic detection of this "auroral hotspot," as it is sometimes called, was the purpose of this study.

Since it was felt that this project could be carried out most advantageously at the Cassegrain focus of the 30-inch reflector, a Cassegrain camera was designed by the author and A. G. Smith. This camera was designed with a

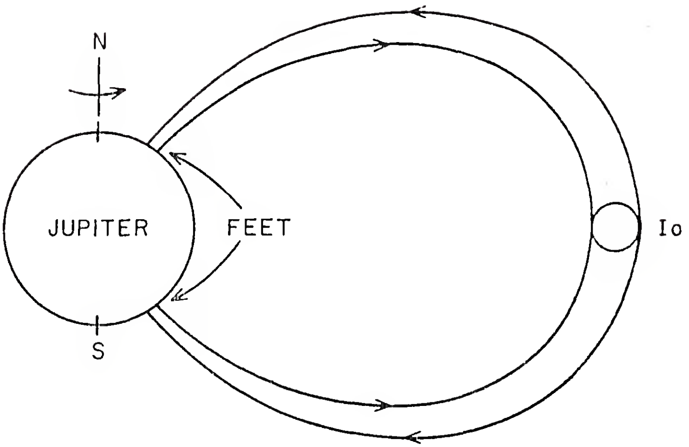

Figure 5. Current sheets in the Io flux tube (not to scale). After Goldreich and Lynden-Bell (1969).

variety of uses in mind; besides planetary photography, it has been used to monitor one of the brighter active quasars on moonlit nights, and it is currently being used by B. Q. McGimsey in polarization studies of quasars. The Cassegrain camera is described in Chapter II, together with the observational techniques used in the remainder of the program.

CHAPTER II

RESEARCH TECHNIQUES AND INSTRUMENTATION

Photographic Studies of Quasars

The University of Florida's 30-inch aperture Tinsley reflector is well suited for a program of optical monitoring of quasars. This instrument, located at Rosemary Hill Observatory near Bronson, Florida, may be used in either an f/4 Newtonian or f/16 Cassegrain focal ratio by exchanging secondary mirrors. Figure 6 shows the 30-inch reflector and the Newtonian and Cassegrain cameras. Figure 7, taken on the evening of January 10, 1974, shows Comet Kohoutek beside the 30-inch dome.

At present, most program objects are photographed with the 30-inch reflector. However, the University's recently acquired 18-inch f/10.3 Ritchey-Chrétien telescope has proven useful for monitoring several of the program's brighter sources. This telescope, which was acquired and refurbished under the guidance of Professor John Oliver, was used during the summer of 1974 by visiting professors Karen and Richard Hackney of Western Kentucky University to study short-term variations of lacertids. These data have also contributed significantly to the author's own studies. The 18-inch reflector is shown in Figure 8; its dome is located about 100 yards north of the 30-inch dome.

Figure 6. The Rosemary Hill Observatory 30-inch Newtonian/Cassegrain Tinsley reflector, with both Newtonian (N) and Cassegrain (C) cameras mounted.

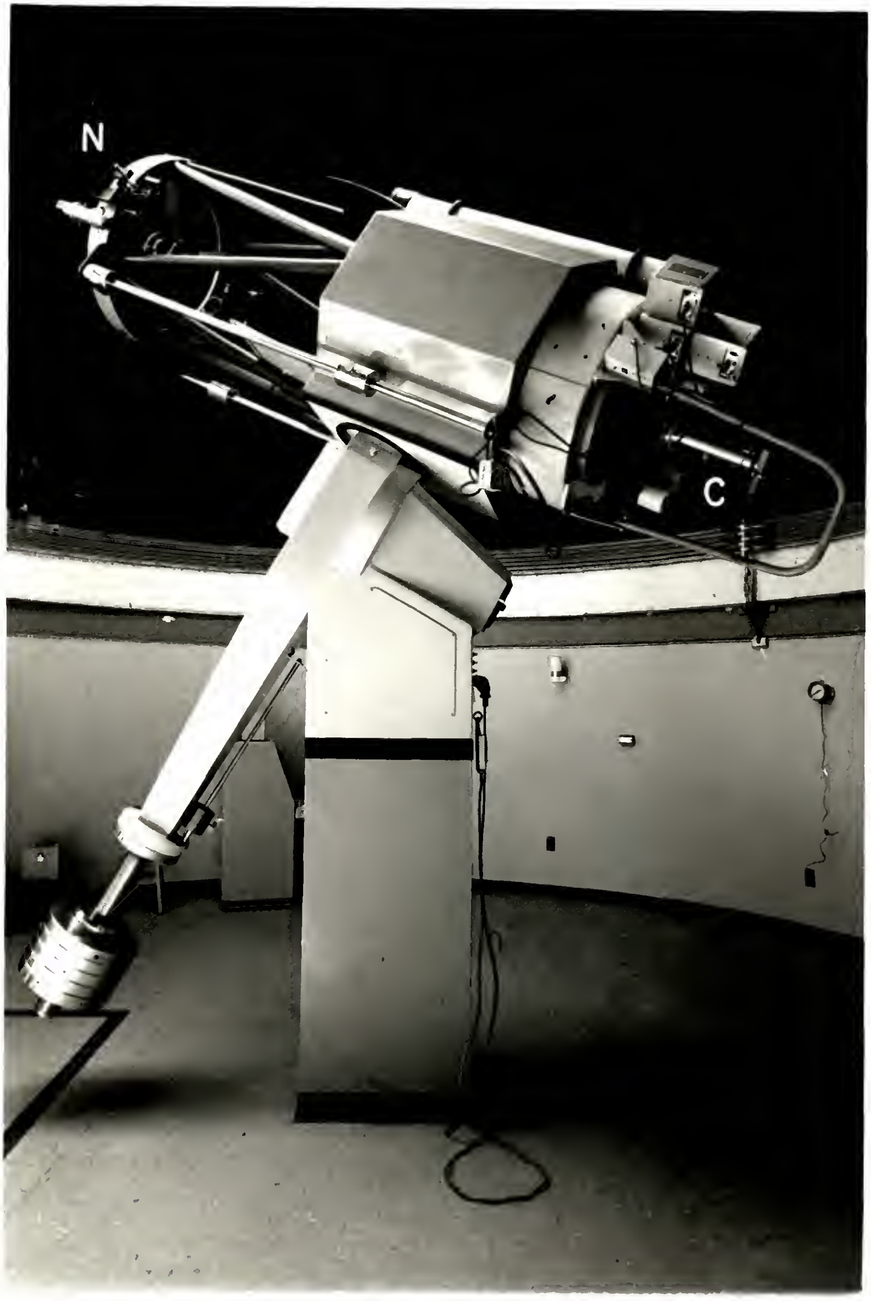
N
C

Figure 7. Comet Kohoutek in the brilliant zodical light, as seen from Rosemary Hill Observatory on the evening of January 10, 1974, at 2030 EDT. This print was made from a contrast enhanced internegative. The original negative was taken with a 50 mm f/1.4 Nikkor lens using an exposure of 30 seconds on Tri-X Pan, which was force developed for added speed and contrast.

Figure 8. The Rosemary Hill Observatory 18-inch Ritchey-Chrétien telescope showing offset guiding telescope (T) and camera (C). The camera bed is similar to the camera beds used at the Newtonian and Cassegrain positions of the 30-inch telescope, and will accept the same plate cassettes as the 30-inch cameras.

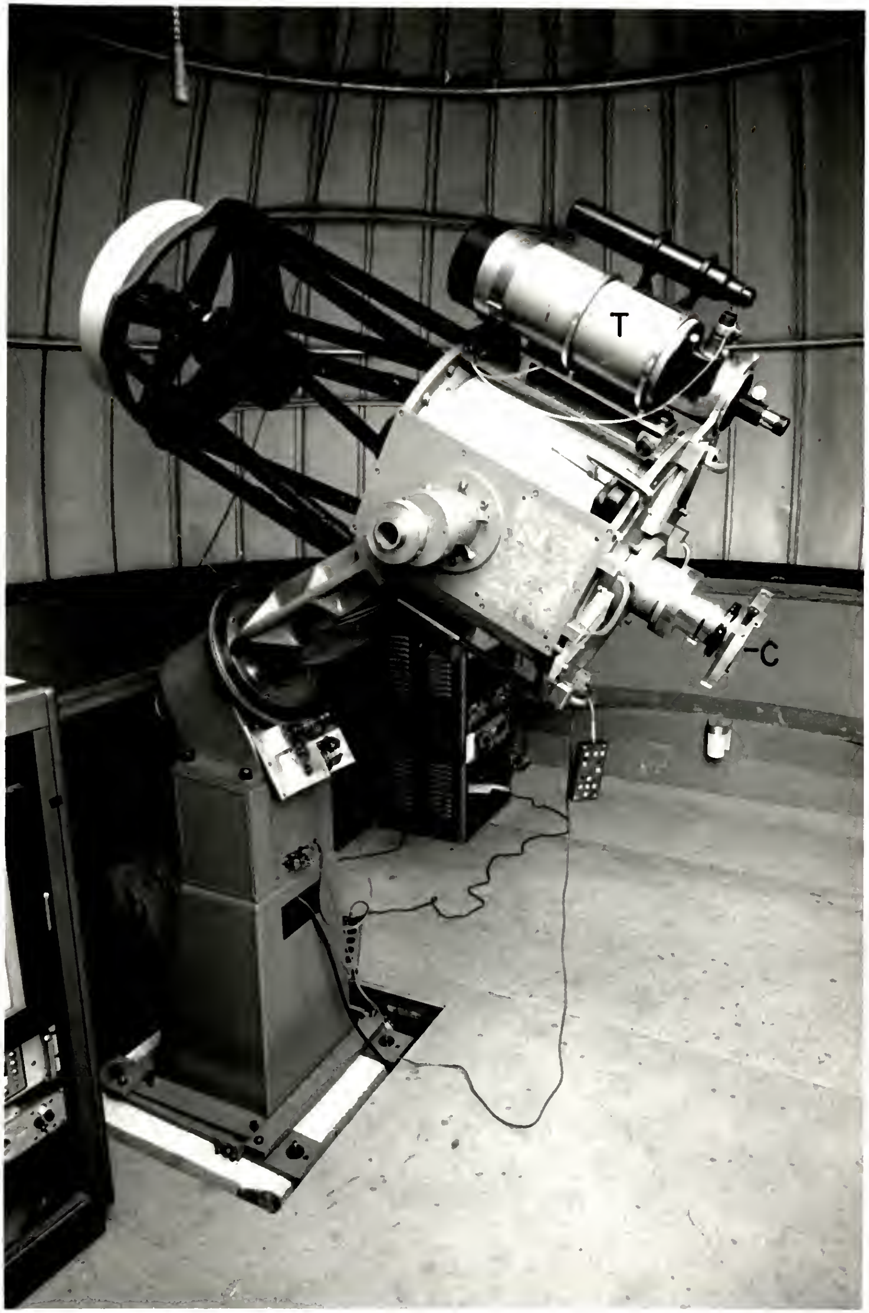
T
C

The majority of the program objects are between 15th and 19th magnitude in the spectral regions studied, which is beyond the practical limit for photoelectric observations with the 30-inch telescope, this being about 14th magnitude due to the limitations of aperture and sky brightness. The technique used is that of photographic photometry; a sky-limited photographic magnitude of 20 to 20.5 can be reached in approximately 15 to 20 minutes at the Newtonian focus, on unfiltered Kodak 103a-0 plates. When hypersensitized by nitrogen baking, as described in Chapter III, such plates can reach the Newtonian limiting magnitude in 10 minutes or less, and they have enabled satisfactory exposures to be made at the slower Cassegrain focus, making possible polarization studies and occasional monitoring of bright sources during periods of moonlight. However, the majority of program objects are photographed at the fast Newtonian focus.

For regular monitoring of many sources, photographic techniques have a further advantage over photoelectric photometry. Studies by Hackney (1973) indicate that on the average 66 percent of the 12 nights per month allotted to quasar monitoring are useful photographically, while only 35 percent of the nights are useful photoelectrically.

Program Techniques

Detailed descriptions of the telescope, Newtonian camera, observing procedures, and data reduction are given by Folsom (1970), R. L. Hackney (1972a), and K. R. Hackney (1973). In general, objects are photographed at the Newtonian focus of the 30-inch telescope; plates are exposed in sealed cassettes charged with dry nitrogen to prevent speed losses due to the excessive humidity of the Florida air. The observer carefully guides the telescope during the exposure, to ensure images of usable quality. Plates are developed immediately, at the observatory, in a darkroom set up for that purpose. The plates are reduced on a Cuffey iris astrophotometer; an on-line Hewlett-Packard 9810 A calculator fits a least-squares calibration curve to the iris readings and magnitudes of a series of comparison stars, and calculates the magnitude of the object. Comparison star magnitudes are smoothed for local field effects with an IBM 370/165; the computer is also used to perform chi-squared tests on the data to determine the confidence level for variability (Hackney 1973).

Magnitude Systems

Most program objects are photographed on unfiltered 103a-0 plates, yielding a photographic magnitude m_{pg}. For studying color changes in a select group of objects, K. R. Hackney used a photographic UBV system which closely approximates the U, B, and V magnitudes of the Johnson-Morgan system (Stock and Williams 1966). A Kodak IIa-0 emulsion is combined with Schott UG-2 and GG-13 filters, to yield photographic U and B magnitudes, respectively. A IIa-D emulsion and a Schott GG-14 filter define the photographic V magnitude. The system response functions of the Rosemary Hill UBV system are described by K. R. Hackney (1973). The IIa-0 and IIa-D plates were chosen initially because it was felt their fine-grained emulsions would contribute to photometric precision. Both plates are baked in dry nitrogen, approximately doubling their speed. Investigations by the author and A. G. Smith, described in Chapter III, have shown that the faster, coarser-grained 103a-0 may be substituted for the IIa-0, with a small loss in photometric precision unimportant in routine monitoring.

The author has used the above UBV system to compare the color indices of various classes of objects, and to investigate the relation between the color indices of quasars and their redshifts. In addition, an infrared system, also described by Stock and Williams (1966), has been used in these studies. Kodak I-N plates combined with a Schott RG-8 filter define the infrared magnitude system. Figure 9 shows the normalized infrared system response function. The I-N emulsion is inherently slow; it must be hypersensitized at the observatory and used within a few hours to obtain sufficient speed for practical use. Using the ammonia hypering procedures described by Barker (1968) and Babcock et al. (1974), sufficient sensitivity has been obtained to reach a limiting infrared magnitude of about 16 with an exposure of 25 minutes at the Newtonian focus.

Figure 9. The infrared system response function used in the QSO studies, obtained by combining the Kodak type I-N emulsion with a Schott RG-8 infrared filter. The curve shows the normalized relative response R_N versus wavelength, and was obtained by a point-by-point multiplication of the plate sensitivity and percent transmission of the filter. The spectral response of the I-N emulsion was obtained from the booklet "Kodak Plates and Films for Scientific Photography," Eastman Kodak Company, 1973. The transmission characteristics of the RG-8 filter were obtained from the Schott "Color Filter Catalog No. 365e."

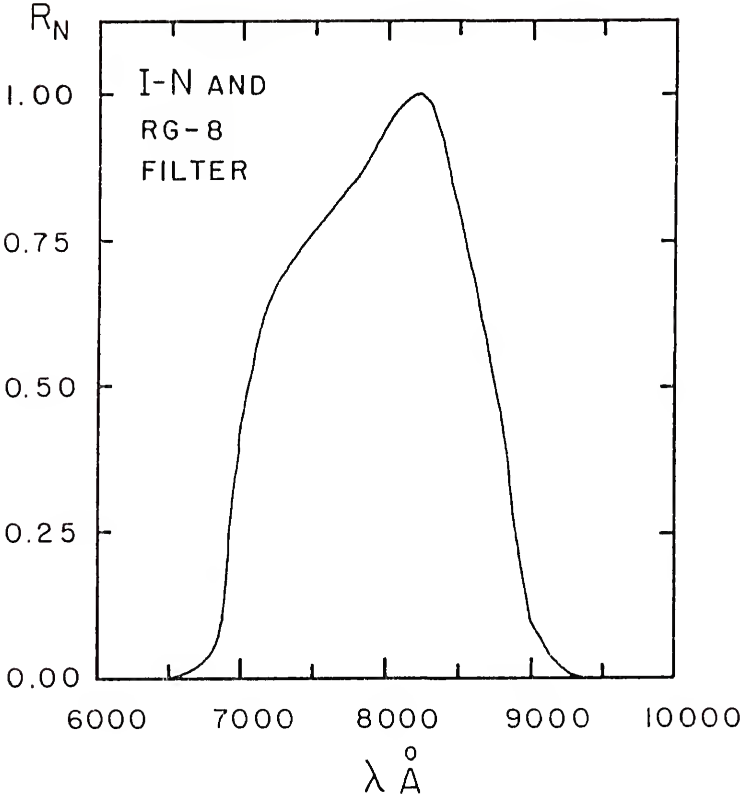
R_N
I-N AND
RG-8
FILTER
1.00
0.75
0.50
0.25
0.00
6000
7000
8000
9000
10000
λ Å

A Photographic Attempt to Detect the Jovian "Hotspot"

The Cassegrain Camera

The Rosemary Hill Observatory Cassegrain camera was designed by the author and A. G. Smith in the summer of 1971. The camera was built by Eli Graves, of the Department of Physics and Astronomy research shop. Though initially conceived with a variety of uses in mind, the major goal at the time of construction was to obtain a convenient image size for the author's photographic study of Jupiter.

Assuming an apparent Jovian diameter of 35 arcsec, the image diameter at the f/4 Newtonian focus will be approximately 1/50 of an inch. It was felt this image size should be increased relative to plate grain in order to obtain adequate resolution. Also, a larger image would aid in the reduction of the plates, yielding a larger area for more convenient examination.

The image size may be boosted by a factor of 4 by working at the f/16 Cassegrain focus. In addition, larger increases can be obtained by eyepiece projection, a standard procedure for increasing image size in planetary photography.

Figure 10 shows the various parts of the Cassegrain camera. Essentially, the camera consists of a flat baseplate connected to a camera bed by a spacing tube designed to align the focal plane of the camera with the f/16 Cassegrain focal plane of the 30-inch reflector. The camera bed is similar to that of the Newtonian camera, and will accept the sealed

Figure 10. The Cassegrain camera mounted on the guidebox of the 30-inch reflector showing offset guider (G), counterweights (W), base tube (T), rotation clamps (R), eyepiece projection tube (E), filter holder (H), shutter (S), with cable release (C), and camera bed (B), with dark slide (D).

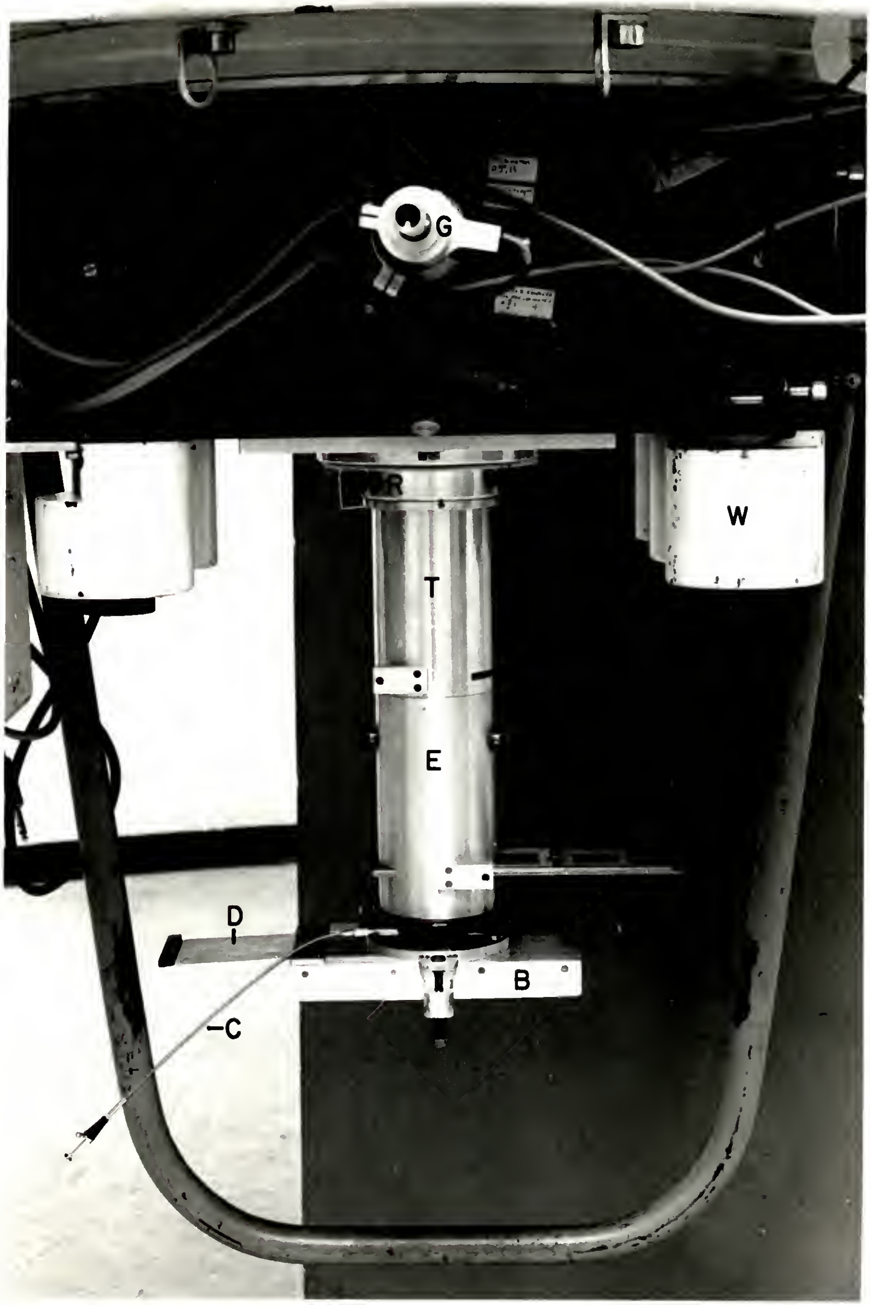
G
R
W
T
E
D
B
C

cassettes used in the quasar program if desired. The bed may be rotated to any desired position angle relative to the guidebox by loosening the rotation clamps.

A shutter is provided for exposures of short duration. It can be set at 1/2 sec, 1/5 sec, 1/10 sec, 1/25 sec, 1/50 sec, "time" and "bulb." For the Jupiter project, where most of the exposures were seconds or sometimes minutes, the shutter was set on "bulb" and the exposure duration was controlled by the observer, using a cable release. For very long exposures, the shutter is set on "time" and opened, and the exposure is controlled with the dark slide.

After removal of the photoelectric photometer, the camera bolts directly to the Cassegrain guidebox of the 30-inch reflector as shown in Figure 10. A series of six counterweights are used to compensate for the 80-lb weight differential between the camera and the photometer. The existing Cassegrain offset guiding mechanism, with slight modification by A. G. Smith, was found to be satisfactory for the guiding of long exposures.

An eyepiece projection tube accepting standard 1-1/4-inch outside-diameter eyepieces can be used if image enlargement is desired over that provided at f/16. With the camera bed unscrewed, the projection tube screws directly onto the base tube; the camera bed is then screwed onto the end of the projection tube. The eyepiece projection tube is shown in Figure 10. The camera is constructed mostly of aluminum; exceptions are the stainless steel dark slide, the steel shutter (from a commercial source), and the eyepiece holder and filter slide for the projection tube, both of which are made of brass.

A filter slide was constructed for the eyepiece projection tube, to allow exposures to be taken through standard tricolor filters in rapid succession. This has enabled the author to construct several tricolor separation prints of Jupiter; Figure 11 is an example. The color print in Figure 11 is a composite of the three black and white exposures taken on fine-grained Kodak Contrast Process Pan film through a red #25, blue #47 B, and green #58 filter, respectively.

To produce such a color print, each of the three black and white negatives is projected one at a time upon ordinary color print paper. Each negative is projected through the same filter used to produce it at the telescope. Accurate superposition is accomplished by use of a cardboard mask, upon which details of the Jovian image are traced with extreme care. With the mask covering the print paper, a negative is carefully aligned with the tracing on the mask and the proper filter is placed in the enlarger. The mask is then removed and the exposure is made. Then the mask is carefully replaced and another negative is aligned with it. When all three negatives have been exposed through their filters, the paper is developed in its usual manner.

Tricolor separation is a standard method used to produce color pictures of planets and, occasionally, celestial objects too faint to photograph successfully on color films without using cooled emulsion techniques. Such a procedure produces

Figure 11. Tricolor separation print of Jupiter from negatives taken on July 29, 1972. A print from the red negative is at upper right, the blue at lower left, and the green at lower right. The red and green exposures were each 25 seconds, the blue 70 seconds. A 25 mm eyepiece was used to project the primary Cassegrain image onto the film plane yielding an equivalent focal length of f/64 or 160 feet. All exposures were made on Kodak Contrast Process Pan 4" x 5" sheet film. The three negatives were superimposed through the corresponding filters to produce the Unicolor print. In the color print the Great Red Spot predominates, along with a double equatorial band crossed with white wisps, and a white spot to the right of the red spot. South is up.

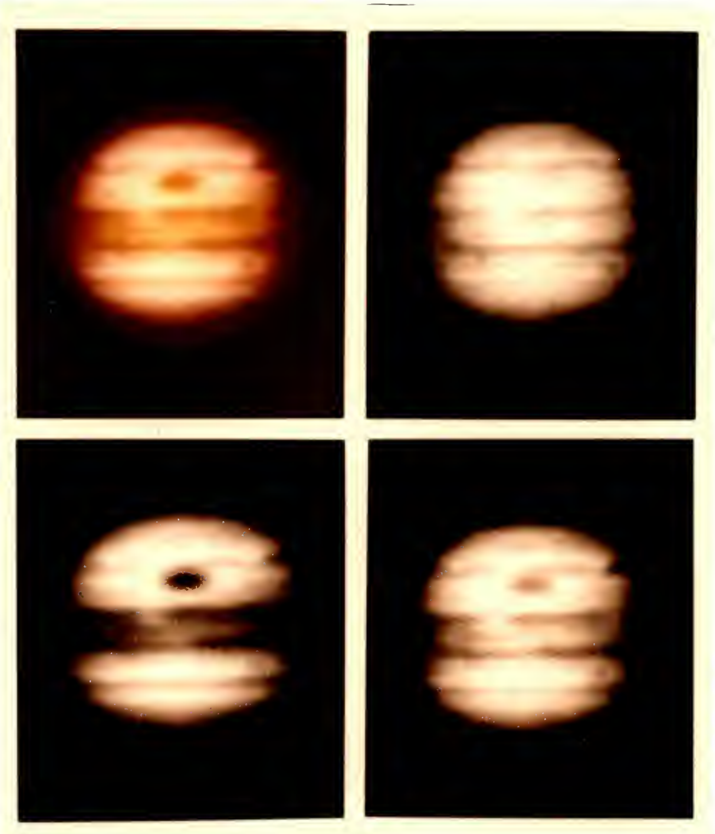

a sharper print than a single exposure, due to suppression of emulsion grain and seeing effects. By manipulating the relative exposures of the tricolor negatives, the desired results may usually be obtained after a little experimentation.

Plates and Filters

According to Goldreich and Lynden-Bell, the intersection of the Io-linked flux tube with Jupiter's ionosphere has an elliptical cross section, with a major axis of 230 km and a minor axis of 120 km. If a Jovian angular diameter of 35 arcsec is assumed, the angular diameter of the foot of the flux tube is approximately 0.05 arcsec. The theoretical resolving power of the 30-inch reflector is 0.15 arcsec, and seeing usually limits the resolution to at least 2 arcsec. However, the real difficulty in detection of the spot is the interference from reflected sunlight. Unresolved stellar images are easily seen or photographed because of their great brightness relative to the sky background. Since Jupiter exhibits considerable limb darkening, confining the search for the hotspot to those times when it should be near the Jovian limb would lessen interference from reflected sunlight.

Pilcher and McCord (1971) show the albedo of Jupiter to be at a minimum between 0.3 and 0.4 microns, and between 0.95 and 1.05 microns. Their curve is shown in Figure 12. Since interference from reflected sunlight would be minimized, these spectral regions are well suited for an attempt at detecting the hotspot, especially the infrared region.

Figure 12. Spectral reflectivity of Jupiter. After Pilcher and McCord (1971). Pilcher and McCord's original albedo curve was normalized to unity at 0.56μ; the normalized albedos have been replaced with estimates of the true albedo obtained from Danielson (1966).

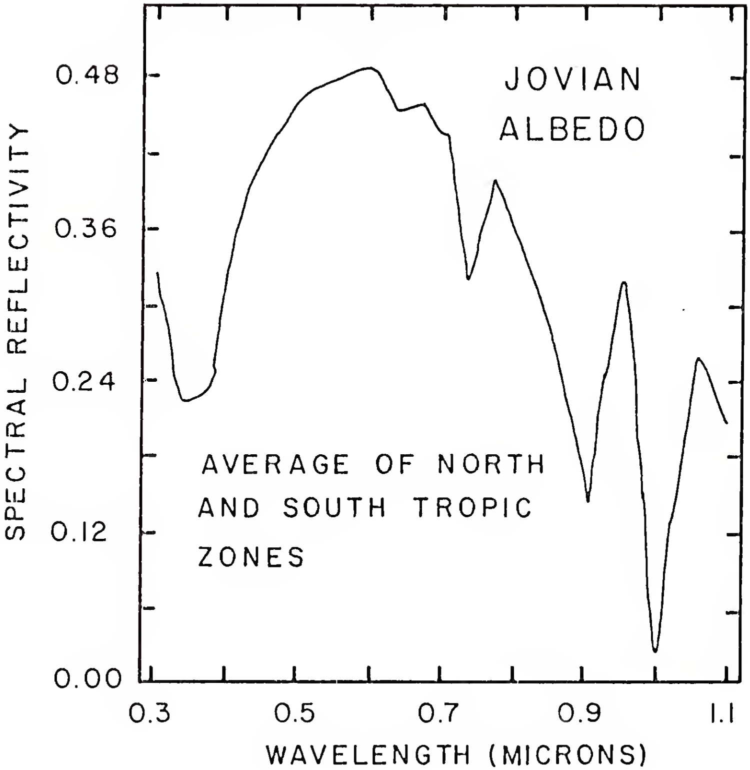
JOVIAN
ALBEDO
AVERAGE OF NORTH
AND SOUTH TROPIC
ZONES
SPECTRAL REFLECTIVITY
0.00
0.12
0.24
0.36
0.48
0.3
0.5
0.7
0.9
1.1
WAVELENGTH (MICRONS)

Kodak 103a-0 plates, combined with a Kodak #18 A filter, approximate the above ultraviolet region. Kodak I-Z plates, combined with a Schott RG-8 or Corning 7-56 filter, will give broad and narrow band coverage of the above infrared region respectively. The normalized system response functions of these plate and filter combinations are shown in Figures 13 and 14.

To obtain maximum speeds and reduce exposure times, the 103a-0 plates were nitrogen baked. The I-Z plates, like most infrared emulsions, must be hypersensitized before use. They were treated with ammonia, following a procedure described by Pope and Kirby (1967).

Choosing Observation Times

A computer-generated ephemeris, programmed by G. R. Lebo and W. W. Richardson, is used by the University of Florida Radio Observatory in predicting Io-related Jovian radio storms. This ephemeris also gives the geocentric longitude of Io, Europa, and Ganymede for each hour of Universal Time, for each day of the year. The longitude is computed relative to superior geocentric conjunction, the point at which the satellite is farthest from earth in its orbit. This ephemeris was used to select optimum times for photographing the hotspot, by determining what times Io, and thus the hotspot, would be near the Jovian limb.

Goldreich and Lynden-Bell suggest that the spot may lead Io in longitude by as much as 12°, depending upon the conductivity of the Jovian ionosphere. Such a lead should be at a

Figure 13. The ultraviolet response function used in the Jupiter studies, obtained by combining the Kodak type 103a-0 emulsion with a Kodak #18 A filter. The curve shows the normalized relative response R_N versus wavelength, and was obtained by a point-by-point multiplication of the plate sensitivity and percent transmission of the filter. The spectral response of the 103a-0 emulsion was obtained from the booklet "Kodak Plates and Films for Scientific Photography," Eastman Kodak Company, 1973. The transmittance of the #18 A filter was obtained from the booklet "Kodak Filters for Scientific and Technical Uses," Eastman Kodak Company, 1970.

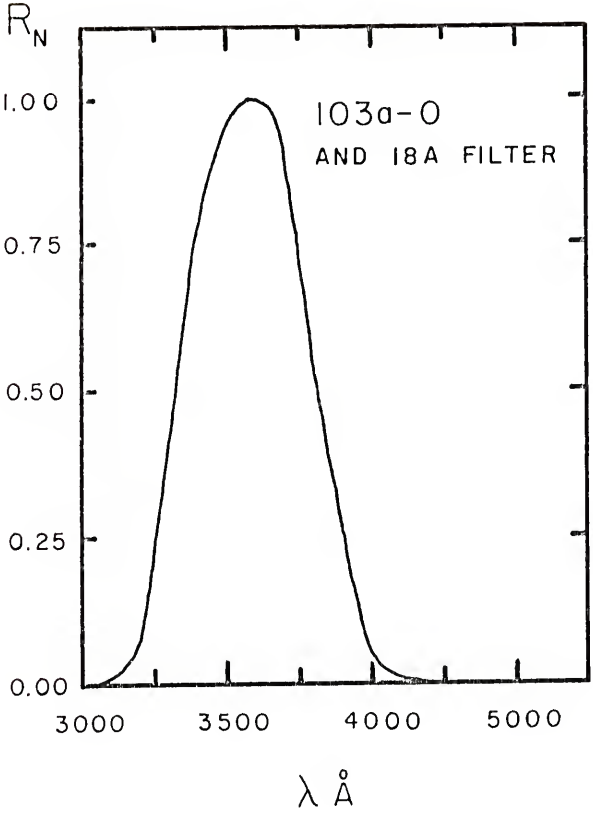
R_N
1.00
0.75
0.50
0.25
0.00
103a-O
AND 18A FILTER
3000
3500
4000
5000
λ Å

Figure 14. The infrared system response functions used in the Jupiter studies, obtained by combining the Kodak type I-Z emulsion with a Schott RG-8 filter for broad band coverage (dotted curve), and a Corning 7-56 filter for narrow band coverage (solid curve). The curves show the normalized relative response R_N versus wavelength, and were obtained by a point-by-point multiplication of the plate sensitivity and the percent transmission of the filters. The spectral response of the I-Z emulsion was obtained from the booklet "Kodak Plates and Films for Scientific Photography," Eastman Kodak Company, 1973. The transmittance of the RG-8 filter was obtained from the Schott "Color Filter Catalog No. 365e." The transmittance of the 7-56 filter was obtained from the booklet "Glass Color Filters," Corning Glass Works, 1965.

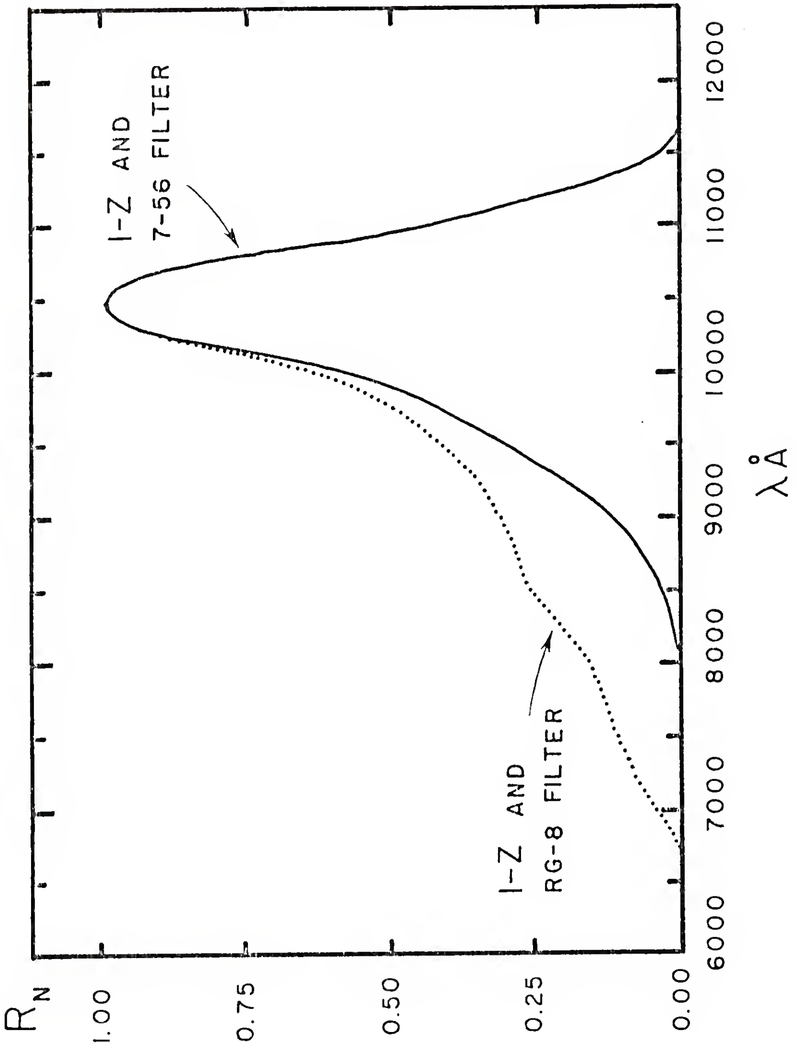
R_N
1.00
0.75
0.50
0.25
0.00
6000
7000
8000
9000
10000
11000
12000
$\lambda \mathring{A}$
I-Z AND 7-56 FILTER
I-Z AND RG-8 FILTER

minimum as the spot emerges from the terminator on the east limb of Jupiter, and at a maximum as the spot approaches the western limb. Assuming a 12° lead, the spot will be on the east limb when Io has a geocentric longitude of 78°, and on the west limb when Io is at longitude 258°. Because of the uncertainty in the lead in longitude of the hotspot relative to Io, "hotspot events" were considered to start when Io was near 78° or 258°, and to end when Io reached 90° or 270°, respectively. Since Io moves about 8.4° per hour in its orbit, such an event lasts about 1-1/2 hours. If possible, Jupiter was photographed continuously during these times.

Observing Techniques

Due to the short exposures required for this study it was not felt necessary to use the sealed quartz-window cassettes used in the quasar program. Instead, nonsealed cassettes containing no optical windows were used; they can be unloaded and loaded quickly, making it possible to take a series of exposures in rapid succession.

At the start of observing sessions, the camera was given a careful knife-edge focus. Focus plates have shown that there is no significant change in focus introduced by the ultraviolet and infrared filters. After focusing, the wide field Erfle eyepiece used in the quasar program was inserted, and Jupiter was placed near the "top" of the field. Then the eyepiece was removed and the desired filter was placed in the camera. A series of exposures was now taken; they were spaced by sliding the cassette relative to a scale on the side of the camera bed. Usually five or six exposures were taken in such a series. Then the eyepiece was replaced, Jupiter placed in the center or "bottom" of the field, and another series of exposures was taken. In this manner, several rows of Jovian images could be placed on a single plate. The starting time of each exposure was determined to the nearest second with WWV and this, together with the duration of each exposure, was recorded in a logbook.

Since the expected brightness of the hypothetical spot is known only roughly at best, exposures were bracketed in such a manner as to range from images that showed detail in the Jovian cloud features to burned-in disks which showed no surface features at all. Because of the slowness of the I-Z emulsion, infrared exposures were taken at f/16, and required exposure times of nearly a minute to several minutes in length. Using the RG-8 filter, infrared exposures of about 40 seconds showed the best detail in Jovian cloud features. Longer exposures of several minutes showed little detail and were often surrounded by a halo. When using the 7-56 filter, exposures of approximately 2 minutes showed the best Jovian cloud detail, while exposures of up to 5 minutes could be made without burning in the planetary disk. The longer exposures were guided with the Cassegrain offset guiding mechanism.

The fast 103a-0 plates yielded satisfactory ultraviolet images with exposures of only a few seconds, and occasionally eyepiece projection was used to increase the size of the image. At f/16, ultraviolet exposures of 1 to 1/2 seconds showed the best cloud detail, while exposures of 5 seconds and greater produced totally burned-in images with no visible detail. The reduction of the plates is discussed in Chapter VII.

CHAPTER III

NITROGEN BAKING AND EMULSION COOLING AS METHODS OF HYPERSENSITIZATION

Introduction

Two hypersensitization techniques are discussed in this chapter: the effect of nitrogen baking on the Kodak type 103a-0 spectroscopic emulsion, and the speed gains obtained by cooling various emulsions. The nitrogen baking of the 103a-0 was found to be a practical aid in the routine monitoring of QSO's at Rosemary Hill; a discussion of this technique was published in the Astronomical Journal (Scott and Smith 1974).

The speed gains obtained by nitrogen baking or emulsion cooling apparently arise due to a lessening of "low intensity reciprocity failure." According to the reciprocity law for photochemical reactions, the product of a photochemical reaction is dependent upon the total energy involved (Eastman Kodak 1973). Applying the reciprocity law to photographic emulsions would imply that the density of the image formed is dependent upon the energy of the exposure; the energy may be expressed as the product of the intensity of the exposure and the exposure duration. For most photographic materials the density produced by a long exposure of low intensity will be less than that produced by a shorter exposure of higher intensity, even if the total energy in the two cases is the same. This is an example of low intensity reciprocity failure, and it shows that image density is dependent upon both intensity and time of exposure.

The currently accepted theory of latent image formation is that of Gurney and Mott (1938). The typical photographic emulsion is composed of silver halides, usually a mixture of silver bromide and silver iodide, suspended in gelatin. The latent image is assumed to be formed of metallic silver and arises from the combination of photoelectrons and silver ions, which forms a speck of metallic silver on or in the silver halide crystal. The latent image photolysis reactions for a silver bromide emulsion are given below (Stock and Williams 1966):

$$Br^{-} + h\nu \rightarrow Br + e \qquad (3.1)$$

$$e + Ag^{+} \rightarrow Ag \qquad (3.2)$$

where $h\nu$ is a quantum of radiation and e an electron. At low intensity levels many of the liberated photoelectrons are believed to recombine with positive holes before a stable latent image can be formed; this is the suggested explanation for low intensity reciprocity failure.

Kodak spectroscopic plates of "a" designation, such as IIIa-J or 103a-0, are chemically treated by Eastman Kodak during manufacture to partially compensate for low intensity reciprocity failure. Nitrogen baking can usually be used to hypersensitize "a" plates; the baking presumably extends the chemical sensitization initiated by Kodak, reducing the probability that photoelectrons will recombine with positive holes. Oxygen and water are also removed by baking; their presence in the emulsion is also believed to hinder latent image formation. Though impressive speed gains may be obtained by baking, they are accompanied by an increase in background fog level. The shelf life of baked materials is also greatly reduced unless stored at a low temperature in nitrogen. It should be pointed out that it has long been a standard practice at many observatories to bake plates in air; the current more efficient practice of baking in nitrogen was pioneered by Dr. A. G. Smith at the University of Florida (Smith et al. 1971).

The cooling of photographic emulsions is believed to retard "thermal regression" of the latent image (Hoag 1964). At low intensity levels thermal activity tends to break up the latent image specks before they are stable enough for development. Cooling of the emulsion reduces this effect, presumably increasing the number of photoelectrons trapped by silver ions, while reducing the mobility of positive holes (Eastman Kodak 1973). Unlike baking, which is carried out prior to exposure, the cooling process must be carried out during the exposure interval. Cooling is most effective for materials designed for short exposures, such as Tri-X Pan or Ektachrome-X. Such materials have a large inherent low intensity reciprocity failure. Kodak spectroscopic materials which have been chemically treated during manufacture to reduce low intensity reciprocity failure do not respond well to cooling. Though intricate equipment is usually required for emulsion cooling, an advantage over baking is that considerable speed gains can be achieved without the gain in background fog that baking produces.

Hypersensitization of Kodak 103a-0 Plates by Nitrogen Baking

Earlier work at Rosemary Hill by Smith *et al*. (1971) showed that baking Kodak type IIIa-J spectroscopic plates in an atmosphere of dry nitrogen provided the greatest gain in speed of any method evaluated. Because of its simplicity and reproducibility this process has also been adopted for the Kodak type IIa-0 and IIa-D emulsions. These three baked emulsions, together with untreated type 103a-0 plates, have been used extensively in the Rosemary Hill quasar monitoring program described in Chapters I and II.

Since the 103a-0 emulsion approaches its limiting magnitude with an exposure of 15 to 20 minutes at the f/4 Newtonian focus of the 30-inch reflector, there has been little incentive to increase the speed of this plate. However, photographic monitoring of bright quasars recently was inaugurated at the f/16 Cassegrain focus to extend light curves through periods of moonlight, and to compensate for the considerably increased exposure times hypersensitization of the 103a-0 emulsion has now been investigated.

Experimental Procedure

All plates were baked in specially designed aluminum boxes whose lids are sealed with high temperature O-rings. Dry nitrogen from a commercial cylinder flowed continuously through the boxes at a rate of 0.2 l/min. To insure dryness, the gas passed through a silica gel column prior to entering the oven, and inside the oven it was preheated by flowing through a copper coil before entering the baking box.

To simulate a reasonable period of storage before use at the telescope each plate was held for 16 hours at 5°C in a static atmosphere of the gas in which it had been baked (the exception to this was the 1L3 batch, which is discussed later). The plate was then transferred to a sealed cassette charged with nitrogen (again to simulate practice at the telescope) and exposed for 10 minutes on a Smithsonian-type tube sensitometer (Latham 1969). The plates were developed 9 minutes in MWP-2 developer (Diffley 1968) and the characteristic curves were obtained by means of a commercial densitometer that measures diffuse densities. Plate speed was defined as the reciprocal of the exposure producing a density of 0.6 above the background fog. Unless baking times are excessive, the effect is merely that of shifting the characteristic curve of the conventional D vs log E plot to the left without changing the slope of the linear portion of the curve. Thus the contrast or gamma is unaltered except in the toe of the curve, which is of course elevated as the fog level rises.

Results

Since it is well known that emulsions vary significantly from batch to batch, five different emulsion batches (designated 1L1, 1E2, 1F2, 1K2, and 1L3) were tested. The initial investigation was conducted with an oven temperature of 65°C, the standard adopted for other emulsions at Rosemary Hill. The speed gains achieved in these runs are summarized in Table 2.

Table 2

Speed Gains Relative to Unbaked 1L1 for Five Emulsion Batches Baked at 65°C

Baking time in hours	1L1	1E2	1F2	1K2	1L3
0	1.00	1.10	1.01	1.07	1.00
8	1.47	2.16		2.44	1.74
16	1.55	2.33		2.59	1.94
30	2.27	3.77	2.20	3.22	2.44
50	2.31	3.66		4.00	

Figure 15 shows the speed and fog curves for batches 1L1 and 1K2, which are representative. In this plot, the speed of an unbaked 1L1 plate has been taken as unity. The anticipated difference between batches is immediately evident, as well as the fact that a speed gain of three can be achieved before fog becomes excessive. In testing the 1E2 batch, the effect of the nitrogen atmosphere was compared with that of ordinary air by simultaneously baking a second plate in a box

Figure 15. Speed and fog curves for emulsion batches 1L1 (dashed curves) and 1K2 (solid curves), baked in nitrogen at 65°C. Speed is measured relative to the untreated 1L1 emulsion.

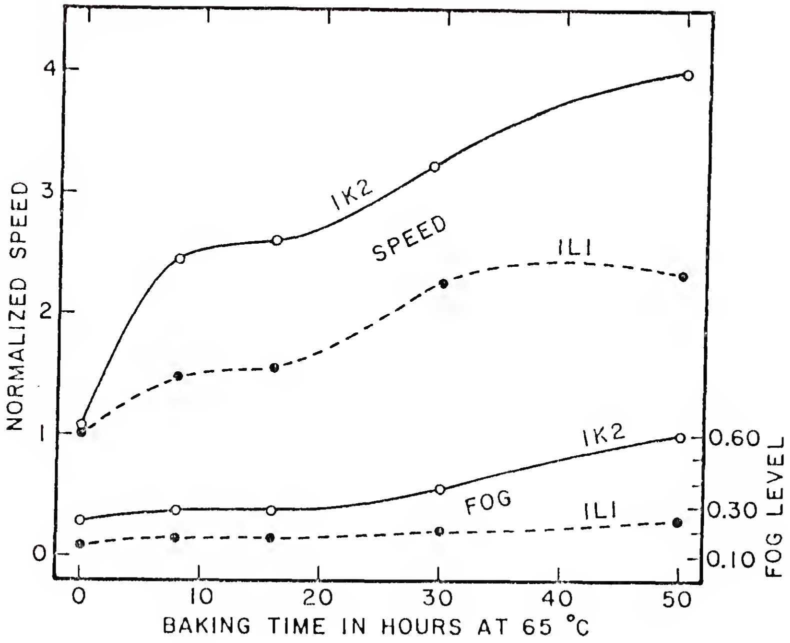
NORMALIZED SPEED
0
1
2
3
4
IK2
SPEED
IL1
IK2
FOG
IL1
0.60
0.30
0.10
FOG LEVEL
0
10
20
30
40
50
BAKING TIME IN HOURS AT 65 °C

whose valves were open to the oven air. The results of this experiment are shown in Figure 16. The fog levels in air are somewhat higher, but this does not become disastrous until excessive baking times are reached. Similarly, the speed curves are comparable up to baking times of about 30 hours. The plateau that occurs in both the speed and fog curves at baking times near 15 hours appears to be a real feature, since it is present in all three sets of data in Figures 15 and 16; it suggests the completion of one ripening process and the onset of another.

Inspection of the several runs indicates that a baking time of about 30 hours at 65°C represents a reasonable compromise between speed and fog. In each case, a speed gain from about two to four over an untreated plate was realized. It is interesting that the plates which were initially fastest tended to reach the highest final speed. This is somewhat in contrast to the behavior of the IIIa-J emulsion, where the slower plates seem to be speeded up more so that all tend to reach a similar ultimate speed.

Because 30 hours is an inconveniently long baking time, a higher temperature was tried as a means of shortening the process. In view of Miller's (1970) warning against possible emulsion damage at temperatures in excess of 75°C, 72.5°C was selected for additional tests on three emulsion batches, 1F2, 1K2, and 1L3. The results shown in Figure 17 suggest that eight to ten hours at 72.5°C is roughly the equivalent of 30

Figure 16. Speed and fog curves for batch 1E2 baked at 65°C in air (dashed curves) and in dry nitrogen (solid curves). Speed is measured relative to the untreated 1L1 emulsion.

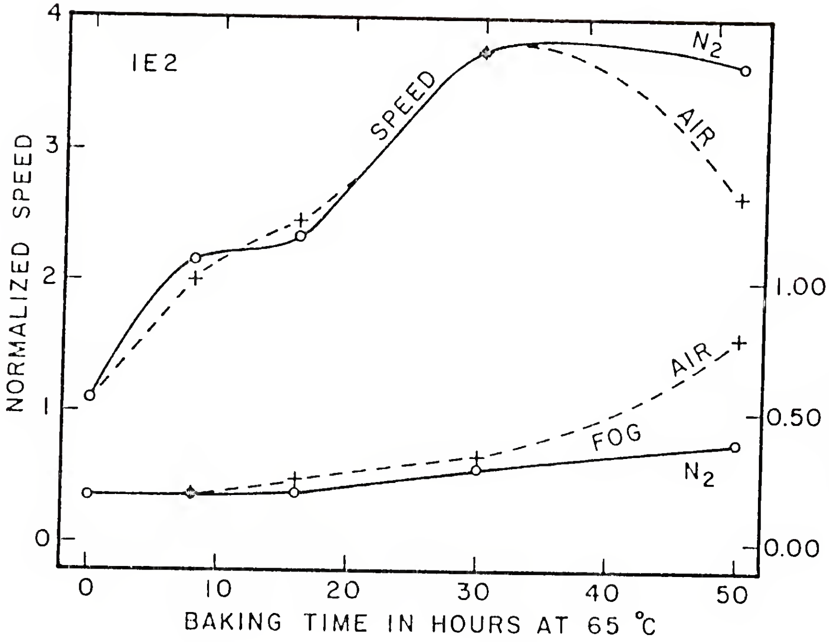
IE2
SPEED
N2
AIR
AIR
FOG
N2
NORMALIZED SPEED
FOG LEVEL
0
1
2
3
4
1.00
0.50
0.00
0
10
20
30
40
50
BAKING TIME IN HOURS AT 65 °C

Figure 17. Speed and fog curves for batches 1L3 (dashed lines) and 1K2 (solid lines) baked in dry nitrogen at 72.5°C. Speed is measured relative to the untreated 1L1 (and 1L3) emulsions. The "X" shows the small loss in speed of a 20-hour 1L3 plate stored for 16 hours.

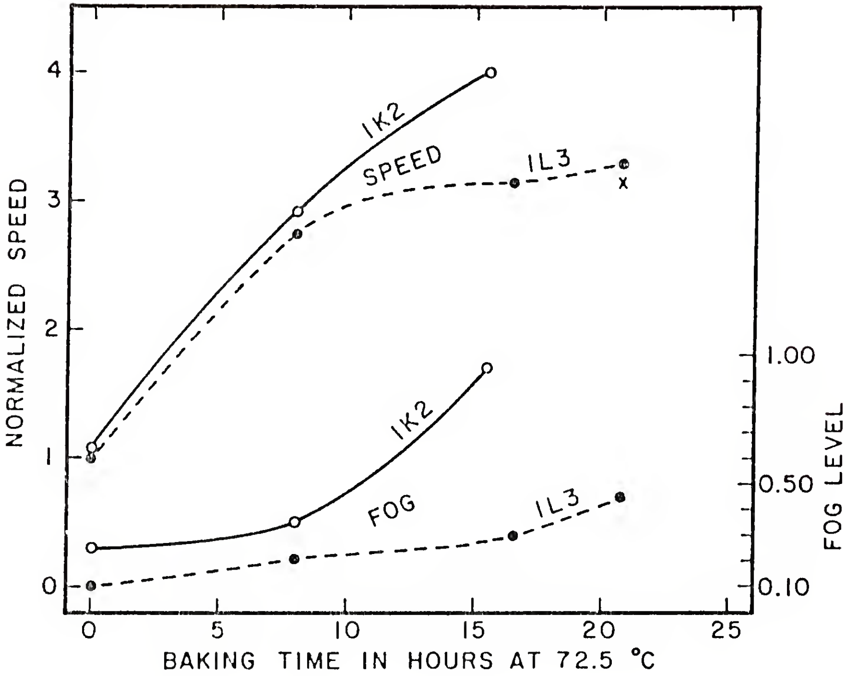
NORMALIZED SPEED
0
1
2
3
4
IK2
SPEED
IL3
x
IK2
FOG
IL3
FOG LEVEL
1.00
0.50
0.10
0
5
10
15
20
25
BAKING TIME IN HOURS AT 72.5 °C

hours at 65°C, and Rosemary Hill has now adopted 72.5°C as its standard temperature for baking the 103a-0 emulsion.

In testing the 1L3 batch at both temperatures, plates carried to the maximum baking times were sensitometered immediately after cooling, while comparison plates were held 16 hours in nitrogen at 5°C before testing. As the "X" in Figure 17 shows, there was a small drop in speed of the stored plate. Additional storage tests have shown that there is no further appreciable change in speed or fog for baked plates stored for two weeks at 4°C in dry nitrogen. Plates stored for a month at -26°C show a moderate increase in fog but little loss in speed.

Sensitometric tests conducted with the 1L3 emulsion have shown that, as anticipated, the speed gains derived from baking are even greater for the long exposures that might be encountered, for example, in Cassegrain photography. For a ten-minute exposure, a plate baked eight hours at 72.5°C in nitrogen was 2.76 times faster than an unbaked plate (Figure 17). At an exposure of one hour, the gain rose to 3.07, and at two hours it was 4.80; at such exposures the reciprocity failure of the unbaked emulsion is of course becoming extremely serious.

Photometric Tests

An obvious question is whether hypersensitization impairs the precision of photometric measurements. Fortunately, the author was able to compare a sample of 96 unbaked plates of the variable source BL Lacertae with a more recent sample of 92 baked plates for the same field. All plates were reduced with an on-line calculator that generates a least-squares calibration curve from the magnitudes and iris readings of the comparison stars. The rms scatter of the comparison stars relative to this curve is taken as a measure of the quality of each plate.

In the case of the two samples of BL Lac plates, the unbaked plates showed an average rms of $0\overset{\mathrm{m}}{.}053$, while the corresponding figure for the baked plates was $0\overset{\mathrm{m}}{.}074$. Application of standard statistical tests indicates that the difference between the baked and unbaked plates is highly significant for samples of this size; that is, the hypersensitization process does slightly degrade the photometric quality of the plates. However, the observed small difference is not regarded as important in routine monitoring.

Summary

The response of Kodak type 103a-0 plates to nitrogen baking varies considerably from batch to batch, both in speed gain and in increase in background fog. In general, the speed can be increased by a factor of from two to three without excessive fog by baking for about 30 hours at 65°C or for eight to ten hours at 72.5°C. Similar results may be produced by baking in air if nitrogen is unavailable, but the fog tends to increase more rapidly. Plates stored in nitrogen at refrigerator or freezer temperatures have adequate shelf life for most practical purposes. Because of batch variability, it is probably wise to determine the optimum baking time for each batch.

Extensive experience at the telescope confirms the sensitometer tests, showing the exposures can safely be reduced by a factor of two to three. This experience also shows that there is only a small loss in photometric precision with the baked plates. Baking of the 103a-0 emulsion has been adopted as standard procedure at Rosemary Hill for exposures at both the Newtonian and Cassegrain foci of the 30-inch reflector. Baked plates are of course also used with the recently installed 18-inch reflector.

Hypersensitization by Emulsion Cooling

The fact that photographic emulsions can be made more sensitive to exposures of low intensity by cooling is not a newly discovered effect; rather this work was pioneered in the early 1900's by E. S. King of Harvard Observatory (Hoag 1964). King found that plates cooled to exterior winter temperatures yielded half a magnitude gains in exposure, when compared with plates warmed over a heat register in his laboratory. King also discovered that cooling reduces the sensitivity for intense exposures, probably due to temperature-imposed limits on the rate of migration of silver ions to emulsion sensitivity centers (Hoag 1964), which limits the response of the emulsion. The discovery that moisture lowers emulsion speed is also attributed to King, arising from his experiments in cooling plates with snowballs.

Much of the modern work in cold emulsion photography was initiated by Hoag (1961,1964). In his early experiments Hoag used dry ice (-78°C) and a frozen liquid mercury mixture as refrigerants, and he experimented with evacuated plate chambers and a plate chamber flushed with cold dry oxygen, in order to prevent moisture from forming on the emulsion. Hoag's latest camera uses a thermoelectric device for cooling; the plates are enclosed in a vacuum to prevent frost formation. In all Hoag's cameras plates are cooled by physical contact with a refrigerated metal platen. Using temperatures as low as -65°C, Hoag has studied the effect of cooling on a number of emulsions. Hoag's work has shown that many amateur films such as Panatomic-X respond well to cooling, yielding not only increased speed but better exposure latitude, enabling objects with a large brightness differential, such as many nebulae, to be photographed with more detail in both bright and faint areas. Many of Hoag's experiments were with color reversal emulsions, showing that cooling greatly increases their speed and color balance, enabling more accurate color renditions to be made of faint astronomical objects.

Experimental Procedure

The range of temperatures achievable with dry ice refrigeration is very restricted, and thermoelectric devices are relatively expensive. In order to achieve a reasonable range in temperature without resorting to thermoelectric devices, liquid nitrogen was used as the refrigerant in the author's studies, following procedures outlined by Stong (1969). The exposures were made in a "cold cassette" designed by the author and A. G. Smith for a Smithsonian-type tube sensitometer (Latham 1969). A schematic diagram of the cassette is shown in Figure 18; Figure 19 is a photo of the cassette with its lid removed.

The principle of the cassette was suggested by R. L. Hackney (1972b); the cooling is accomplished by a flow of cold nitrogen directly across the emulsion surface; the nitrogen then flows across the back of the plate and exits. A double window separates the emulsion from the air; warm dry nitrogen flows continuously through the window to prevent frost formation. The warm nitrogen was supplied from a commercial cylinder at room temperature (20°C). The cold nitrogen flow was supplied by a dewar of liquid nitrogen; a 300 ohm power resistor was used as a heating element to obtain sufficient cold gas flow for adequate cooling. To provide adequate insulation for the cold chamber the cassette was constructed of Bakelite, a material of extremely low thermal conductivity. The cold chamber temperature was monitored by thermocouples mounted on brass springs which pressed directly against the emulsion when the plate was positioned for exposure. Valves were mounted at the cold-gas inlet and outlet to provide additional control over the flow of cold gas.

Figure 18. Schematic diagram of the cold cassette (not to scale). Cooling is accomplished by a flow of cold nitrogen vapor across the emulsion surface. The cold gas then flows across the back of the plate and exits, cooling both sides of the plate and avoiding stresses that might cause the plate to crack. Before flowing across the emulsion the cold gas passes through a series of baffles to assure a more uniform flow. Valves are located at the cold-gas inlet and outlet to provide additional control over the cold gas flow. The cold gas is boiled out of a dewar by a 300 ohm power resistor. Warm nitrogen at room temperature from a commercial cylinder flows between windows 1 and 2 to prevent frost formation. The warm nitrogen flow is also baffled to provide a more uniform flow. The lid of the cassette is sealed with an O-ring; the lid is held firmly in place by thumb screws. The cassette is constructed of Bakelite to keep thermal conduction at a minimum. The windows are made from 0.040-inch thick glass plates from which the emulsion and backing have been removed.

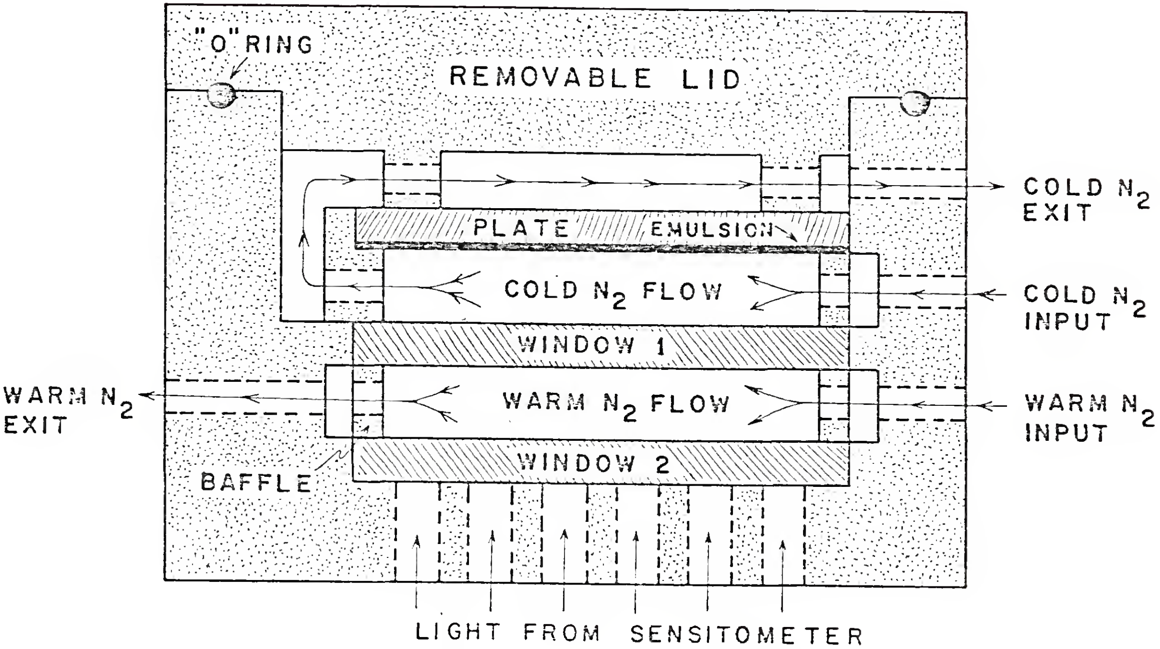

COLD CASSETTE SCHEMATIC DIAGRAM

Figure 19. Photograph of the cold cassette. The removable lid is shown at the top; the cassette with the cold chamber exposed is at the bottom. The cold-gas inlet and exit valves are mounted on the right; the vertical pipes are the warm-gas inlet and exit. The wires are the thermocouple leads; the thermocouples, which can be placed at any position in the cold chamber, are mounted on the triangular brass springs. The window mask has holes that exactly align with those on the tube stack of the sensitometer. The O-ring seal can be seen around the perimeter of the cold chamber.

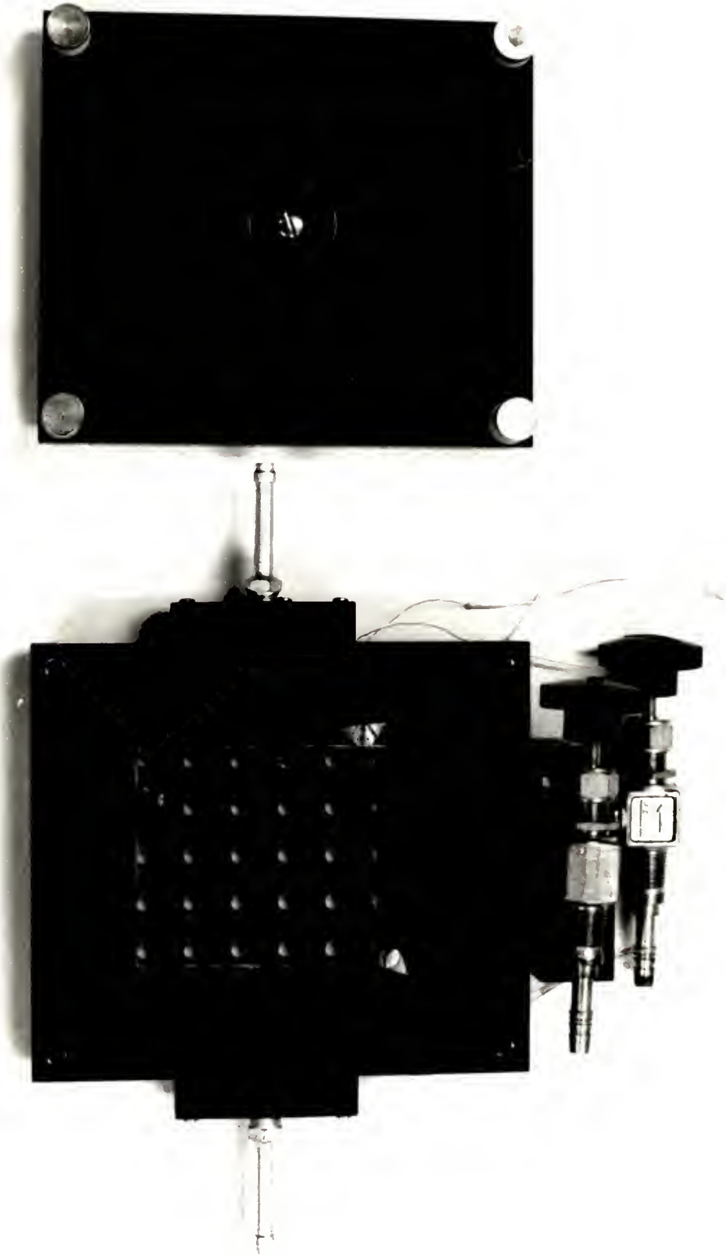
F1

Before it was cooled the cold chamber was flushed with dry nitrogen at room temperature to remove moisture that might condense on the emulsion or inner window. The cold chamber temperature was regulated by the cold gas flow; about 30 minutes was required for the temperature to stabilize before starting each exposure. A rather vigorous gas flow was required to maintain the coldest temperatures; a temperature of about -68°C was the lowest that could be achieved. A thermal gradient of about 15°C was present in the cold chamber during the exposures; the coldest end of the plate was near the cold-gas inlet valve. As soon as the cassette temperature stabilized heavy frost would form on the cassette and cold-gas feed tube; at the lowest temperature traces of frost formed on the outer window surface in spite of the warm gas flow between the windows.

Results

The response of four emulsions to cooling was tested: Kodak Tri-X Pan, Kodak Contrast Process Pan, Kodak 103a-0 (1E2), and Kodak IIIa-J (1G1). The results are summarized in Table 3. Figure 20 shows speed gains obtained by cooling Tri-X Pan and Contrast Process Pan, both in a 4" x 5" format. The characteristic curves and speeds for the cold emulsion work were determined in the same manner as those for the nitrogen baking experiments. In Figure 20 the speeds have been normalized to exposures made at room temperature. The Tri-X showed the largest increase in speed of any emulsion

Key to Table 3

Table 3 is a summary of the initial cold emulsion experiments. The fog level was measured with the commercial densitometer used to obtain the characteristic curves; it measures diffuse densities. N is the speed relative to an exposure made at room temperature (20°C). The exposure temperatures are listed at the left.

Table 3

The Effect of Cooling on Emulsion Speed

	Tri-X Pan		Contrast Process Pan		103a-0 (1E2)		IIIa-J (1G1)	
Temperature	Fog	N	Fog	N	Fog	N	Fog	N
20°C	0.21	1.00	0.09	1.00	0.11	1.00	0.24	1.00
-34°C	0.21	1.69	--	--	0.11	1.18	0.24	1.11
-68°C	0.23	2.94	0.11	1.50	0.11	1.03	0.33	1.44

Figure 20. Speed and fog curves obtained by cooling Kodak Tri-X Pan and Kodak Contrast Process Pan. The speeds are normalized to exposures made at room temperature (20°C).

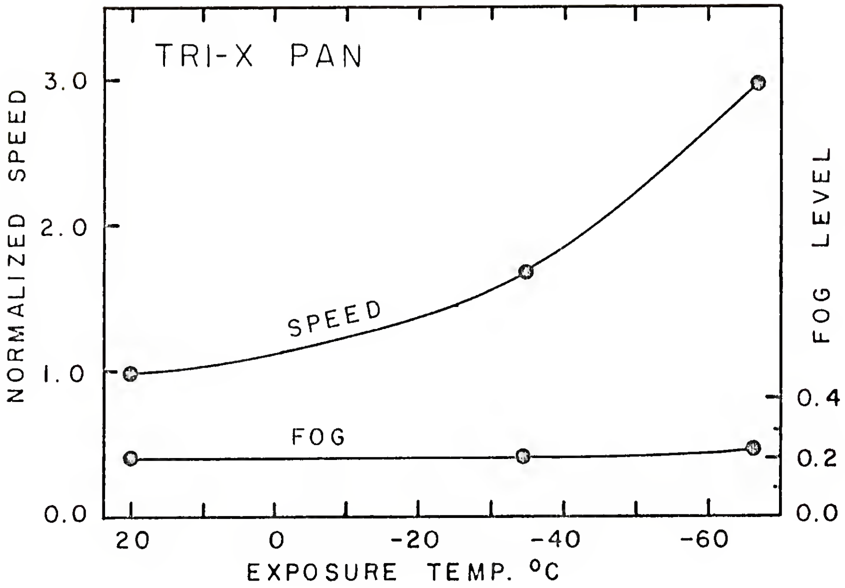
TRI-X PAN
NORMALIZED SPEED
3.0
2.0
1.0
0.0
SPEED
FOG
FOG LEVEL
0.4
0.2
0.0
20
0
-20
-40
-60
EXPOSURE TEMP. °C

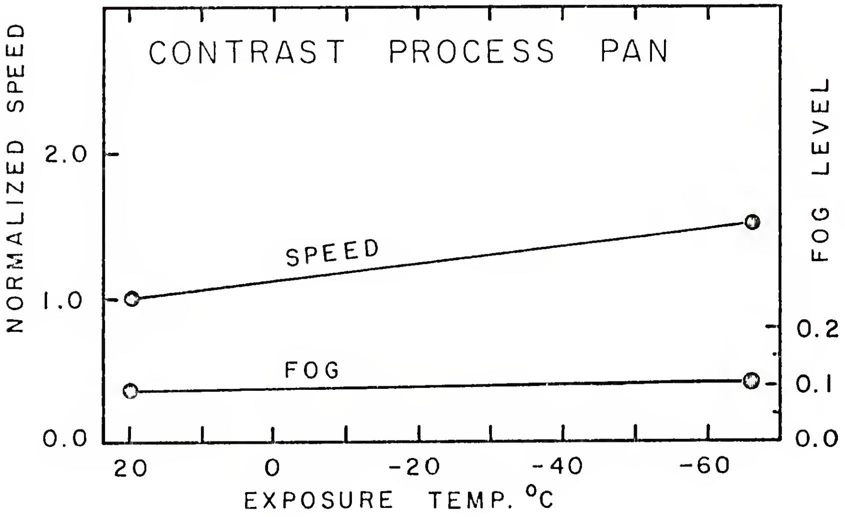
CONTRAST PROCESS PAN
NORMALIZED SPEED
2.0
1.0
0.0
SPEED
FOG
FOG LEVEL
0.2
0.1
0.0
20
0
-20
-40
-60
EXPOSURE TEMP. °C

tested; cooling to -68°C yielded a speed gain of about 3 over uncooled exposures. Cooling to -68°C yielded a speed gain of 1.50 for the Contrast Process Pan. The large gain in speed exhibited by the Tri-X is not surprising, since this emulsion, while relatively fast for short exposures of high intensity, has a large low intensity reciprocity failure. As expected, little increase in fog occurred during the cooling of either emulsion.

Figure 21 shows the results obtained by cooling Kodak 103a-0, emulsion batch 1E2, and Kodak IIIa-J, emulsion batch 1G1. Speed gains are normalized to an uncooled exposure. As predicted by Hoag, small or moderate gains were obtained by cooling the Kodak spectroscopic plates, due to their low intensity reciprocity failure having already been partially corrected by chemical sensitization at the factory. At -68°C the 103a-0 shows a decrease in speed; the maximum gain of 1.18 was obtained at -34°C. The results for the IIIa-J look more promising. At -68°C a gain of almost 1.50 was achieved, comparable to the gain achieved for Contrast Process Pan. This probably indicates that the factory sensitization is more effective for 103a-0 than for IIIa-J. However, since there are differences in the responses of different emulsion batches, several more batches of each emulsion should be tested before conclusions are drawn. The speed curve for IIIa-J indicates that a greater gain might be obtained by cooling to a lower temperature, but -68°C was the lowest temperature that could be achieved.

Figure 21. Speed and fog curves obtained by cooling Kodak 103a-0 (1E2) and Kodak IIIa-J (1G1). The speeds are normalized to exposures made at room temperature.

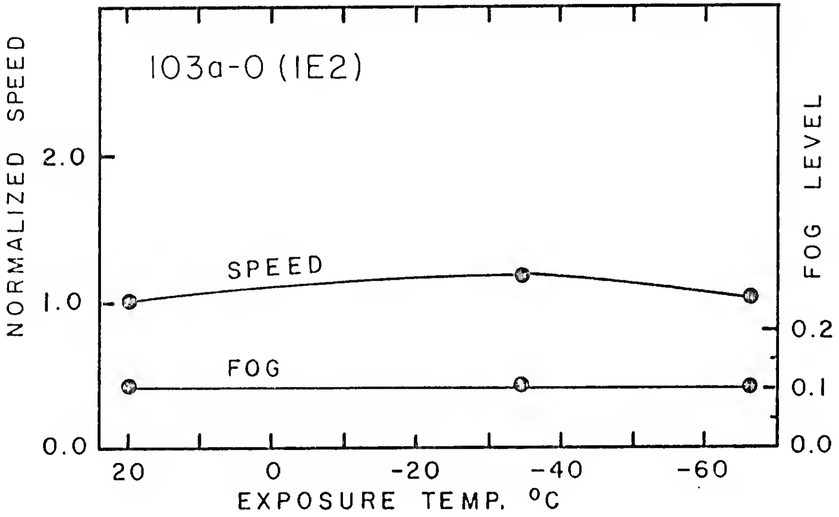
103a-O (IE2)
NORMALIZED SPEED
FOG LEVEL
SPEED
FOG
2.0
1.0
0.0
0.2
0.1
0.0
20
0
-20
-40
-60
EXPOSURE TEMP. °C

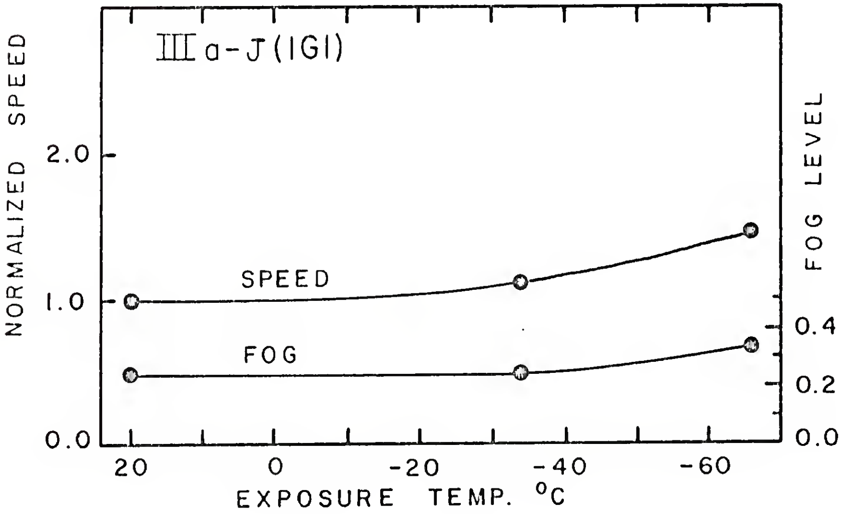
IIIa-J (IGI)
NORMALIZED SPEED
FOG LEVEL
SPEED
FOG
2.0
1.0
0.0
0.4
0.2
0.0
20
0
-20
-40
-60
EXPOSURE TEMP. °C

The speed gains achieved by cooling the IIIa-J suggested that the effects of baking and cooling might be added together. Stong (1969) reports slight speed gains due to the additive properties of baking and cooling for High Speed Ektachrome. Nitrogen baking of IIIa-J is discussed by Smith _et_ _al_. (1971). The results of cooling a baked IIIa-J are shown in Table 4. A plate baked 8 hours at 65°C in nitrogen and cooled to -68°C had only 40 percent of the speed of a similar plate exposed at room temperature (20°C). Surprisingly cooling also reduced the fog level, suggesting that the effect of baking may have been partially neutralized. Speed is normalized relative to the uncooled exposure.

Table 4

Effect of Cooling on Baked IIIa-J (1G1)

Baking time	Exposure temp.	Fog	N
8 hours	20°C	0.46	1.00
8 hours	-68°C	0.39	0.40

Summary

The largest speed gain was obtained by cooling Tri-X Pan, a film with a large low intensity reciprocity failure. Moderate gains were obtained by cooling Contrast Process Pan and IIIa-J; little gain was obtained by cooling 103a-0. Cooling a baked IIIa-J reduced its speed by 60 percent.

The data suggest that lower temperatures would yield still larger speed gains except in the case of 103a-0. The lowest achievable temperature was -68°C, believed to be limited by the gas flow rates and conductive properties of the cassette. Thermal gradients of about 15°C were present across the cold chamber during all the exposures. Such gradients do not greatly interfere when testing the general response of an emulsion to cooling, but they might prove undesirable at the telescope as density gradations might be introduced in the field area. It is suggested that in the future the present system be upgraded to achieve lower and more uniform temperatures, and that the response of various emulsions to cooling be further investigated along with the additive properties of baking and cooling. Color reversal emulsions should not be neglected. It is expected that if future investigations show emulsion cooling to be a practical and useful process, a cold cassette will be designed for use at Rosemary Hill.

CHAPTER IV

A STUDY OF THE OPTICAL VARIABILITY OF A SAMPLE OF QUASARS AND RELATED OBJECTS

Introduction

In this chapter the photometric history of 14 sources from the Florida program will be discussed. Included will be light curves for all the objects and the results of a chi-squared test for variability. Comparison sequences for several of the objects were calibrated by the author; sequence finders are included for these sources. The objects studied are listed in Table 5 along with their colors, redshifts, and the confidence level for variability.

The comparison sequences for the objects were obtained by photographic transfers from selected areas in the Brun Atlas (Brun 1957) or from globular clusters. Two of the objects have tertiary transfers from the fields of objects already calibrated. While tertiary transfers increase the probability of zero-point shifts and calibration-curve slope errors, the author feels such transfers allow a much more accurate testing of variability than simple visual examination of the source image. All comparison sequences were computer smoothed to correct for local field errors of the Rosemary Hill Observatory 30-inch reflector. A discussion

Key to Table 5

(1) Name of source.

(2) Classification of optical counterpart (from references).

(3) Mean m_{pg} from Florida data followed by the number of plates reduced (in parentheses).

(4) Total range of variation (in magnitudes) observed at Rosemary Hill.

(5) Average rms of a single observation (in magnitude units).

(6) Confidence level for detected variability.

(7) (U-B) color index (from references).

(8) (B-V) color index (from references).

(9) Redshift (from references).

(10) The references keyed to the footnotes under the table.

Table 5

A Sample of Objects from the Florida Program

(1) Source	(2) Classification	(3) Mean m_{pg}	(4) Range	(5) RMS Error	(6) Confidence Level	(7) (U-B)	(8) (B-V)	(9) z	(10) References
PKS 0048-09	Galaxy	17.8(17)	0.54	0.11	99.9 %				a
0420-01	Quasar	18.8(43)	1.03	0.15	99.9			1.74 0.915	a b
0725+14	Quasar	17.6(12)	0.23	0.09	55.0	-1.02	0.43	1.382	c
0735+17	Lacertid ?	16.0(30)	1.72	0.11	99.9				d
0736+01	Quasar	16.0(22)	1.09	0.12	99.9	-0.77	0.43	0.191	b,c
0906+01	Quasar	17.0(96)	1.80	0.11	99.9	-0.97	1.24	1.018	c,e
1004+13	Quasar	14.6(21)	0.24	0.16	30.0	-0.82	0.13	0.240	c
1055+20	Quasar	16.6(12)	0.50	0.15	98.0	-0.81	0.44	1.110	c
1116+12	Quasar	18.6(17)	1.03	0.20	55.0	-0.76	0.14	2.118	c
4C 09.42	Galaxy	18.3(10)	0.48	0.12	98.0				f
PKS 1510-08	Quasar	17.0(16)	0.85	0.08	99.9	-0.74	0.17	0.361	b,c
1645+17	Quasar ?	17.4(11)	0.59	0.16	40.0				a
2145+06	Quasar	16.0(32)	0.51	0.12	50.0	-0.82	0.38	0.367	b,c
2349-01	N-galaxy	15.8(21)	0.94	0.18	99.5				a

Key to references: (a) Ekers (1969); (b) Medd *et al.* (1972); (c) Setti and Woltjer (1973); (d) Burbidge and Strittmatter (1972); (e) Hackney (1973); (f) Wills *et al.* (1973).

of calibration procedures and the errors inherent in photographic transfers is given by Hackney (1973).

Photometric History and Discussion

PKS 0048-09

This Parks object was identified by Bolton and Ekers (1966a) as an 18th magnitude galaxy within a small cluster of galaxies. It was found to be variable at 8,000 MHz by Stull (1970), who reported that the object's radio spectrum was similar to that of BL Lac.

Hackney (1973) established a tertiary comparison sequence by a photographic transfer from the calibrated field of the quasar PKS 2345-16. Hackney found the object to be variable with a confidence level of 99.8 percent, based upon four observations. The author recalibrated the comparison sequence of PKS 0048-09 with a photographic transfer from SA 117 (Brun 1957) using a plate exposed on September 30, 1973. The recalibrated comparison star magnitudes are listed in Table 6. The sequence finder for PKS 0048-09 is given by Hackney (1973).

Table 6

The Photographic Comparison Star Magnitudes
for PKS 0048-09

(1)	17.07	(5)	17.83	(9)	17.63
(2)	16.35	(6)	17.58	(10)	14.87
(3)	17.22	(7)	13.16	(11)	14.40
(4)	17.32	(8)	17.55	(12)	17.68

The Florida light curve of PKS 0048-09 is shown in Figure 22. The confidence level for variability is 99.9 percent; the average rms error is $0\overset{m}{.}11$. The object's light curve suggests rapid optical variability with a range of about $0\overset{m}{.}30$ with a burst in late 1973 of $0\overset{m}{.}50$.

PKS 0420-01

The optical counterpart of this radio source was identified by Bolton and Ekers (1966b) as an 18th magnitude stellar object. The object has two redshifts; they are listed in Table 5. The source is variable at radio frequencies; Dent and Kojoian (1972) and Medd *et al*. (1972) reported a steady decline in intensity at centimeter wavelengths between 1968 and 1971. Medd *et al*. describe the spectrum as having a centimeter excess. The Florida light curve of PKS 0420-01 is shown in Figure 22. The optical variability appears to be characterized by rapid fluctuations of about $0\overset{m}{.}5$ on a time scale of about a month. The rms error is $0\overset{m}{.}15$ and the confidence level for variability is 99.9 percent. It is interesting to note that the average optical intensity increased by nearly a magnitude during the centimeter wavelength decline mentioned above.

The comparison sequence for PKS 0420-01 was obtained by a photographic transfer from SA 96 using the photometry of Brun (1957). The magnitudes of the comparison stars and a sequence finder are given by Hackney (1973).

Figure 22. The Florida light curves of PKS 0048-09, PKS 0420-01, and PKS 0725+14. The error bars indicate twice the average rms error of a single measurement.

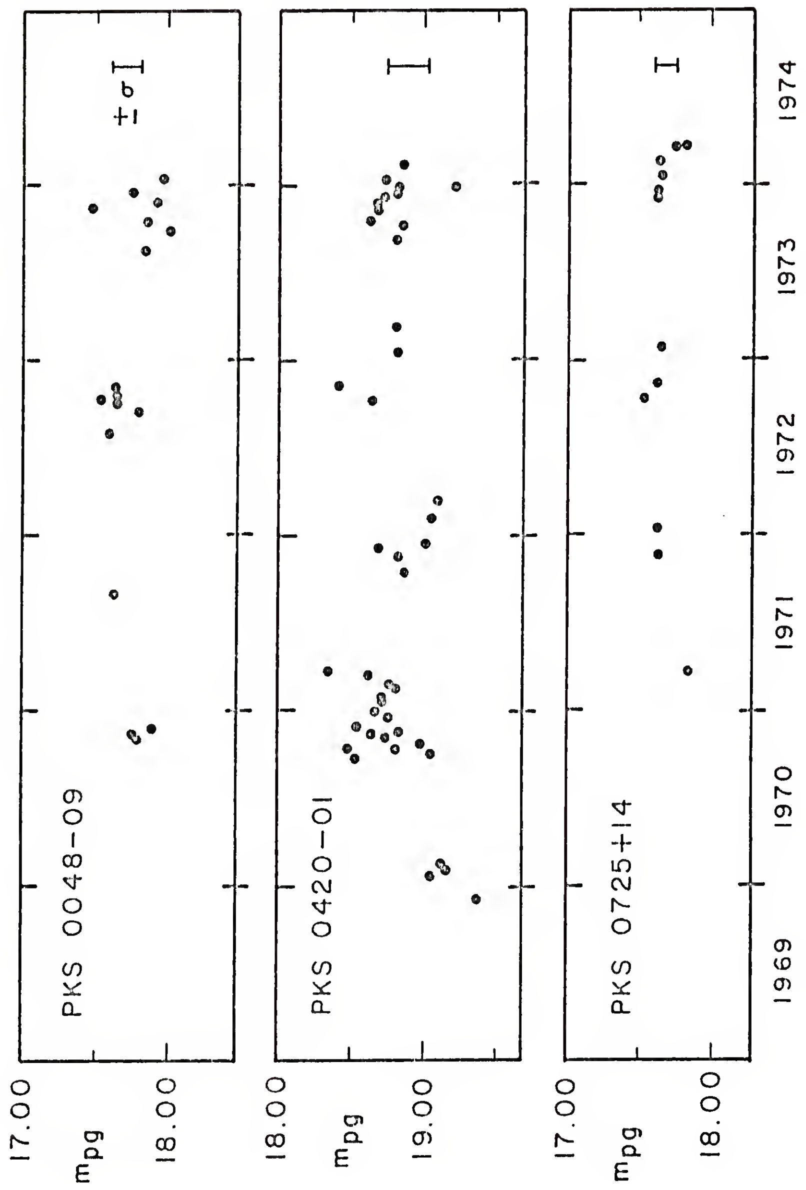
PKS 0048-09
PKS 0420-01
PKS 0725+14
m_{pg}
17.00
18.00
18.00
19.00
17.00
18.00
1969
1970
1971
1972
1973
1974
$\pm\sigma$

PKS 0725+14

This 17.5 magnitude quasar is alternatively known as 3C 181. The object exhibits a double radio structure with the optical counterpart in the center (Setti and Woltjer 1973). Hunter and Lü (1969) report $0\overset{m}{.}3$ variations in early 1967 and 1969; Peach (1969) reports a brightening of $0\overset{m}{.}5$. The Florida light curve of PKS 0725+14 is shown in Figure 22. No significant variations were seen between 1971 and 1974. The confidence level for variability is 55 percent and the average rms error is $0\overset{m}{.}09$. The Florida data agree with the observations of Lü (1972), who reports that the object showed very little variation after 1969.

The comparison sequence for PKS 0725+14 was obtained by a photographic transfer from SA 76 using the photometry of Brun (1957). Figure 23 shows the sequence finder for PKS 0725+14.

PKS 0735+17

The optical counterpart of PKS 0735+17 was identified by Blake (1970). An alternative designation is VRO 17.07.02. Burbidge and Strittmatter (1972) report large optical variations and a lineless spectrum, which suggests that the object is a lacertid. The object is also variable at radio wavelengths. Dent and Kojoian (1972) report that observations at 3.8 cm and 1.9 cm show clearly defined maxima in 1969 and 1970, and they suggest that the object undergoes repeated outbursts at radio frequencies. The trends reported by Medd

Figure 23. The sequence finder for PKS 0725+14. The comparison star photographic magnitudes were obtained by a photographic transfer from SA 76 using a plate exposed on December 2, 1973, at Rosemary Hill Observatory. This photograph is reproduced from the above plate. The scale is 2.4 arcmin per inch. North is at the top and east is to the left. The quasar PKS 0725+14 is denoted by Q. The comparison star magnitudes are as follows: (1) 17.88, (2) 17.59, (3) 17.22, (4) 18.10, (5) 18.08, (6) 16.53, (7) 17.60, (8) 17.53, (9) 16.21, (10) 16.96, (11) 17.51.

6
-5
10
11
3
1
Q
4
7
2
-9
8

et al. (1972) at 2.8 cm and 4.5 cm show considerable variability and confirm the observations of Dent and Kojoian. Medd et al. describe the object's radio spectrum as having a centimeter excess.

Figure 24 shows the Florida light curve of PKS 0735+17. Optical fluctuations of an extremely violent nature are apparent, similar to those observed for BL Lac. The object is concluded to be an OVV with a confidence level for variability of 99.9 percent. The average rms error is $0\overset{m}{.}11$. The average range of the optical fluctuations seems to be about $0\overset{m}{.}5$ on a time scale of a few weeks. Occasionally much greater variations occur; in early 1974 the object flared nearly $1\overset{m}{.}5$ and then rapidly declined to its preflare intensity level. The object's obvious similarity to BL Lac prompted the author to search for intraday variations; the results are discussed in Chapter VI.

The comparison sequence for PKS 0735+17 was obtained by a photographic transfer from SA 76 using the photometry of Brun (1957). The sequence finder for PKS 0735+17 is given by Hackney (1973).

PKS 0736+01

An alternate designation for PKS 0736+01 is OI 061. Kellerman et al. (1970) report a complex radio structure at 13 cm. Medd et al. (1972) report large variations at 2.8 cm and 4.5 cm with three well-defined maxima occurring in 1968, 1969, and 1970, respectively, and they describe its spectrum

Figure 24. The Florida light curves of PKS 0735+17 and PKS 0736+01. The error bars indicate twice the average rms error of a single measurement.

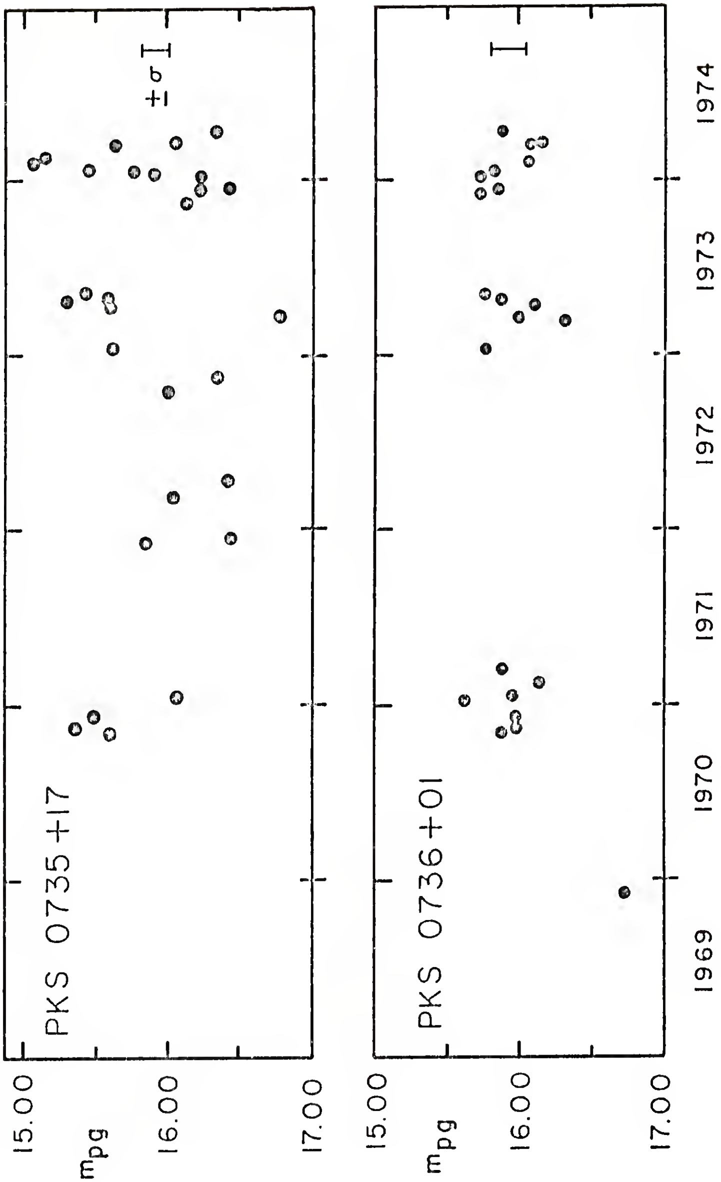
PKS 0735+17
PKS 0736+01
m_{pg}
15.00
16.00
17.00
1969
1970
1971
1972
1973
1974
±σ

as having a centimeter excess. The Florida light curve of PKS 0736+01 shown in Figure 24 suggests variations of $0^{m}_{.}5$ on a time scale of weeks or months. The confidence level for variability is 99.9 percent and the average rms error is $0^{m}_{.}12$.

The comparison sequence for PKS 0736+01 was obtained by a photographic transfer from SA 99 using the photometry of Brun (1957). Figure 25 shows the sequence finder for PKS 0736+01.

PKS 0906+01

The optical counterpart of PKS 0906+01 was found to have irregular optical variations of approximately $1^{m}_{.}0$ by Folsom and Smith (1969), who reported an ultraviolet excess and concluded that the object was probably a quasar. This was confirmed by Burbidge and Strittmatter (1972), who determined a redshift of 1.018 and concluded that PKS 0906+01 was definitely a quasar. Ekers (1969) and Setti and Woltjer (1973) report a flat radio spectrum. Variability at 8,000 MHz was reported by Stull (1972) and Brandie (1972).

The Florida light curve of PKS 0906+01 is shown in Figure 26. The closed circles are m_B observations; the open circles are m_{pg} observations corrected to m_B by the addition of $0^{m}_{.}4$. Optical activity of an interesting nature is suggested. The object exhibited violent optical fluctuations in 1970 and 1971 with an amplitude of about $1^{m}_{.}0$ on a time scale of a month. During 1972 and 1973 the object slowly declined in intensity, and the amplitude of the variations

Figure 25. The sequence finder for PKS 0736+01. The comparison star photographic magnitudes were obtained by a photographic transfer from SA 99 using a plate exposed on April 20, 1973, at Rosemary Hill Observatory. This photograph is reproduced from a Rosemary Hill plate taken on March 20, 1974. The scale is 2.4 arcmin per inch. North is at the top and east is to the left. The quasar PKS 0736+01 is denoted by Q. The comparison star magnitudes are as follows: (1) 16.67, (2) 16.36, (3) 15.51, (4) 15.11, (5) 16.72, (6) 16.07, (7) 16.81, (8) 17.52, (9) 15.57, (10) 17.11.

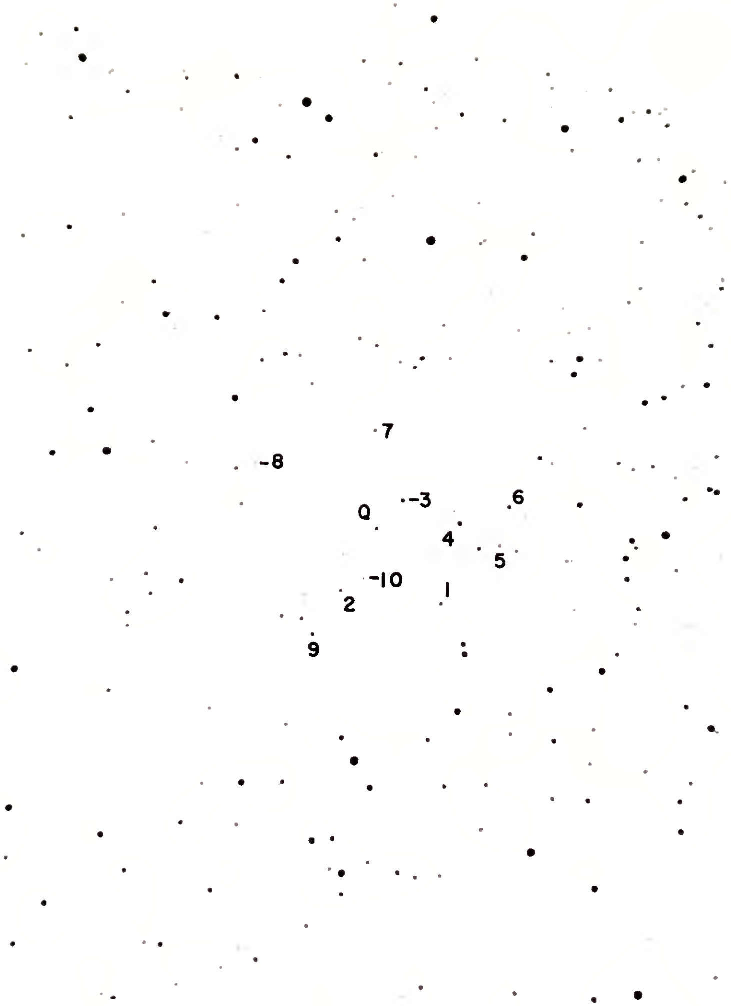
-8
Q
-3
-10

Figure 26. The Florida light curve of PKS 0906+01. The error bars indicate twice the average rms error of a single measurement. The filled circles indicate m_B observations; the open circles are m_{pg} observations corrected to m_B by the addition of $0\overset{m}{.}4$.

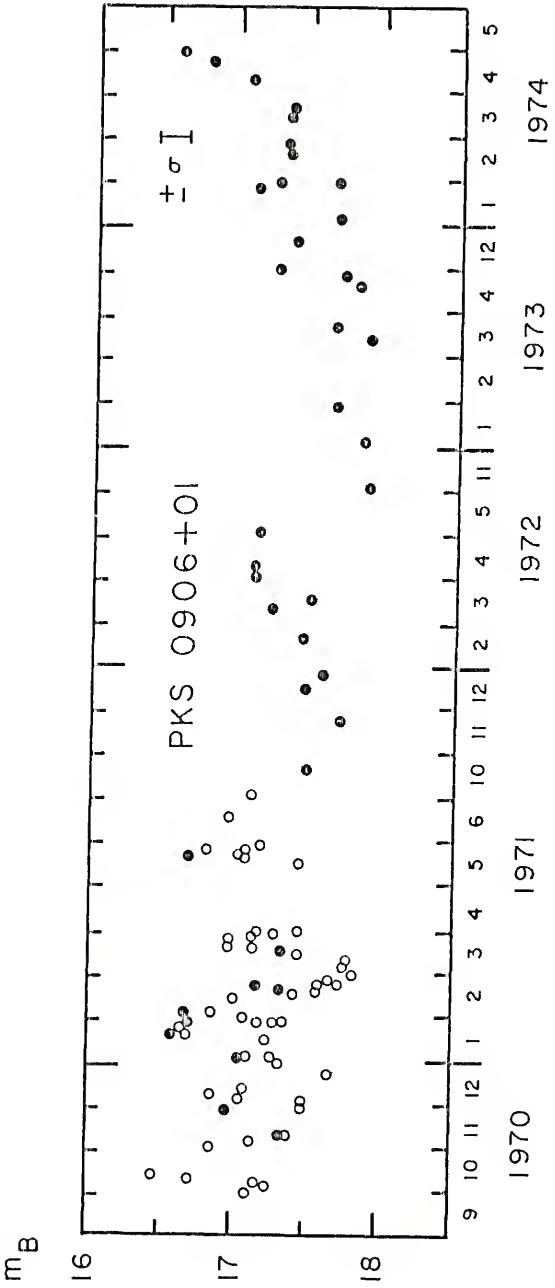
PKS 0906+01
± σ
m_B
16
17
18
9
10
11
12
1
2
3
4
5
6
10
11
12
2
3
4
5
11
1
2
3
4
12
1
2
3
4
5
1970
1971
1972
1973
1974

decreased to an apparent minimum m_B near 18th magnitude, as reported by Scott et al. (1973). In late 1973 and the first half of 1974 the optical activity and average intensity increased, flaring almost to the maximum brightness reached in October of 1970. The average rms error is $0^m.11$ and the confidence level for variability is 99.9 percent. It is concluded that PKS 0906+01 is an OVV whose short-term activity appears to be correlated with apparent long-term intensity variations; the short-term optical activity is most vigorous at high average intensity levels.

The comparison sequences for PKS 0906+01 were obtained by photographic transfers from M 3; the sequence finder is given by Hackney (1973).

PKS 1004+13

The Florida light curve of PKS 1004+13 is shown in Figure 27. No significant variations were observed. The confidence level for variability is 30 percent and the average rms error is $0^m.16$. This is in contrast to the observations of Hunter and Lü (1969), who report a $0^m.3$ decline and those of Lü (1972) who reports a $1^m.0$ decline between March of 1969 and May of 1970. About ten observations by Kinman et al. (1968) detected no significant variations. This object appears to undergo long quiescent periods during which no optical variations occur.

A tertiary comparison sequence for PKS 1004+13 was established by a photographic transfer from the field of the

Figure 27. The Florida light curves of PKS 1004+13, PKS 1055+20 and PKS 1116+12. The error bars indicate twice the average rms error of a single measurement.

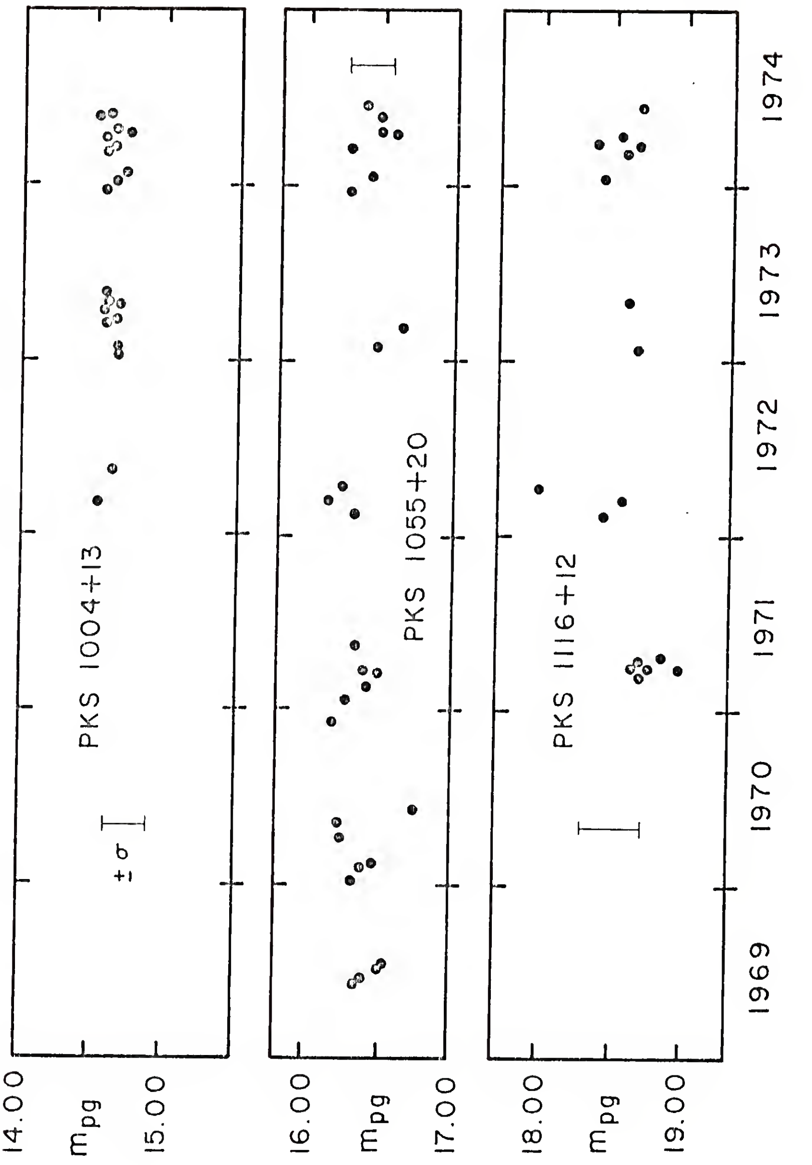
PKS 1004+13
PKS 1055+20
PKS 1116+12
± σ
m_{pg}
14.00
15.00
16.00
17.00
18.00
19.00
1969
1970
1971
1972
1973
1974

quasar PKS 1055+20. Figure 28 shows the sequence finder for PKS 1004+13.

PKS 1055+20

The optical counterpart of PKS 1055+20 was identified by Bolton *et al*. (1968). Setti and Woltjer (1973) report a double radio structure. The Florida light curve of PKS 1055+20 is shown in Figure 27. No large optical fluctuations were observed; the light curve suggests monthly variations of about $0\overset{m}{.}2$ with a confidence level of 98 percent. The average rms error is $0\overset{m}{.}15$.

The comparison sequence for PKS 1055+20 was obtained by a photographic transfer from SA 79 using the photometry of Brun (1957). Figure 29 shows the sequence finder for PKS 1055+20.

PKS 1116+12

The optical counterpart of PKS 1116+12 was identified by Bolton *et al*. (1965b). The Florida light curve of the object is shown in Figure 27. Even though variations as large as $1\overset{m}{.}0$ are suggested the high rms error, whose average value is $0\overset{m}{.}20$, has lowered the confidence level for variability to 55 percent.

The comparison sequence for PKS 1116+12 was obtained by a photographic transfer from SA 79 using the photometry of Brun (1957). Figure 30 shows the sequence finder for PKS 1116+12. Due to the high rms generated by this sequence it is felt that PKS 1116+12 should be recalibrated in the future;

Figure 28. The sequence finder for PKS 1004+13. The comparison star photographic magnitudes were obtained by a photographic transfer from the field of PKS 1055+20 using a plate exposed on March 13, 1972, at Rosemary Hill Observatory. This photograph is reproduced from a Rosemary Hill plate taken on January 29, 1973. The scale is 2.4 arcmin per inch. North is at the top and east is to the left. The quasar PKS 1004+13 is denoted by Q. The comparison star magnitudes are as follows: (1) 14.38, (2) 13.96, (3) 14.84, (4) 15.95, (5) 14.56, (6) 15.87, (7) 15.10, (8) 15.17, (9) 14.27.

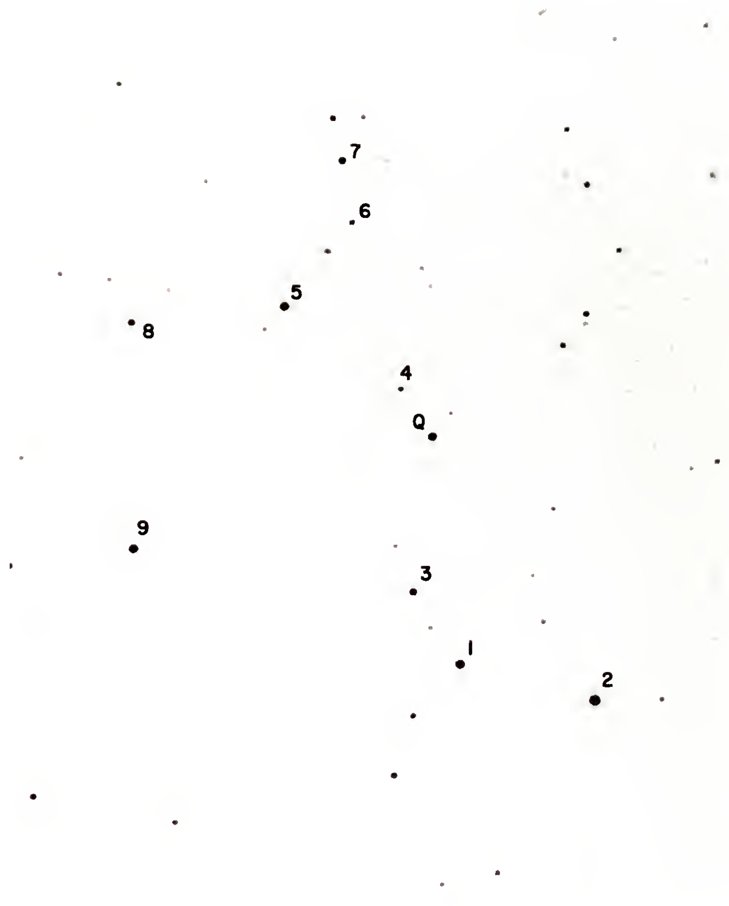
Q

Figure 29. The sequence finder for PKS 1055+20. The comparison star photographic magnitudes were obtained by a photographic transfer from SA 79 using a plate exposed on March 4, 1973, at Rosemary Hill Observatory. This photograph is reproduced from the above plate. The scale is 2.4 arcmin per inch. North is at the top and east is to the left. The quasar PKS 1055+20 is denoted by Q. The comparison star magnitudes are as follows: (1) 16.33, (2) 16.82, (3) 15.50, (4) 16.24, (5) 17.28, (6) 17.79, (7) 15.22, (8) 17.01, (9) 16.75, (10) 16.89, (11) 16.16.

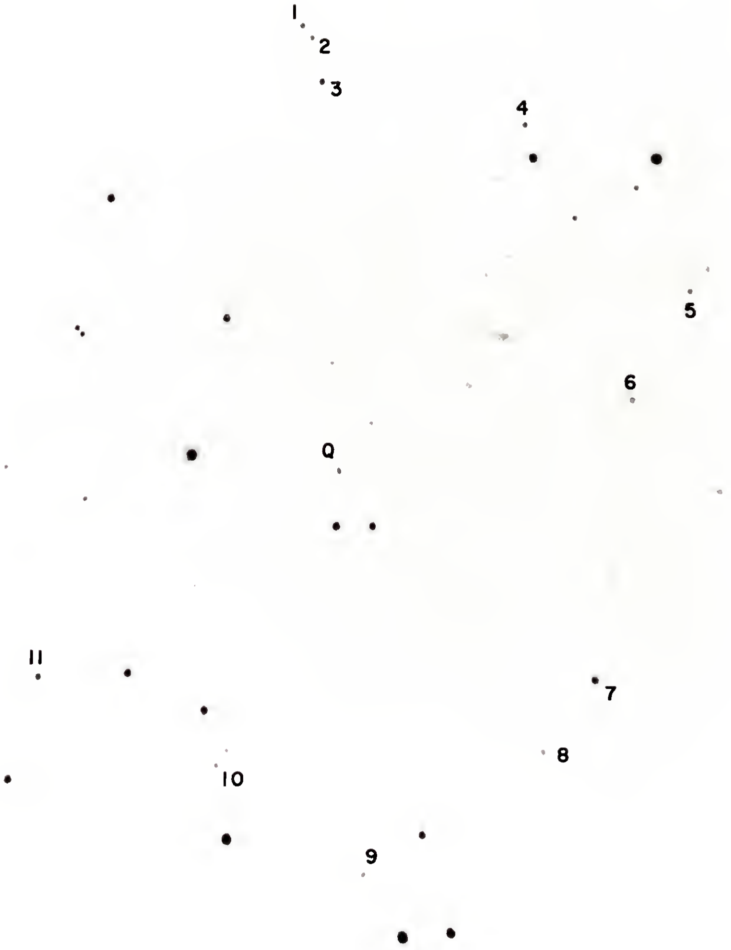
Q

Figure 30. The sequence finder for PKS 1116+12. The comparison star photographic magnitudes were obtained by a photographic transfer from SA 79 using a plate exposed on January 31, 1973, at Rosemary Hill Observatory. This photograph is reproduced from a Rosemary Hill plate taken on March 2, 1974. The scale is 2.4 arcmin per inch. North is at the top and east is to the left. The quasar PKS 1116+12 is denoted by Q. The comparison star magnitudes are as follows: (1) 18.42, (2) 18.93, (3) 19.00, (4) 18.05, (5) 17.79, (6) 19.24, (7) 18.48, (8) 16.29, (9) 17.05, (10) 16.65.

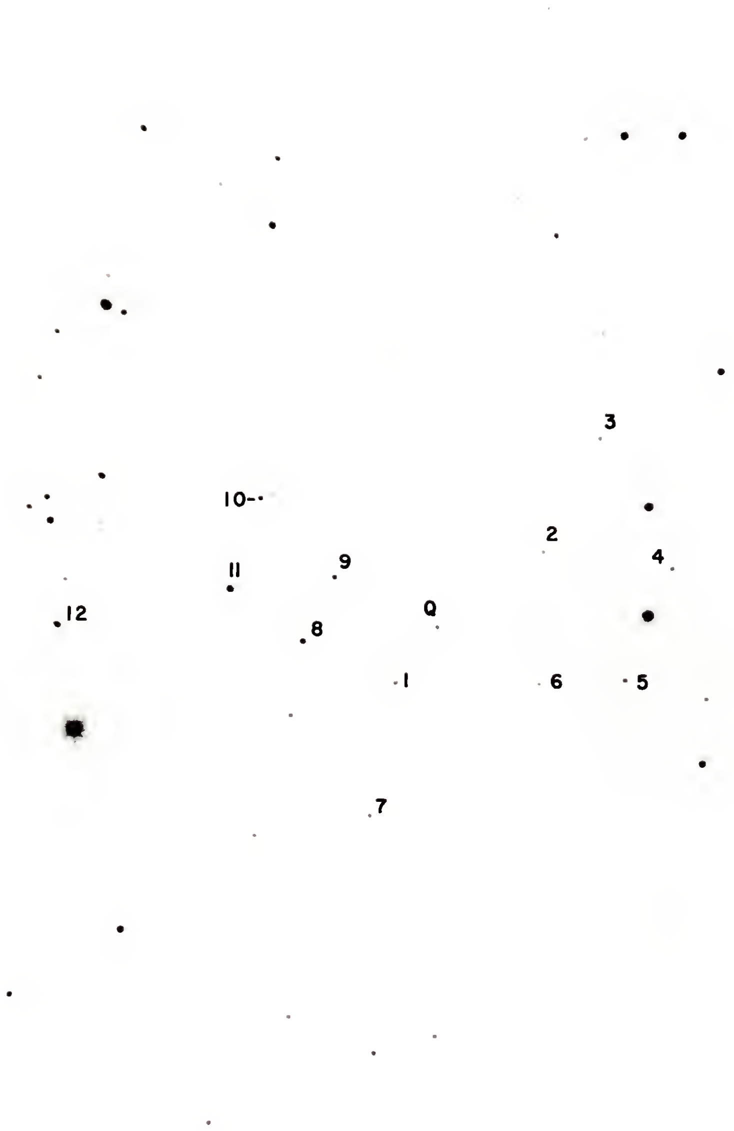
3
10
2
4
11
9
12
Q
8
1
6
5
7

lowering the rms to a reasonable value should greatly increase the statistical confidence for variability.

4C 09.42

This source was identified by Wills *et al*. (1973) as an 18.5 magnitude blue galaxy. The Florida light curve of 4C 09.42 is shown in Figure 31. Optical variations of around $0\overset{m}{.}5$ are suggested over a time scale of a few months with a confidence level for variability of 98 percent. The average rms error is $0\overset{m}{.}12$.

The comparison sequence for 4C 09.42 was obtained by a photographic transfer from SA 81 using the photometry of Brun (1957). Figure 32 shows the sequence finder for 4C 09.42.

PKS 1510-08

The optical counterpart of PKS 1510-08 was identified by Bolton and Kinman (1966). Medd *et al*. (1972) report rapid fluctuations at 2.8 cm and 4.5 cm between 1967 and 1971, and describe the radio spectrum as having a centimeter excess. Lü (1972) reports optical variations; the greatest range was about $0\overset{m}{.}6$. The Florida light curve of PKS 1510-08 is shown in Figure 31. Optical variations were observed with a confidence level of 99.9 percent; a sharp decline in intensity occurred in mid 1972. The average rms error is $0\overset{m}{.}08$.

The comparison sequence for PKS 1510-08 was obtained by a photographic transfer from SA 132 using the photometry of Brun (1957). Figure 33 shows the sequence finder for PKS 1510-08.

Figure 31. The Florida light curves of 4C 09.42, PKS 1510-08 and PKS 1645+17. The error bars indicate twice the average rms error of a single measurement.

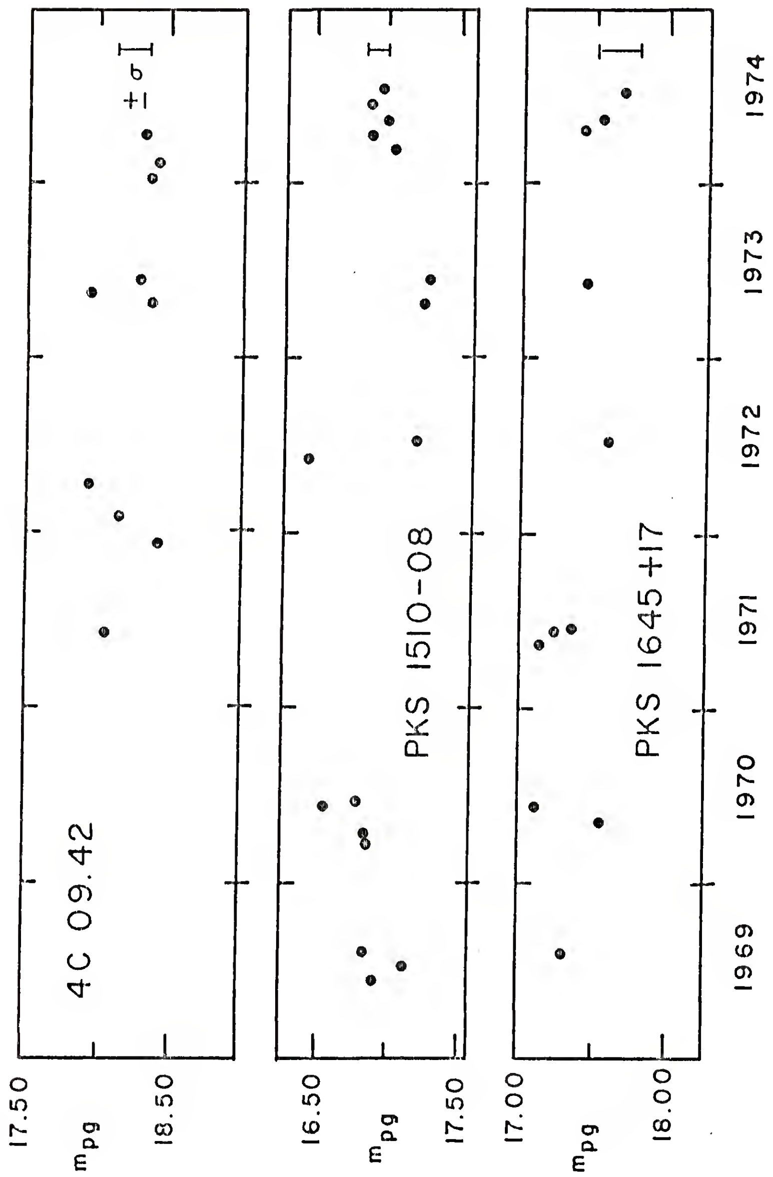
4C 09.42
PKS 1510-08
PKS 1645+17
$\pm\sigma$
m_{pg}
17.50
18.50
16.50
17.50
17.00
18.00
1969
1970
1971
1972
1973
1974

Figure 32. The sequence finder for 4C 09.42. The comparison star photographic magnitudes were obtained by a photographic transfer from SA 81 using a plate exposed on February 19, 1974, at Rosemary Hill Observatory. This photograph is reproduced from a Rosemary Hill plate taken on February 21, 1972. The scale is 2.4 arcmin per inch. North is at the top and east is to the left. The galaxy 4C 09.42 is denoted by G. The comparison star magnitudes are as follows: (1) 18.36, (2) 17.80, (3) 18.72, (4) 18.31, (5) 17.58, (6) 17.35, (7) 16.38, (8) 15.91, (9) 16.09.

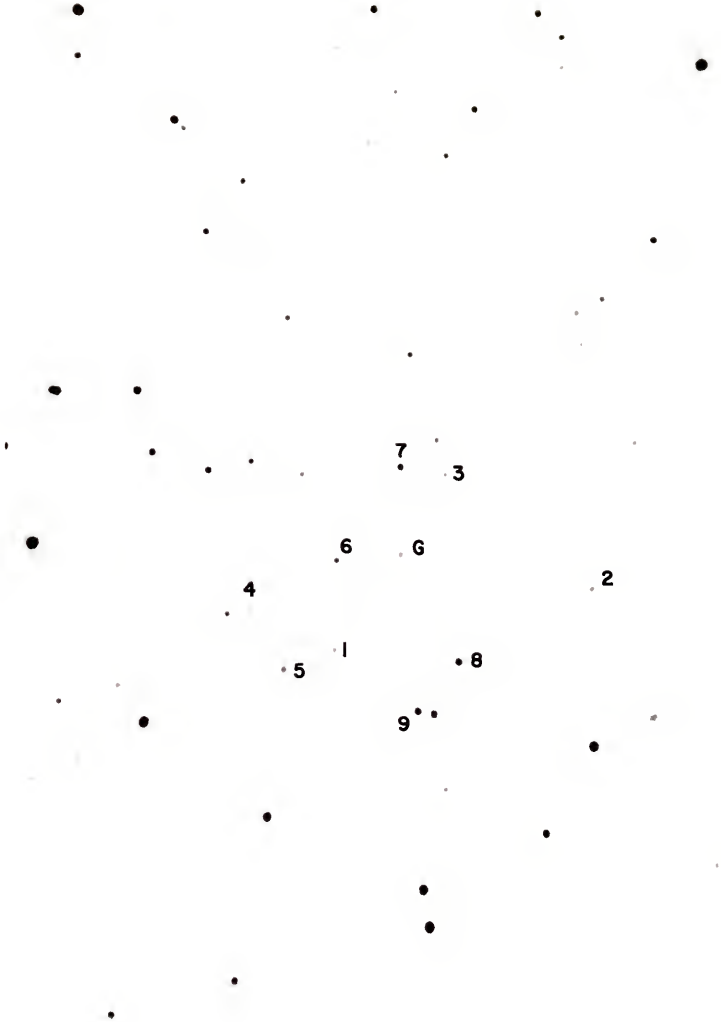
7
3
6
G
2
4
1
8
5
9

Figure 33. The sequence finder for PKS 1510-08. The comparison star photographic magnitudes were obtained by a photographic transfer from SA 132 using a plate exposed on April 29, 1973, at Rosemary Hill Observatory. This photograph is reproduced from a Rosemary Hill plate taken on July 10, 1972. The scale is 2.4 arcmin per inch. North is at the top and east is to the left. The quasar PKS 1510-08 is denoted by Q. The comparison star magnitudes are as follows: (1) 15.60, (2) 15.38, (3) 17.13, (4) 17.67, (5) 17.18, (6) 17.09, (7) 17.93, (8) 16.80, (9) 17.40, (10) 16.54.

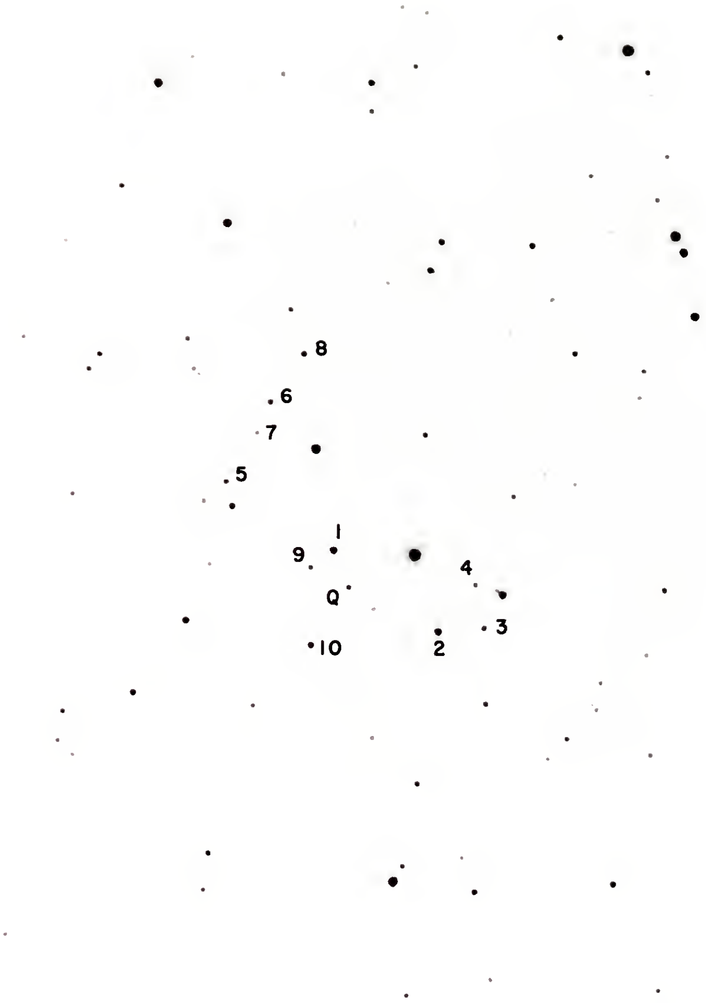
8
6
7
5
1
9
4
Q
3
10
2

PKS 1645+17

The Parks Catalog (Eckers 1969) identifies this source as a possible quasar. The Florida light curve of PKS 1645+17 is shown in Figure 31. No significant optical variations were observed. The confidence level for variability is 40 percent and the average rms error is $0\overset{m}{.}16$.

A tertiary comparison sequence for PKS 1645+17 was established by a photographic transfer from the field of PKS 1607+26. The sequence finder for PKS 1645+17 is shown in Figure 34.

PKS 2145+06

The optical counterpart of PKS 2145+06 was identified by Kinman *et al*. (1967). Medd *et al*. (1972) report a slight decline at 2.8 cm and 4.5 cm between 1967 and 1971, and describe its spectrum as having a centimeter excess. Observations by Dent and Kojoian (1972) at 3.8 cm and 1.9 cm show a decline in intensity between 1969 and 1971, agreeing with Medd *et al*. Tritton and Selmes (1971) found no significant optical variations between August of 1967 and August of 1970. The Florida light curve of PKS 2145+06 is shown in Figure 35. Generally the light curve shows little variability, though variations of $0\overset{m}{.}4$ are occasionally suggested. Though the confidence level for variability is only 50 percent and therefore not statistically significant, the decline in intensity seen by Medd *et al*. at centimeter wavelengths is also suggested by the Florida observations. The average rms error is $0\overset{m}{.}12$.

Figure 34. The sequence finder for PKS 1645+17. The comparison star photographic magnitudes were obtained by a photographic transfer from the field of PKS 1607+26 using a plate exposed on June 3, 1970, at Rosemary Hill Observatory. This photograph is reproduced from a Rosemary Hill plate taken on May 20, 1974. The scale is 2.4 arcmin per inch. North is at the top and east is to the left. The source PKS 1645+17 is denoted by S. The comparison star magnitudes are as follows: (1) 18.21, (2) 16.02, (3) 17.37, (4) 17.89, (5) 18.50, (6) 18.24, (7) 15.62, (8) 17.72, (9) 17.29, (10) 17.73, (11) 15.74, (12) 17.06.

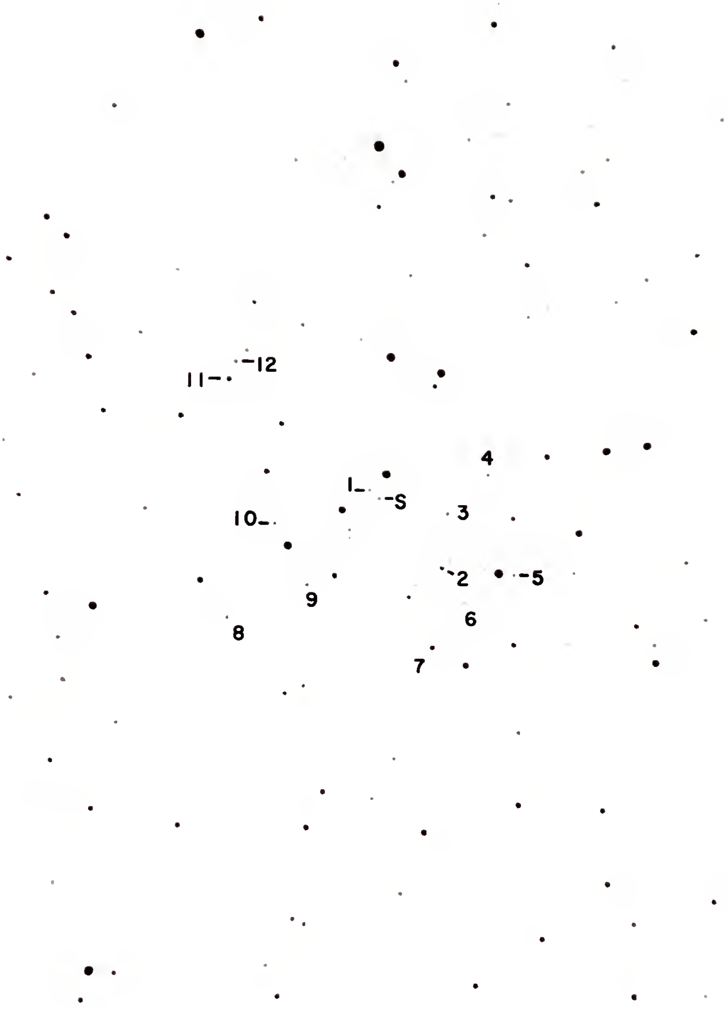
11
12
4
1
S
3
10
2
5
9
6
8
7

Figure 35. The Florida light curves of PKS 2145+06 and PKS 2349-01. The error bars represent twice the average rms error for a single measurement.

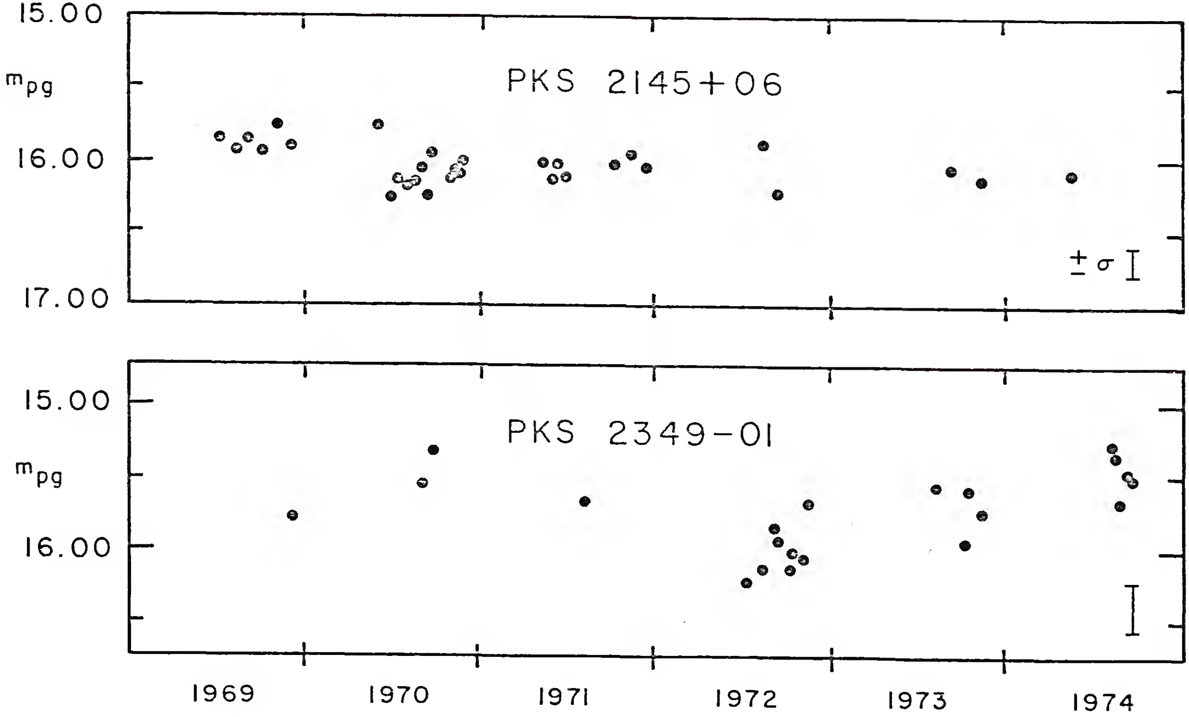
15.00
m_pg
16.00
17.00
PKS 2145+06
± σ
15.00
m_pg
16.00
PKS 2349-01
1969
1970
1971
1972
1973
1974

The comparison sequence for PKS 2145+06 was established by a photographic transfer from SA 114 using the photometry of Brun (1957). The sequence finder for PKS 2145+06 is shown in Figure 36.

PKS 2349-01

The Parks Catalog (Ekers 1969) identifies this source as an N galaxy. The Florida light curve is shown in Figure 35. The Florida observations suggest variations of approximately $0^{m}.5$ over a time scale of a few months with a confidence level of 99.5 percent.

The comparison sequence for PKS 2349-01 was established by a photographic transfer from SA 92 using the photometry of Brun (1957). The sequence finder for PKS 2349-01 is shown in Figure 37.

Summary

Of the 14 objects studied, 7 showed statistically significant variations with a confidence level equal to or greater than 99.5 percent. The probable lacertid PKS 0735+17 and the quasar PKS 0906+01 exhibit the range and rapidity of variations characteristic of OVVs; the latter object was classified as such by Folsom et al. (1969). The quasar PKS 1055+20 and the galaxy 4C 09.42 have a confidence level for variability of 98 percent and should be considered as possible variables. It is suggested that PKS 1116+12 is a probable variable also; the high rms scatter in the observations of

Figure 36. The sequence finder for PKS 2145+06. The comparison star photographic magnitudes were obtained by a photographic transfer from SA 114 using a plate exposed on August 2, 1970, at Rosemary Hill Observatory. This photograph is reproduced from the above plate. The scale is 2.4 arcmin per inch. North is at the top and east is to the left. The quasar PKS 2145+06 is denoted by Q. The comparison star magnitudes are as follows: (1) 16.41, (2) 16.33, (3) 14.88, (4) 15.85, (5) 15.37, (6) 17.03, (7) 16.52, (8) 16.03, (9) 15.56, (10) 14.76, (11) 15.01.

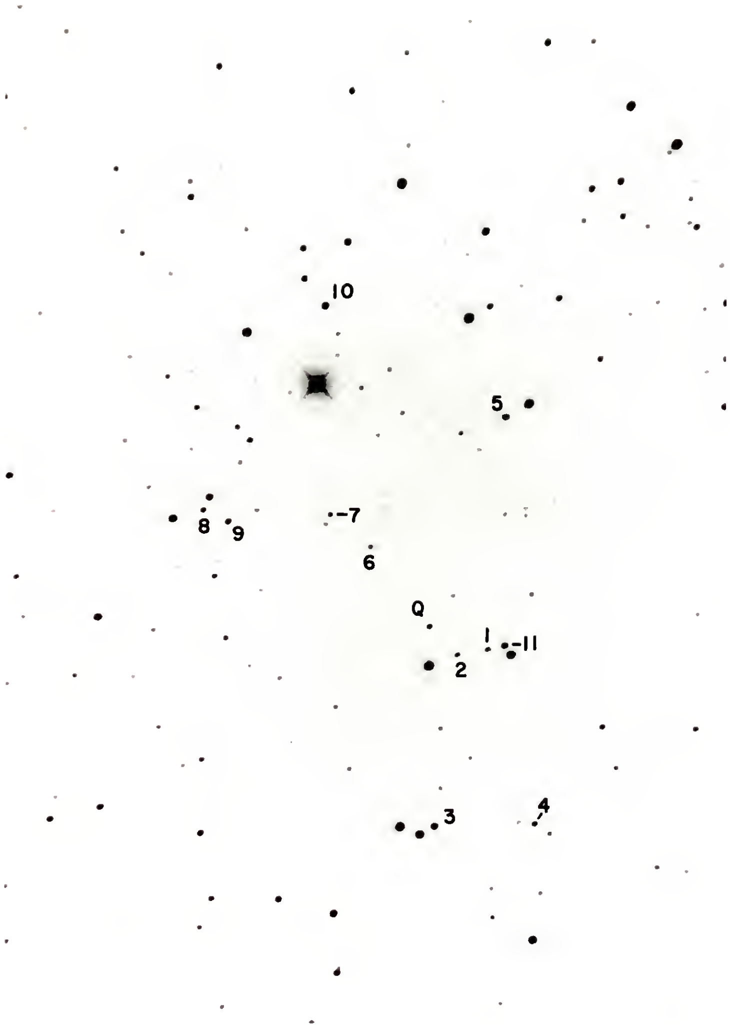
10
5
7
8
9
6
Q
1
11
2
3
4

Figure 37. The sequence finder for PKS 2349-01. The comparison star photographic magnitudes were obtained by a photographic transfer from SA 92 using a plate exposed on September 24, 1974, at Rosemary Hill Observatory. This photograph is reproduced from a Rosemary Hill plate taken on July 20, 1972. The scale is 2.4 arcmin per inch. North is at the top and east is to the left. The N-galaxy PKS 2349-01 is denoted by N. The comparison star magnitudes are as follows: (1) 15.80, (2) 14.10, (3) 15.33, (4) 16.87, (5) 13.48, (6) 17.02, (7) 16.34, (8) 13.42, (9) 15.83, (10) 14.34.

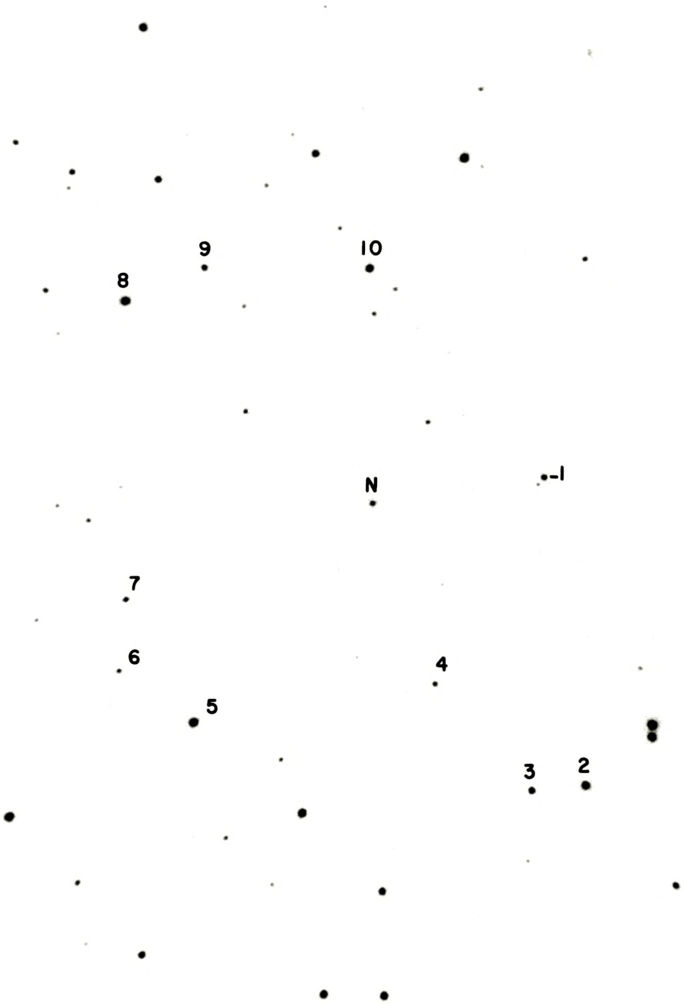
9
10
8
N
-1
7
6
4
5
3
2

this object are probably responsible for the low confidence level for variability.

The two objects showing the least variability were the quasars PKS 0725+14 and PKS 1004+13. PKS 1004+13 is apparently in a quiescent period at the present time, since it has shown indications of variability in the past. The behavior of this object tends to support the hypothesis of Lü (1972) that some QSOs may show occasional violent optical activity but at other times remain relatively quiet. It is Lü's opinion that probably all QSOs will show variability if they are observed over a long enough period. The author suggests that PKS 1004+13 should be monitored frequently in order to observe a possible resumption of activity.

CHAPTER V

COLOR STUDIES OF QUASARS AND RELATED OBJECTS

Introduction

The observed similarities between classes of objects and the assumption that QSO redshifts are of cosmological origin suggest an evolutionary sequence starting with quasars and ending with normal galaxies. Such a relationship would imply a gradation of average properties relative to distance and retarded time. As a consequence of this hypothesis an evolutionary component might be expected in the relationship between the redshifts of QSOs and their color indices, assuming the high-redshift objects are seen at a very early epoch in the age of the universe. In addition, the color indices and range and frequency of variation of low-redshift QSOs should resemble those of Seyfert and N-type galaxies if the latter objects are indeed intermediate stages between QSOs and galaxies like our own.

The observed characteristics of several objects from the Florida program have been compared in order to study the above hypothesis. The color indices of five quasars have been compared with their redshifts, and the color indices and variability of these objects have been compared with those of an N galaxy, a Seyfert galaxy, and two lacertids.

These objects are listed in Table 7 along with their (B-V) and (U-B) color indices, redshifts, and average B magnitudes. The first values listed of an object's color indices were obtained from Florida data; the values in parentheses are from the indicated references.

Several of these objects exhibit large variations in magnitude and color index. The Florida values given in Table 7 are average values; the values obtained from different sources will not necessarily agree. The study of the Florida sources has enabled the author to estimate the range of variation in the color indices of individual objects; these ranges and the recent photometric history of each object are discussed in later sections of this chapter.

The Recent Photometric History of the Florida Objects

A brief history and description of the Florida objects is now given; they are discussed in the order that they are listed in Table 7. The Florida program has amassed considerable color data on 3C 120, BL Lac, OJ 287 and 3C 345; light curves are given for these objects. Only a few color observations have been made of the remainder of the objects, which were monitored principally to study short-term fluctuations in magnitude and the range and average values of their color indices. The author's observations of these objects are listed in Table 8. When examining the data it is helpful to remember that an increase in color index indicates a reddening

Key to Table 7

The first values of the color indices were obtained from Florida data are are average values. The color indices in parentheses were obtained from the references listed at the right of the table. These references, along with those for the redshifts, are listed below. M_B is the average photographic B magnitude obtained from Florida data.

(1) Kinman (1967)

(2) Penston *et al*. (1971)

(3) Sandage (1966a)

(4) DuPuy *et al*. (1969)

(5) Oke and Gunn (1974)

(6) Dyck *et al*. (1971)

(7) De Veny *et al*. (1971)

(8) Haro and Luyten (1962)

(9) Setti and Woltjer (1973)

Table 7

The Objects Used for the Color Studies

Class of Object	Name	(B-V)	(U-B)	M_B	z	Color Reference	Redshift Reference
Seyfert Galaxy	3C 120	0.56(0.50)	-0.89(-0.84)	15.0	0.032	1	1
N Galaxy	3C 390.3	0.58(0.58)	-0.40(0.037)	16.0	0.057	2	3
Lacertid	BL Lac	1.15(0.68)	-0.10(-0.36)	14.7	0.07	4	5
Lacertid	OJ 287	0.40(0.39)	-0.65(-0.63)	14.0	?	6	--
QSO	3C 273	0.28(0.21)	-0.46(-0.85)	13.1	0.158	7	7
QSO	3C 345	0.38(0.29)	-0.49(-0.50)	16.3	0.595	7	7
QSO	3C 454.3	0.27(0.47)	-0.67(-0.66)	16.9	0.859	7	7
QSO	2134+004 (PHL 61)	0.61(-0.1)	-1.11(-0.40)	17.5	1.94	8	8
QSO	4C 05.34	(0.37)	0.11(-0.04)	18.2	2.877	9	9

Table 8

The Rosemary Hill U, B, and V Observations of 3C 390.3, 3C 273, 3C 454.3, PKS 2134+004, and 4C 05.34

Object	Date	U	RMS Error	B	RMS Error	V	RMS Error	(U-B)	(B-V)
3C 390.3	7/2/73	15.91	0.34	--	--	--	--	--	--
	7/3/73	--	--	15.72	0.14	15.06	0.08	--	0.66
	8/28/73	15.54	0.03	16.23	0.06	15.17	0.09	-0.69	0.06
	9/30/73	15.70	0.36	15.90	0.07	15.16	0.03	-0.20	0.74
	10/16/73	15.99	0.29	16.11	0.08	15.36	0.03	-0.12	0.75
	10/20/73	15.61	0.11	16.04	0.03	14.97	0.03	-0.43	0.67
	4/19/74	15.37	0.08	15.95	0.03	--	--	-0.58	--
3C 273	1/24/74	--	--	13.30	0.19	13.10	0.15	--	0.20
	2/25/74	12.58	0.10	12.93	0.06	12.74	0.16	-0.35	0.19
	3/19/74	12.78	0.16	13.35	0.12	13.00	0.83	-0.57	0.35
	4/23/74	12.99	0.37	13.45	0.21	13.07	0.21	-0.46	0.38

Table 8 - Continued

Object	Date	U	RMS Error	B	RMS Error	V	RMS Error	(U-B)	(B-V)
3C 454.3	8/10/73	15.79	0.21	16.56	0.10	16.01	0.08	-0.77	0.55
	8/25/73	--	--	16.80	0.17	--	--	--	--
	9/7/73	16.14	0.30	16.79	0.07	16.85	0.15	-0.65	-0.06
	9/23/73	--	--	16.68	0.06	--	--	--	--
	10/20/73	15.97	0.25	16.72	0.11	16.23	0.06	-0.75	0.49
	11/27/73	16.48	0.34	16.97	0.16	--	--	-0.49	--
	12/21/73	16.15	0.05	16.84	0.05	16.74	0.05	-0.69	0.10
2134+004	9/6/73	15.96	0.32	17.38	0.11	16.80	0.10	-1.42	0.58
	9/20/73	16.59	0.54	17.47	0.10	16.94	0.11	-1.08	0.53
	10/18/73	15.93	0.30	17.64	0.19	16.81	0.11	-1.71	0.83
	10/27/73	16.42	0.56	17.61	0.12	16.99	0.09	-1.19	0.62
	7/27/74	--	--	17.52	0.03	--	--	--	--
	8/18/74	--	--	17.40	0.23	16.85	0.08	--	0.55
	9/16/74	16.48	0.03	--	--	--	--	--	--
4C 05.34	11/4/73	18.32	0.16	18.21	0.10	--	--	0.11	--
	1/29/74	18.25	0.13	18.17	0.05	--	--	0.08	--
	2/18/74	18.30	0.03	18.14	0.03	--	--	0.15	--
	4/13/74	18.27	0.06	--	--	--	--	--	--

of the object; a decrease in color index indicates a shift in color toward shorter wavelengths.

Sequence finders are given for comparison star fields not shown by Folsom (1970), Hackney (1972a) or Hackney (1973). Photoelectric sequences were used when available to avoid the zero level shifts and slope errors inherent in photographic transfers. Comparison star magnitudes were computer smoothed as described by Hackney (1973) to correct for systematic errors present in the Rosemary Hill photographic UBV system or in the original photoelectric observations.

3C 120

Folsom *et al.* (1971) classify the Seyfert galaxy 3C 120 as an OVV that undergoes violent optical variations of a magnitude or more on a time scale of days or weeks. Kinman (1968) found it to be variable at both radio and optical wavelengths.

The Florida U, B, V, and I light curves of 3C 120 are shown in Figure 38. Figure 39 is a plot of the corresponding color indices. The blue light curve is most complete; it shows the object at a maximum optical intensity during the latter part of 1972, at a minimum intensity during the latter part of 1973, with a sharp burst of activity occurring in early 1974. The overall range in the U and B is about $1\overset{m}{.}0$ and approximately $0\overset{m}{.}4$ in the V. Surprisingly, the object is quite active in the infrared; the outburst in February of 1974 is correlated in all four colors. Generally the apparent

Figure 38. The Florida four-color light curve of 3C 120. The error bars represent twice the average rms error of a single measurement.

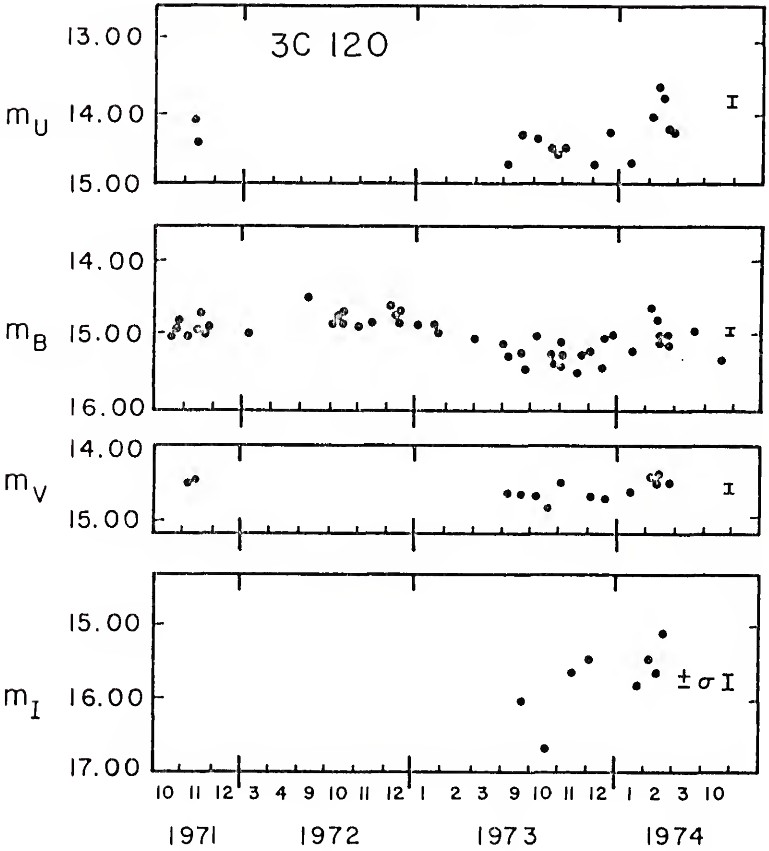
3C 120
m_U
13.00
14.00
15.00
m_B
14.00
15.00
16.00
m_V
14.00
15.00
m_I
15.00
16.00
17.00
±σ I
10 11 12 3 4 9 10 11 12 1 2 3 9 10 11 12 1 2 3 10
1971
1972
1973
1974

Figure 39. Apparent variations in the color indices of 3C 120. The straight lines through the data points are least-squares fits. The error bars represent twice the average rms error of a single measurement. The least-squares lines suggest long-term trends in (U-B) and (B-V) of about $0\overset{\mathrm{m}}{.}1$ per year.

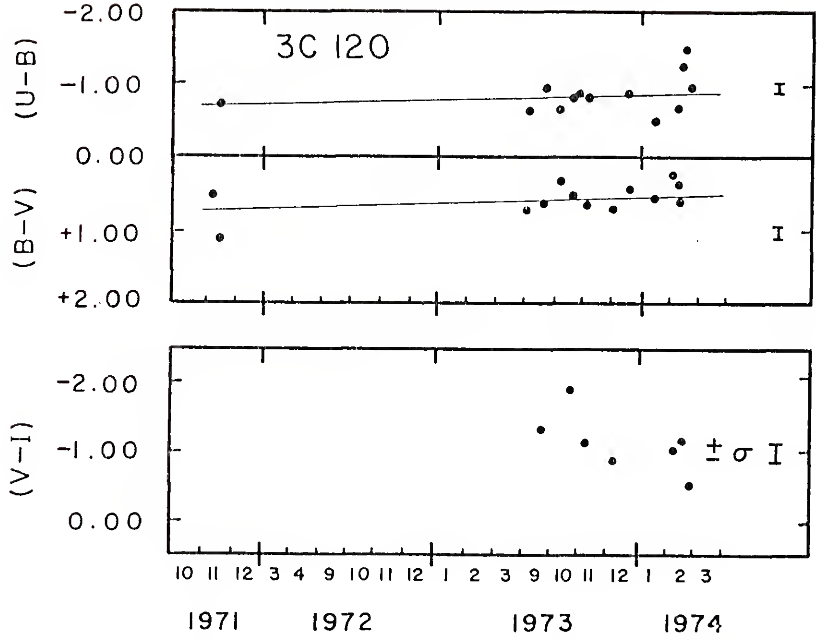
3C 120
(U-B)
(B-V)
(V-I)
-2.00
-1.00
0.00
+1.00
+2.00
-2.00
-1.00
0.00
±σ I
10 11 12 3 4 9 10 11 12 1 2 3 9 10 11 12 1 2 3
1971
1972
1973
1974

short-term variations in the color indices suggest that the object becomes bluer as it brightens and redder as it declines.

For the UBV observations of 3C 120 the combined photoelectric sequences of Kinman (1968) and Angione (1971) were used. A photographic transfer from a plate of M 67 taken on January 26, 1974, using magnitudes supplied by Eggen (1972) was used as the infrared sequence. The comparison stars for 3C 120 are listed in Table 9. The sequence finder for 3C 120 is given by Hackney (1973).

Table 9

The Comparison Stars for 3C 120

Star	U	B	V	I
1	14.85	14.34	12.82	12.77
2	16.33	16.08	15.39	16.35
3	16.10	15.45	14.54	15.36
4	16.75	15.69	14.46	14.89
5	--	15.70	15.02	16.07
6	--	14.36	13.47	14.34
7	--	15.02	14.30	15.57
8	--	15.11	14.27	15.47

In the above sequence only the first four stars are calibrated in the ultraviolet. The author attempted to calibrate the last four stars using the first four as standards, but obtained very poor photometric results. Due to the close agreement between the average Florida colors of 3C 120 and those quoted in the literature, the author feels that the U sequence for 3C 120 is reasonably free from zero-point shift and slope error and is sufficiently accurate for the purpose of this study.

3C 390.3

The optical variability of the N galaxy 3C 390.3 was established by Sandage (1967) and Cannon, Penston, and Penston (1968). Shen, Usher, and Barrett (1972) report a brightness decrease of 1.15 magnitudes in 3 days and a total range of variation of about 2 magnitudes; they observed no long-term intensity trends.

The spectrum of 3C 390.3 differs from that of a typical quasar in that it has two emission line redshifts: 0.056 and 0.042 (Burbidge and Burbidge 1971). Many QSOs have two or more redshifts; one is usually an emission-line system while the other arises from absorption lines. The redshift of 0.056 also reported by Sandage (1966a) was assumed by the Burbidges to arise from the central mass of the N galaxy; this is the redshift listed in Table 7. The weaker redshift of 0.042 is attributed to gas ejected from the central core with a line-of-sight velocity component.

The author's observations of 3C 390.3 are listed in Table 8. A brightening trend is suggested throughout the latter part of 1973 and early 1974, with a minimum occurring in mid October of 1973. There is the suggestion of short-term trends in the color indices indicating that the object becomes bluer as its optical intensity increases and redder as it declines.

The comparison sequence for 3C 390.3 was established from a photoelectric sequence by Penston, Penston, and Sandage (1971). The sequence finder for 3C 390.3 is shown in Figure 40; the magnitudes of the comparison stars are shown below in Table 10.

Table 10

The Comparison Stars for 3C 390.3

Star	U	B	V
1	13.58	14.19	11.70
2	14.49	14.37	12.29
3	15.12	15.05	14.28
4	16.58	17.08	16.18
5	15.75	15.38	14.65
6	16.55	16.40	15.48

BL Lac

The Florida light curves of the lacertid prototype BL Lac shown in Figure 41 indicate optical activity of an extremely violent nature. As discussed in previous chapters BL Lac has been studied by a number of independent sources who confirm this violent activity.

The minimum in intensity that occurred in the latter part of 1973 allowed Oke and Gunn (1974) to block out the central core with an occulting disk and obtain a redshift for the faint outer envelope, using the 200-inch telescope. Oke and Gunn report that the energy distribution of the envelope

Figure 40. The sequence finder for the N galaxy 3C 390.3. This photograph is reproduced from a B exposure taken on the night of May 19, 1974, at Rosemary Hill Observatory. The scale is 2.4 arcmin per inch. North is at the top and east is to the left. The N galaxy 3C 390.3 is denoted by N. The magnitudes of the comparison stars are listed in Table 10.

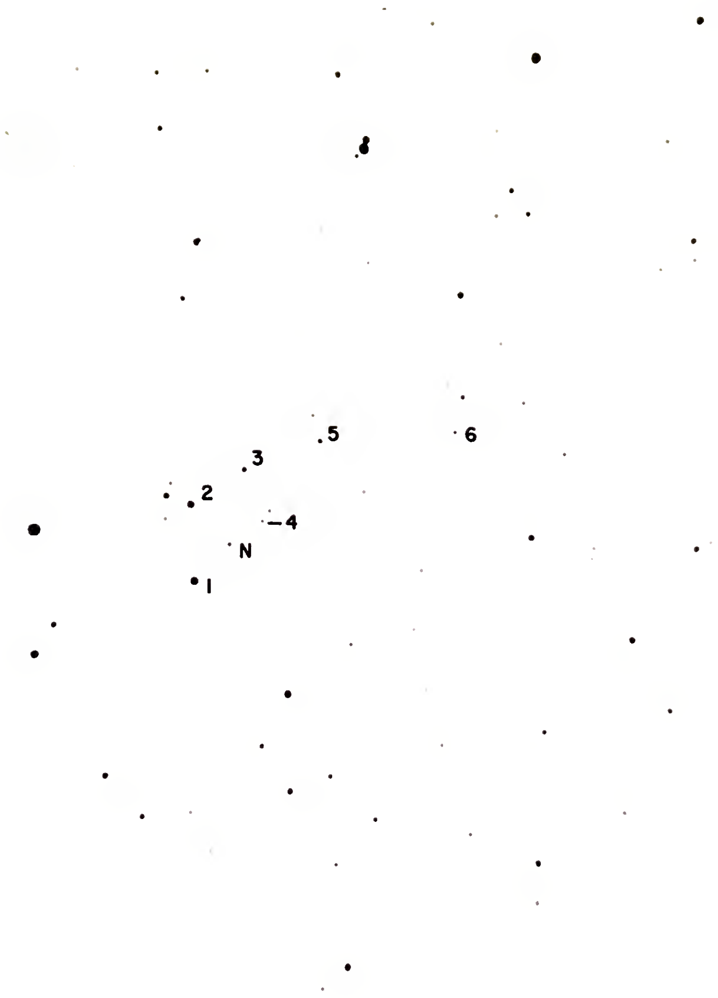
5
6
3
2
4
N
1

Figure 41. The Florida four-color light curve of BL Lac. The error bars represent twice the average rms of a single measurement. The error bars for the B and I curves are the same size as the data points and are not shown.

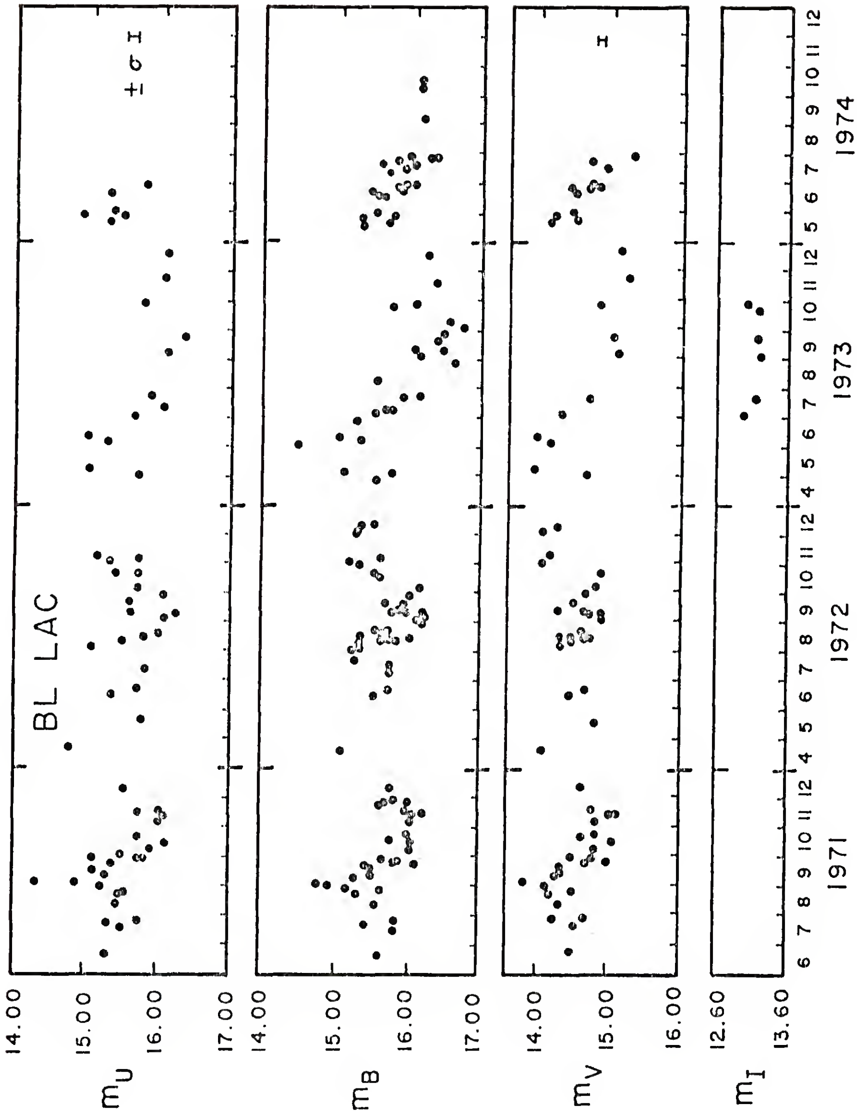
BL LAC
±σ
m_U
m_B
m_V
m_I
14.00
15.00
16.00
17.00
12.60
13.60
6 7 8 9 10 11 12
4 5 6 7 8 9 10 11 12
4 5 6 7 8 9 10 11 12
5 6 7 8 9 10 11 12
1971
1972
1973
1974

is similar in character to that of a giant elliptical galaxy which suggests that the other lacertids may be similar objects.

The intensity variations are well correlated in all four colors. Figure 42 shows the color indices corresponding to Figure 41. The optical fluctuations, together with short-term trends in the color indices, suggest that the greatest optical variations take place at the shorter wavelengths, supporting the conclusions of Hackney (1973). While there are considerable short-term color fluctuations, there appear to be no significant long-term color changes. This is illustrated by the small slopes of the least-squares fits through the (U-B) and (B-V) data in Figure 42; they are both less than $0\overset{m}{.}05$ per year.

The maximum range of variations observed was approximately $2\overset{m}{.}0$ in the U and B, $1\overset{m}{.}25$ in the V, and $0\overset{m}{.}20$ in the I. The small infrared activity of BL Lac is in contrast to that of 3C 120, which exhibited infrared variations similar to those in the U and B during the outburst in February of 1974.

The UBV comparison sequence for BL Lac was chosen from a photoelectric sequence of 8 stars published by Bertaud _et al_. (1969). The infrared sequence is a photographic transfer from M 92 using a plate taken on October 19, 1973. The infrared photometry of M 92 was obtained from Eggen (1972). The magnitudes of the comparison stars are listed in Table 11. The sequence finder for BL Lac is given by Hackney (1973).

Figure 42. The color indices of BL Lac corresponding to the light curves shown in Figure 41. The error bars represent twice the average rms error of a single measurement. The lines drawn through the (U-B) and (B-V) plots are least-squares fits; their small slopes indicate that there are no significant long-term color trends.

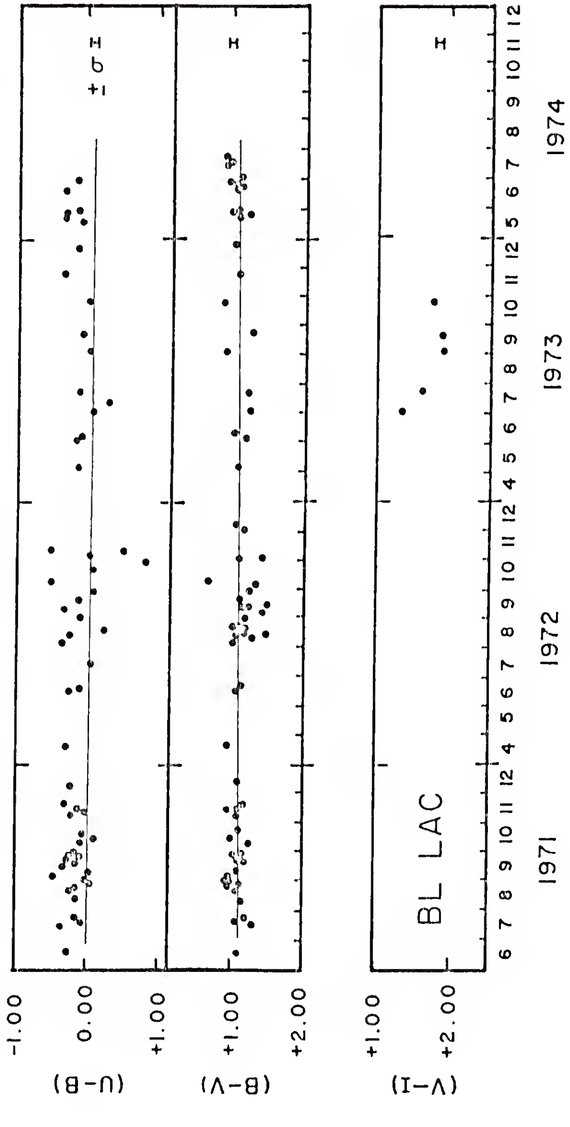
(U-B)
(B-V)
(V-I)
-1.00
0.00
+1.00
+1.00
+2.00
+1.00
+2.00
± σ
BL LAC
6 7 8 9 10 11 12 4 5 6 7 8 9 10 11 12 4 5 6 7 8 9 10 11 12 5 6 7 8 9 10 11 12
1971
1972
1973
1974

Table 11

The Comparison Stars for BL Lac

Star	U	B	V	I
1	16.55	14.63	12.89	11.30
2	14.99	14.35	13.28	12.40
3	15.42	15.09	14.10	12.97
4	15.73	15.21	14.27	13.06
5	16.64	16.40	15.48	13.13
6	16.77	15.77	14.40	12.95

OJ 287

This compact extragalactic source, whose lineless optical spectrum and rapid variability class it as a lacertid, has an extremely intriguing photometric history. It was first monitored by the Florida program in 1969 as one of 17 Ohio State radio sources identified as having peculiar radio spectra (Kraus *et al*. 1968). The Florida observations showed that OJ 287 was an OVV, exhibiting rapid and violent optical intensity fluctuations (Folsom *et al*. 1971). When these results were communicated to Stull at the University of Michigan his group found that OJ 287 exhibited violent activity at radio wavelengths as well (Brandie and Stull 1971).

In 1971 three-color monitoring of OJ 287 was begun by Hackney (1973) to study possible color changes associated with the optical intensity fluctuations. These observations were continued by the author, starting in late 1972, and extended into the infrared. Figure 43 shows the Florida

Figure 43. The Florida four-color light curve of OJ 287. The error bars represent twice the average rms error of a single measurement. Parabolic least-squares fits are drawn through the U, B, and V data points; they suggest rapid and violent short-term fluctuations superimposed upon a steadily declining background component.

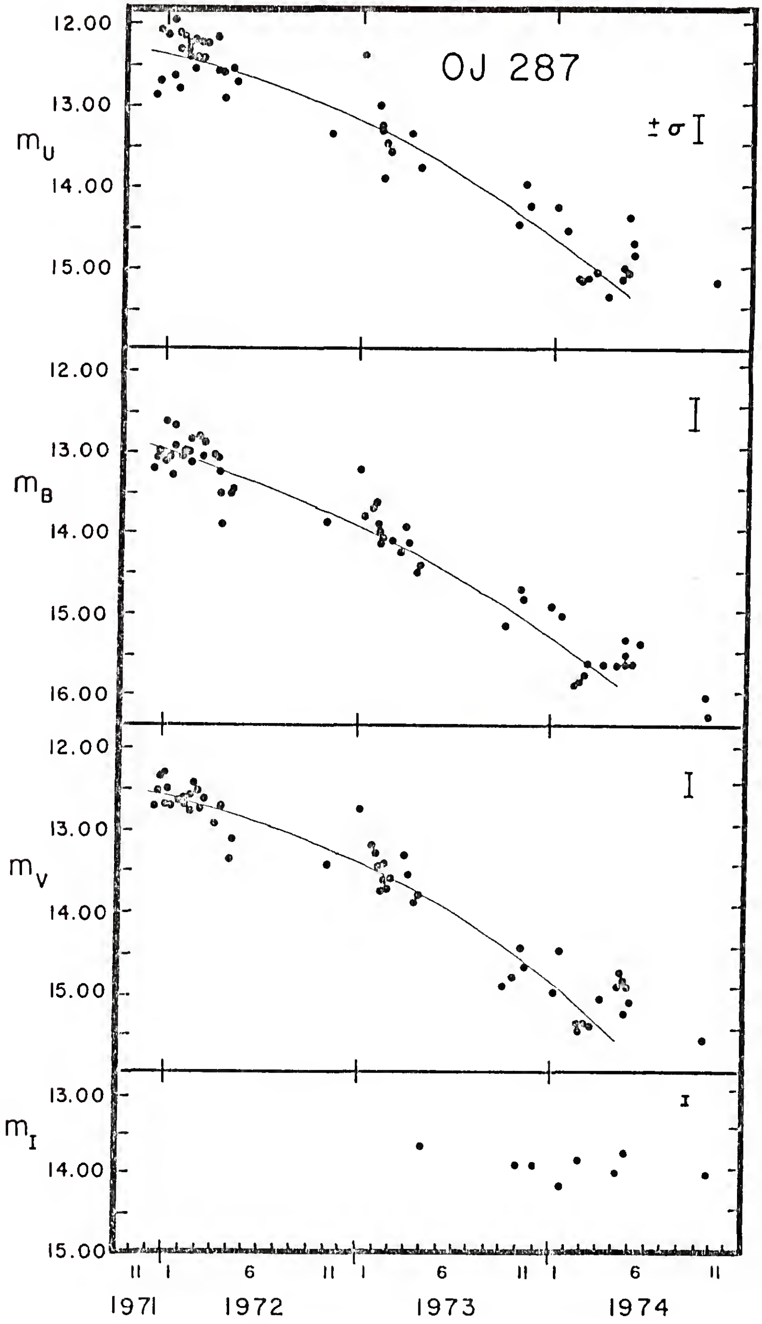
OJ 287
± σ
m_U
12.00
13.00
14.00
15.00
m_B
12.00
13.00
14.00
15.00
16.00
m_V
12.00
13.00
14.00
15.00
m_I
13.00
14.00
15.00
11
1
6
11
1
6
11
1
6
11
1971
1972
1973
1974

four-color light curve of OJ 287. A long-term intensity decline is immediately evident; the curved lines through the data points are parabolic least-squares fits and suggest rapid and violent short-term fluctuations superimposed upon a steadily declining background component.

At the start of the color observations OJ 287 was the brightest of the quasar-like sources; its B magnitude of 12.4 exceeded even that of the brightest quasar 3C 273, whose minimum B magnitude is around 12.7. The overall decline in the U, B, and V is greater than 3.25 magnitudes in each color. Figure 44 shows the (U-B), (B-V), and (V-I) color indices corresponding to the light curves of Figure 43.

Though there are considerable short-term color fluctuations, the least-squares lines through the data points show that there are no significant long-term changes in (U-B) and (B-V). The short-term fluctuations appear to be centered about baselines of -0.65 and 0.39 for the (U-B) and (B-V), respectively. These values are very close to the values of -0.63 and 0.41 derived from data published by Dyck et al. (1971). Though the data points are sparse, the large variations in (V-I) suggest that the short-term infrared fluctuations are less than in the other three colors. The long-term decline also seems to be less steep in the infrared.

The short-term trends in color index appear to be correlated with intensity variations; in general the (U-B) index suggests that the object becomes bluer as it brightens. However, in many instances the (B-V) index suggests greater

Figure 44. The color indices of OJ 287 corresponding to the light curves of Figure 43. The error bars represent twice the average rms error of a single measurement. The lines drawn through the (U-B) and (B-V) data points are least-squares fits; their small slopes suggest the absence of long-term color trends.

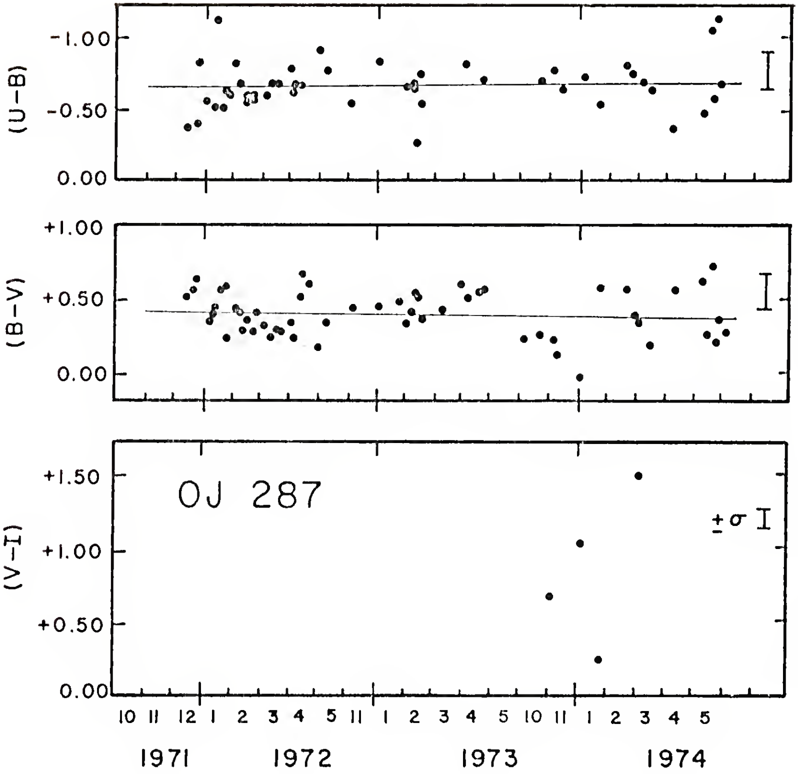
-1.00
-0.50
0.00
(U-B)
+1.00
+0.50
0.00
(B-V)
+1.50
+1.00
+0.50
0.00
(V-I)
OJ 287
±σ
10 11 12 1 2 3 4 5 11 1 2 3 4 5 10 11 1 2 3 4 5
1971
1972
1973
1974

activity in the V than in the B, with the object reddening as it brightens. Examination of the light curves does give the impression that there are bursts of activity where the short-term fluctuations are of equal or greater amplitude in the V than in the B.

Figure 45 shows the Rosemary Hill Observatory light curve of OJ 287 from 1970 to the present. The points represented by the circles are m_{pg}, those represented by dots are m_B. The photographic magnitudes were corrected to B magnitudes by the addition of $0\overset{m}{.}4$. It is apparent that the long-term component was increasing in intensity throughout 1970 and reached a maximum in intensity in mid-1971 before starting the decline shown by the color curves. During May and June of 1974 the object seemed to be making a recovery; however, this appeared to be only a short-term disturbance and the general intensity has continued to decline.

The general trends shown by the Florida light curves are in agreement with observations at 10.5μ and 0.44μ by Rieke and Kinman (1974). However, the Florida infrared observations, as stated previously, show a slower long-term decline than the other colors. The Florida infrared band pass is centered on approximately 0.82μ.

Two comparison sequences have been used for the UBV observations of OJ 287. The first was derived from photoelectric observations made with the Rosemary Hill 30-inch reflector; it is described by Hackney (1973). From late 1972 to the present, Florida reductions have been made with the

Figure 45. The Rosemary Hill Observatory light curve of OJ 287 from early 1970 to the present, showing an increase in the long-term component before the long decline shown in the color observations. The dots represent m_B; the open circles are m_{pg} corrected to m_B by the addition of $0\overset{m}{.}4$.

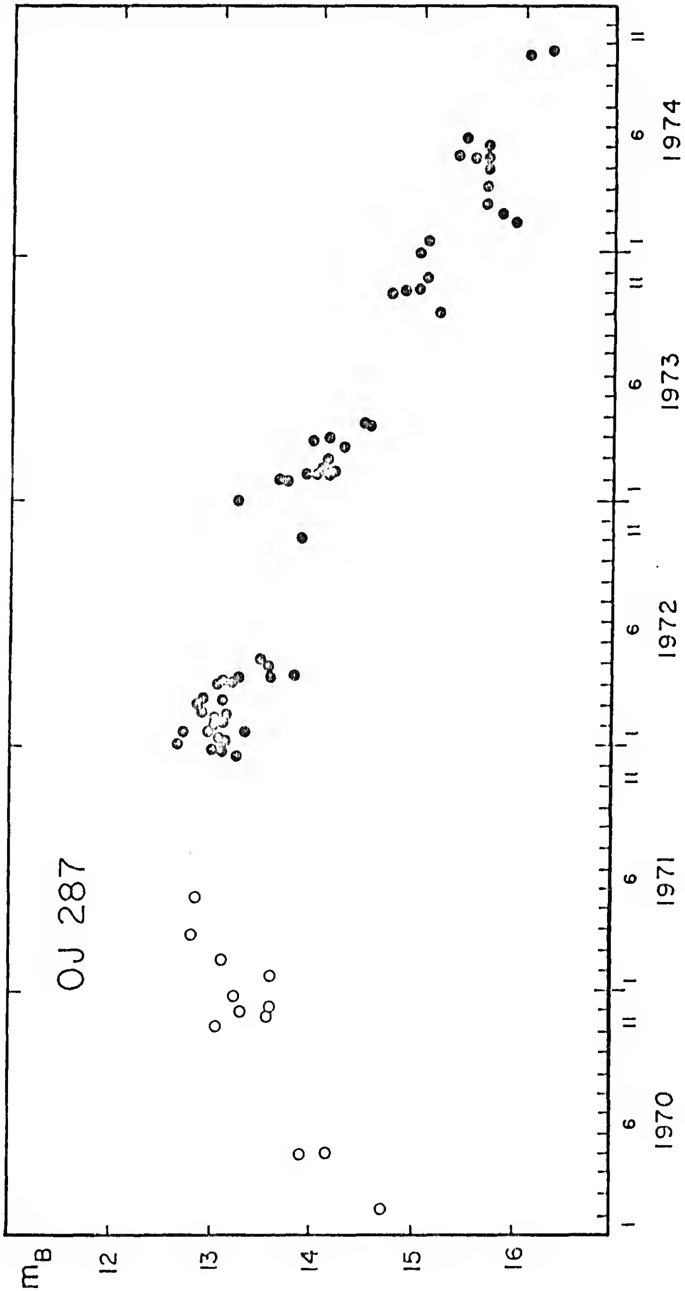
OJ 287
m_B
12
13
14
15
16
1
6
11
1970
1971
1972
1973
1974

photoelectric sequence of Penston and Wing (1973), which was received as a preprint prior to publication. The infrared magnitudes were obtained by a photographic transfer from a plate of M 67 taken on April 29, 1973, using the infrared photometry of Eggen (1972). Penston and Wing's sequence finder for OJ 287 is shown in Figure 46. The magnitudes of the comparison stars are listed in Table 12.

Table 12

The Comparison Stars for OJ 287

Star	U	B	V	I
1	12.34	12.13	11.47	12.03
2	13.55	13.45	12.79	12.91
3	14.08	14.14	13.69	13.63
4	15.57	15.07	14.14	13.66
5	12.02	12.03	11.52	12.09
6	13.81	13.88	13.39	13.45
7	14.61	14.16	13.38	13.28

Difficulty was encountered in computer smoothing Penston and Wing's sequence; this is probably due to the extended area of the sequence in the field. Use of the Wynne field corrector described by Hackney (1973) appears to have solved the problem. The magnitudes listed in Table 12 were obtained by smoothing plates taken with the field corrector.

Figure 46. The sequence finder for the lacertid OJ 287. This photograph is reproduced from a B plate taken on the night of February 13, 1972, at Rosemary Hill Observatory. The scale is 2.8 arcmin per inch. North is at the top and east is to the left. The variable source OJ 287 is denoted by S. The comparison star magnitudes are listed in Table 12.

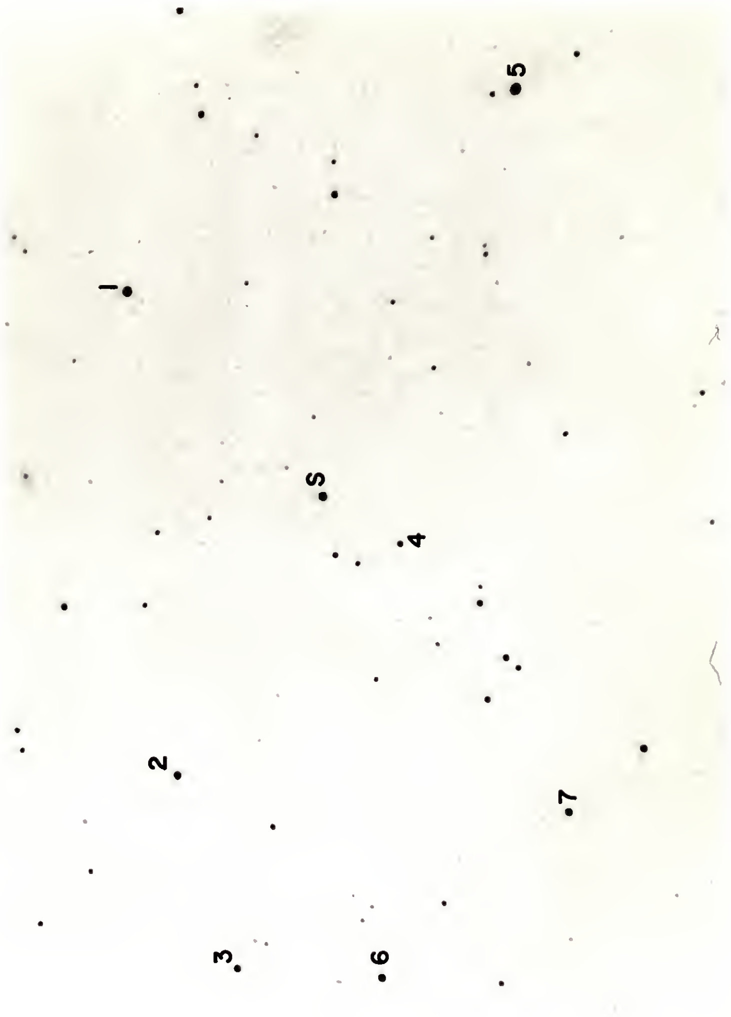
5
1
S
4
2
7
3
6

3C 273

This prototype quasar usually exhibits moderate variations at both optical and radio wavelengths. Tritton and Selmes (1971) report B magnitude fluctuations on the order of $0\overset{m}{.}25$ on a time scale of about two months. Sandage (1966b) reported that 3C 273 exhibited moderate optical fluctuations about a more or less constant intensity level over a 2-year observing period. Others such as Smith and Hoffleit (1963) have reported large optical variations over a considerably longer time interval. Dent (1965) reports a 40 percent increase in the radio flux of 3C 273 at 8,000 MHz over a 2.5-year time interval.

The author's observations of 3C 273 are listed in Table 8. Over a period of 2 months the object dimmed about $0\overset{m}{.}5$ in the U and B, and $0\overset{m}{.}4$ in the V. Previous to the decline the object had brightened about $0\overset{m}{.}4$ in the B and V, reaching a maximum in intensity in late February of 1974.

A photoelectric comparison sequence published by Penston, Penston, and Sandage (1971) was used for the Florida observations. Figure 47 shows the sequence finder for 3C 273; the magnitudes of the comparison stars are listed below in Table 13.

3C 345

This quasi-stellar radio source is a well-known OVV. Dent (1965) showed that 3C 345 was variable at 8,000 MHz and Goldsmith and Kinman (1965) found that the object was also

Figure 47. The sequence finder for the quasar 3C 273. This photograph is reproduced from a B plate taken on the night of January 24, 1974, at Rosemary Hill Observatory. The scale is 5.2 arcmin per inch. North is at the top and east is to the left. The quasar 3C 273 is denoted by Q. The comparison star magnitudes are listed in Table 13.

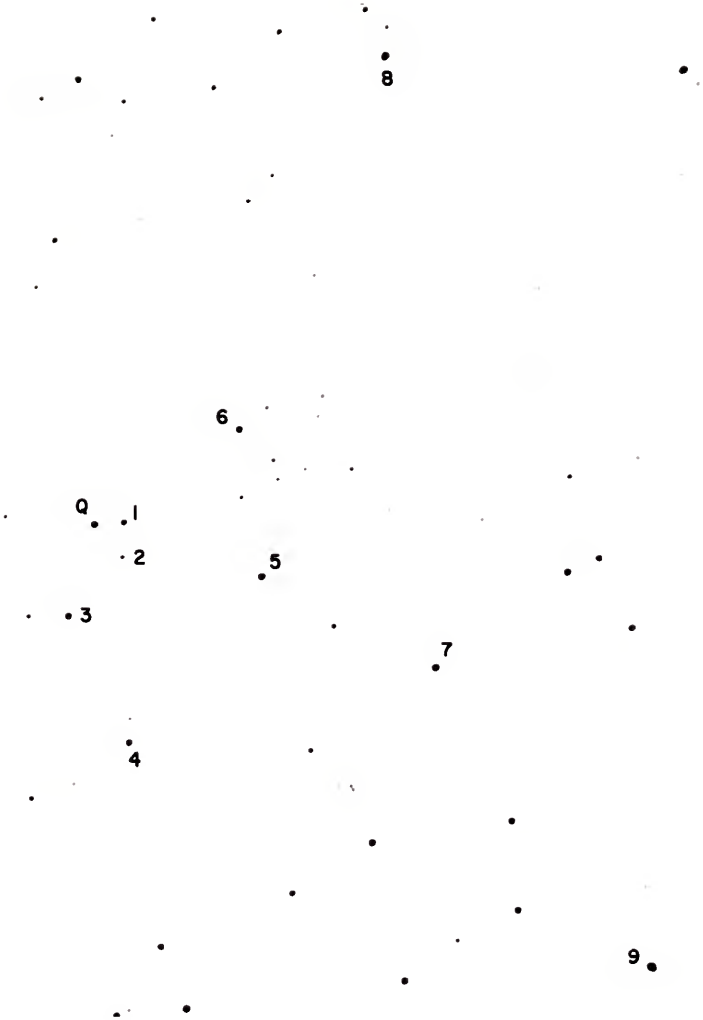
Q

Table 13

The Comparison Stars for 3C 273

Star	U	B	V
1	14.22	14.16	13.59
2	16.85	16.03	14.85
3	13.29	13.38	12.76
4	14.99	13.98	12.75
5	13.20	12.89	12.02
6	13.06	13.18	12.75
7	12.76	12.71	12.17
8	12.83	12.58	11.72
9	13.78	11.87	10.47

variable at optical wavelengths. A detailed B light curve composed of data from several sources is given by Hackney (1973) and shows the object's characteristic bursts of violent activity interspaced with apparent quiescent periods.

Figure 48 shows the Florida U, B, and V light curves of 3C 345; the corresponding color indices are shown in Figure 49. Since the outburst of 1971 a steady long-term decline in intensity is apparent in all three colors. The data suggest a minimum was reached near the end of 1973 as a slight brightening trend was seen in early 1974.

It is interesting to note that, like OJ 287, the amplitude of the variations does not appear to decrease toward longer wavelengths but at times appears as large or larger in the V as in the B. During the outburst of 1971 short-term

Figure 48. The Florida three-color light curve of 3C 345. The error bars represent twice the average rms error of a single measurement. The curves drawn through the data points are parabolic least-squares fits and suggest that 3C 345 like OJ 287 undergoes violent short-term optical activity superimposed upon a slowly varying background component.

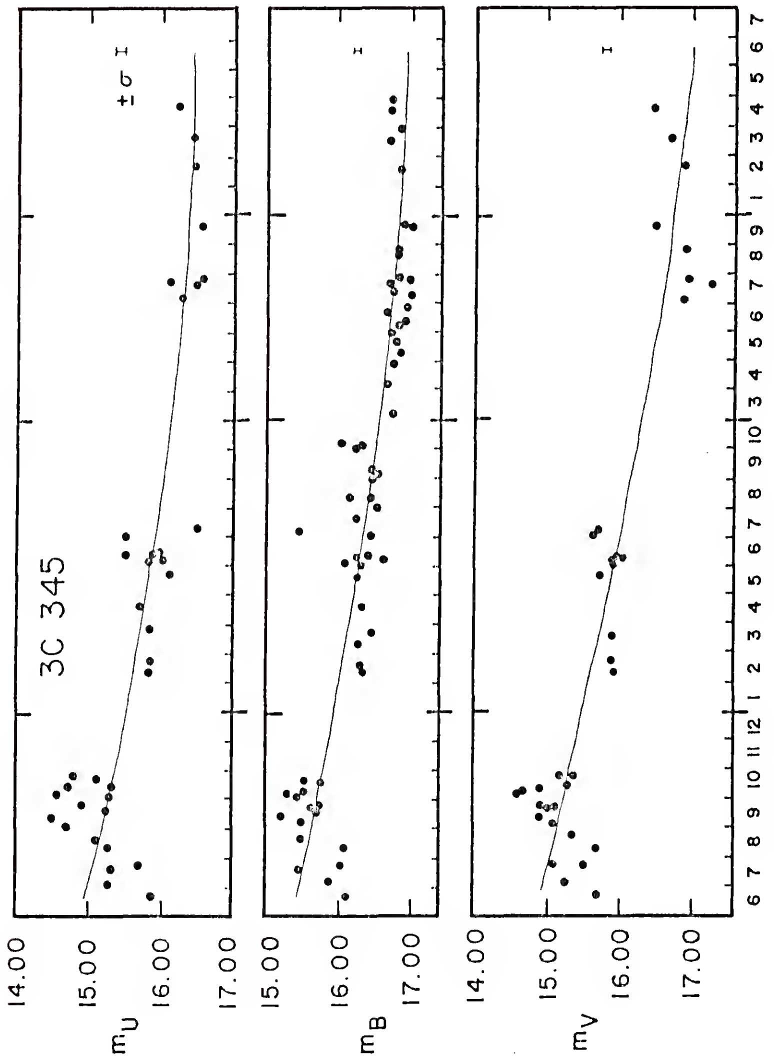
3C 345
± σ
m_U
14.00
15.00
16.00
17.00
m_B
15.00
16.00
17.00
m_V
14.00
15.00
16.00
17.00
6 7 8 9 10 11 12 1 2 3 4 5 6 7 8 9 10 3 4 5 6 7 8 9 1 2 3 4 5 6 7
1971
1972
1973
1974

Figure 49. The color indices of 3C 345 corresponding to the light curves of Figure 48. The error bars represent twice the average rms error of a single measurement. The lines drawn through the data points are least-squares fits. The line through the (U-B) data suggests no appreciable long-term color changes while the line through the (B-V) data suggests that the object has become bluer by a decrease in (B-V) of nearly $0\overset{m}{.}2$ per year.

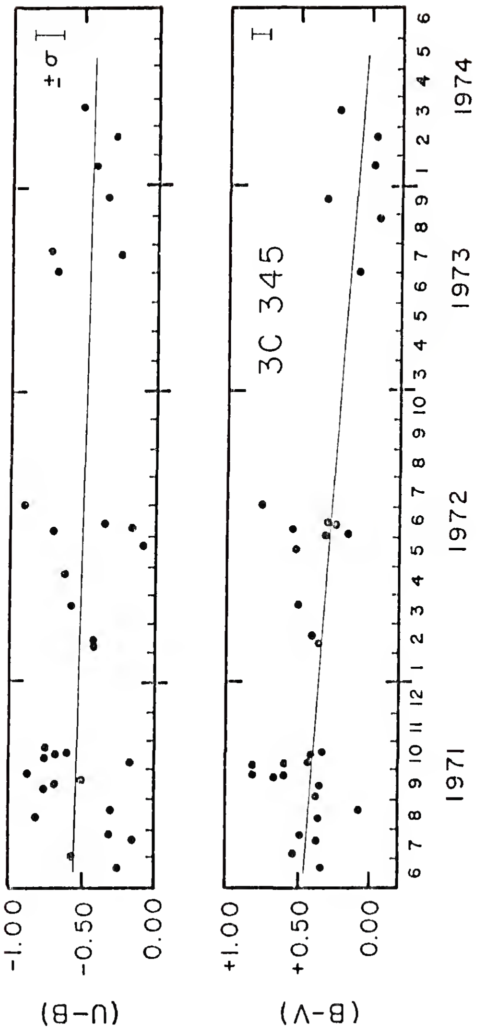
3C 345
(U-B)
-1.00
-0.50
0.00
± σ
(B-V)
+1.00
+0.50
0.00
6 7 8 9 10 11 12 1 2 3 4 5 6 7 8 9 10 3 4 5 6 7 8 9 1 2 3 4 5 6
1971
1972
1973
1974

ranges of $1\overset{m}{.}5$, $1\overset{m}{.}0$, and $1\overset{m}{.}3$ were seen in the U, B, and V respectively.

The color indices of 3C 345 appear to undergo considerable short-term changes apparently correlated with intensity variations. Short-term trends in the (U-B) index suggest that the object becomes bluer as it brightens, but in general the (B-V) index suggests that the object reddens as it brightens, analogous to OJ 287. The statistical significance of the color fluctuations of these two objects will be discussed later in this chapter.

The long-term trend in (U-B) shows a slight and hardly significant reddening as the object declines in intensity. The long-term trend in (B-V) suggests that the object has become bluer as it dimmed. Examination of the light curves does suggest that the long-term decline in intensity was greater in the V than in the B. The sequence finder for 3C 345 is given by Hackney (1973).

3C 454.3

The Florida observations of the quasar 3C 454.3 were begun in 1968 by Folsom (1970), who found it to show the least activity of the then known variables studied. Tritton and Selmes (1971) report a variation in the B of approximately $1\overset{m}{.}5$ over a period of 500 days. Sandage (1966b) reported optical variations with an amplitude of about $1\overset{m}{.}0$ between 1954 and 1965.

The author's observations of 3C 454.3 are listed in Table 8. The largest variations were observed in the V; the first two observations show a decline of nearly a magnitude in the V and about $0\overset{\mathrm{m}}{.}5$ in the U and B.

A photoelectric comparison sequence published by Angione (1971) was used for the current observations. The sequence finder for 3C 454.3 is shown in Figure 50. The magnitudes of the comparison stars are shown below in Table 14.

Table 14

The Comparison Stars for 3C 454.3

Star	U	B	V
1	17.23	16.86	15.89
2	17.93	17.02	15.67
3	15.81	15.87	15.21
4	15.25	14.71	13.78
5	16.98	16.34	15.45
6	15.89	14.89	13.75
7	15.34	15.16	14.43
8	16.66	16.08	15.29
9	15.92	15.61	14.87

PKS 2134+004

The quasar PKS 2134+004 is alternately known as Phl 61, DA 553, and OX 057. Shimmins *et al.* (1968) report an apparent brightening of $1\overset{\mathrm{m}}{.}0$ over its appearance on the Palomar Sky Survey. Medd *et al.* (1972) report an almost constant flux density at 2.8 cm and 4.5 cm during 1968, 1969, and 1970.

Figure 50. The sequence finder for the quasar 3C 454.3. This photograph is reproduced from a B plate taken on the night of October 20, 1973, at Rosemary Hill Observatory. The scale is 2.4 arcmin per inch. North is at the top and east is to the left. The quasar 3C 454.3 is denoted by Q. The comparison star magnitudes are listed in Table 14.

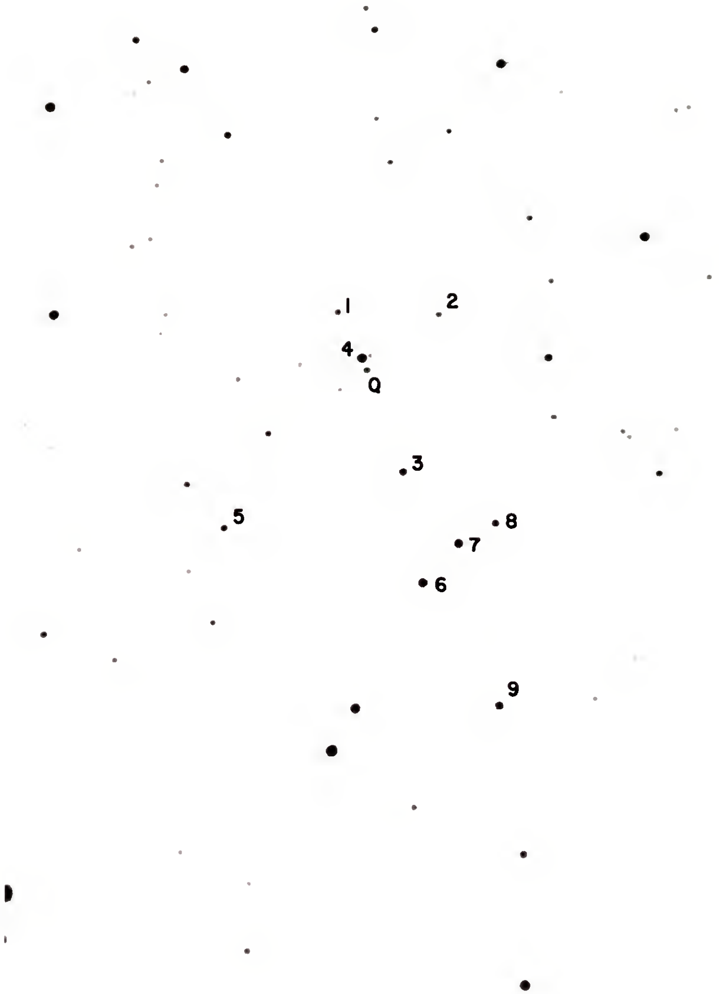
Q

The author's observations of this object are listed in Table 8.

No photoelectric comparison stars were found in the literature for color observations of 2134+004; the comparison sequence was calibrated using photographic transfers from M 15 and the photometry of Sandage (1970). The U calibration plate was taken on September 15, 1974, the B on July 27, 1974, and the V on August 17, 1974. The sequence finder for 2134+004 is shown in Figure 51; the magnitudes of the comparison stars are listed below in Table 15.

Table 15

The Comparison Stars for PKS 2134+004

Star	U	B	V
1	18.64	18.17	17.19
2	17.80	17.46	16.25
3	17.43	16.89	15.62
4	16.16	16.01	14.75
5	18.12	18.21	17.19
6	16.59	17.09	16.55
7	18.82	18.03	16.96
8	18.05	17.85	16.99
9	18.45	17.61	16.06
10	15.18	14.62	13.47

4C 05.34

The quasar 4C 05.34 is of special interest, as it has the largest redshift of the objects included in this study

Figure 51. The sequence finder for the quasar PKS 2134+004. This photograph is reproduced from a B plate taken on the night of October 5, 1972, at Rosemary Hill Observatory. The scale is 2.4 arcmin per inch. North is at the top and east is to the left. PKS 2134+004 is denoted by Q. The comparison star magnitudes are listed in Table 15.

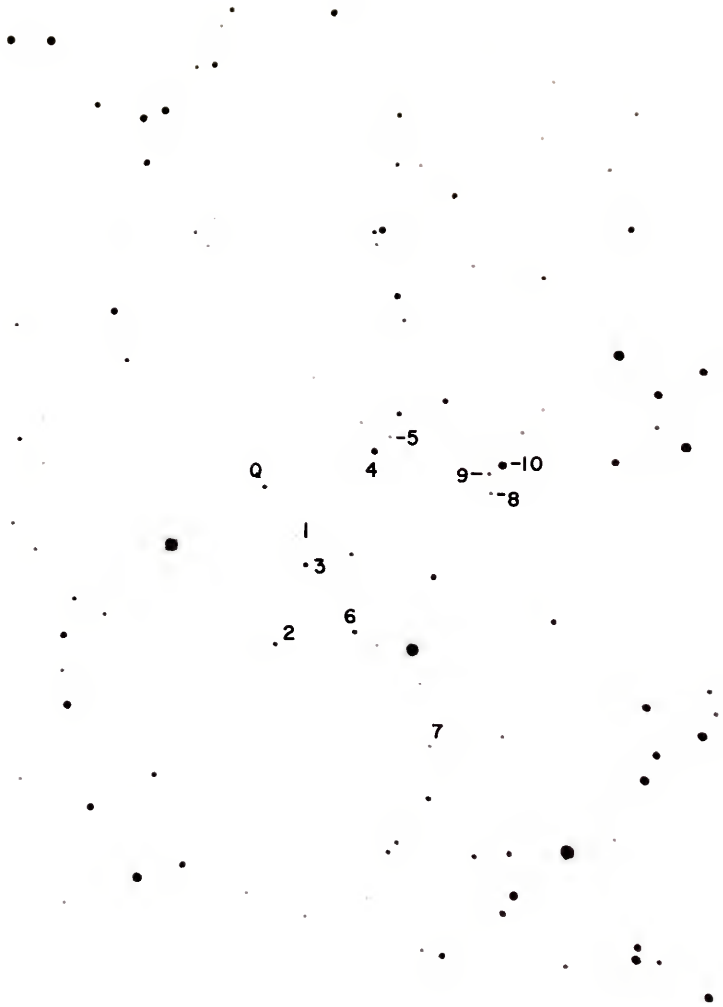
Q
4
-5
9-
-10
-8
1
3
6
2
7

and may be one of the most distant objects yet observed. At the present its redshift of 2.877 is surpassed only by that of OH 471 (Carswell and Strittmatter 1973) and OQ 172 (Wampler et al. 1973) which have redshifts of 3.40 and 3.53, respectively. The optical counterpart of 4C 05.34 was identified by Wills and Bolton (1969). The extreme distance of the object, combined with its apparent magnitude of about 18.0, suggests that it ranks among the most luminous of the quasar-like objects.

Observations of 4C 05.34 by Hackney et al. (1972a) and Scott et al. (1973) show no large short-term optical fluctuations but suggest that the object undergoes long-term low amplitude variations of about $0^{m}.1$ per year.

The author's U and B observations of 4C 05.34 are listed in Table 8. A chi-squared test indicates a confidence level for variability of 0.00 percent in the U and 25 percent in the B with no significant fluctuations in the (U-B) color index.

No photoelectric comparison stars were found in the literature for color observations of 4C 05.34; the comparison sequence was calibrated using photographic transfers from M 67 and the photometry of Johnson and Sandage (1955). The U calibration plate was taken on March 17, 1974, and the B calibration plate was taken on February 13, 1974. The faintness of the object puts it at about the practical limit for calibrating in the U, B, and V using the 30-inch reflector; a V calibration was not obtained. The sequence finder for

4C 05.34 is shown in Figure 52; the magnitudes of the comparison stars are listed below in Table 16.

Table 16

The Comparison Stars for 4C 05.34

Star	U	B
1	18.31	17.75
2	18.46	18.29
3	18.08	17.87
4	18.25	18.17
5	18.42	18.25
6	18.36	18.11
7	18.19	17.95
8	18.54	18.31
9	18.23	18.07
10	18.39	18.20

Color Variations of the Florida Objects

Table 17 shows the estimated maximum short-term ranges in UBV magnitudes and (U-B) and (B-V) color indices of the Florida objects. The ranges were estimated by examining all of the Florida observations of an object and estimating the maximum short-term excursions in magnitude and color that could occur within an arbitrarily selected time of four months.

The largest ranges in color were encountered during bursts of short-term optical activity. However, the largest

Figure 52. The sequence finder for the quasar 4C 05.34. This photograph is reproduced from an m_{pg} plate taken on the night of March 5, 1972, at Rosemary Hill Observatory. The scale is 2.4 arcmin per inch. North is at the top and east is to the left. The quasar 4C 05.34 is denoted by Q. The comparison star magnitudes are listed in Table 16.

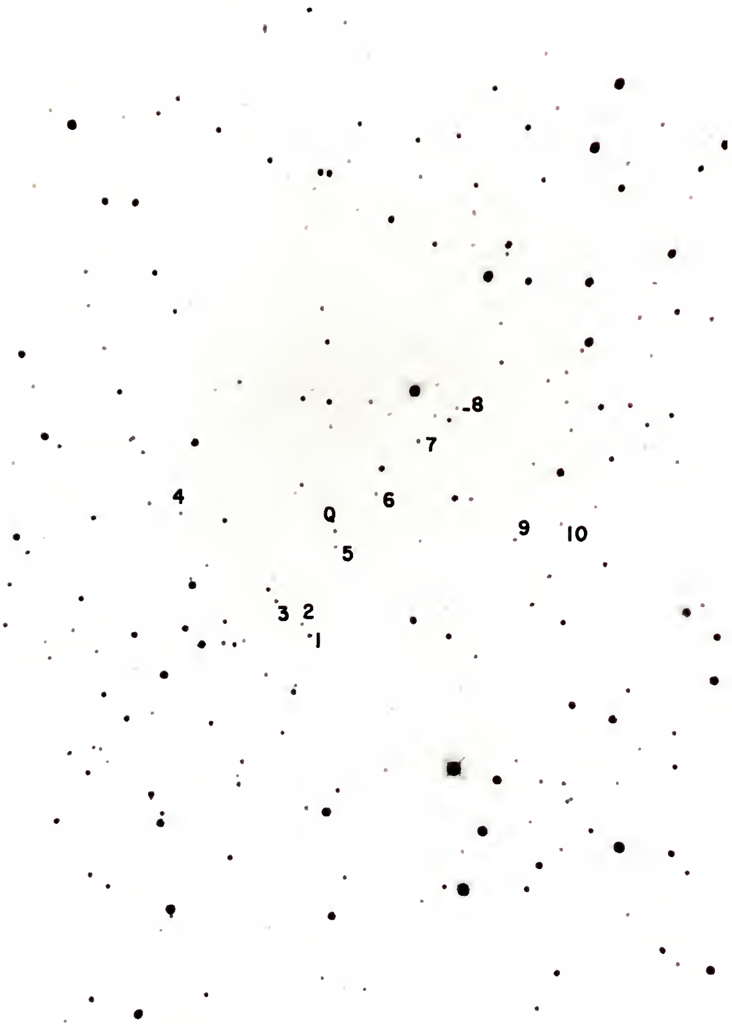
8
7
4
6
Q
5
9
10
3
2
1

Key to Table 17

Under each heading the first number in parentheses is the number of observations used for each estimate. The second number is the observed short-term range in magnitude or color index; the third number is the average rms error of a single measurement.

Table 17

The Observed Short-Term Ranges in Magnitude and Color of the Florida Objects

Object	Range in U		Range in B		Range in V		Range in (B-V)		Range in (U-B)	
3C 120	(15)1.08	0.15	(51)0.47	0.08	(15)0.22	0.12	(15)0.35	0.14	(13)0.93	0.17
3C 390.3	(6) 0.62	0.18	(6) 0.51	0.07	(5) 0.39	0.04	(5) 0.69	0.08	(5) 0.57	0.17
BL Lac	(55)1.86	0.14	(59)1.69	0.07	(59)1.31	0.09	(59)0.82	0.11	(55)1.35	0.16
OJ 287	(63)0.96	0.16	(74)0.95	0.23	(65)1.01	0.13	(58)0.60	0.26	(55)0.75	0.28
3C 273	(3) 0.41	0.26	(4) 0.52	0.12	(4) 0.36	0.13	(4) 0.19	0.17	(3) 0.22	0.29
3C 345	(36)1.31	0.18	(65)0.90	0.10	(36)1.17	0.10	(32)0.70	0.14	(31)0.80	0.21
3C 454.3	(5) 0.69	0.20	(7) 0.41	0.10	(4) 0.84	0.09	(4) 0.61	0.13	(5) 0.28	0.22
2134+004	(5) 0.39	0.40	(6) 0.26	0.13	(5) 0.14	0.08	(5) 0.31	0.15	(4) 0.71	0.41
4C 05.34	(4) 0.07	0.10	(3) 0.07	0.08	no data		no data		(3) 0.05	0.13

variations in magnitude and in color index were not necessarily correlated. Table 17 does suggest a rough correlation between the range of short-term optical variability and the range of fluctuation in color index. However, it must be remembered that the data are weighted by a selection effect; the more active objects have been monitored much more frequently than the less active ones.

With the exceptions of OJ 287, 3C 345, and 3C 454.3 the apparent short-term fluctuations in (U-B) and (B-V) color indices suggest that an increase in optical intensity results in the optical spectrum becoming flatter or bluer, and as the intensity declines the spectrum becomes steeper or redder. The (U-B) index of all the objects follows this trend but the (B-V) index of the above three objects suggests that their optical activity in the V may be equal to or more vigorous at times than that at blue wavelengths. If this effect is real it suggests that as their intensity fluctuates the amplitude does not decrease toward longer wavelengths as with the rest of the objects.

The infrared observations of BL Lac and OJ 287 both show less activity than in the other three colors. By contrast, 3C 120 shows quite vigorous infrared activity which is at times as great as that observed at blue wavelengths. Due to the color trends suggested by the OJ 287 data, large infrared variations might be expected for this object also. Other astronomers working at longer wavelengths than the Florida observations have reported such variations, which will be discussed in the next section.

No significant color variations were observed for 3C 273, 2134+004, and 4C 05.34. Of those objects showing significant variations 3C 120 showed marginal evidence for variability in (B-V) and 3C 454.3 showed no significant variation in (U-B). However, even when statistical support is lacking, the apparent variations follow the previously discussed trends.

A possible long-term color change is suggested by the (B-V) data of 3C 345. During the decline in intensity shown in Figure 48 the object appears to have become bluer by a decrease in (B-V) of about $0\overset{\mathrm{m}}{.}2$ per year. No significant long-term change was observed in (U-B).

Attempts to correlate fluctuations in color index with short-term optical variations in order to determine the statistical confidence of the previously described color trends have been made by Hackney (1973) and the author. Though the correlations in many instances support the observed trends, statistical support is at best marginal and yields a 50 percent confidence level for the reality of the trends. The author's investigations of the apparent color trends of OJ 287 and 3C 345 are discussed in the next section.

The Short-Term Color Trends of OJ 287 and 3C 345

The large V fluctuations exhibited by the lacertid OJ 287 and the quasars 3C 345 and 3C 454.3 set them apart from the other objects of this study. The Florida observations of 3C 454.3 are sparse but large variations in the V are seen on plates with low standard error.

Although there appears to be no significant long-term trends in the color indices of OJ 287, the short-term optical fluctuations apparently superimposed upon a slowly varying background component suggest that the optical intensity of this object might arise from two separate mechanisms, each capable of producing different color effects. To test this hypothesis the least-squares curves shown in Figure 43 were fitted through the data points in order to remove the long-term decline in magnitude. The U, B, and V residuals about these least-squares curves were used to compute normalized color indices with the long-term component subtracted out.

Figure 53 shows the normalized OJ 287 (U-B) index plotted versus normalized m_U, and the normalized (B-V) index plotted versus normalized m_V. Superficially the plots appear to show definite trends which if real would be highly significant. The slopes of the least-squares lines through the data points in Figure 53 appear to confirm that the largest optical fluctuations of OJ 287 take place in the U and V rather than decreasing toward longer wavelengths.

Figure 54 shows similar normalized plots for 3C 345. Unlike the unnormalized plots for OJ 287, which show no correlation between magnitude and color, a strong hint of the relations suggested by Figure 54 is present in the unnormalized 3C 345 data. Perhaps the greater decline in intensity of OJ 287 has completely "washed out" such trends from the raw data.

Figure 53. The normalized color regression plots of OJ 287; the long-term decline in intensity has been removed. The error bars represent twice the average rms error of a single measurement. The correlation coefficients of the least-squares lines are denoted by r. The slopes of the lines suggest that a brightening of $1\overset{\mathrm{m}}{.}0$ in V is accompanied by an increase or reddening in (B-V) of $0\overset{\mathrm{m}}{.}25$, and that a brightening of $1\overset{\mathrm{m}}{.}0$ in U is accompanied by a decrease or blueing in (U-B) of $0\overset{\mathrm{m}}{.}4$.

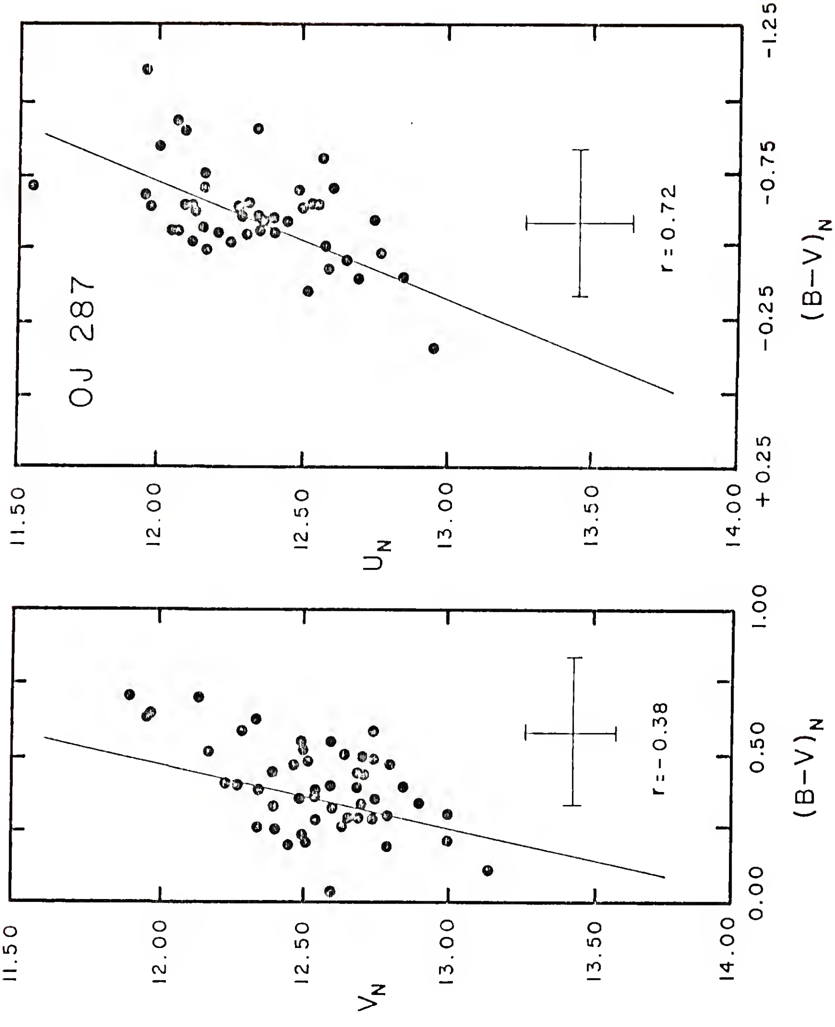
OJ 287
r = 0.72
U_N
11.50
12.00
12.50
13.00
13.50
14.00
+0.25
−0.25
−0.75
−1.25
$(B-V)_N$
r = −0.38
V_N
11.50
12.00
12.50
13.00
13.50
14.00
0.00
0.50
1.00
$(B-V)_N$

Figure 54. The normalized color regression plots of 3C 345; the long-term decline in intensity has been removed. The error bars represent twice the average rms error of a single measurement. The correlation coefficients of the least-squares lines are denoted by r. The slope of the lines suggests that a brightening of $1^{m}.0$ in V is accompanied by an increase of reddening in (B-V) of $0^{m}.30$, and that a brightening of $1^{m}.0$ in U is accompanied by a decrease or blueing in (U-B) of $0^{m}.45$.

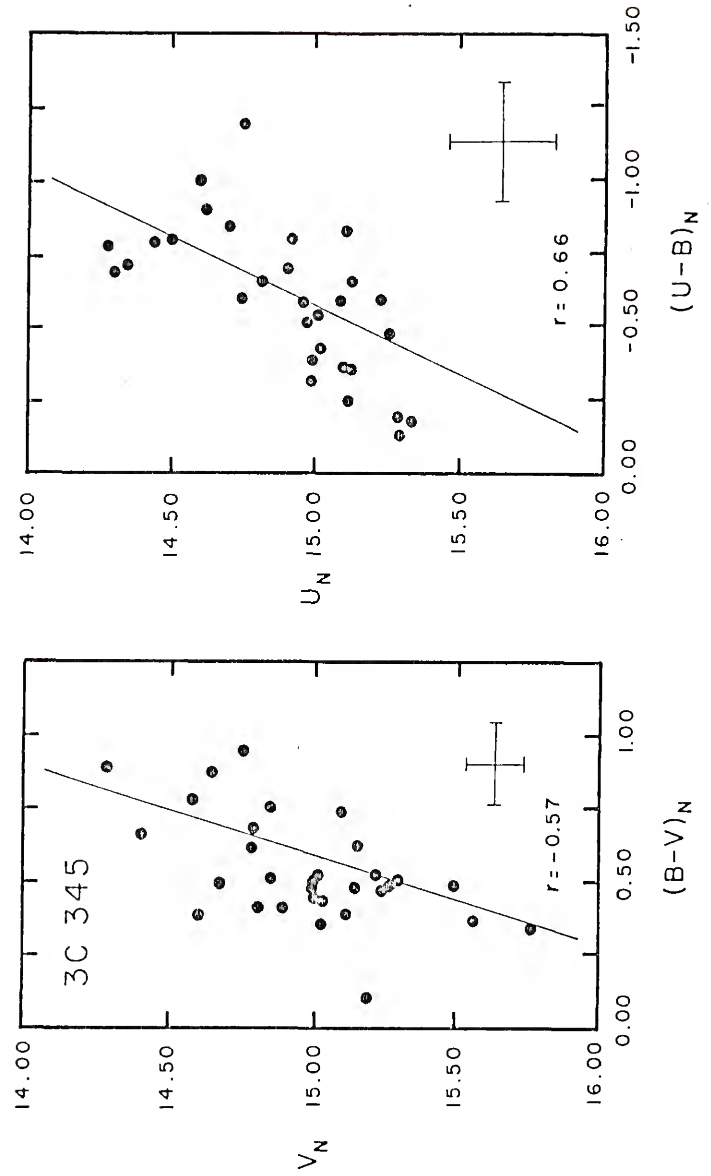
3C 345
r = -0.57
V_N
(B-V)_N
14.00
14.50
15.00
15.50
16.00
0.00
0.50
1.00
r = 0.66
U_N
(U-B)_N
0.00
-0.50
-1.00
-1.50

A cautionary note is now in order. Superficially the plots appear to show definite trends which confirm those suggested by visual examination. Unfortunately, the observed effects for both objects are hardly significant in terms of the error bars shown in Figures 53 and 54. In addition, U and (U-B) are not independent variables; neither are V and (B-V). The above difficulties leave the author unconvinced of the reality of the color trends. However, it is felt that the above investigation deserves additional study. Visvanathan (1973) points out the close similarity of OJ 287 to the OVV quasars 3C 279, 3C 345, 3C 454.3 and 3C 446 in such properties as their variability, nonthermal continuum with variable polarization, star-like images and inverted radio spectra. Also, there is other evidence that the slope of the optical continuum of QSOs may not necessarily flatten as they brighten. The spectra of 3C 446 and 3C 279 were observed to become redder as the objects dimmed, but an earlier observation of 3C 446 had shown its spectrum to be much bluer at a time when the object's intensity was less (Oke 1967). This suggests that the slope of the optical continuum may not be simply correlated with brightness. Furthermore, three simultaneous U and V observations of OJ 287 made on September 22, October 27, and October 28 of 1971 by Dyck et al. (1971) show short-term variations with the largest amplitude in the V.

Evidence that the expanding source model (Vander Laan 1966), which predicts a decrease in the amplitude of variations with increasing wavelength, may not apply to OJ 287 is reported by Kinman _et al_. (1974). Observations of OJ 287 at 11.1, 4.5, 3.7, 0.95, and 0.35 cm and 0.44μ showed little difference in the variations of the long-term component. Though the short-term variations were not resolved in time, the delay between variations at different wavelengths predicted by the Vander Laan model was not seen and it was concluded that the expanding source model may not be applicable.

Hackney (1973) describes a spectral model to explain the apparent flattening of the optical spectrum of BL Lac as its optical intensity increased. This model assumed a steep infrared spectral component showing little or no short-term activity and a less steep variable synchrotron component. Their resultant is concave up. As the variable component increases in intensity the spectrum flattens out; the greatest flattening occurs at longer wavelengths, causing the greatest variations in intensity to occur at shorter wavelengths.

The shape of the continuum of OJ 287 is quite different from that of BL Lac; the spectral index of OJ 287 is approximately equal to 1.0, much flatter than the values of 2.85 to 3.17 of BL Lac, which has the steepest continuum of any OVV (Visvanathan and Elliot 1973). Rieke and Kinman (1974) report that the spectrum of OJ 287 appears to have positive curvature and becomes flatter as one goes from the optical to the infrared.

It is conceivable that the optical variations at long wavelengths could be as great or greater than those at short wavelengths if the optical spectrum were convex at low intensities but became more linear as the intensity increased. This is illustrated in Figure 55. The curve represents the resultant of the synchrotron component and a hypothetical thermal component whose energy distribution peaks in the middle of the optical spectrum. Such an energy distribution is produced by a blackbody at approximately 6000°K, which is also a good approximation of the solar energy distribution. The centers of the color band passes used in this study are denoted by U, B, and V. The two vertical lines delimit the optical portion of the spectrum. It is assumed that as the synchrotron component increases in intensity it swamps out the thermal component and the spectrum can then be described by a simple power law. Visvanathan (1973) observed the spectral energy distribution of OJ 287 from 0.33μ to 1.0μ on January 18, 19, 20, and 21 of 1972 and found it could be represented by a straight line of slope 1.248 in a log F_ν versus log ν plot. Florida observations show that not only was the object near its maximum long-term brightness level but that it was undergoing a short-term flare at this time. Assuming that the spectrum does become more linear at high intensities the apparent fluctuations in intensity will be greatest in the V and U, the "hump" in the middle of the spectrum having been overpowered.

It is difficult to visualize how a separate infrared component like the one described by Hackney for BL Lac could be included in the model for OJ 287. Such a component would

Figure 55. A model to explain the color trends suggested by OJ 287 and 3C 345. The heavy black lines represent a variable synchrotron continuum which varies in intensity without changing slope. The synchrotron line at the bottom has added to it a hypothetical thermal continuum; the resultant is convex in the optical region. The centers of the spectral band passes used in this study are denoted by U, B, and V. As the synchrotron component increases in intensity it overpowers the thermal component and the spectrum becomes linear. The greatest intensity variations will take place in the U and V.

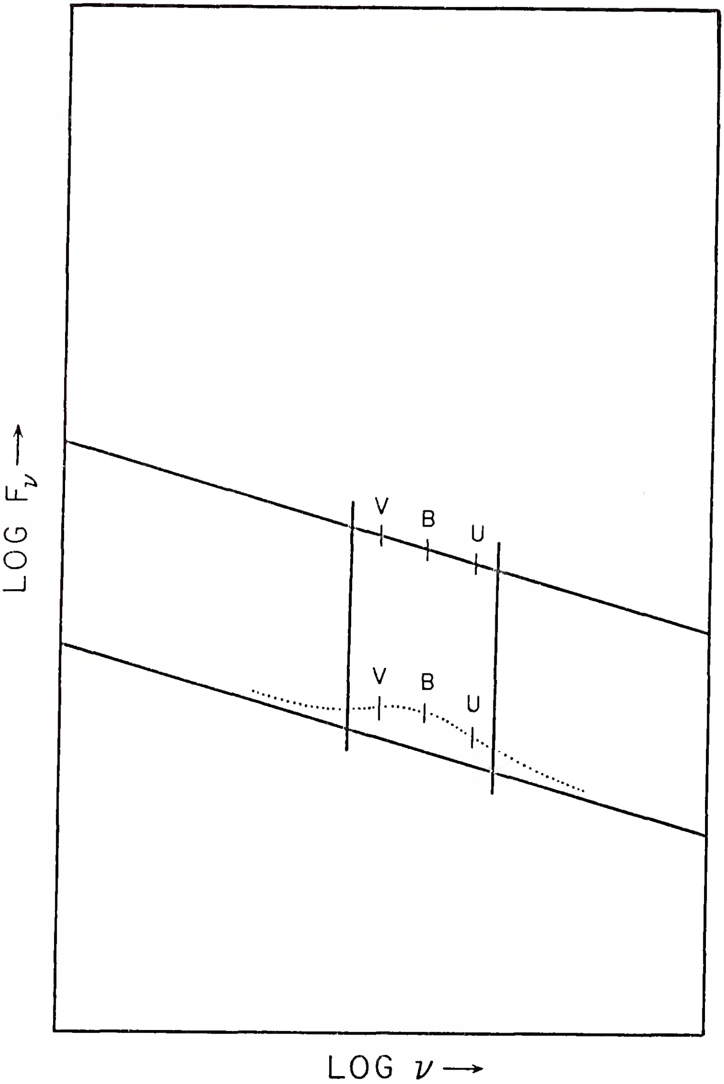
LOG F_ν →
V
B
U
V
B
U
LOG ν →

cause the spectrum to rise steeply from the optical into the infrared and be concave. Kinman et al. (1974) report that the behavior of the optical polarization of 3C 345 and OJ 287 is very similar; they both tend to show sudden changes from a smooth trend and then return to the original value. Observations at 3.7 cm show similar behavior and Kinman et al. conclude that this suggests a similar emission mechanism at different wavelengths in OJ 287 and 3C 345. The author concludes that the infrared spectrum of OJ 287 is most likely a smooth continuation of the optical spectrum and arises from the same cause. This is further substantiated by Rieke (1972), who reports variations in OJ 287 at 2.2, 3.5, 5, and 10μ which are correlated with optical variations, and by Rieke and Kinman (1974), who report that the long-term decline of OJ 287 at 10.5μ and 0.44μ has been approximately the same. As mentioned previously, Florida observations of OJ 287 have shown a less rapid long-term decline in the infrared than at optical wavelengths. However, the Florida observations were made at the much shorter wavelength of 0.82μ and the slope of the Florida long-term decline is very dependent upon a single observation made in early 1973.

There are obvious difficulties with the author's model. One of them is the source of the thermal component. A possible clue is provided by Oke and Sargent (1968), who report on the energy distribution of the nucleus of NGC 4151, a variable Seyfert galaxy. After subtracting out the emission lines from the spectrum of the galaxy a spectrum was obtained which resembled a straight synchrotron spectrum except for a hump in the ultraviolet believed to be caused by a thermal component generated by bound-free and free-free hydrogen recombination.

The position of the thermal component in the optical spectrum (i.e., its temperature) is very critical. For the correct results the peak of its energy distribution must be located at the shorter wavelengths or in the middle of the optical spectrum. It is interesting to note that a thermal component peaking toward long optical wavelengths will allow the largest variations to take place at shorter wavelengths, analogous to the variations exhibited by BL Lac. Another source of the thermal component might be an envelope of stars surrounding the active region; in the case of OJ 287 the spectral lines would be washed out by the strong nonthermal component.

Other difficulties arise when the spectra of OJ 287 and 3C 345 are compared. Unlike the featureless spectrum of OJ 287, which flattens out toward longer wavelengths, the spectrum of 3C 345 rises steeply into the infrared (Oke _et al_. 1970). Oke _et al_. also report that the short-term variations in 3C 345 take place with little obvious change in the shape of the visual energy distribution. However, the magnitudes of the suggested color effects are not large and the observed color fluctuations take place over a short interval of time. The observations of Oke _et al_. were made over a number of years and most likely were measuring intensity changes of the long-term component.

Though the color trends in Figures 53 and 54 are statistically unconvincing, it is concluded that the observational similarities of OJ 287 and 3C 345 suggest that these two objects, perhaps along with 3C 454.3, may have similar mechanisms for the generation of energy and are quite possibly more closely related to each other than to the other objects studied.

Possible Relationships Between Classes of Objects

The observed similarities between the nuclei of Seyfert galaxies, N galaxies and QSOs hint that these objects may somehow be related or perhaps represent different aspects of the same phenomenon. Generally Seyfert and N type galaxies fall intermediate in color characteristics between QSOs and normal galaxies. This suggests that peculiar galaxies may represent a transitory stage between QSOs and galaxies such as the Milkey Way.

It is felt that the strongest evidence for kinship among the objects studied exists for OJ 287 and 3C 345. As has been pointed out, OJ 287 resembles the OVV quasar 3C 345 much closer in observed characteristics than it does its fellow lacertid BL Lac. This suggests that OJ 287 and BL Lac may really represent two classes of objects, their lineless spectra arising from unusually strong nonthermal emission in their active regions. In all characteristics except its lineless spectrum OJ 287 resembles a typical OVV quasar, while BL Lac more closely resembles the peculiar galaxies; this observation is further strengthened by the determination of a redshift of 0.07 for the envelope of BL Lac by Oke and Gunn (1974). This redshift is compatible with those measured for Seyfert and N galaxies. No envelope has ever been observed for OJ 287; it has a completely starlike image like that of 3C 345.

Figure 56 shows the Florida objects plotted on the color-color diagram described in Chapter I. The positions of the objects were determined using average color values from Florida data. Due to the short-term variations in color intrinsic in several of the objects, their positions on the diagram may shift significantly in a period of days or weeks. However, the large number of observations of OJ 287, 3C 345, 3C 120, and BL Lac have enabled average values for their colors to be determined with a fair degree of accuracy; the long-term trend suggested for 3C 345 will not shift the object appreciably on the diagram. The large difference in color between OJ 287 and BL Lac is readily apparent in Figure 56 and does suggest that BL Lac is more closely related to the variable Seyfert N galaxies than to the OVV quasars.

No significant evidence for evolutionary trends was found by the author when comparing the colors and characteristics of variability of the objects in this study. The peculiar object BL Lac, having one of the lowest redshifts,

Figure 56. The positions of the objects used in the color study on a color-color diagram. Average values of their colors obtained from Florida data were used to plot their positions. The regions normally occupied by QSOs, Seyfert galaxies, and N galaxies are denoted by Q, S, and N, respectively. Because of the large number of color observations of 3C 345, OJ 287, BL Lac and 3C 120 their positions are probably determined most accurately. The (B-V) index of the N galaxy 3C 390.3 places it in the region normally reserved for Seyfert galaxies, but the class regions are not rigid boundaries and the Florida average value of 0.58 agrees with that found in the literature. The key to the Florida objects is given below.

(1) 3C 120
(2) 3C 390.3
(3) BL Lac
(4) 3C 273
(5) 3C 345
(6) 3C 454.3
(7) PKS 2134+004
(8) 4C 05.34
(9) OJ 287

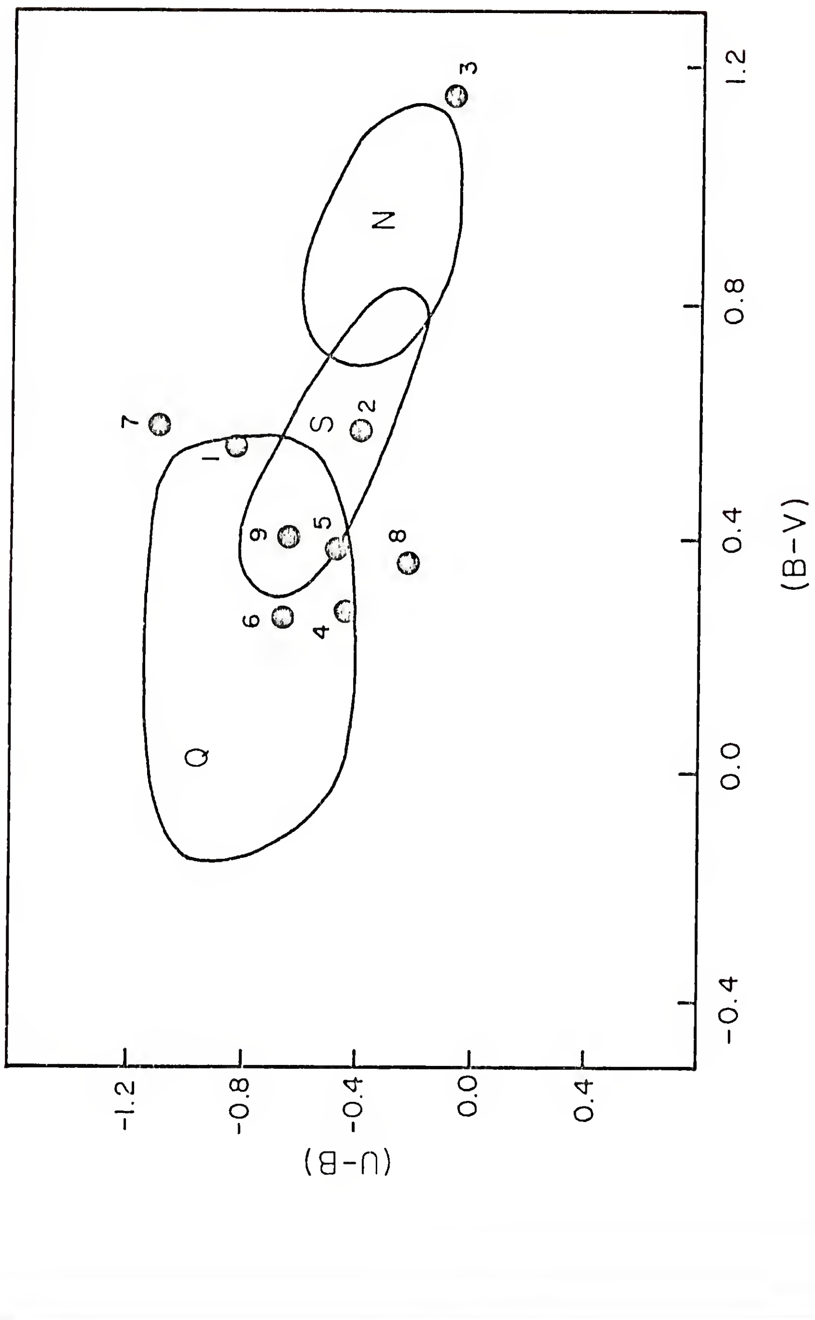
(U-B)
-1.2
-0.8
-0.4
0.0
0.4
(B-V)
-0.4
0.0
0.4
0.8
1.2
Q
S
N
1
2
3
4
5
6
7
8
9

exhibited the largest short-term activity of any of the objects studied. The two most distant objects, PKS 2134+004 and 4C 05.34, did not exhibit any significant variability, but there are not enough data to suggest a decrease in activity with an increase in redshift. It is suggested that OH 471 and OQ 172, the objects with the largest known redshifts at this date, should be monitored to investigate the possibility of a relationship between variability and redshift. If high-redshift objects were in general to show less variability than those of moderate redshift such as 3C 345, it might imply that variability was an evolved characteristic; the high-redshift objects presumably are seen at an earlier epoch in the age of the universe.

It is felt that the most significant result of the comparison of the various classes of objects is the apparent kinship of 3C 345 and OJ 287. The observational differences between BL Lac and OJ 287 suggest that they represent different classes of objects, their line-free spectra and violent optical activity being their most similar characteristics. The great similarities between classes of objects are obvious, but whether they represent different evolutionary stages or are merely different aspects of the same phenomenon remains unsolved.

The Color-Redshift Relation for Quasi-Stellar Objects

The color-redshift relation for quasi-stellar objects has been well established; McCrea (1966) showed that a correlation exists between the (U-B) and (B-V) color indices of quasars and their redshifts. McCrea's results were verified by similar studies performed independently by Kardashev and Komberg (1966) and Barnes (1966). The purpose of the author's color redshift investigations was to search for an evolutionary component in the color-redshift relation which might be distinguished from the reddening caused by cosmological recessional velocities.

Sandage (1966c) found that the correlation of the colors of 43 QSOs with their redshifts could be approximated by the shifting of an assumed universal continuum energy distribution across the U, B, and V spectral band passes. Strittmatter and Burbidge (1967) argue that the nonredshifted continuum is not unique and that the observed correlation is the result of various emission lines shifted through the UBV band passes.

Goldsmith (1972) checked the theoretical curves of Sandage, and of Strittmatter and Burbidge, with a much larger sample of objects using U, B, and V colors from a catalog of quasars published by De Veny *et al*. (1971). Goldsmith concluded that the theoretical curves of Strittmatter and Burbidge were a better fit to the data than those of Sandage. Figure 57 shows the plots made by Goldsmith. The five quasars studied by the author have been added; they are represented by circles. The first three objects showed significant short-term color variations; the observed ranges of these variations are indicated by the bars. The redshift range has been extended upward from Goldsmith's original plot so that the high-redshift quasar 4C 05.34 could be added. The dotted line represents the theoretical curve of Sandage; that of Strittmatter and Burbidge is represented by the solid line.

In general, the Florida objects appear roughly to fit the general trend of the data. The position of 4C 05.34 lies beyond the range of the theoretical curves, which were computed only up to a redshift of 2.2. It is suggested that the high-redshift trend of the K correction is represented by 4C 05.34.

The intrinsic variations in the colors of the first three Florida objects make it difficult to choose which of the theoretical curves they best fit. Similar color variations in the objects from the catalog of De Veny _et al_. probably contribute significantly to the large scatter in the color redshift relationships. Due to the variations in color of the Florida objects it is concluded that valid color measurements of optically variable quasars cannot be made except with a large number of observations; the resulting values of the objects' colors will be average values. It is further concluded that the color variations observed for the Florida objects are probably typical of objects showing similar optical variability. The resulting scatter in Figure

57 would probably mask any evolutionary trend significantly different from the theoretical reddening curves. The author therefore concludes that no evidence for evolutionary trends can be detected in the color-redshift relation for quasars.

Figure 57. The observed correlations between the color indices of quasars and their redshifts. The solid dots are from a catalog of quasars by De Veny *et al.* (1971). The five quasars studied by the author are represented by open circles; those showing short-term color variations have their observed color ranges indicated by bars. Average colors from Florida data were used to plot the Florida objects. Objects 1, 2, and 3 are also listed in the catalog by De Veny *et al.* The theoretical curve of Sandage (1966c) is represented by the dotted line and that of Strittmatter and Burbidge (1967) by the solid line. After Goldsmith (1972). The key to the Florida objects is given below.

(1) 3C 273
(2) 3C 345
(3) 3C 454.3
(4) PKS 2134+004
(5) 4C 05.34

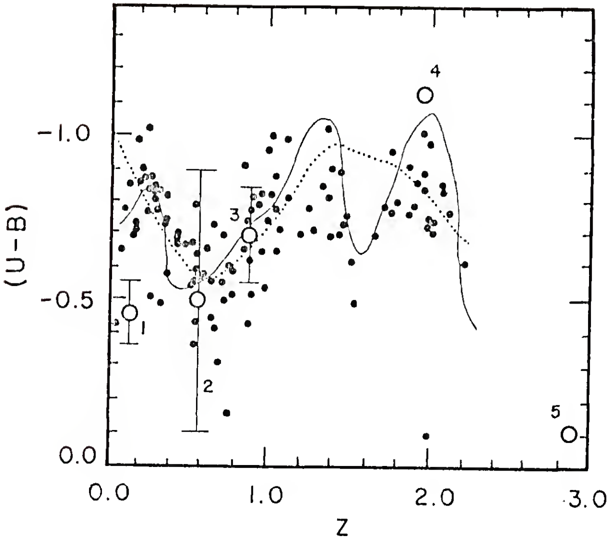
(U-B)
-1.0
-0.5
0.0
0.0
1.0
2.0
3.0
Z
1
2
3
4
5

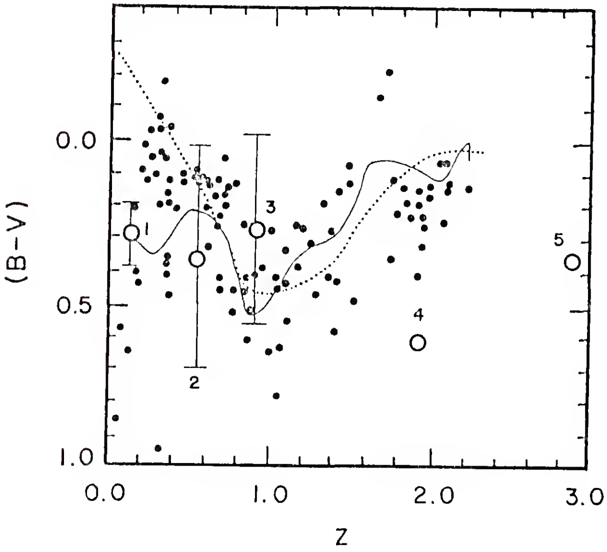
(B-V)
0.0
0.5
1.0
0.0
1.0
2.0
3.0
Z
1
2
3
4
5

CHAPTER VI

A STUDY OF THE SHORT-TERM OPTICAL ACTIVITY OF FIVE LACERTIDS

Introduction

Evidence was presented in Chapter V that lacertids are not a homogeneous class of objects, but they do have many observational similarities. Lacertids resemble quasars in their spectral energy distributions but they are distinguished from the latter objects by their featureless optical spectra and the rapidity of their violent optical fluctuations. These objects are further characterized by large intensity variations at radio wavelengths; both the radio and optical fluxes exhibit strong and rapidly varying polarization.

In order to study the rapid optical fluctuations of these objects, the lacertids PKS 1514-24 (AP Librae), ON 231 and ON 325 have been observed with a time resolution of months or days. Hackney (1973) made a study of the intraday variations of the lacertids BL Lac and OJ 287 and the Seyfert galaxy 3C 120. The time resolution was largely limited by the plate sensitivity required to obtain adequate exposures. Using the nitrogen baking procedure described in Chapter III (Scott and Smith 1974), it was felt that intraday studies could be made with an improved time resolution. The author has further studied the intraday variations of BL Lac and has attempted to detect intraday variations in the probable lacertid PKS 0735+17.

A large portion of the short-term studies made by the author and his colleagues at Rosemary Hill was a cooperative effort involving other astronomers. Visiting professors Dr. Richard L. Hackney and Dr. Karen R. H. Hackney of Western Kentucky University took most of the Rosemary Hill 18-inch plates indicated in the following sections. The Drs. Hackney were also responsible for making the final adjustments to the 18-inch reflector, allowing it to become photographically operational. On a number of nights simultaneous intraday campaigns were run on BL Lac and PKS 0735+17 with Dr. George H. Folsom and Dr. Hugh R. Miller working at Bradley Observatory of Agnes Scott College in Atlanta, Georgia. In addition, several intraday runs on PKS 0735+17 made exclusively at Bradley Observatory are included in this study.

The Optical Activity of PKS 1514-24, ON 231 and ON 325

PKS 1514-24

The optical counterpart of the radio source PKS 1514-24 was identified by Bolton *et al*. (1965a) with a 16th magnitude elliptical galaxy. Westerlund and Wall (1969) identified this object as an N-type galaxy. Searle and Bolton (1968) reported that the optical spectrum had no emission lines. Bond (1971) identified the position of the optical counterpart with the variable object AP Librae.

The rapid optical variability of PKS 1514-24 has been established by a number of observers. Biraud (1971) reports variations of $0^{\mathrm{m}}.8$ on a time scale of a few days, and a few instances where plates taken a few hours apart show fluctuations of about $0^{\mathrm{m}}.7$. Biraud also remarks on the similarities between the optical variations of PKS 1514-24 and those of BL Lac. Rodgers (1971) reports that the energy distribution of the continuous spectrum has a marked resemblance to that of BL Lac. Miller *et al*. (1975) report extremely rapid optical variability with fluctuations as great as $0^{\mathrm{m}}.5$ in 20 minutes.

The Florida light curve of PKS 1514-24 is shown in Figure 58. The closed circles represent 30-inch observations; the open circles are 18-inch observations. The light curve suggests variations of $1^{\mathrm{m}}.0$ on a time scale of a month, with the largest range of variation being about $1^{\mathrm{m}}.5$. The confidence level for variability is 99.9 percent and the average rms error is $0^{\mathrm{m}}.16$. It is concluded that PKS 1514-24 is an OVV whose variations in many ways resemble those of BL Lac but are generally of lesser amplitude.

A B-magnitude comparison sequence was established for PKS 1514-24 by a photographic transfer from SA 107, using the photometry of Purgathofer (1969). The sequence finder for PKS 1514-24 is shown in Figure 59. The magnitudes of the comparison stars were computer smoothed to correct for local

Figure 58. The Florida light curve of PKS 1514-24. The closed circles are 30-inch observations; the open circles are 18-inch observations. The error bars represent twice the average rms error of a single measurement.

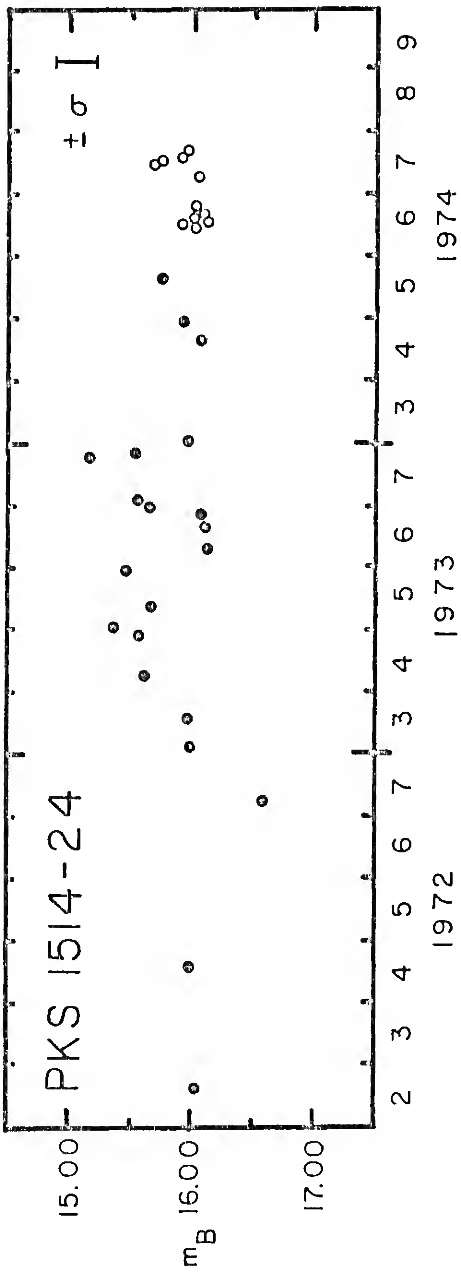
PKS 1514-24
±σ
m_B
15.00
16.00
17.00
2
3
4
5
6
7
3
4
5
6
7
3
4
5
6
7
8
9
1972
1973
1974

Figure 59. The sequence finder for PKS 1514-24. The comparison star B magnitudes were obtained by a photographic transfer from SA 107 using a plate exposed on April 10, 1973, at Rosemary Hill Observatory. This photograph is reproduced from a Rosemary Hill plate taken on April 8, 1973. The scale is 2.4 arcmin per inch. North is at the top and east is to the left. The variable source PKS 1514-24 is denoted by S. The comparison star magnitudes are as follows: (1) 15.86, (2) 13.72, (3) 15.35, (4) 16.94, (5) 16.02, (6) 14.55, (7) 14.89, (8) 16.11, (9) 14.34, (10) 14.20.

3
2
8
1
10
S
4
9
7
6
5

field errors of the 30-inch reflector. The 18-inch plates yielded satisfactory photometric results when reduced with this sequence; a separate 18-inch sequence should probably be established if more plates are taken with this instrument in the future.

ON 231

The optical counterpart of ON 231 was identified by Browne (1971) as the variable star W Coma Berenices, a $14^{m}.5$ stellar object which appears neutral in color on the Palomar Sky Survey. Browne reports that an 18th magnitude "galaxy like" object resembling a "jet" lies 12 arcsec from the main star on the Sky Survey prints. Browne also reports that the object has an inverted radio spectrum. Stull and Carpenter (1973) observed ON 231 at 8,000 MHz over a 10-month period but failed to detect any significant variations. Craine and Warner (1973) report that data on the optical variations of ON 231 are sparse, but that Wolf (1916) reported that W Coma Berenices varied from photographic magnitudes 11.5 to 14. Craine and Warner also report that later observations of this object have shown it to vary between magnitudes 13 to 15.5; the possibility of a long-term trend toward fainter magnitudes is suggested.

The Florida 2-color light curve of ON 231 is shown in Figure 60. The closed circles represent 30-inch observations, the open circles 18-inch observations. Rapid optical variations are apparent in both colors with an amplitude of about

Figure 60. The Florida B and V light curves of ON 231. The closed circles are 30-inch observations; the open circles are 18-inch observations. The error bars represent twice the average rms error of a single measurement.

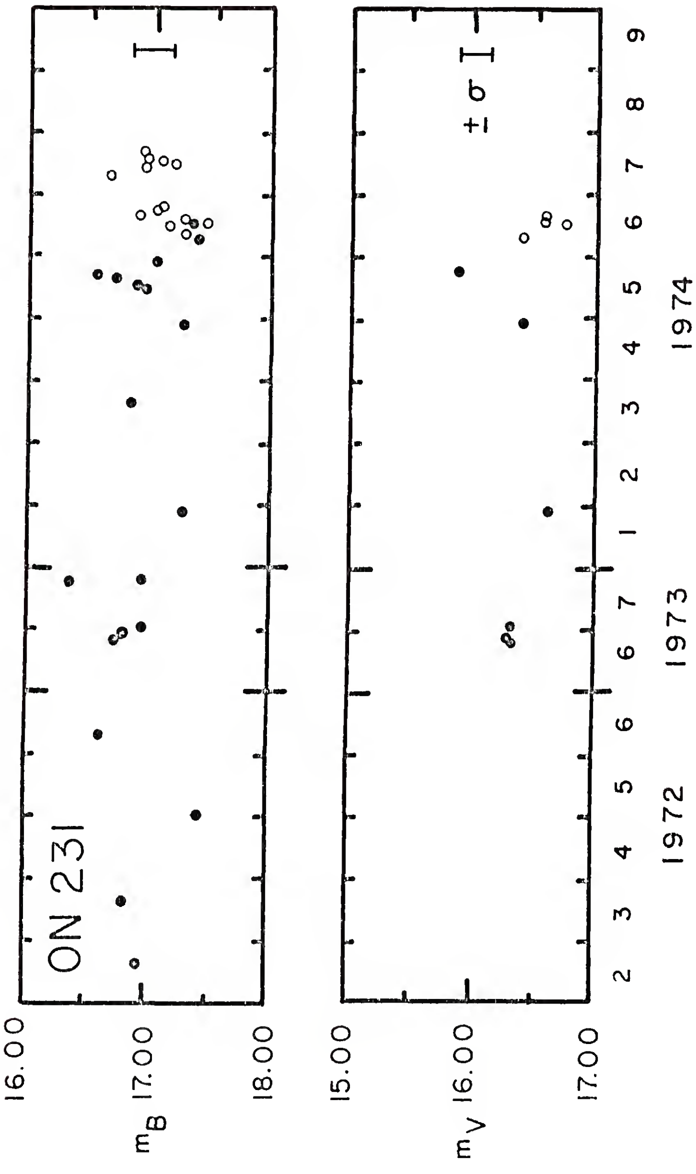
ON 231
m_B
16.00
17.00
18.00
m_V
15.00
16.00
17.00
± σ
2 3 4 5 6
1972
6 7
1973
1 2 3 4 5 6 7 8 9
1974

$1^{m}.0$ over a time scale of a month. The average B magnitude is 16.91 and the average V magnitude is 16.40, supporting the suggestion of Craine and Warner that the object's average intensity is decreasing. The confidence level for variability in both the B and V is 99.9 percent. The average rms error is $0^{m}.18$ in the B and $0^{m}.14$ in the V. It is concluded that ON 231 is an OVV whose short-term optical fluctuations appear similar to those of PKS 1514-24.

Comparison sequences for ON 231 were established by computer smoothing B and V photoelectric sequences published by Wing (1973), to correct for field errors of the 30-inch reflector. The 18-inch plates were reduced satisfactorily with this sequence; an 18-inch sequence should be established whenever a suitable number of plates have been taken. The sequence finder for ON 231 is shown in Figure 61. The magnitudes of the comparison stars are shown below in Table 18.

Table 18

The Comparison Stars for ON 231

Star	B	V
1	12.72	12.15
2	17.01	16.66
3	14.43	13.46
4	17.52	16.79
5	16.40	14.83
6	13.63	13.01
7	16.53	15.70

Figure 61. The sequence finder for ON 231; the magnitudes of the comparison stars are listed in Table 18. This photograph is reproduced from a Rosemary Hill Observatory plate taken on July 24, 1973. The scale is 2.4 arcmin per inch. North is at the top and east is to the left. The variable source ON 231 is denoted by S.

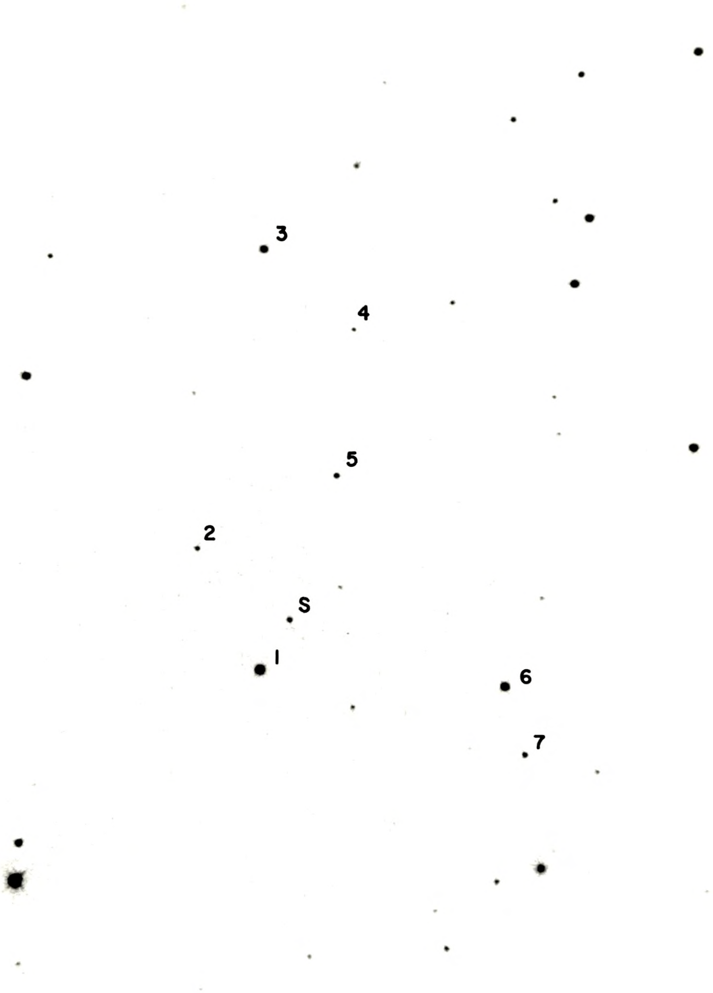
S

ON 325

The optical counterpart of this source was identified by Browne (1971) with a $14^{m}.5$ object on the Palomar Sky Survey. An alternate designation is B2 1215+30. Like ON 231, ON 325 appears neutral in color on the Sky Survey. While the image of ON 231 is completely stellar on both the red and blue Sky Survey prints, there is an indication that ON 325 is slightly non-stellar on the red print. There is also a faint nebulosity lying to the south of ON 325. ON 231 and ON 325 are in the same region of the sky, being separated by less than two degrees. Browne reports that the radio spectrum of ON 325 is relatively flat.

Lucchetti and Usher (1971) report that ON 325 is optically variable with a range of more than two magnitudes. They also report intraday variations with discernable brightness changes over time scales of hours, and long-term intensity trends on a time scale of years. The Florida two-color light curve of ON 325 is shown in Figure 62. The closed circles are 30-inch observations; the open circles are 18-inch observations. The B light curve is most complete; it suggests that the object's optical intensity remained relatively constant during 1972 and 1973, declined to a minimum in late April of 1974 and then rapidly returned to its previous intensity level. The confidence levels for variability are 99.9 percent in the B and 99.5 percent in the V. The average rms error is $0^{m}.12$ in both colors.

Figure 62. The Florida B and V light curves of ON 325. The closed circles are 30-inch observations; the open circles are 18-inch observations. The error bars represent twice the average rms error of a single measurement.

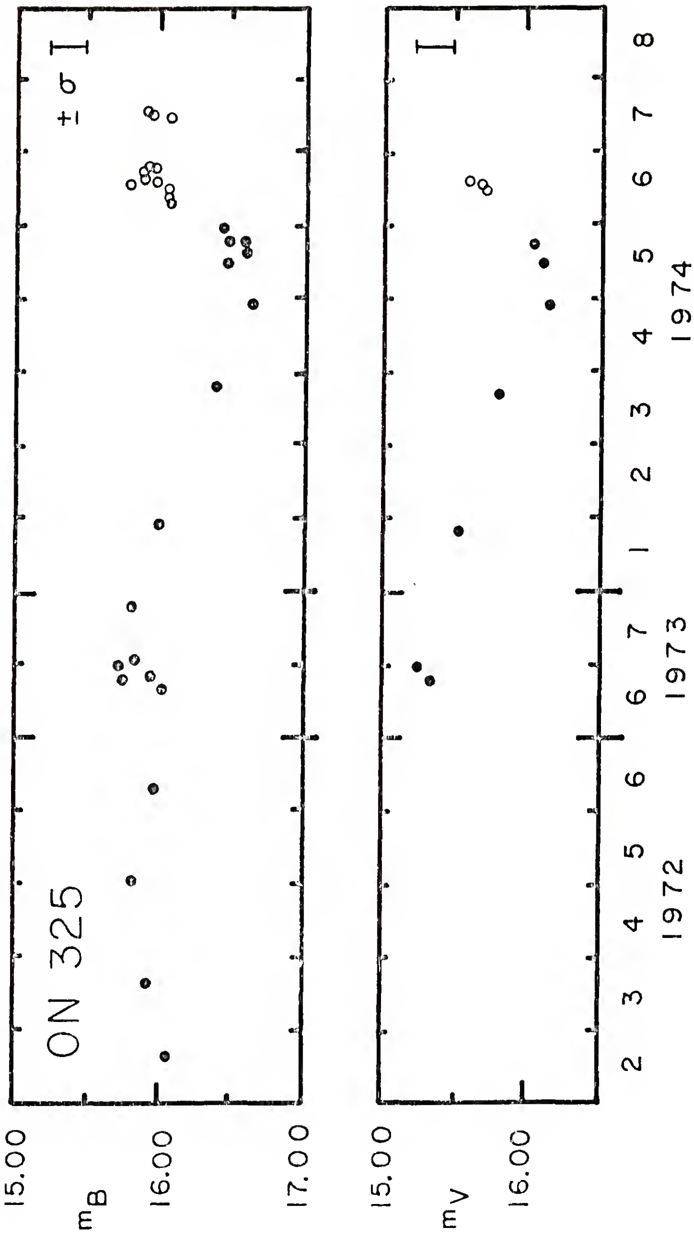
ON 325
± σ
m_B
15.00
16.00
17.00
m_V
15.00
16.00
2
3
4
5
6
6
7
1
2
3
4
5
6
7
8
1972
1973
1974

The Florida light curves suggest that the optical variations of ON 325 are different in character from those of PKS 1514-24 and ON 231. The optical variations of the latter two objects resemble those of BL Lac; they show little evidence of long-term trends during the time of observations and appear to fluctuate violently about a more or less constant baseline. By contrast the light curves of ON 325 show definite long-term trends; the short-term fluctuations appear to be much less violent than in PKS 1514-24 and ON 231. ON 231 does appear to have declined in intensity over a large number of years as discussed previously. However, its average intensity was relatively constant during the Florida observations and its long-term fluctuations appear to cover a much longer time span than those of ON 325.

Comparison sequences were established for ON 325 by computer smoothing B and V photoelectric sequences published by Wing (1974) to correct for field errors of the 30-inch reflector. The 18-inch plates were reduced satisfactorily with this sequence; an 18-inch sequence should be established whenever a suitable number of plates have been taken. The sequence finder for ON 325 is shown in Figure 63. The magnitudes of the comparison stars are shown below in Table 19.

Figure 63. The sequence finder for ON 325; the magnitudes of the comparison stars are listed in Table 19. This photograph is reproduced from a Rosemary Hill Observatory plate taken on July 24, 1973. The scale is 2.4 arcmin per inch. East is at the top and north is at the right. The variable source ON 325 is denoted by S.

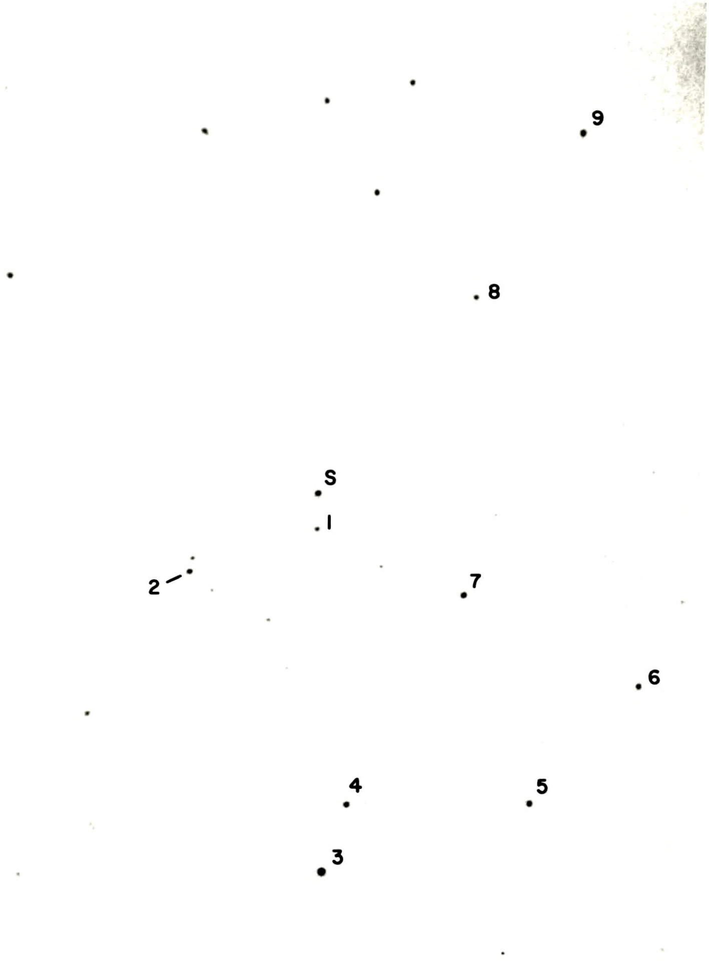
9
8
S
1
2
7
6
4
5
3

Table 19

The Comparison Stars for ON 325

Star	B	V
1	17.05	16.48
2	16.43	15.88
3	14.42	13.70
4	16.31	15.62
5	15.85	15.49
6	16.15	15.31
7	15.53	14.99
8	16.63	15.88
9	15.56	15.18

A Search for Intraday Optical Activity in BL Lac and PKS 0735+17

BL Lac

The optical counterpart of the lacertid prototype VRO 42.22.01 (BL Lac) was identified by MacLeod and Andrew (1968) with a 14th magnitude object on the Palomar Sky Survey. The optical image is mostly starlike though it is slightly elliptical and has a faint envelope, most easily seen on the Sky Survey red print. The overall brightness appears slightly greater on the Sky Survey blue print. The optical counterpart was identified by Schmitt (1968) with the variable star BL Lac. Semakin (1955) found that between 1950 and 1954 BL Lac ranged between photographic magnitudes 13 to 16. DuPuy *et al*. (1969) found the spectrum of BL Lac to be featureless;

they were observing at times of minimum brightness to lessen possible masking of spectral features by the nonthermal continuum.

BL Lac is a rapid variable at both radio and optical wavelengths. Andrew *et al.* (1969) report that the total radio flux density varies with time scales as short as one month, and Olsen (1969) reports changes in the linearly polarized flux density in one week. MacLeod *et al.* (1971) report possible repetitive outbursts at centimeter wavelengths and conclude that BL Lac is a rapid radio variable. At optical wavelengths BL Lac exhibits rapid and violent variability; the Florida observations discussed in Chapter V are good examples of this behavior. The spectral index of the continuum ranges from 2.85 to 3.17; the continuum of BL Lac has the steepest slope of any of the optically violent variables (Visvanathan and Elliot 1973).

Intraday variations have been reported for BL Lac by a number of observers. Racine (1970) reported fluctuations of $0^{m}.1$ in a time of a few hours, and "flickers" of approximately $0^{m}.03$ in times as short as 2 minutes. Milone (1972) reported a decrease of $0^{m}.4$ in 4 minutes; 15 minutes later the object had returned to its original intensity. Large variations in the photographic V were reported by Weistrop (1973); the largest was a decrease of $1^{m}.2$ in a time of 23 minutes. Observations by Hackney (1973) suggested oscillatory behavior with a range of $0^{m}.3$ in the photographic B with a period of an hour.

The author's BL Lac campaigns are listed in Table 20; light curves are shown in Figures 64, 65, and 66. In order to reduce field errors introduced by slightly different centerings of the object and its comparison stars in the telescope from night to night, smoothings of the comparison sequence were performed separately with the data from individual campaigns. This resulted in the lowest possible rms error and the maximum confidence level for variability. In addition, on the night when observations were made at both Rosemary Hill and Bradley Observatories, the comparison sequence was smoothed with the data from each telescope separately, as combining the field errors of the two instruments would produce a larger rms error. Comparison star 5 (Hackney 1973) was closest to the object's magnitude at the times of observation; its apparent magnitude is plotted along with that of the object. Due to the separate computer smoothings, the magnitude of star 5 and presumably the calibration curve zero point will shift from night to night. When using different instruments the local field effects of each telescope probably contribute to this effect; the greatest shift observed was about $0^{m}.06$ and this effect is therefore considered insignificant. The average m_B, the largest observed intensity variations of the object and star 5, the confidence level for variability, and the average rms error for each campaign are listed in Table 20. A brief description of each campaign is now given.

Key to Table 20

(1) Campaign date--All exposures were made at Rosemary Hill unless otherwise indicated.

(2) Average B magnitude during the campaign.

(3) Largest observed magnitude change for BL Lac and time interval of change.

(4) Largest observed magnitude change for comparison star 5 and time interval of change.

(5) Result of chi-square test for variability.

(6) Average rms error of a single observation (in magnitude units).

Table 20

Intraday Observations of BL Lac

(1)	(2)	(3)		(4)		(5)	(6)
Date	Avg. m_B	Δm BL Lac	Δt	Δm star 5	Δt	Confidence level	Avg. rms
8/9/73	15.62	0.25	6 min	0.10	6 min	75.0 %	0.09
10/2/73	16.67	0.60	33 min	0.05	6 min	99.9	0.08
10/4/73 Fla.	16.48	0.40	9 min	0.10	6 min	99.9	0.07
10/4/73 Ga.	16.31	0.40	15 min	0.10	6 min	80.0	0.05
6/23/74 30-inch	15.74	0.25	15 min	0.10	15 min	60.0	0.05
6/23/74 18-inch	15.88	0.15	24 min	0.05	24 min	96.0	0.03
7/16/74 30-inch	16.01	0.30	15 min	0.10	15 min	70.0	0.04
7/16/74 18-inch	15.93	0.15	15 min	0.10	15 min	75.0	0.04

Figure 64. Light curves of BL Lac intraday campaigns held on August 9 and October 2 at Rosemary Hill Observatory. The f/4 Newtonian focus of the 30-inch reflector was used for the observations. The error bars represent twice the rms error of each measurement. The apparent fluctuations of comparison star 5 are plotted above each light curve.

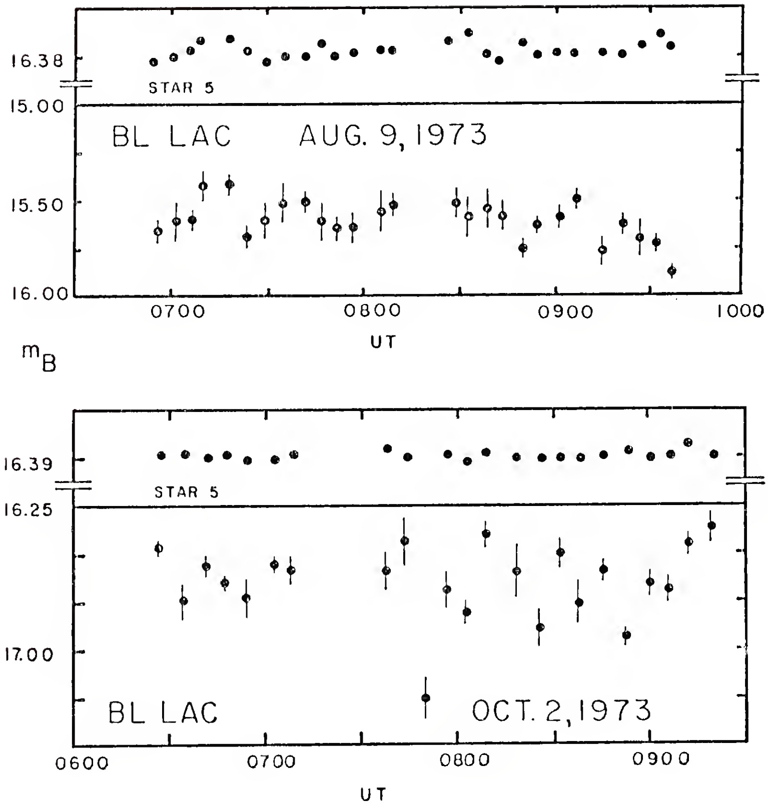
16.38
STAR 5
15.00
BL LAC
AUG. 9, 1973
15.50
16.00
0700
0800
0900
1000
UT
m_B
16.39
STAR 5
16.25
17.00
BL LAC
OCT. 2, 1973
0600
0700
0800
0900
UT

Figure 65. Light curves of the joint Florida-Georgia BL Lac intraday campaign held on October 4, 1973. The Florida observations were made at the f/4 Newtonian focus of the Rosemary Hill 30-inch reflector; the Georgia observations were made at the f/14.7 Cassegrain focus of the 30-inch reflector at Bradley Observatory of Agnes Scott College. The error bars represent twice the rms error of each measurement. The apparent fluctuations of comparison star 5 are plotted adjacent to each light curve.

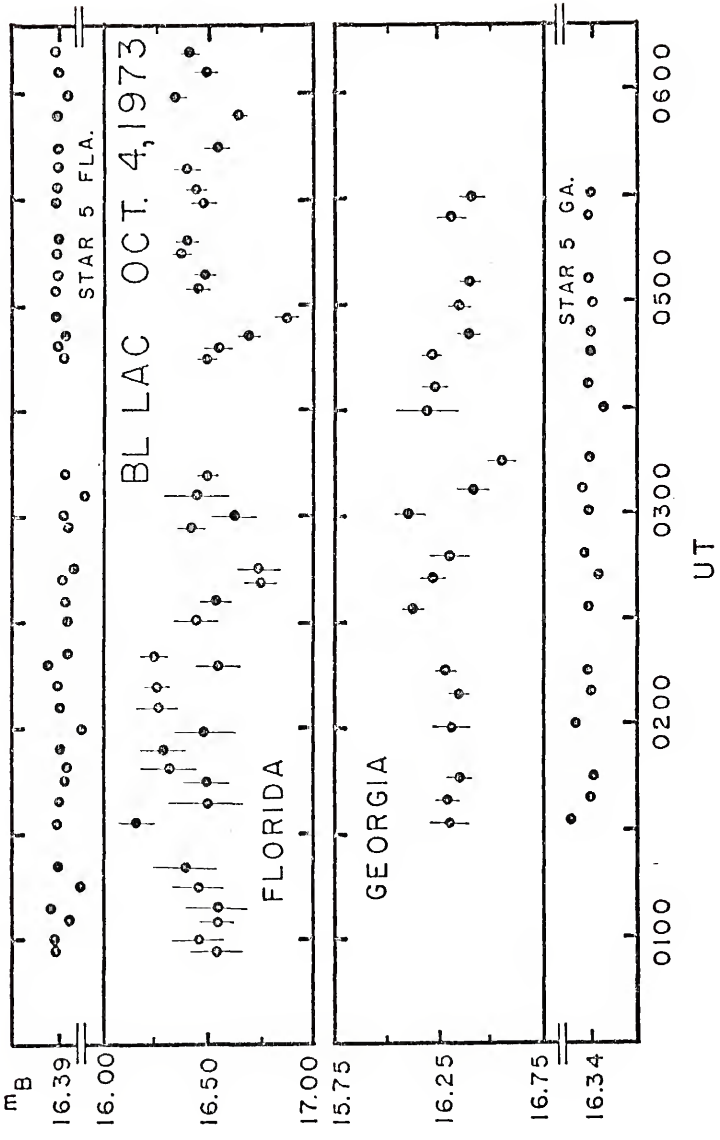
BL LAC OCT. 4, 1973
STAR 5 FLA.
FLORIDA
GEORGIA
STAR 5 GA.
m_B
16.39
16.00
16.50
17.00
15.75
16.25
16.75
16.34
0100
0200
0300
0500
0600
UT

Figure 66. Light curves of BL Lac intraday campaigns held at Rosemary Hill on June 23 and July 16 of 1974 using the 30-inch and 18-inch reflectors. In the June 23 light curves the error bars represent twice the rms error of each measurement; the error bars shown adjacent to the July 16 light curves represent twice the average rms error of a single measurement. The apparent fluctuations of comparison star 5 are plotted adjacent to the light curves. On the night of July 16 the 18-inch observations are represented by open circles, the 30-inch observations by closed circles.

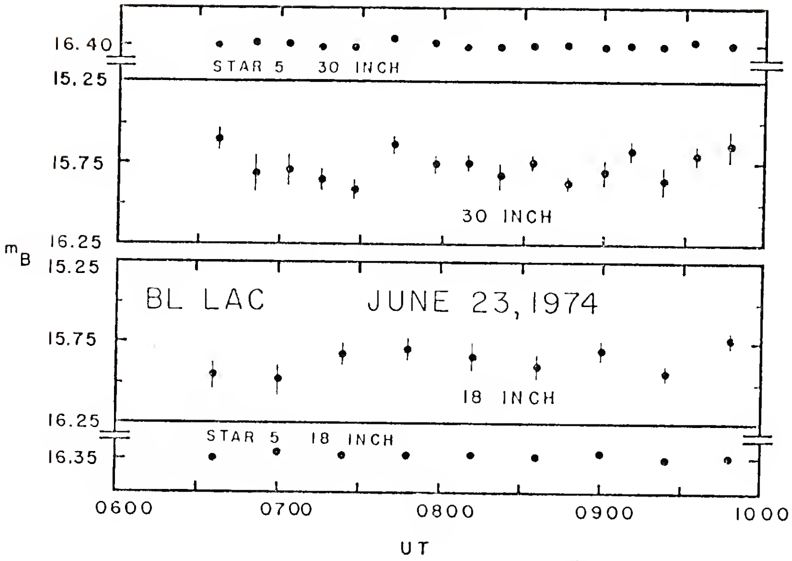
16.40
STAR 5 30 INCH
15.25
15.75
30 INCH
16.25
m_B
15.25
BL LAC JUNE 23, 1974
15.75
18 INCH
16.25
STAR 5 18 INCH
16.35
0600
0700
0800
0900
1000
UT

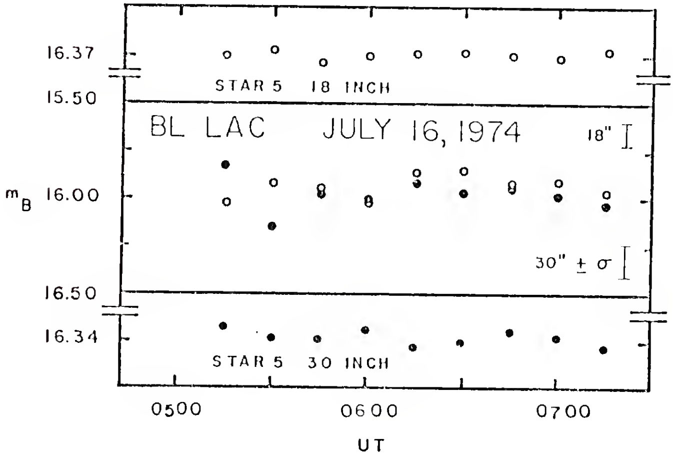
16.37
STAR 5 18 INCH
15.50
BL LAC JULY 16, 1974
18"
m_B 16.00
30" ± σ
16.50
16.34
STAR 5 30 INCH
0500
0600
0700
UT

Figure 64 shows the light curves obtained on August 9 and October 2 of 1973 using the f/4 Newtonian focus of the Rosemary Hill 30-inch reflector. By use of a mask to reduce the apparent field size, up to four exposures were placed on a 4" x 5" plate. The magnitude system for all the campaigns was photographic B, achieved by combining a nitrogen baked 103a-0 with a Schott GG 13 filter. The above field mask and the fast hypersensitized plates allowed suitable exposures to be made in approximately 5 minutes. This enabled a time resolution of about 6 minutes to be achieved under good sky conditions; usually a minute was required to reposition the cassette for the next exposure.

On the night of August 9 an oscillatory behavior with an amplitude of $0^{m}.3$ and a period of less than an hour is suggested; the confidence level for variability is 75 percent and the average rms error is $0^{m}.09$. The object appeared to be much more active on the night of October 2; violent activity is suggested with a confidence level of 99.9 percent and average rms error of $0^{m}.08$. An apparent increase starting just before 0900 UT is particularly convincing, as it involves a succession of 5 exposures. The apparent decrease in intensity to $17^{m}.25$ occurring at 0750 UT is most likely spurious as this field and the preceding were mistakenly superimposed. On both August 9 and October 2 the apparent fluctuations of star 5 were less than those of BL Lac and no greater than twice the average rms error.

Figure 65 shows the light curves of the Florida-Georgia campaign of October 4, 1973. The f/4 Newtonian focus of the Rosemary Hill 30-inch was used; the Bradley Observatory 30-inch reflector is instrumented for photography at its f/14.7 Cassegrain focus. Exposures of 3 to 4 minutes were used at Rosemary Hill; longer exposures of approximately 6 minutes were required at Bradley Observatory. The starting times of exposures were not synchronized at the two observatories; rather the object was monitored over a common time interval. The Florida light curve suggests vigorous activity with a confidence level of 99.9 percent and an average rms error of $0\overset{m}{.}07$. Surprisingly, the object appeared to be less active at Bradley Observatory; the confidence level for variability is 80 percent and the average rms error is $0\overset{m}{.}05$. Also, the average magnitude of BL Lac was $0\overset{m}{.}17$ brighter as observed at Bradley Observatory.

The difference in magnitude and the level of activity seen at the two observatories suggests that polarization or color effects may be involved. The continuum of BL Lac is characterized by strong and rapidly varying polarization. The polarization characteristics of the Georgia Cassegrain system and the Florida Newtonian system are quite different; the Florida system introduces plane polarization into all fields due to the Newtonian diagonal mirror. Slight color effects might be introduced by differences in atmospheric transparency or the reflectivity of optical surfaces. The difference in time resolution between the two observatories could have contributed to the different levels of activity seen; fast fluctuations unresolved by the Georgia system may have been detected at Florida. At both observatories the fluctuations of star 5 were less than those of BL Lac and no greater than twice the average rms error.

Figure 66 shows light curves of BL Lac campaigns held on June 23 and July 16 of 1974 at Rosemary Hill using the 30-inch and 18-inch reflectors. The observations were primarily made to investigate the relative responses of the two instruments. On June 23 the Newtonian focus of the 30-inch was used; the focal ratio of the 18-inch is f/10.3. The average brightness of the object was $0^{\mathrm{m}}.14$ greater on the 30-inch plates. Exposures at both telescopes were 7 minutes; the starting times of exposures were not synchronized. The confidence level for variability of the 30-inch observations is 60 percent and the average rms error is $0^{\mathrm{m}}.05$. The 18-inch confidence level for variability is 96 percent and the average rms error is $0^{\mathrm{m}}.03$. Since the general level of activity appears less, the higher confidence level of the 18-inch data is probably due to the smaller rms error.

On July 16 the f/16 Cassegrain focus of the 30-inch reflector was used in an attempt to decrease the average magnitude difference between the two instruments. All exposures were 7 minutes and the exposure times were synchronized. On this night the average magnitude was $0^{\mathrm{m}}.08$ brighter on the 18-inch plates, suggesting that the magnitude difference of June 23 may have been due in part to differences in relative exposure. If the more intense exposures detect part of the object's envelope this is the effect that would be expected. The 30-inch confidence level for variability is 70 percent and the average rms error is $0\overset{\mathrm{m}}{.}04$. The 18-inch confidence level for variability is 75 percent, also with an average rms error of $0\overset{\mathrm{m}}{.}04$. Except for the first two points the light curves are in good agreement. On both June 23 and July 16 the apparent fluctuations of star 5 were less than twice the average rms error achieved with either instrument. It is concluded that any magnitude difference between the 18-inch and the 30-inch is unimportant in routine long-term monitoring. When making intraday comparisons it is probably best to use the 30-inch Cassegrain focus to lessen exposure and polarization effects; due to the large aperture difference the author feels that exposure effects predominate.

PKS 0735+17

The identification and photometric history of PKS 0735+17 have been discussed in Chapter IV. Though no intraday variations have been reported by other observers, the object's violent optical activity and lineless spectrum suggest its similarity to BL Lac. In an attempt to detect intraday activity, intraday campaigns were held during the first three months of 1974; 6 campaigns were run exclusively at the Bradley Observatory of Agnes Scott College. On February 25 and March 18 of 1974 simultaneous observations were made at Bradley Observatory and Rosemary Hill. The start of all exposures at the two observatories was synchronized. All Florida observations in this study were made at the Newtonian focus of the Rosemary Hill 30-inch telescope. Unfiltered 103a-0 plates were used for all exposures at both observatories.

Light curves of the campaigns are shown in Figures 67 through 70. Star 5 of the comparison sequence (Hackney 1973) was used as a control; its apparent fluctuations are plotted adjacent to the PKS 0735+17 light curves. A list of the campaigns is given in Table 21, along with the average photographic magnitude, the largest observed intensity variations of the object and star 5, the confidence level for variability, and the average rms error. The comparison sequence was smoothed individually for each campaign using the same procedure as for BL Lac. A brief discussion of the campaigns now follows.

Figure 67 shows the light curve of the campaign held on the night of January 24 at Rosemary Hill. The confidence level for variability is 80 percent and the average rms error is $0\overset{m}{.}08$. The fluctuations of comparison star 5 are of the same magnitude as those of the object, suggesting that no real variations were observed. The large gap in the observations was caused by clouds; the transparency was variable throughout the campaign.

Figure 68 shows the light curves of campaigns held at Bradley Observatory on January 31, February 1, and February 12 of 1974. The object appeared very steady on January 31; the confidence level for variability is only 10 percent; the

Figure 67. Light curve of PKS 0735+17 intraday campaign held at Rosemary Hill on January 24, 1974. The error bars represent twice the rms error of each measurement. The apparent fluctuations of comparison star 5 are plotted below the light curve. The large gap in the observations was caused by clouds.

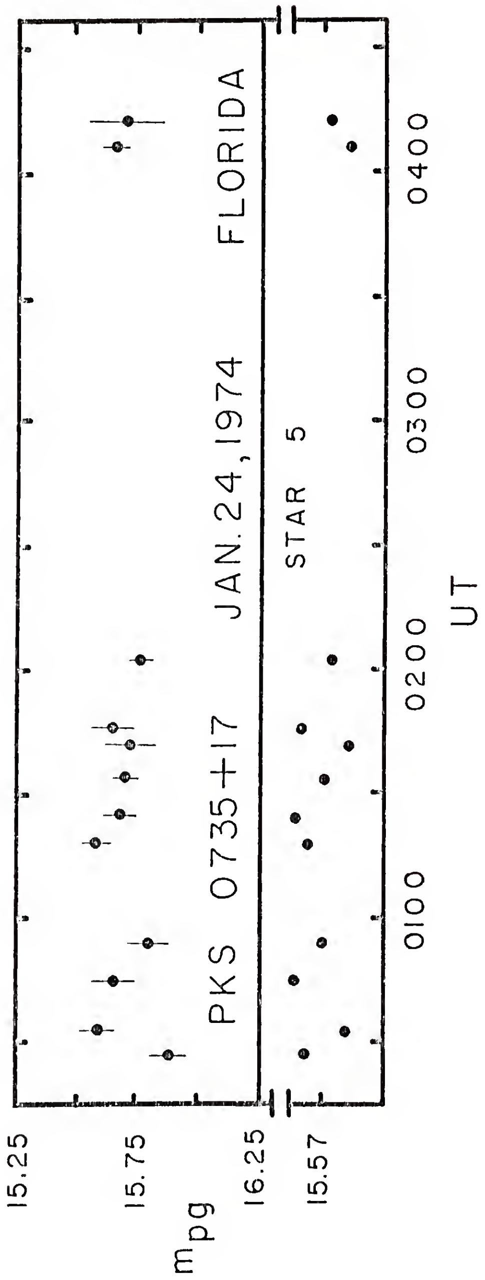
PKS 0735+17
JAN. 24, 1974
FLORIDA
STAR 5
m_{pg}
15.25
15.75
16.25
15.57
0100
0200
0300
0400
UT

Figure 68. Light curves of PKS 0735+17 intraday campaigns held at Bradley Observatory on January 31, February 1, and February 12 of 1974. The error bars represent twice the rms error of each measurement. The apparent fluctuations of comparison star 5 are plotted below each light curve.

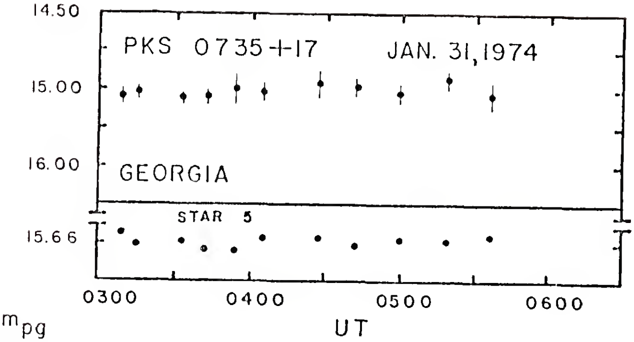
14.50
15.00
16.00
15.66
PKS 0735+17
JAN. 31, 1974
GEORGIA
STAR 5
0300
0400
0500
0600
m_{pg}
UT

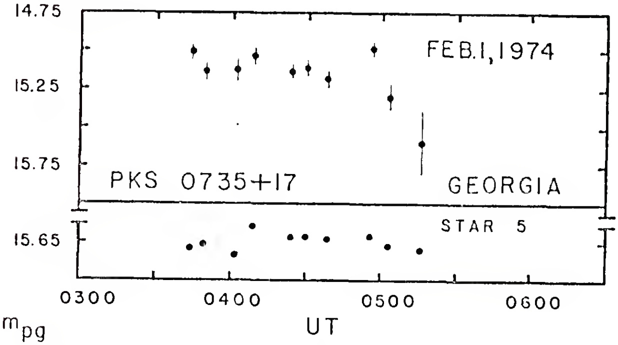
14.75
15.25
15.75
15.65
FEB. 1, 1974
PKS 0735+17
GEORGIA
STAR 5
0300
0400
0500
0600
m_{pg}
UT

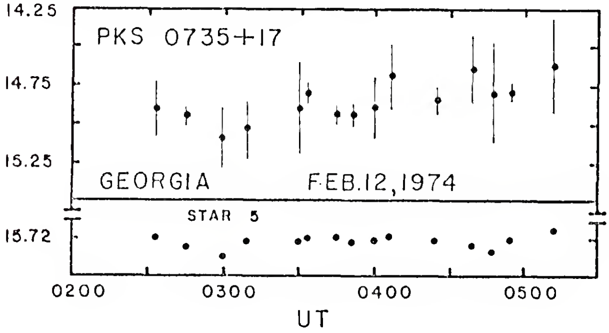
14.25
14.75
15.25
15.72
PKS 0735+17
GEORGIA
FEB. 12, 1974
STAR 5
0200
0300
0400
0500
UT

Figure 69. Light curves of PKS 0735+17 intraday campaigns held at Bradley Observatory on February 18, February 27, and March 15 of 1974. The error bars represent twice the rms error of each measurement. The apparent fluctuations of comparison star 5 are plotted below each light curve.

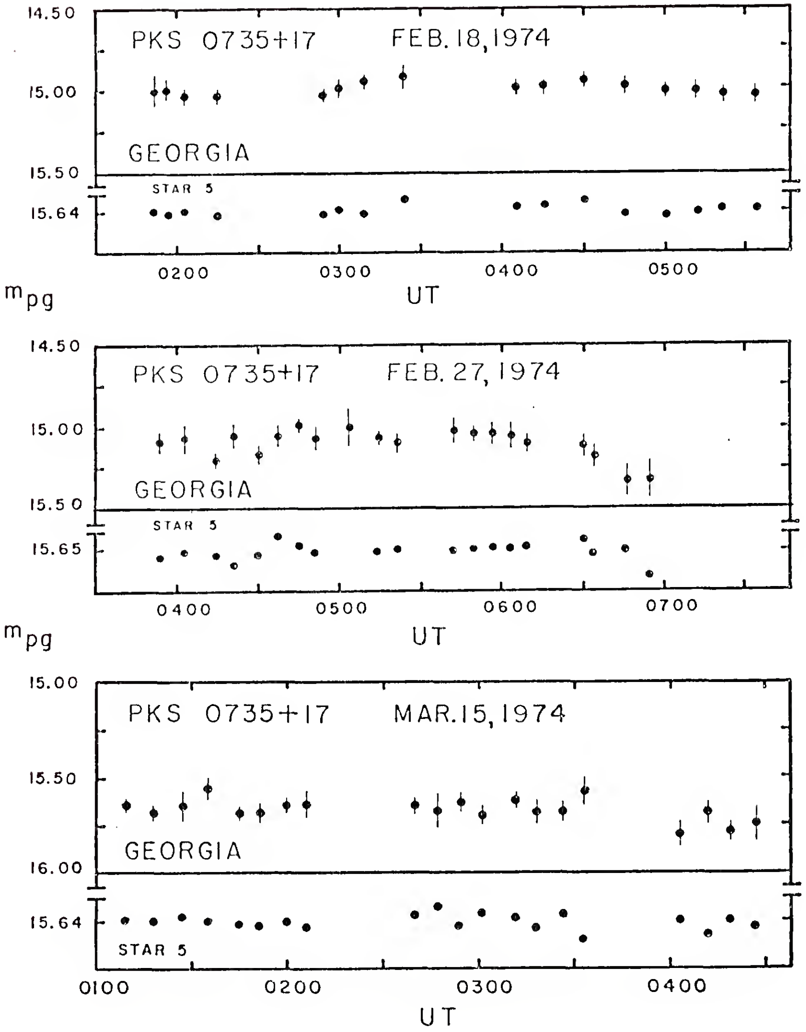
PKS 0735+17 FEB. 18, 1974
GEORGIA
STAR 5
14.50
15.00
15.50
15.64
0200
0300
0400
0500
UT
mpg
PKS 0735+17 FEB. 27, 1974
GEORGIA
STAR 5
14.50
15.00
15.50
15.65
0400
0500
0600
0700
UT
mpg
PKS 0735+17 MAR. 15, 1974
GEORGIA
STAR 5
15.00
15.50
16.00
15.64
0100
0200
0300
0400
UT

Figure 70. Light curves of joint Florida-Georgia PKS 0735+17 intraday campaigns held on February 25 and March 18 of 1974. The starting of exposure times at the two observatories was synchronized. The error bars represent twice the rms error of each measurement. The apparent fluctuations of comparison star 5 are plotted below each light curve.

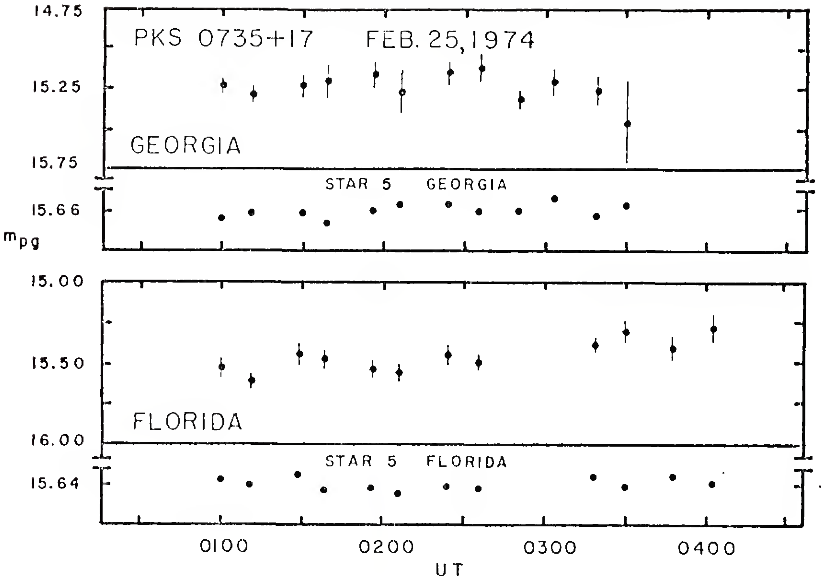
PKS 0735+17 FEB. 25, 1974
GEORGIA
STAR 5 GEORGIA
FLORIDA
STAR 5 FLORIDA
14.75
15.25
15.75
15.66
m_{pg}
15.00
15.50
16.00
15.64
0100
0200
0300
0400
UT

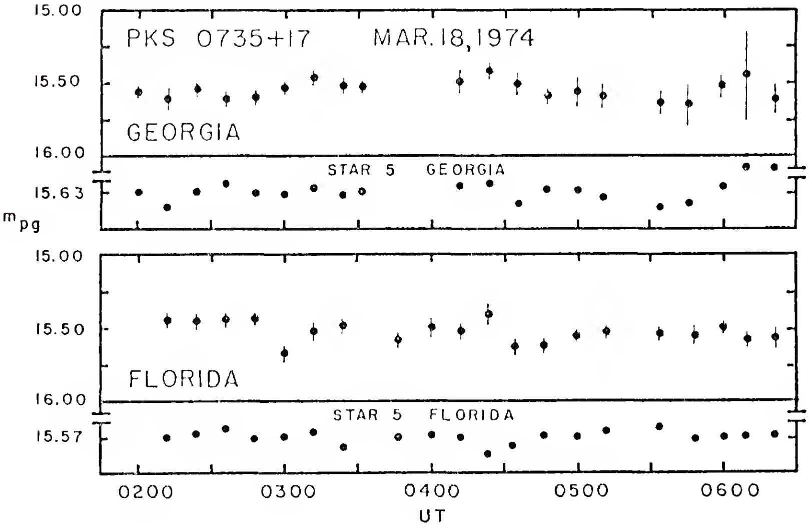
PKS 0735+17 MAR. 18, 1974
GEORGIA
STAR 5 GEORGIA
FLORIDA
STAR 5 FLORIDA
15.00
15.50
16.00
15.63
m_{pg}
15.00
15.50
16.00
15.57
0200
0300
0400
0500
0600
UT

Key to Table 21

(1) Date and place of observation.

(2) Average photographic magnitude during the campaign.

(3) Largest observed magnitude change for PKS 0735+17 and time interval of change.

(4) Largest observed magnitude change for comparison star 5 and time interval of change.

(5) Result of chi-square test for variability.

(6) Average rms error of a single observation (in magnitude units).

Table 21

Intraday Observations of PKS 0735+17

(1) Date	(2) Avg. m_{pg}	(3) Δm 0735+17	 Δt	(4) Δm star 5	 Δt	(5) Confidence level	(6) Avg. rms
1/24/74 Fla.	15.70	0.25	6 min	0.20	12 min	80.0 %	0.08
1/31/74 Ga.	15.03	0.10	18 min	0.10	12 min	10.0	0.07
2/1/74 Ga.	15.10	0.60	20 min	0.15	24 min	97.0	0.07
2/12/74 Ga.	14.90	0.45	132 min	0.15	24 min	30.0	0.20
2/18/74 Ga.	15.01	0.15	30 min	0.10	15 min	25.0	0.05
2/25/74 Fla.	15.49	0.30	150 min	0.10	9 min	98.0	0.06
2/25/74 Ga.	15.27	0.30	18 min	0.10	27 min	60.0	0.11
2/27/74 Ga.	15.08	0.30	111 min	0.20	24 min	80.0	0.07
3/15/74 Ga.	15.66	0.25	30 min	0.15	7 min	30.0	0.05
3/18/74 Fla.	15.54	0.25	11 min	0.15	12 min	99.0	0.04
3/18/74 Ga.	15.54	0.20	36 min	0.25	36 min	11.0	0.20

average rms error is $0^{m}.07$. On February 1 a $0^{m}.6$ decline was observed, starting around 0500 UT; the confidence level for variability is 97 percent and the average rms error is $0^{m}.07$. On February 12 an apparent increase of about $0^{m}.5$ was seen over a 2-hour period starting at 0300 UT. However, poor transparency conditions prevailed throughout the observations; the confidence level for variability is 30 percent and the average rms error is $0^{m}.2$.

Figure 69 shows the light curves of PKS 0735+17 intraday campaigns held at Bradley Observatory on February 18, February 27, and March 15 of 1974. On February 18 the object appeared steady; the confidence level for variability is 25 percent and the average rms error is $0^{m}.05$. On February 27 a higher level of activity is suggested; the confidence level for variability is 80 percent and the average rms error is $0^{m}.07$. The decline starting around 0630 UT is also seen in the trends shown by star 5; similar instances are present in portions of other PKS 0735+17 campaign light curves. Examination of the plates show them to be underexposed, suggesting that proper exposure time is very critical for accurate intraday monitoring. On March 15 a slight decline is suggested over the course of the campaign with superimposed fluctuations of around $0^{m}.15$. However, the confidence level for variability is only 30 percent; the average rms error is $0^{m}.05$.

Figure 70 shows the light curves of joint Florida-Georgia campaigns held on February 25 and March 18 of 1974. On February 25 the confidence level for variability at Rosemary

Hill is 98 percent and at Bradley Observatory 60 percent; the average rms errors are $0\overset{m}{.}06$ and $0\overset{m}{.}11$, respectively. The larger Georgia error probably accounts for the lower confidence level for variability. Synchronized exposure times of 6 and 12 minutes were used at the two observatories. The exposure times were alternated on successive exposures with the first observation being a 6-minute exposure. The purpose was to investigate the effect of exposure on rms error. Though there are exceptions, the longer exposures seem to give the lowest rms error. The light curves are in rough agreement during the first hour of observations, suggesting that simultaneous events may have been marginally detected. On the night of February 25 the average magnitude of the object was $0\overset{m}{.}22$ brighter at Bradley Observatory; on March 18 the average magnitude was the same at both observatories. The cause of this zero point shift remains unknown; the apparent change in the shift from night to night suggests that relative atmospheric transparency rather than instrumental effects may have been a major contributing factor.

On the night of March 18 synchronized exposures of 8 minutes were used at both observatories. The confidence level for variability at Rosemary Hill is 99 percent and at Bradley Observatory 11 percent; the average rms errors are $0\overset{m}{.}04$ and $0\overset{m}{.}20$, respectively. Poor transparency prevailed at times at Bradley Observatory; this contributed to the high rms error and the low confidence level for variability. Little activity was observed other than small fluctuations of about $0^{m}.20$; the lack of similarity between the light curves suggests that no real simultaneous events were observed.

Summary

Florida observations show that PKS 1514-24 and ON 231 are OVV's reminiscent of BL Lac, except that their ranges of fluctuation are apparently not as great as those of the lacertid prototype. ON 325 exhibits optical activity of a different character; its short-term excursions are less than either PKS 1514-24 or ON 231, and long-term intensity changes over a time of several months are shown by the Florida light curves. Long-term trends are absent from the Florida observations of the latter objects.

Statistically significant intraday variations were observed for the lacertid prototype BL Lac on October 2 and October 4 of 1973 at Rosemary Hill Observatory. Lesser activity observed at Bradley Observatory on October 4, 1973, could have been due to the non-synchronization of exposure times and possible polarization effects. Polarization and color effects along with local field characteristics are believed to have contributed to magnitude zero-point shifts observed between Bradley and Rosemary Hill observatories. However, the observed change in the magnitude of the shift from night to night suggests that differences in the atmospheric transparency at the two observatories may have played a major role.

Zero point shifts observed between the Rosemary Hill 30-inch and 18-inch reflectors are believed to have been caused by relative exposure differences, though polarization probably contributes. These magnitude shifts are concluded to be unimportant in routine long-term monitoring; for intraday work the author suggests using the Cassegrain focus of the 30-inch if simultaneous observations are to be made with the 18-inch.

Based upon a lower limit of 99.5 percent no statistically significant intraday variations were observed for PKS 0735+17. However, on three nights probabilities of 97 percent or greater were determined. Florida-Georgia campaigns were held on two of these nights; the object's confidence level for variability was greater at Rosemary Hill. The higher rms error of the Georgia data on these nights, probably due to varying transparency, is believed to have contributed to this effect. On the night of February 25, 1974, the data suggest that simultaneous PKS 0735+17 fluctuations may have been marginally detected at Bradley and Rosemary Hill observatories.

Exposure time appears to be very important in intraday studies, even more than in routine long-term monitoring. As evidenced by several of the PKS 0735+17 plates, inadequate image densities may cause zero-point shifts; the apparent magnitude of a comparison star should always be plotted adjacent to the object's light curve in intraday work to check for this effect. In the case of BL Lac, comparison star 5 remained mostly steady during the intraday observations and appeared to vary much less than the object, strengthening the suggestion that the observed object variations were real.

Assuming that real intraday variations were observed for BL Lac, the following relation derived from Terrell (1967) can be used to estimate the maximum size of the active region, assuming non-relativistic motion in the source:

$$D = \frac{4}{1+z}\,\frac{\Delta t}{\Delta m} \tag{6.1}$$

where D is the size of the active region, z is the redshift, and Δm is the magnitude change observed in time Δt. Using Oke and Gunn's redshift of 0.07 (1974) and the change of $0\overset{m}{.}60$ in 33 minutes observed on October 2, 1973, a maximum size of $3^h\ 26^m$ in light travel time is indicated for the active region. Such a small size combined with the observed luminosity puts severe restraints on emission models if correct.

CHAPTER VII

A PHOTOGRAPHIC SEARCH FOR AN IO-RELATED JOVIAN HOTSPOT

Introduction

During the 1973 Jovian apparition a total of 93 ultraviolet and 71 infrared images of Jupiter were taken at Rosemary Hill, in the spectral regions described in Chapter II. A complete list of these images is given in Appendix I. The data reduction consisted of the following four steps: (1) determining the expected location of the auroral spot on the images, (2) visual examination of the images to note their characteristics and to hunt for evidence of the hotspot, (3) digitization of suitable images, and (4) computer superposition of the digitized images and interpretation of the computer output. A rough estimate of the differential brightness between the spot and the surrounding Jovian limb is given in the next section. In the following sections the major steps in the data reduction are outlined.

The Estimated Brightness of the Spot

Using a standard Jovian atmospheric model by Tan (1974), Prasad (1974) has estimated the photon flux that should be generated in the above spectral regions due to excitation by the current sheets proposed by Goldreich and Lynden-Bell. This model and Prasad's calculations are based upon pre-Pioneer 10 and 11 information. Prasad estimates that most of the emissions will arise from molecular hydrogen; atomic hydrogen contributions will be predominantly due to the dis-associative excitation of H_2. Using the parameters of Goldreich and Lynden-Bell, Prasad estimates that the emissions from H_2 are about 200 kilorayleighs (2.0×10^{11} photons/cm^2/sec) from 3,000 to 4,000 Å, and approximately 1,100 kilorayleighs (1.1×10^{12} photons/cm^2/sec) from 6,000 to 9,000 Å. Molecular hydrogen emissions are expected to be negligible in the 10,000 to 11,000 Å range, but a possible methane contribution might arise if all the precipitant electron energy is not dissipated at high altitudes.

At the earth's distance from the sun the solar flux is approximately 2.0×10^{16} photons/cm^2/sec between 3,000 and 4,000 Å (Shimazaki and Ogawa 1974). The approximate flux between 6,000 and 9,000 Å is 6.6×10^{16} photons/cm^2/sec, according to Shimazaki and Ogawa, and approximately 4.4×10^{16} photons/cm^2/sec between 9,000 and 11,000 Å, according to Campen *et al*. (1961). Extrapolating these fluxes to the average distance of Jupiter from the sun will attenuate them by a factor of about 25.

Albedo curves for Jupiter given by Pilcher and McCord (1971) and Danielson (1966) indicate that the albedo in the ultraviolet and infrared regions of interest is approximately 0.25. Pilcher and McCord assumed a Lambert-sphere model for limb-darkening corrections in their photometric work. In such a model the reflected intensity of a distant illuminated gaseous sphere falls off as the cosine of the angle from the apparent center of the body. The results of the above albedo and limb-darkening corrections to sunlight reflected from the Jovian limb are shown in Table 22. The table indicates that the brightness of the auroral spot is slightly greater than that of the Jovian limb for central meridian angles approaching 90°. The estimates of the hotspot intensity are for emissions from molecular hydrogen. As mentioned previously, a contribution from methane might arise in the 10,000 to 11,000 Å region. If intense methane emissions were to occur, the infrared region would offer the best chance for detecting the hotspot.

The Jovacentric Coordinates of the Spot

The first step in the search for the hotspot was to calculate the approximate expected position of the spot for each image. An outline of these calculations now follows.

According to Goldreich and Lynden-Bell (1969) the magnetic co-latitude of the foot of the Io flux tube, and thus the spot, is 24°. In computing the position of the spot it was assumed that this magnetic co-latitude remains constant and that the only shift in true co-latitude was due to the precession of a symmetrical dipole field inclined 10° relative to Jupiter's rotational axis.

Key to Table 22

(1) Solar flux at earth's distance from the sun in units of photons/cm^2/sec from Shimazaki and Ogawa (1974) and Campen *et al*. (1961).

(2) Solar flux reflected from the Jovian limb in units of photons/cm^2/sec at an angle from the central meridian of 89.90°.

(3) Solar flux reflected from the Jovian limb in units of photons/cm^2/sec at an angle from the central meridian of 89.95°.

(4) The expected intensity of the auroral hotspot in units of photons/cm^2/sec (Prasad 1974) arising from molecular hydrogen emissions.

Table 22

A Comparison of the Expected Brightness of the Auroral Hotspot and the Jovian Limb

	3,000-4,000 Å, photons/cm^2/sec	6,000-11,000 Å, photons/cm^2/sec
(1) Solar flux at 1 A.U.	2.00×10^{16}	11.00×10^{16}
(2) Reflected at 89.90°	3.49×10^{11}	1.92×10^{12}
(3) Reflected at 89.95°	1.75×10^{11}	0.96×10^{12}
(4) Expected hotspot intensity	2.00×10^{11}	1.10×10^{12}

The plates used in this study were taken between July 14, 1973, and November 14, 1973. During this time the tilt of Jupiter's rotational axis relative to the ecliptic was less than 1° and was decreasing. It was therefore assumed that the observer was always viewing the Jovian rotational axis at an angle of 90°.

Figure 71 shows the Jovacentric hotspot coordinates X and Y and their relationship to the co-latitude ψ. For simplicity the spot is assumed to be on the Jovian limb. Since ψ varies between 14° and 34°, Y ranges from 0.83 R to 0.97 R. Due to the high latitude of the spot, the apparent polar radius was used as R. Likewise, X ranges from 0.56 R to 0.24 R. For times when the spot is located on the limb, these calculations indicate that it is located within a rectangle on the Jovian disk of width 0.32 R and height 0.14 R, whose central coordinates are

$$X = R(\sin 24°) \tag{7.1}$$

and

$$Y = R(\cos 24°). \tag{7.2}$$

This rectangle is indicated by the shaded area in Figure 71.

Figure 72 is a polar view of the positional geometry showing the general case where the spot is not quite on the limb. Angle θ is the angle of the spot from the central meridian; the spot is assumed to lead Io in longitude by 12°. The value of Y remains unchanged but the projected X coordinate is now X_1, equal to $X(\sin \theta)$. Thus, in general the

Figure 71. The projected Jovacentric coordinates X and Y of the hotspot. Angle ψ is the true co-latitude and varies from 14° to 34° due to the 10° tilt of Jupiter's magnetic axis relative to its rotational axis. For simplicity the spot is assumed to be on the western limb. The shaded rectangle indicates the area most likely to contain the hotspot. The values of X and Y are: $X = R(\sin \psi)$ and $Y = R(\cos \psi)$.

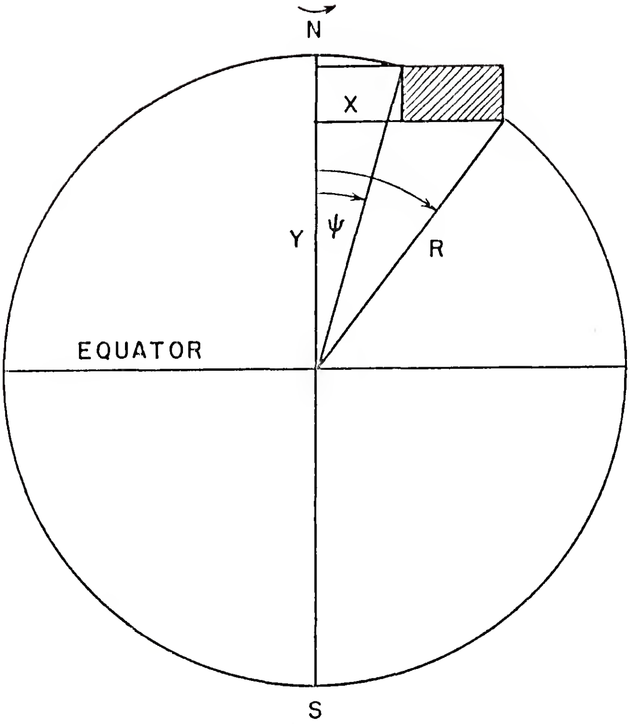
N
X
Y
ψ
R
EQUATOR
S

Figure 72. A polar view of the flux tube projected positional geometry. Angle θ is the angle of the hotspot from the central meridian. The spot is assumed to lead Io in longitude by 12°. For spot positions where θ is less than 90° the projected X coordinate becomes $X_1 = X(\sin\ \theta)$.

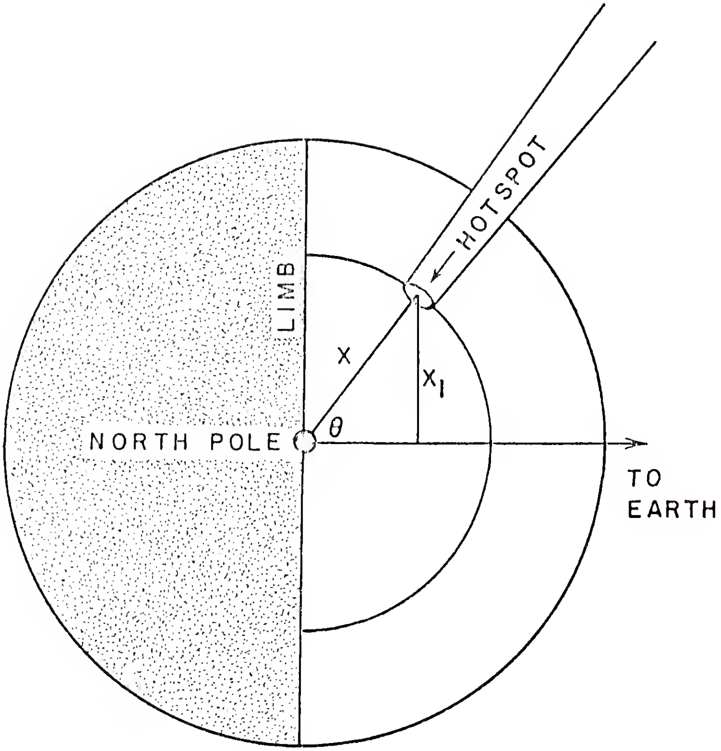
HOTSPOT
LIMB
X
X_1
θ
NORTH POLE
TO
EARTH

rectangle on the Jovian disk containing the hotspot has a height of 0.14 R, a width of 0.32 R(sin θ) and central coordinates

$$X_1 = R(\sin 24° \sin \theta) \tag{7.3}$$

and

$$Y = R(\cos 24°). \tag{7.4}$$

Assuming a symmetrical Jovian dipole field, an analogous location for the hotspot exists in the southern Jovian hemisphere. This positional rectangle is simply the mirror image of the search area in the northern hemisphere. It must be kept in mind that the instantaneous coordinates are not equal; when the co-latitude is at a minimum in the northern hemisphere it is at a maximum in the southern hemisphere, etc. While the above procedure was used to locate the most probable location of the hotspot, a much larger area of each image was actually examined during the reduction of the data.

After locating the area on each disk in which to search for the hotspot, the images were given a visual examination with a stereo-zoom microscope. Though no sign of the hotspot was seen, the details of each image, such as defects, bands, satellite shadows and density were carefully noted. Each image was assigned a number which, along with the above information, was assembled into a "Jupiter-image library." This library is listed in Appendix I.

After the visual examination of the images was completed, the first major step in the data reduction was initiated.

Even though the hotspot was not visible to the eye, it was felt that it might be made visible by averaging over a large number of images to reduce the noise by a factor sufficient to allow detection of a very weak source. Such operations are frequently carried out in the darkroom by printing a composite of several "identical" negatives, analogous to the procedure described in Chapter II, except that no filters are used.

Since the spot would be near the Jovian limb, its motion would be greatly foreshortened and it would not appear to move appreciably during the time a series of exposures was taken. As an example, let angle ψ equal 24°. If an observing session is started when the spot is 14° from the limb and ended when the spot reaches the limb, the projected X coordinate X_1 changes by only 0.01 R. A typical value for R is 20 arcsec. Using this value for R yields a change in X_1 of 0.2 arcsec. Since the average seeing disk at Rosemary Hill is usually at least 2.0 arcsec in diameter, the change in X_1 is insignificant. The above change in angle θ is far larger than any encountered in the actual observing sessions. Thus the superposition of several images should raise the signal-to-noise ratio between the spot and the Jovian limb.

For the purpose of this study it was felt that computer processing would be a more powerful tool than darkroom techniques. With the images in a digital form acceptable by the computer, very involved manipulations can be performed, and if the presence of the hotspot is suggested, the data are already in a suitable form for further reductions. The preparation of the data for computer processing is now described.

Digitizing the Jovian Images

The Jovian images were digitized by scanning them with a model MK III C Joyce-Loebl scanning microdensitometer, and feeding the voltage output of this machine into an analog-to-digital converter which was designed and built by Dr. M. A. Lynch. This device read the data onto magnetic tape in a form usable by the computer. The scanning microdensitometer is shown in Figure 73 and Dr. Lynch's digital converter in Figure 74.

The microdensitometer automatically scans in the x direction; the y increments are made by adjusting a micrometer screw which drives the specimen support stage. The stage is moved in the x direction by a lever arm with a variable fulcrum connected to a driven record platform designed to hold a sheet of graph paper, at the rear of the instrument. As the record platform is driven past a pen-drive mechanism the specimen support stage is moved in the opposite direction by the lever arm, the rate of drive depending on the position of the fulcrum. Potentiometers geared to the pen-drive mechanism and record table generate voltages proportional to the specimen density and x-position, respectively. These two voltage outputs were fed into separate channels of the

Figure 73. The model MK III C Joyce-Loebl scanning microdensitometer. The driven record platform is denoted by (R), the specimen support stage by (S), and the lever arm that drives the specimen support stage by (L). The control box (B) at the right was used to send "scan" and "frame" signals to the analog-to-digital converter.

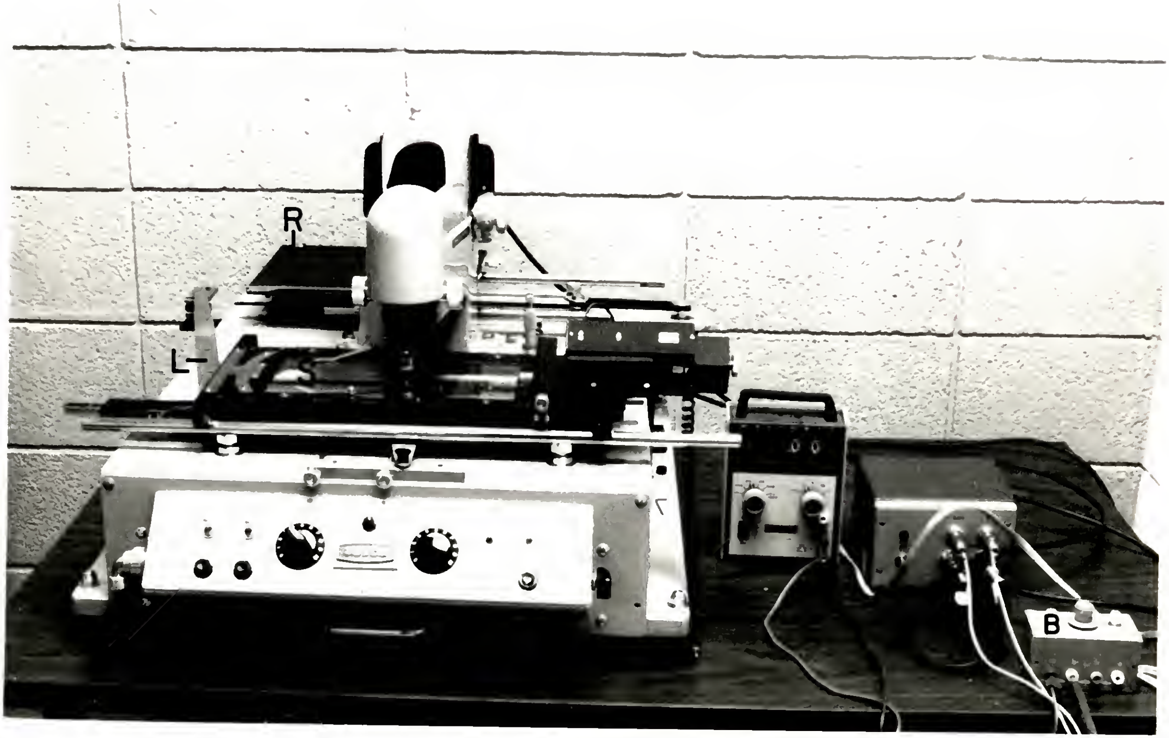
R
L
B

Figure 74. The analog-to-digital converter designed and built by Dr. M. A. Lynch. The tape drive unit is at the bottom; the wires leading from the panel off to the right of the photo are the inputs from the scanning microdensitometer.

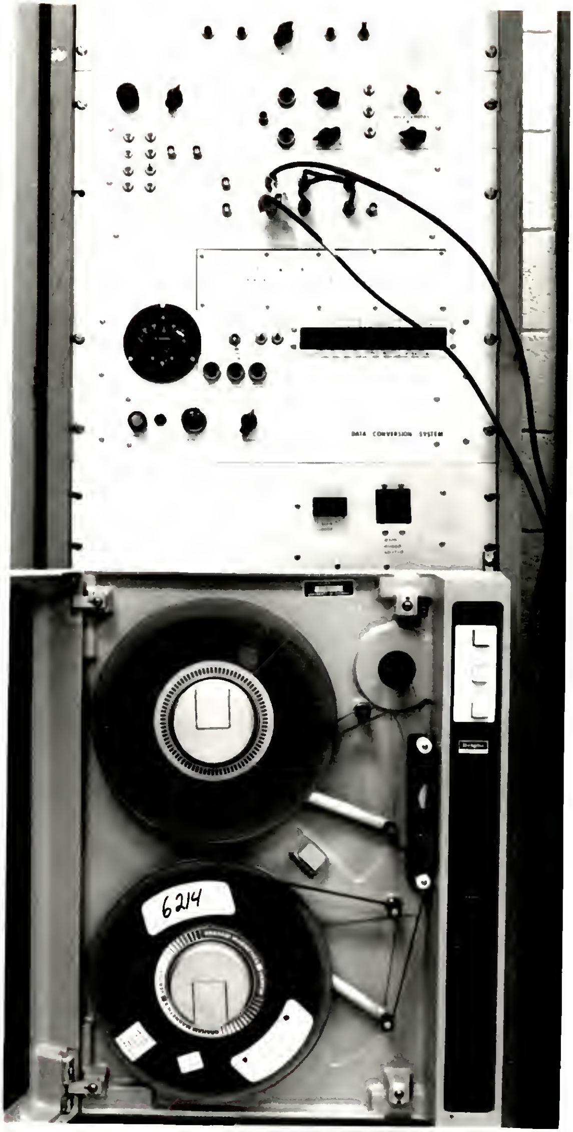
DATA CONVERSION SYSTEM
6214

digital converter through shielded cable. The position channel was designated "X," the density channel "Z." Graphical records were not desired during the digitization process; the pen is easily removed if not needed. These density readings are accurate to 2 percent (McPeters 1974), which was felt to be satisfactory for this study.

The Jovian images averaged about 3 mm in equatorial diameter at f/16, and about 9 mm in equatorial diameter at f/50. All of the infrared images were taken f/16, but occasionally ultraviolet images were enlarged to f/50 by eyepiece projection. Many of the ultraviolet images were found to be too dense for the range of the densitometer. Very dense images peg the pen-potentiometer drive mechanism.

Average image densities ranged from a density of about 0.3 to greater than 3.0 as measured with a Photovolt photometer model 520 A. The density scanning range of the microdensitometer is controlled by a series of exchangeable variable density wedges. With the most dense "F" wedge in place, an image up to density 2.0 could be scanned at the required slit setting without pegging the pen-potentiometer drive. No images of greater density were scanned.

In all, a total of seventy infrared images and four ultraviolet images were scanned. Twenty-six ultraviolet images suitable for scanning were not scanned due to a breakdown of the digitizing system. All of the images scanned were taken at a magnification of f/16.

All images were scanned with the 10 X objective and a slit setting of 50 microns. Each image was divided up into 50 scan lines; the y-adjust micrometer screw was incremented 3 units of 25 microns each between successive scans. This gave a y resolution of 1.27 arcsec on the scanned image. The length of the x scan was controlled by the x-positional voltage. An x voltage of 0.260 volts corresponds to a scan distance of 4.20 mm. The computer program which assembled the digitized images disregarded all data after it had detected an x voltage of 0.260 volts, thus ending the scan. The digital converter sampled the density voltage at a rate of 50 to 70 times per second. However, the assembly program divided the voltage range of 0.260 volts into 70 increments and disregarded the rest of the data. This yielded an x resolution of 1.02 arcsec. Thus a rectangular area of 3.75 mm x 4.20 mm, containing the image, was converted into a 50 x 70 element array, the resolution of approximately 1.0 arcsec being considerably smaller than the average seeing disk at Rosemary Hill.

The procedure for scanning an image was as follows. The densitometer was first allowed to warm up for at least an hour. Next the machine was carefully focused and the slit set to 50 microns. The wedge was checked to be sure it was suitable for the density range of the images to be scanned. The plate was aligned on the specimen stage so that the scan beam would move parallel to the equator of the images. Then the plate was tightly clamped, for if the images were to be properly superimposed this alignment must remain constant. The specimen stage was checked to be sure that it was in its zero position. The specimen stage was now unclamped from both the x and y drives and the desired image positioned for scanning. This does not disturb the zero setting of the platform. When the image was correctly positioned the platform was reclamped.

A digital voltmeter was used to monitor the x voltage at all times; it was approximately 0.09 volts when the stage was in its zero position. The scanning densitometer has two drive modes: "fast" and "slow." The "fast" mode was used for all the images. The scan rate was not constant; it slowed down to a very slow rate when scanning regions of great density gradation due to a differential drive control used to aid resolution.

All images were scanned with the fulcrum in the "5 to 1" position; the specimen stage moves at 1/5 the speed of the record platform in this position. The average scan took about 20 seconds, an entire image around 20 minutes.

Dr. Lynch operated the digital converter. At the start of a scan session the author and Dr. Lynch communicated by telephone; the digital converter is located in 304 SSRB, the densitometer in 317 SSRB. The two rooms are separated by about 200 feet; shielded cables were strung down the hall between the two rooms in order to interface the machines. The data tape was allowed to run for about 15 seconds before starting a scan session to minimize possible noise at the start of the tape.

Throughout the scanning session a control box was used to place markers on channel "X," the channel containing the x-positional voltage, for the benefit of the computer programs. At the start of a scan session the author placed a -4.5 volt signal on channel "X"' this was a "frame signal" and told the computer assembly program that an image was about to be scanned. Before making the first scan a +4.5 volt "scan signal" was also placed on channel "X." Then the platform drive switch was turned to "fast" and the x-positional voltage was watched closely. When it reached 0.270 volts, 0.01 volts beyond the maximum scan value, the drive switch was placed on "return" and the platform quickly returned to the original x position. This position was very repeatable, as attested by the accuracy with which the x voltage always returned to exactly the same zero value during a scan session.

After each scan the y adjust was incremented 3 units of 25 microns each. Then another scan signal was placed on channel "X" and another scan was made as described above. Another frame signal was not made until all the scans for one image were completed and the next image positioned for scanning. A log of each frame signal, scan signal, and scan was made for each image in order to avoid becoming confused during the long scan sessions. A typical scan session involved about 9 or 10 images and took about three and a half hours.

After a scan session was completed the scanned images were calibrated. To initiate a calibration, two frame signals were placed on channel "X" in succession. Then, after placing a scan signal on channel "X" a scan was made across a neutral density filter of known density. Then another scan signal was given and a filter of different density was scanned. Usually three such filters were scanned; their densities, along with the actual digital values corresponding to the densities, were printed out by the image assembly program. The range in density of the neutral density filters was chosen to be roughly equal to the density range encountered in the scanned images.

The Computer Programs

The computer programs used for the reduction of the Jupiter data were written by Dr. Richard L. Hackney of Western Kentucky University. They were modified as the need arose by Dr. Michael A. Lynch of the University of Florida. In addition, Dr. Lynch helped the author with many tape-related computer program problems.

Two 1,200-foot magnetic tapes for the IBM 370/165 tape drives were used in the data reduction. One tape was named "JOVE" and was used by Dr. Lynch as the raw-data collection tape. This tape was initialed as a nonstandard-label tape (NL) to enable the digital converter to write on it. The second tape was called "ZEUS" and was initialed as a standard label tape (SL), enabling the computer to write on it. This tape was used as a library tape to hold the entire series of data files. A data file was generated by each scan session.

The image assembly program is called "JSCAN." JSCAN reads the raw data from JOVE, assembles and punches each scanned image on cards, prints out each image as a 10-density level 50 x 70 pixel image array, and writes the raw data on the library tape ZEUS, excluding the data not used to produce the images. The calibration scans are also printed out in digital form, allowing a calibration curve to be plotted if desired. Due to the abbreviated nature of the files on ZEUS, it easily held all of the image data files, while the first two files of JOVE had to be rewritten in order to complete the scanning sessions.

Each completed image frame is punched on 100 standard computer cards with 35 elements per card. Thus, two cards were required per scan line of 70 elements. Blank cards are inserted every 100 cards to separate the image decks. The punch feature of JSCAN is optional and can be deleted by switching two cards in the program deck. The punch feature of the superposition program described below is controlled in the same manner.

The 10-level pixel images, using periods and the numbers from 1 to 9 as pixel elements, were used to examine briefly all of the scanned images. Not only was the hotspot looked for, but also scanning defects such as missing scan lines or improper density gradation due to overriding the pen-potentiometer drive mechanism. Any such defective images were noted and their image decks withdrawn from the cumulative decks of all the scanned images. This cumulative image was used as the input for the superposition program, which is named "JSUPER."

JSUPER centers all the images relative to the borders of the array, punches the centered images on cards if desired, and prints out the centered images with 35 levels of contrast gradation, using both numerals and all the letters of the alphabet. The centered images are then superimposed by adding together corresponding array elements. The superimposed image is also printed out with 35 levels of gradation and is punched out on 350 cards if desired. All of the superimposed pixel information is tabulated in its original digital form, preserving the total range of density gradations. The contour profiles of each scan line of the superimposed image are printed out in graphical form with 35 levels of resolution. The output from JSUPER was used to make the final search for the hotspot.

The following figures are examples of output from the computer programs. Figure 75 shows the 10-level pixel array from JSCAN of infrared image no. 72, compared with a standard print of image no. 72. Figure 76 shows the 35-level centered pixel of image no. 72 generated by JSUPER, also compared with a standard print of image no. 72. In the 10-level array the numerals 8 and 9 indicate areas of highest density while in the 35-level array, using both numerals and letters to

Figure 75. The 10-level pixel array of infrared image no. 72 generated by JSCAN, compared with a standard print of image no. 72. In the pixel array the numeral "9" indicates the areas of highest density. Density gradation is reversed between the array and print since the array corresponds to a negative image. Areas of the greatest density in the array correspond to the lightest areas of the print. North is up.

```
     0        10        20        30        40        50        60        70
     *         *         *         *         *         *         *         *

   1  ......................................................................  1
   2  ......................................................................  2
   3  ......................................................................  3
   4  ......................................................................  4
   5  ......................................................................  5
   6  ......................................................................  6
   7  ......................................................................  7
   8  ................................1111111111111.........................  8
   9  ............................1122222222333322221.......................  9
  10  ...........................12223333333334433332211....................  10
  11  .......................1112333445544444444444443221...................  11
  12  ......................1233344455555555555555554444221.................  12
  13  .....................123444455556666666666666655554322................  13
  14  ...................1123444555556666777766667665566544311..............  14
  15  ..................12234445566666666777776777766766655421..............  15
  16  ..................1234455566666677777777887777777765553211............  16
  17  .................13334555556676777778888878778777766664322............  17
  18  ................123445566677777777888888898889887777765522............  18
  19  ................2344456667777888988999989988888887777754432...........  19
  20  ..............113344466677788888999899898888887887777755432...........  20
  21  ..............1233456677777888888888988888888987787776555421..........  21
  22  ..............1233455566677777677788888887888877777676654431..........  22
  23  ..............12334555666667777667778888888988877777776554311.........  23
  24  ..............22334456667667676688889999988888888877676654421.........  24
  25  ..............22335566666776777788888999888888877777776555311.........  25
  26  ..............22445555566777777788888889888888888887776655321.........  26
  27  ..............2233555667777777788898888888888878787777655541..........  27
  28  ..............22344556676787988888889889999899888897776655411.........  28
  29  ..............2233455667778888899899999999999999888887655531..........  29
  30  ..............1233455677777889999999999999999898888877555421..........  30
  31  ..............113345556777788889999999999998888888877755442...........  31
  32  ................1244457777777777789899888888888777776654332...........  32
  33  ................113445556677777778898888887887777776654421............  33
  34  .................1234445666777777777788888777777766555321.............  34
  35  ..................123345556666767777777787777766665544221.............  35
  36  ...................113444456556666677777776666655554431...............  36
  37  ...................11234444555566666666666655555443331................  37
  38  ......................23333444555555555555555544442111................  38
  39  ......................11123333444444444444444433331...................  39
  40  .........................1122333333344444433333221....................  40
  41  ...........................111222233333333322211......................  41
  42  ..............................11111222211111..........................  42
  43  ......................................................................  43
  44  ......................................................................  44
  45  ......................................................................  45
  46  ......................................................................  46
  47  ......................................................................  47
  48  ......................................................................  48
  49  ......................................................................  49
  50  ......................................................................  50
```

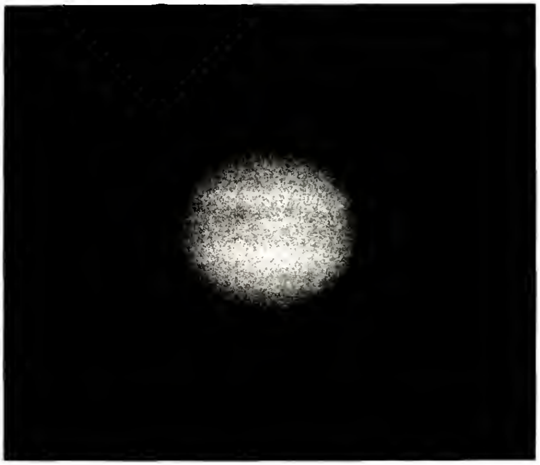

Figure 76. The 35-level centered pixel array of image no. 72 generated by JSUPER compared with a standard print of image no. 72. Due to the greater tonal gradation, this image array appears slightly larger than the image array generated by JSCAN shown in Figure 75. The letter "Z" indicates the areas of greatest density. Again the tonal gradation is reversed between the array and print. North is up.

```
    0        10        20        30        40        50        60        70
    *         *         *         *         *         *         *         *

 1    ......................................................................   1
 2    ......................................................................   2
 3    ....................................2.................................   3
 4    ......................................................................   4
 5    ......................................................................   5
 6    ......................................................................   6
 7    ............................222233333333332...........................   7
 8    .......................233566778668888977654222.......................   8
 9    ......................236679ABBCDDDDDDDCBBA76443......................   9
10    ...................245569ABCDFEFGFFGGGGFEECBA87422....................  10
11    ...................5699BDDEHHKKIIIIIJJJIIIIHECB7652...................  11
12    ..................48ADDDGHIKKLLLLLLLLLLLMKKIIGGCA952..................  12
13    ..............3348BDGGGHKLLLNNNNMONNNNNNNNNMKLKHDCA42.................  13
14    ...............477AEGHHKLMLMMPOPRQQQPQQPQPPMMNNKIHD863322.............  14
15    .............2379AEGJJLMNNNPOPPRRRQSPRRRRQPQQPPMKJIA854...............  15
16    .............459DEHIJKMNOPQQQRQSSSSSTRTTSRQRRRQUKKKFD963..............  16
17    ...........2267DEFHKLLLOQQQQRSSTTUUUUTSTTSUSRRRPNNNIFBA322............  17
18    ...........239AEGHKMOUUPQRRTTTTTUUUUWVVVVVUUTSSRRRQKJCC632............  18
19    ...........65ADGIILNPPQSRRVUVWWWWXXXVZZWWVVWVUUTSSQMJGFB322...........  19
20    ...........77FGJJJOOPQQTWWVUWXXWWWYXWXWVVWUVTVUSSSSLKHFC54............  20
21    ...........8AFFHKNNQRRRSTUUUUVVWVWYUWVUTVTUURSTRRRPMKJJ863............  21
22    ...........9ADEIKMMPPPPTRSSPRSTTUUUVUTTTUUUTSSSSQQPNLJIE752...........  22
23    ..........29PFFILLLJPPPQQRQPPTSSTVUUJWWWVVUTSTSTQQRQLKIF97............  23
24    ..........3ACEGJJMOPPQQQQRQPPTTUUWXXXXXWVVVVTTTRQPQONLIHA63...........  24
25    ..........4ABEFKLOOOPRQQSSRSUUUUUVXXXUUVWUUVTTTSSSRPMKKF972...........  25
26    ..........4ABGGJKLMOPSSSSRTUUUUUVWVVXVVVUVWVUUUTQQRONMKEA73...........  26
27    ..........3CCEELKMNOFQQRSSSSTUUTVWWVVVVVVVTTVSTTSSRNMMKG9632..........  27
28    ..........2BDFHILMNDFPPTTUTTVUUVWWWXWXXVWWWWVUUUTSPUUMLH872...........  28
29    ...........AJFGIMMNOSQSTUUVWXXWWXYYYZZYYYYYXXWWUUTRPMLKF652...........  29
30    ...........9AEGJKLPRRTSTVWWXXYXYYYYZZXXYYYWXWVUUTTSMMLIC632...........  30
31    ...........7BEFILMMPRRRTUUVWWXXXXXYYYXXXXVVVUUUTRQRLKHGB422...........  31
32    ...........569BGIJLOOPRSTTTTTVVWWWXWWWVVVTVURRSSGUOKIEDB322...........  32
33    ...........2577EHIKLMNPQFSSSTTTUUVVVUVUTTTTSRQQQNNLJGA9532............  33
34    ............256CGHIJMNNOQRRSPSSSTTUTUUUTSSSRQQQNMMKDC863..............  34
35    .............448CDFILKLNPPPQQRSSSSSSSTSRSSQQPQGMKJGA9652..............  35
36    ..............2499DHIJJKNMMPPPPPQQQQQRQQPPPNMLLJIID7643...............  36
37    ...............477ADGIIIMLKMNNNOUUNNNNNNMMLLJIIFLD94422...............  37
38    ...............2336BEEEFHIJKJJJLLLLLMLLLLLKJHGGB98632.................  38
39    ..................3679BDFFGGIIHIJJJJJJJIIIIFFFF9542...................  39
40    ....................4669CCDFFFFGGGHHGGGGGGDDBA8433....................  40
41    .....................345779BBBCDDEFFEEEDCBA86442......................  41
42    ........................344777799AAA9999765432........................  42
43    ..........................333344445555544332..........................  43
44    .................................2222222..............................  44
45    ......................................................................  45
46    ......................................................................  46
47    ......................................................................  47
48    ......................................................................  48
49    ......................................................................  49
50    ......................................................................  50
```

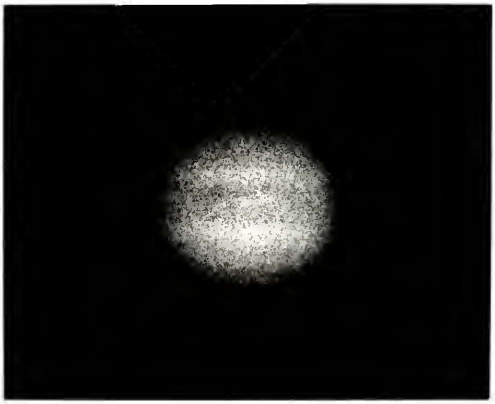

express density gradation; letters near the end of the alphabet indicate the areas of greatest density. The superimposed images from all the scan runs are shown in Appendix II along with the scan lines which pass through the search areas for the hotspot.

Examination of the Computer Output

A total of eight scan sessions was required to scan the 74 images involved in the computer data reduction. Occasionally one or more of the images in a scan session was deleted due to image defects, missed scan lines, or improper density gradation. A list of all the scanned images is given at the beginning of Appendix II.

The pixel arrays for all the scanned images were examined in detail at shading levels of both 10 and 35. A considerable area around the expected area of the spot was examined. In all the pixel arrays of separate images and in the composite arrays there was no evidence of the hotspot. Band structure, satellite shadows and image defects could easily be located when compared with the original image on the photographic plate.

Examination of the scan lines of the composite images in the expected regions of the hotspot showed no anomalies or peaks that could be interpreted as a region of higher density near the limb in the expected position of the spot. Occasional slight changes in density exhibited by the scan lines in the spot search area were found to be identical in character to gradations found over the entire disk area. In general, the scan lines in the spot search area were consistent with a smoothly contoured limb with no evidence of density anomalies.

The author concludes that no evidence of the hotspot is suggested by the data, either by visual examination or by computer superposition of a selected number of images. It is estimated that if the spot had been at least three times the brightness of the limb it should have been marginally detected with the plate-filter combinations used in this experiment. It is concluded that the spot is either below the detection level of this study or is nonexistent.

In view of the results of this experiment it is interesting to note that the recent Pioneer 11 flyby of Jupiter in December of 1974 also failed to detect any evidence of the Io-flux tube (Elson 1974). The trajectory of the spacecraft supposedly intersected the hypothetical flux tube in the vicinity of Io. However, the failure of Pioneer 11 to detect the flux tube does not necessarily invalidate the theory of Goldreich and Lynden-Bell, for there is doubt among the experimenters as to whether the spacecraft actually passed through the expected region of the flux tube.

CHAPTER VIII

CONCLUSIONS

While initially conceived as an aid to Cassegrain photography with the 30-inch reflector, the hypersensitization of Kodak type 103a-0 plates by nitrogen baking has proven helpful in the routine QSO monitoring program at Rosemary Hill, and now is standard procedure. The speed gains obtained by this process have enabled exposure times to be reduced by a factor of from 2 to 3; this has increased the number of sources that may be monitored on a given night and has made possible high-time-resolution studies of the variability of a few of the more active objects. Nitrogen baking of 103a-0 has also proven useful in exposures made with the recently installed Ritchey-Chrétien 18-inch telescope.

The experiments in hypersensitization by emulsion cooling have not yet progressed to the point where this process is practical for use at the telescope. However, the response of four emulsions has been studied, verifying the results of Hoag (1961,1964). A thermal gradient of about 15°C was observed across the cassette cold chamber during exposures; such gradients were also reported by Hoag and should cause no difficulty in the routine testing of emulsion response to cooling. It is suggested that future work in this direction be concentrated toward investigating the additive properties of baking and cooling, and in studying the response of various common color-reversal emulsions such as Ektachrome-X to exposures at low temperatures. If emulsion cooling proves to be a practical and useful process, the eventual goal will be to upgrade the present equipment and procedures to enable cooled exposures to be made at the telescope, perhaps capturing the delicate structure of a faint nebula or galaxy directly on color film.

Studies of the optical variability of quasars made at Rosemary Hill by Folsom (1970), R. L. Hackney (1972a), K. R. Hackney (1973), McGimsey (1974), and the author have shown that there are many different types and forms of variability exhibited by these objects. This suggests that QSO's are not a homogeneous species, but rather a class of objects that, though bound together by certain identifying characteristics, exhibit many divergent properties.

One of the most interesting aspects of QSO variability is the different degree of variability exhibited by various sources. Of the objects studied by the author, 50 percent showed statistically significant optical variations based upon a confidence level of 99.5 percent. The largest observed short-term optical intensity fluctuations were those of the lacertid prototype BL Lac; B-magnitude changes of $1\overset{m}{.}50$ on a time scale of days or weeks are characteristic of this object. The Florida observations of PKS 1004+13 are in sharp contrast, as 20 observations from 1972 to 1973 show a very constant intensity level of about $14^{m}.50$ in m_{pg}. Small fluctuations of approximately $0^{m}.20$ are vaguely suggested, but the confidence level for variability is only 30 percent. Hunter and Lü (1969) and Lü (1972) report moderate to large declines in the intensity of this object over a few years time, prior to the Florida observations. It is concluded that PKS 1004+13 is presently in a quiescent period, and that monitoring should be continued in an attempt to detect a resumption of activity.

Florida observations of PKS 0906+01 from 1970 to the present show a type of optical behavior now known to be characteristic of several of the OVV quasars. This object's light curve exhibits fluctuations suggestive of the behavior of a damped harmonic oscillator. Violent and rapid outbursts are followed by a decrease in activity and average intensity; when last observed the object appeared to be increasing in activity and should be monitored closely in the future.

These examples of QSO variability, and others throughout the course of this study and in other investigations made at Rosemary Hill, have shown that not only are there large differences in the degree of variability shown by different objects but that there appear to be several distinct types of optical fluctuations. One example is the previously discussed "ringing" behavior suggested by PKS 0906+01, where a large outburst apparently triggers violent optical oscillations which slowly die down over a course of months or years. Hackney (1972a) concluded that NRAO 512 and OX 074 also exhibit this kind of activity.

Extremely violent and rapid optical activity about an apparently constant average intensity is exhibited by BL Lac; studies of PKS 1514 -24 and ON 231, also classified as lacertids, show this type of behavior although their intensity fluctuations are not as large as those of the prototype lacertid. Optical activity very similar in degree and character to that of BL Lac was shown by PKS 0735+17 over a time scale of a few weeks. In early 1974 this object flared nearly $1\overset{\mathrm{m}}{.}50$ and then rapidly declined to its preflare intensity level. The lineless spectrum (Burbidge and Strittmatter 1972) and violent optical activity of this object suggest that it definitely belongs in the lacertid class and should be monitored closely in the future.

When considering long intervals of time the majority of objects in this study appear to fluctuate around a more or less average intensity level, but definite long-term intensity declines over a time scale of years have been observed for 3C 345 and OJ 287. Since 1971 they have both declined in average intensity; OJ 287 has declined over $3\overset{\mathrm{m}}{.}25$ in this time, changing from the brightest known QSO to a B magnitude fainter than 16. The long-term intensity declines of these objects, in particular OJ 287, were accompanied by rapid and violent short-term variations on a time scale of days or weeks.

In the sample of objects whose variations were studied in Chapter IV, no statistically significant variations, based upon a confidence level of 99.5 percent, were seen for PKS

0725+14, PKS 1004+13, PKS 1055+20, PKS 1116+12, 4C 09.42, PKS 1645+17, and PKS 2145+06. However, PKS 1055+20 and 4C 09.42 both have confidence levels for variability of 98 percent and should be considered probable variables; monitoring should be continued in the future to try to resolve the nature of their suspected variability. The monitoring of the objects with low confidence levels for variability should not be discontinued; Lü (1972) believes all quasars will show variability if observed over a long enough period. Observations of sudden variability in a long quiescent object could provide important clues as to the nature of the source emission model.

These examples of QSO variability suggest that there may be no unique source model or perhaps that the degree and type of variability is an acquired evolutionary trait. However, if this were so there should be a relationship between the degree of variability and redshift, assuming high redshift objects are seen at an early epoch in the age of the universe. The observations of PKS 2134+004 and 4C 09.34, both high redshift objects, do show little variability. However, the data are too sparse to suggest a decrease in variability with increasing redshift; it is suggested that these objects, along with the objects with the highest known redshifts at the present, OQ 172 and OH 471, be monitored in the future to test this hypothesis.

Studies of the variations in the optical spectral indices occurring during optical intensity fluctuations have given new insight into the relationships between classes of objects, and have suggested that a simple thermal-nonthermal component model may explain many of the observed color changes. In general it is concluded that the more active objects show the largest fluctuations in color indices; however, the selection effect of more frequent monitoring of the active objects must be kept in mind.

Color studies of OJ 287 and 3C 345 suggest that the slope of the optical continuum of QSO's may not be simply correlated with brightness as predicted by the expanding source model (Vander Laan 1966). Such behavior was first noticed in the Florida three-color light curves of OJ 287; the short-term optical fluctuations apparently superimposed upon a slowly varying background component suggest that the optical intensity of this object might arise from two separate mechanisms, each capable of producing different color effects. Though no long-term color trend was observed, removal of the long-term intensity decline by computing the residual short-term fluctuations about least-squares parabolic fits to the data suggests possible short-term color effects.

Using the normalized data, color regression plots of $(m_B - m_V)$ versus m_V and $(m_U - m_B)$ versus m_U appear to show that the short-term optical fluctuations may have equal or greater range at long wavelengths as at short wavelengths, contradicting the expanding source model. Observations of OJ 287 by Kinman et al. (1974) at radio and optical wavelengths support the hypothesis that the expanding source model may not be applicable to OJ 287. Similar color trends were observed for 3C 345. However, statistical support for the color relationships of both objects is at the 50 percent confidence level and hardly significant. Even though statistical support is lacking, a review of Chapter V will show that considerable evidence exists from observations by other astronomers that the color trends may be real. Due to the significance of the apparent color trends it is concluded that these objects should be closely studied in the future to test further the validity of the apparent color relationships.

The color studies of OJ 287 and 3C 345, and of BL Lac by Hackney (1973), suggest that the observed changes in color may be explained by a two-component continuum model consisting of a constant-intensity thermal component perhaps arising from an envelope of stars, and a variable nonthermal component. The nonthermal component is assumed to have the greatest intensity, and a linear spectrum described by a simple power law. The addition of the thermal component makes the shape of the optical continuum slightly convex; at high intensity levels of the nonthermal component, the thermal component is washed out and the spectrum becomes linear in shape. The portion of the spectrum where the "peak" of the thermal component occurs, determined by its temperature, will exhibit a lower range of intensity fluctuations during variations of the nonthermal component, than the surrounding spectral regions. A thermal component peaking in the middle of the optical spectrum would explain the color trends of OJ 287; the color trends of BL Lac could be explained by a thermal component peaking at longer wavelengths. Though there are obvious theoretical and observational difficulties with such a model, the simplicity of this hypothesis adds a certain attractiveness. In addition, a supposed thermal envelope surrounding BL Lac does show up in long exposures with large instruments and is best seen at long wavelengths in the optical. No envelope has been detected for OJ 287; if this object has an envelope whose energy distribution peaks toward shorter wavelengths it could conceivably be masked by the intense nonthermal continuum.

The close similarity of OJ 287 to the OVV quasars 3C 279, 3C 345, 3C 454.3 and 3C 466 in such properties as variability, nonthermal continuum with variable polarization, star-like images and inverted radio spectra (Visvanathan 1973) suggests that the sub-class of lacertids is itself a nonhomogeneous class of objects. It is conceivable that the lineless optical spectra of various lacertids arise from intense nonthermal emissions of different causes, and that the objects are really quite dissimilar. However, the strong resemblance of several lacertids to BL Lac cannot be disputed and this hypothesis remains an interesting speculation at the present.

No evidence for evolutionary trends was observed in a study of the color-redshift relation for quasars, the data seem roughly to fit the theoretical K corrections for reddening of Sandage (1966c) and Strittmatter and Burbidge (1967).

The theoretical curves were not computed beyond a redshift of 2.2; it is suggested that the high-redshift trend of the K correction is represented by 4C 05.34. The intrinsic variations in the colors of the Florida objects made it difficult to decide which of the above two curves best fits the data; Goldsmith (1972), using colors from De Veny *et al.* (1971), concluded that the curves of Strittmatter and Burbidge, which took into account spectral lines, were a better fit to the data than those of Sandage.

Studies of the short-term optical variability of a sample of lacertids have shown that the optical fluctuations of PKS 1514-24 and ON 231 resemble those of BL Lac, as discussed previously. The variations of ON 325 appear to be quite different in character from those of BL Lac. Rather than rapid fluctuations about a more or less constant intensity level, this object exhibits more moderate short-term activity superimposed upon long-term fluctuations of several months' duration. This adds further weight to the hypothesis that several lacertids appear to be rather dissimilar objects whose intense nonthermal emissions mask spectral lines.

Based upon a confidence level of 99.5 percent, statistically significant variations were observed at Rosemary Hill for the lacertid prototype BL Lac; the largest such fluctuation was a decline of $0\overset{\mathrm{m}}{.}60$ which occurred in 33 minutes. The method of Terrell (1967) for estimating the size of the active region, used with the redshift of 0.07 reported by Oke and Gunn (1974), suggests that the above fluctuation took place within a maximum source size of 3.5 hours in light travel time. If correct, such a small size puts severe restraints on the luminosity requirements for source models. However, other more recent interpretations have suggested that the source size or luminosity requirements are not as strict and the size of the active regions of rapid variables such as BL Lac remains open to question.

The identification of BL Lac with an elliptical galaxy at a redshift of 0.07 by Oke and Gunn may have provided an important clue as to the nature of QSO's. However, the validity of the redshift reported by Oke and Gunn is currently being debated. Observations by Baldwin _et_ _al_. (1974), presented at the recent 144th meeting of the American Astronomical Society, do not confirm the observations of Oke and Gunn.

Attempts to detect simultaneous intraday activity in BL Lac at Rosemary Hill and Bradley Observatories yielded inconclusive results; the level of activity appeared to be higher at Rosemary Hill, and the average intensity was $0\overset{m}{.}17$ brighter as observed at Bradley Observatory. The different degree of activity observed might have been due to the higher time resolution achieved at Rosemary Hill; the average intensity difference is attributed to possible polarization or color effects between the two instrument systems.

Simultaneous monitoring of BL Lac with the Rosemary Hill 18-inch and 30-inch telescopes suggests that magnitude shifts between the two instruments are unimportant in routine long-term monitoring; for intraday studies such shifts may be minimized by working at the Cassegrain focus of the 30-inch. The data suggest that, due to the large aperture difference between the two instruments, the small magnitude shifts observed are probably caused by shifts in the calibration curve zero point introduced by relative exposure effects. However, polarization and color effects cannot be ruled out.

No statistically significant intraday activity was observed for PKS 0735+17. However, on three nights variability was detected with a confidence level of 97 percent or greater, suggesting that, though less vigorous than those of BL Lac, intraday variations do occur.

On the night of February 25, 1974, simultaneous monitoring of PKS 0735+17 at Bradley and Rosemary Hill Observatories produced light curves which are in rough agreement during the first hour of observation, suggesting that simultaneous events may have been marginally detected. Synchronized alternating exposures of 6 and 12 minutes suggest that exposure time contributes to the photometric quality of the plate; the longer exposures seem consistently to have lower rms error. Further general investigations of the PKS 0735+17 intraday data suggest that underexposed plates, in addition to having larger rms scatter, can cause calibration curve zero point shifts as evidenced by the apparent similarity between object variations and those of a comparison star. On March 18, 1974, simultaneous monitoring of PKS 0735+17 at Bradley and Rosemary Hill Observatories suggested that no real events were detected.

Magnitude zero point shifts observed between the two observatories are attributed to possible polarization and color effects.

The photographic search for an Io-related Jovian auroral hot spot has ended with essentially negative results. During the 1973 apparition a total of 164 images of Jupiter were taken at the Cassegrain focus of the 30-inch reflector, in low-albedo ultraviolet and infrared regions to reduce the competition from reflected sunlight. To improve further the chance of detecting the spot all observations were made when the spot should have been on the Jovian limb, thus taking advantage of limb darkening to reduce reflected sunlight by an additional factor. The primary emissions expected were those of molecular hydrogen, though a possible methane component might arise in the infrared, if the precipitant electron energy is not dissipated at high altitudes in the Jovian ionosphere. Visual examination of the images revealed no trace of the hot spot. Suitable images were digitized and computer stacked, in a manner analogous to image superposition techniques performed in the darkroom, to try to increase the signal-to-noise ratio between the spot and the Jovian limb. This technique yielded no trace of limb density anomalies that could be interpreted as the auroral hot spot. It is concluded that the spot is either nonexistent or below the threshold detection level of this study. It is estimated that if the spot had been at least three times the brightness of the Jovian limb in the search areas it would have been marginally detected.

It is the author's hope that these studies of QSO's and Jupiter, and the various simultaneously developed photographic techniques, have provided new insight into the various areas of investigation and will stimulate new studies in the future.

APPENDICES

APPENDIX I

LIBRARY OF JUPITER IMAGES

Table A-1 is a complete list of the Jupiter images taken for the hotspot search. All of the images were examined visually; 74 were reduced by computer techniques. The images used in the computer reductions are listed at the beginning of Appendix II.

The image number is an arbitrary identification number assigned to each image. The band pass refers to the spectral regions discussed in Chapter II. All images were taken at either f/16 or f/50. The date is given in the following order: year, month, and day. The time indicates the start of each exposure in Universal Time in the order: hours, minutes, and seconds. The comment column lists characteristics noted during the visual examination, such as a rough description of the image density, the presence of bands or satellite shadows, and image defects. The "E" or "W" at the extreme right of the comment column indicates that the spot was expected on the east or west limb, respectively.

The majority of the infrared exposures were made with the wide-band RG-8 filter. Twelve infrared exposures were taken with the narrow-band 7-56 filter; they are indicated by a "7-56" in the comment column. Offset guiding was used for the 7-56 exposures; the duration of the exposure in minutes is also given in the comment column.

Table A-1

Library of Jupiter Images

Image No.	Band Pass	f/	Date	Time	Comments
1	UV	50	730714	031500	low density W
2	UV	50	730714	031600	low density W
3	UV	50	730714	031700	medium density W
4	UV	50	730714	031730	medium density W
5	UV	50	730714	032000	very low density W
6	UV	50	730714	032020	very low density W
7	UV	50	730714	032040	very low density W
8	UV	50	730714	032200	very low density W
9	UV	50	730714	032230	very low density W
10	UV	50	730714	032300	very low density W
11	UV	50	730714	032400	very dense, faint bands W
12	UV	50	730714	032500	very dense, faint bands W
13	UV	50	730714	032520	very dense opaque W
14	UV	50	730714	032540	very dense opaque W
15	IR	16	730728	052200	very low density, shadow W
16	IR	16	730728	052300	low density, shadow W
17	IR	16	730728	052500	low density, shadow W
18	IR	16	730728	052700	low density, shadow W
19	IR	16	730728	052800	medium density, shadow W
20	IR	16	730728	052900	average density, shadow W

Table A-1 - Continued

Image No.	Band Pass	f/	Date	Time	Comments
21	IR	16	730728	053000	average density, shadow W
22	IR	16	730728	053600	average density, shadow W
23	IR	16	730728	053800	average density, shadow W
24	IR	16	730728	053900	average density, shadow W
25	IR	16	730728	054000	average density, shadow W
26	IR	16	730728	054100	average density, shadow W
27	IR	17	730728	054300	average density, shadow W
28	UV	16	730814	031145	very dense opaque W
29	UV	16	730814	031200	very dense, faint bands W
30	UV	16	730814	031248	dense, well defined bands W
31	UV	16	730814	031300	very dense opaque W
32	UV	16	730814	031315	very dense, faint bands W
33	UV	50	730814	032722	low density W
34	UV	50	730814	032845	dense, well defined bands W
35	UV	50	730814	032905	medium density W
36	UV	50	730814	032933	medium density W
37	IR	16	730819	080300	average density, defects E
38	IR	16	730819	080500	average density E
39	IR	16	730819	080600	average density E
40	IR	16	730819	080700	average density E
41	IR	16	730819	081100	average density E

Table A-1 - Continued

Image No.	Band Pass	f/	Date	Time	Comments
42	IR	16	730819	081300	average density E
43	IR	16	730819	081400	average density E
44	IR	16	730819	081500	average density E
45	IR	16	730819	081600	average density E
46	UV	16	730819	082122	dense, bands show E
47	UV	16	730819	082144	dense, bands show E
48	UV	16	730819	082439	average density E
49	UV	16	730819	082500	average density, scratched E
50	UV	16	730827	070747	very dense opaque W
51	UV	16	730827	070816	very dense, faint bands W
52	UV	16	730827	070838	very dense, faint bands W
53	UV	16	730827	070903	dense, faint bands W
54	UV	16	730827	070923	very dense opaque W
55	UV	16	730827	070950	very dense opaque W
56	UV	16	730827	072203	very dense opaque W
57	UV	16	730827	072231	very dense, faint bands W
58	UV	16	730827	072248	very dense, faint bands W
59	UV	16	730827	072309	very dense, faint bands W
60	UV	16	730827	072326	very dense, faint bands W
61	IR	16	730827	065535	medium density W
62	IR	16	730827	065638	medium density W

Table A-1 - Continued

Image No.	Band Pass	f/	Date	Time	Comments
63	IR	16	730827	065800	medium density W
64	IR	16	730827	065923	medium density W
65	IR	16	730827	070030	dense, bands show W
66	IR	16	730827	070213	medium density W
67	IR	16	730827	071500	low density W
68	IR	16	730827	071616	low density W
69	IR	16	730827	071717	moderate density W
70	IR	16	730827	071819	moderate density W
71	IR	16	730827	071916	moderate density W
72	IR	16	730905	032700	dense, bands show W
73	IR	16	730905	032900	dense, bands show W
74	IR	16	730905	033100	dense, bands show W
75	IR	16	730905	033300	medium density W
76	IR	16	730905	033400	medium density W
77	IR	16	730905	034900	dense, bands show W
78	IR	16	730905	035100	medium density W
79	IR	16	730905	035200	medium density W
80	IR	16	730905	035300	dense, bands show W
81	IR	16	730905	035500	medium density W
82	IR	16	730905	035600	medium density W
83	UV	16	730905	034000	moderate density W

Table A-1 - Continued

Image No.	Band Pass	f/	Date	Time	Comments
84	UV	16	730905	034040	very dense, faint bands W
85	UV	16	730905	034120	very dense opaque W
86	UV	16	730905	034200	very dense opaque W
87	UV	16	730905	034246	moderate density, scratched center W
88	UV	16	730905	040050	very dense opaque W
89	UV	16	730905	040155	very dense opaque W
90	UV	16	730905	040300	very dense, faint bands W
91	UV	16	730905	040404	moderate density, red spot east limb W
92	UV	16	730905	040445	moderate density, red spot east limb W
93	UV	16	730905	040520	moderate density, scratch above red spot W
94	IR	16	730906	010503	dense, bands show fuzzy E
95	IR	16	730906	010700	moderate density, fuzzy E
96	IR	16	730906	010830	moderate density, fuzzy E
97	IR	16	730906	011000	moderate density, fuzzy E
98	IR	16	730906	011100	dense, bands show, fuzzy E
99	IR	16	730906	012600	low density, fuzzy E
100	IR	16	730906	012800	low density, fuzzy E
101	IR	16	730906	013000	dense, bands show, fuzzy E
102	IR	16	730906	013130	moderate density, fuzzy E
103	IR	16	730906	013400	moderate density, fuzzy E
104	IR	16	730906	013900	moderate density, fuzzy E

Table A-1 - Continued

Image No.	Band Pass	f/	Date	Time	Comments
105	IR	16	730906	015310	moderate density, fuzzy E
106	UV	16	730906	011738	very dense opaque E
107	UV	16	730906	011915	very dense opaque E
108	UV	16	730906	012000	very dense, faint bands E
109	UV	16	730906	012044	moderate density, red spot E
110	UV	16	730906	012108	moderate density, red spot E
111	UV	16	730906	014715	very dense opaque E
112	UV	16	730906	014750	very dense opaque E
113	UV	16	730906	014821	very dense opaque E
114	UV	16	730906	014900	moderate density, red spot E
115	UV	16	730906	014925	dense, defect south limb E
116	UV	16	730906	015000	very dense opaque E
117	IR	16	730920	025029	dense, 5 min guided 7-56 E
118	IR	16	730920	025852	dense, 6 min guided 7-56 E
119	IR	16	730920	030656	moderate density, 2 min guided 7-56 E
120	IR	16	730920	030952	dense, 8 min guided 7-56 E
121	IR	16	730920	032059	moderate density RG-8 E
122	IR	16	730920	032214	moderate density RG-8 E
123	IR	16	730920	032316	moderate density RG-8 E
124	UV	16	731014	023615	very dense opaque W
125	UV	16	731014	023725	very dense opaque W

Table A-1 - Continued

Image No.	Band Pass	f/	Date	Time	Comments
126	UV	16	731014	023800	very dense opaque W
127	UV	16	731014	023838	very dense opaque W
128	UV	16	731014	023857	very dense opaque W
129	UV	16	731014	023920	very dense opaque W
130	UV	16	731014	024140	very dense opaque W
131	UV	16	731014	024230	very dense opaque W
132	UV	16	731014	024300	very dense opaque W
133	UV	16	731014	024340	very dense opaque W
134	UV	16	731014	024410	very dense opaque W
135	UV	16	731014	024440	very dense opaque W
136	UV	16	731014	024500	very dense opaque W
137	IR	16	731014	015100	dense, halo, bands, 15 min guided 7-56 W
138	IR	16	731014	021000	dense, bands, 5 min guided 7-56 W
139	IR	16	731014	021800	moderate density, 2 min guided 7-56 W
140	IR	16	731014	022100	dense, halo, bands, 10 min guided 7-56 W
141	IR	16	731014	025330	dense, bands, 5 min guided 7-56 W
142	IR	16	731014	030000	dense, halo, streak, 10 min guided 7-56 W
143	IR	16	731014	031200	moderate density, 2 min guided 7-56 W
144	IR	16	731014	031430	moderate density, 2 min guided 7-56 W
145	UV	50	731114	012300	opaque, 3 min unguided, defect south E
146	UV	50	731114	012700	opaque, 1 min unguided, defect south E

Table A-1 - Continued

Image No.	Band Pass	f/	Date	Time	Comments
147	UV	50	731114	013000	dense, faint bands, defect south E
148	UV	50	731114	013200	dense, defects east-west E
149	UV	50	731114	013300	moderate density, defects east-west E
150	UV	50	731114	013400	low density, defects east-west E
151	UV	50	731114	014000	dense, double exposure E
152	UV	50	731114	014100	very low density E
153	UV	50	731114	014200	dense, faint bands E
154	UV	50	731114	014300	dense, faint bands E
155	UV	50	731114	015200	opaque, defects north-east E
156	UV	50	731114	015400	opaque, defects north-east E
157	UV	50	731114	015500	moderate density, defects north, red spot E
158	UV	50	731114	015600	low density, defects north E
159	UV	50	731114	015630	very low density E
160	UV	50	731114	020100	low density, defects north E
161	UV	50	731114	020120	moderate density, defects north, red spot E
162	UV	50	731114	020200	dense, defect north, red spot E
163	UV	50	731114	020300	dense, defect north, red spot E
164	UV	50	731114	020500	opaque, defects north-south E

APPENDIX II

THE SUPERIMPOSED ARRAYS FROM JSUPER

Appendix II contains the superimposed arrays and their scan lines in the hotspot search areas. The search areas are indicated by rectangles on the pixel images; the corresponding scan-line sections are denoted by vertical lines. All arrays are printed out with 35 levels of contrast; letters near the end of the alphabet indicate the regions of highest density. Occasionally background anomalies are seen surrounding the Jovian limb, especially when the array contains image densities classified as "low" or "average," which indicates a density only a few tenths above the plate background. The arrays constructed from the more dense images in general show a well-defined, symmetrical limb.

A slight "tail" is seen on the west limb of several arrays. This is believed to be due to mechanical damping in the pen-potentiometer drive mechanism, and possibly to capacitance in the interface cables. It is most apparent in the low density arrays; the tail is usually only a few units above the plate background on a scale of 35.

Index

The following is a list of the superimposed arrays and the images composing them. Immediately following the page containing a superimposed array are pages containing the scan lines passing through the spot search areas. Search areas in both the northern and southern hemispheres were examined. All arrays are shown with north up.

Page	Array	Images Superimposed
321	1	15, 16, 17, 19, 20, 21, 22, 23, 24, 25, 26, 27
324	2	37, 38, 39, 40, 41, 42, 43, 44, 45
327	3	46, 47, 48, 49
330	4	61, 62, 64, 66, 68, 69, 70, 71
333	5	72, 73, 74, 75, 76, 77, 78, 79, 80, 81
337	6	94, 95, 96, 97, 99, 100, 101, 102, 103, 104
340	7	117, 118, 119, 120, 121, 122, 123
344	8	138, 139, 140, 141, 142, 143, 144

SUPERIMPOSED JUPITER ARRAY NO 1

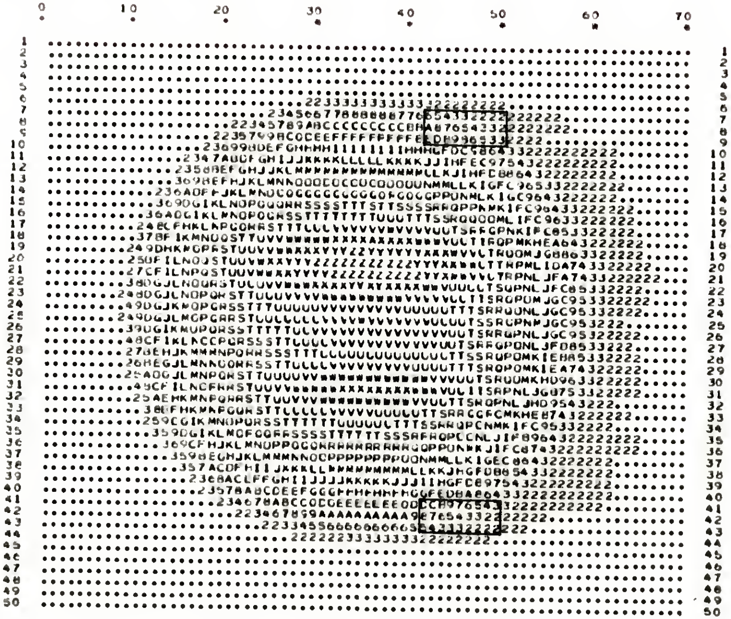
0
10
20
30
40
50
60
70

```
 SUPERPOSITION RECORD
IMAGE  TRIAL  HCENT  VCENT

  15     1     36     27
  16     1     38     26
  17     1     38     27
  19     1     35     29
  20     1     34     28
  21     1     40     30
  22     1     36     23
  23     1     43     24
  24     1     36     30
  25     1     39     29
  26     1     40     28
  27     1     37     26
   0     0      0      0
   0     0      0      0
   0     0      0      0
   0     0      0      0
   0     0      0      0
   0     0      0      0
   0     0      0      0
   0     0      0      0
   0     0      0      0
   0     0      0      0
   0     0      0      0
   0     0      0      0
   0     0      0      0
   0     0      0      0
   0     0      0      0
   0     0      0      0
   0     0      0      0
   0     0      0      0
   0     0      0      0
   0     0      0      0
   0     0      0      0
   0     0      0      0
   0     0      0      0
   0     0      0      0
   0     0      0      0
   0     0      0      0
   0     0      0      0
   0     0      0      0
   0     0      0      0
   0     0      0      0
   0     0      0      0
   0     0      0      0
   0     0      0      0
   0     0      0      0
   0     0      0      0
   0     0      0      0
   0     0      0      0
   0     0      0      0
```

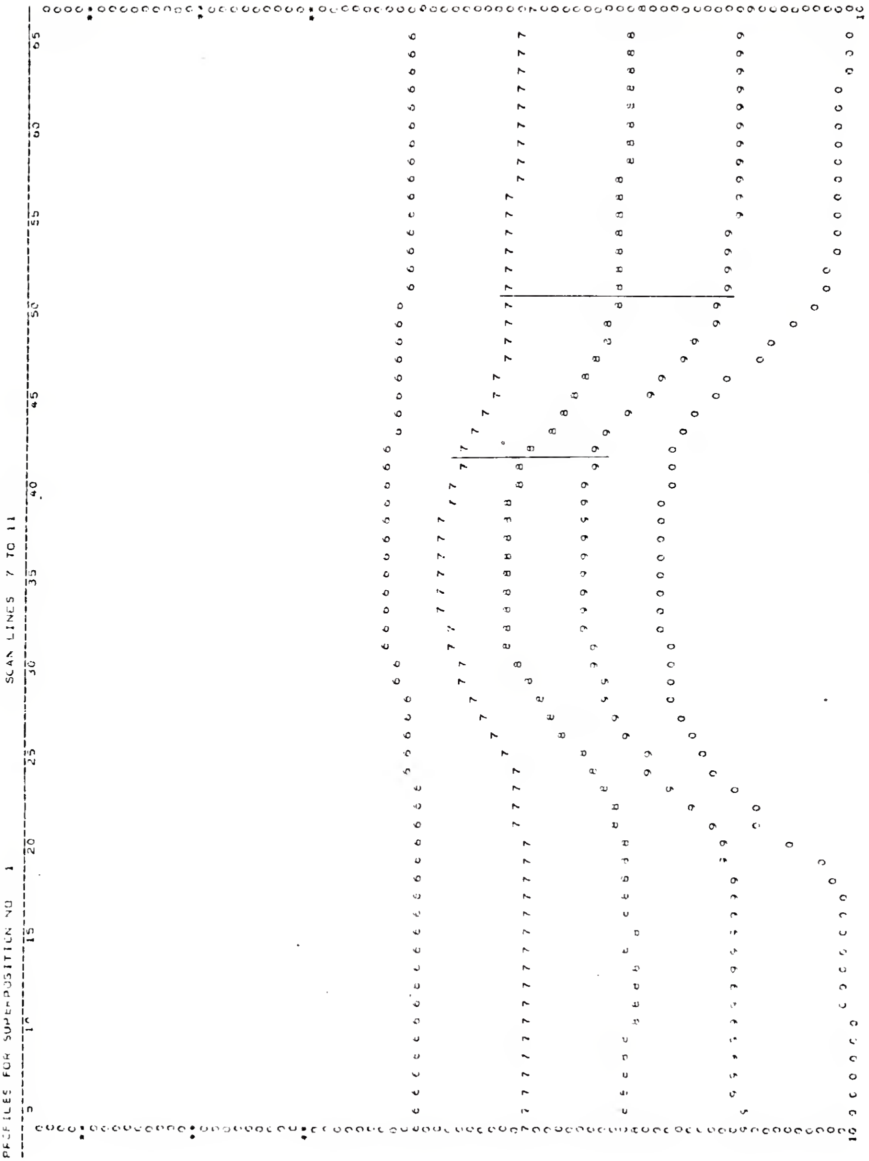
PROFILES FOR SUPERPOSITION NO 1
SCAN LINES 7 TO 11
5
10
15
20
25
30
35
40
45
50
55
60
65
10

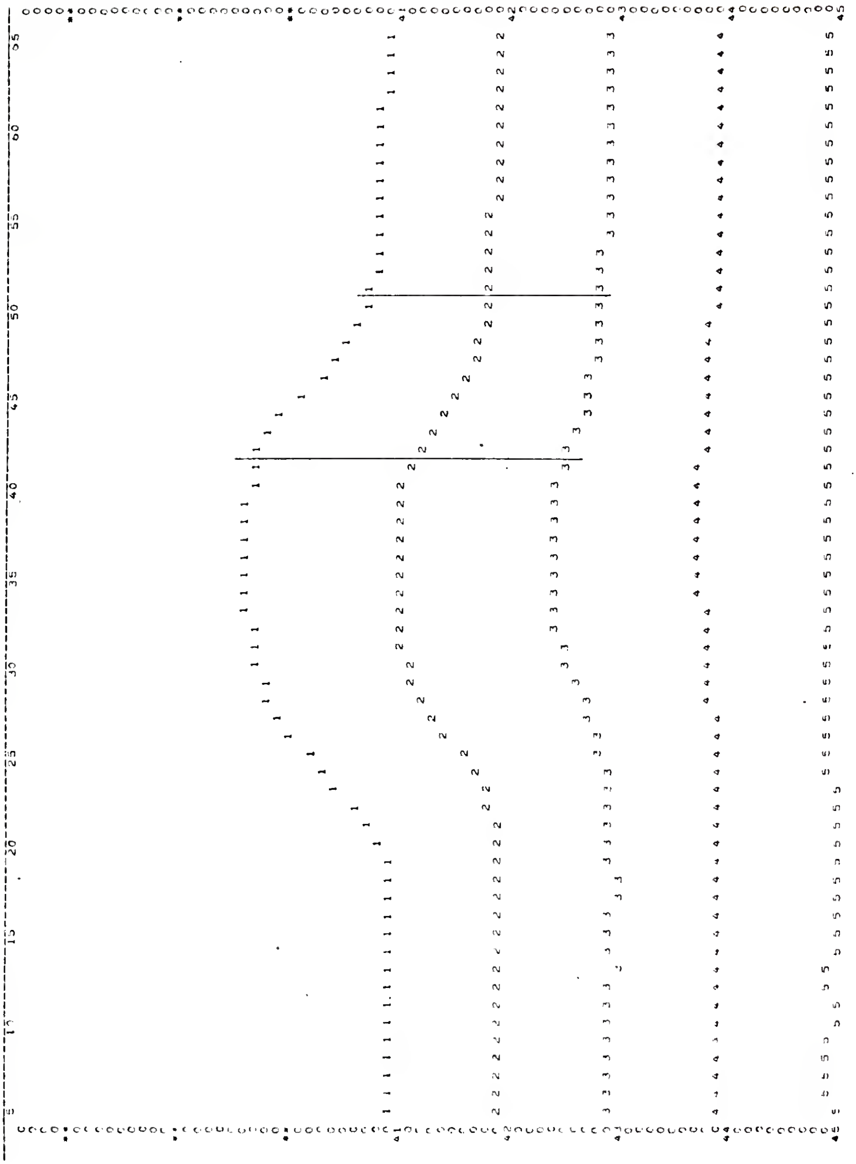

PROFILES FOR SUPERPOSITION NO 1 SCAN LINES 41 TO 46

SUPERIMPOSED JUPITER ARRAY NO 2

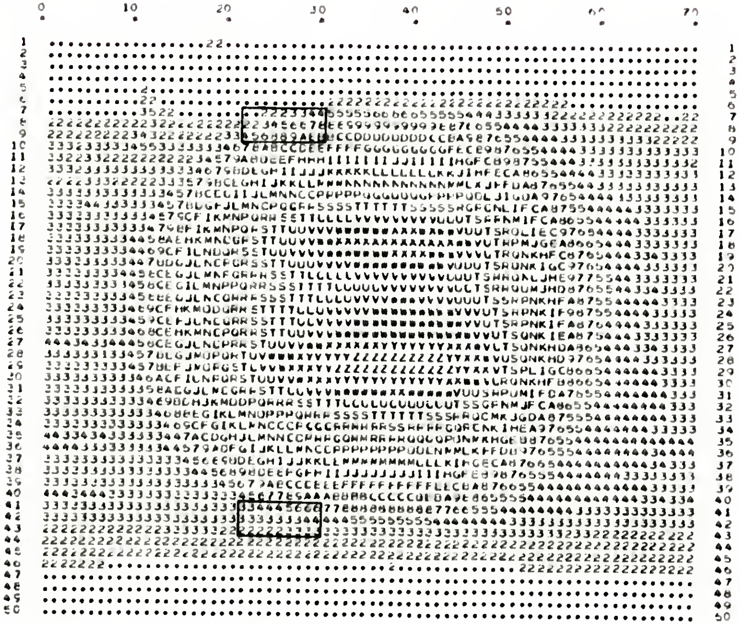

```
   SUPERPOSITION RECORD
IMAGE   TRIAL   HCENT   VCENT
  37      1       31      26
  38      1       38      29
  39      1       42      28
  40      1       39      27
  41      1       39      29
  42      1       35      27
  43      1       40      27
  44      1       39      26
  45      1       35      28
   0      0        0       0
   0      0        0       0
   0      0        0       0
   0      0        0       0
   0      0        0       0
   0      0        0       0
   0      0        0       0
   0      0        0       0
   0      0        0       0
   0      0        0       0
   0      0        0       0
   0      0        0       0
   0      0        0       0
   0      0        0       0
   0      0        0       0
   0      0        0       0
   0      0        0       0
   0      0        0       0
   0      0        0       0
   0      0        0       0
   0      0        0       0
   0      0        0       0
   0      0        0       0
   0      0        0       0
   0      0        0       0
   0      0        0       0
   0      0        0       0
   0      0        0       0
   0      0        0       0
   0      0        0       0
   0      0        0       0
   0      0        0       0
   0      0        0       0
   0      0        0       0
   0      0        0       0
   0      0        0       0
   0      0        0       0
   0      0        0       0
   0      0        0       0
   0      0        0       0
   0      0        0       0
```

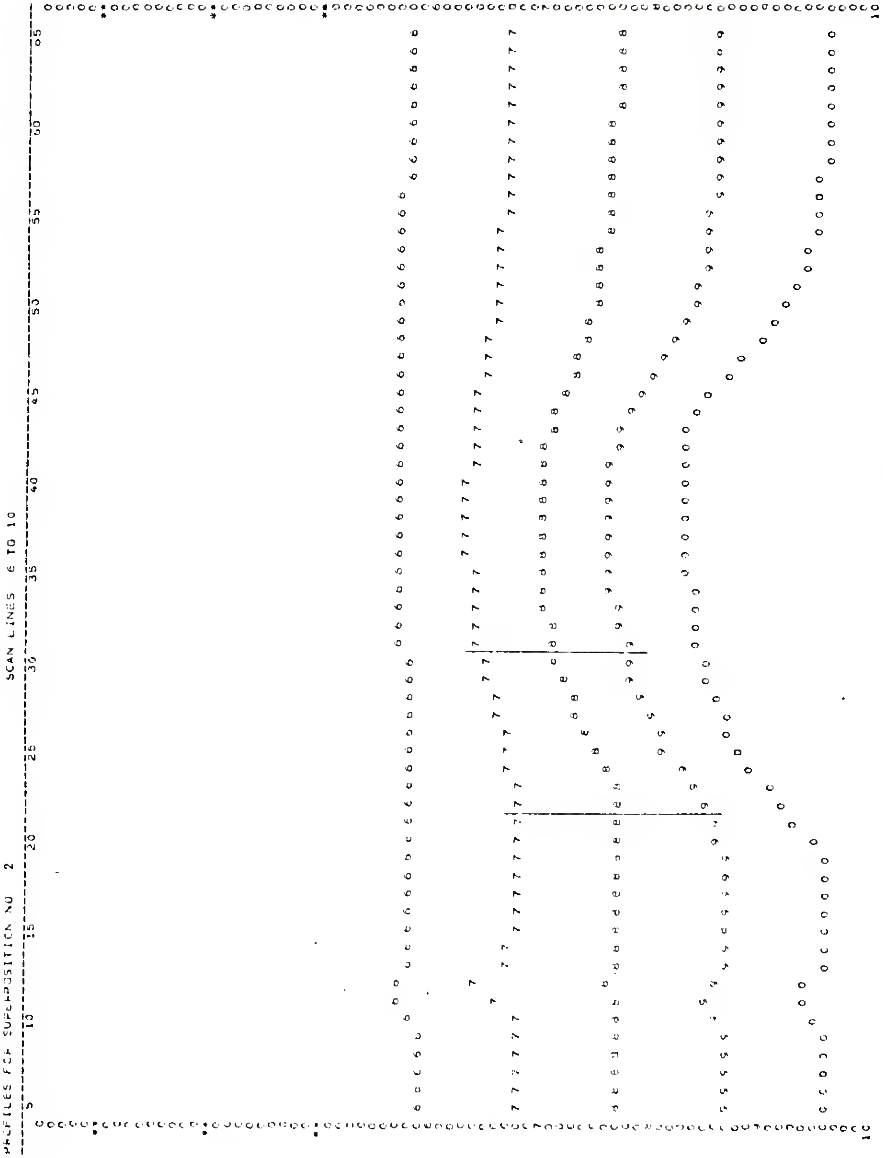
PROFILES FOR SUPERPOSITION NO 2
SCAN LINES 6 TO 10
5
10
15
20
25
30
35
40
45
50
55
60
65

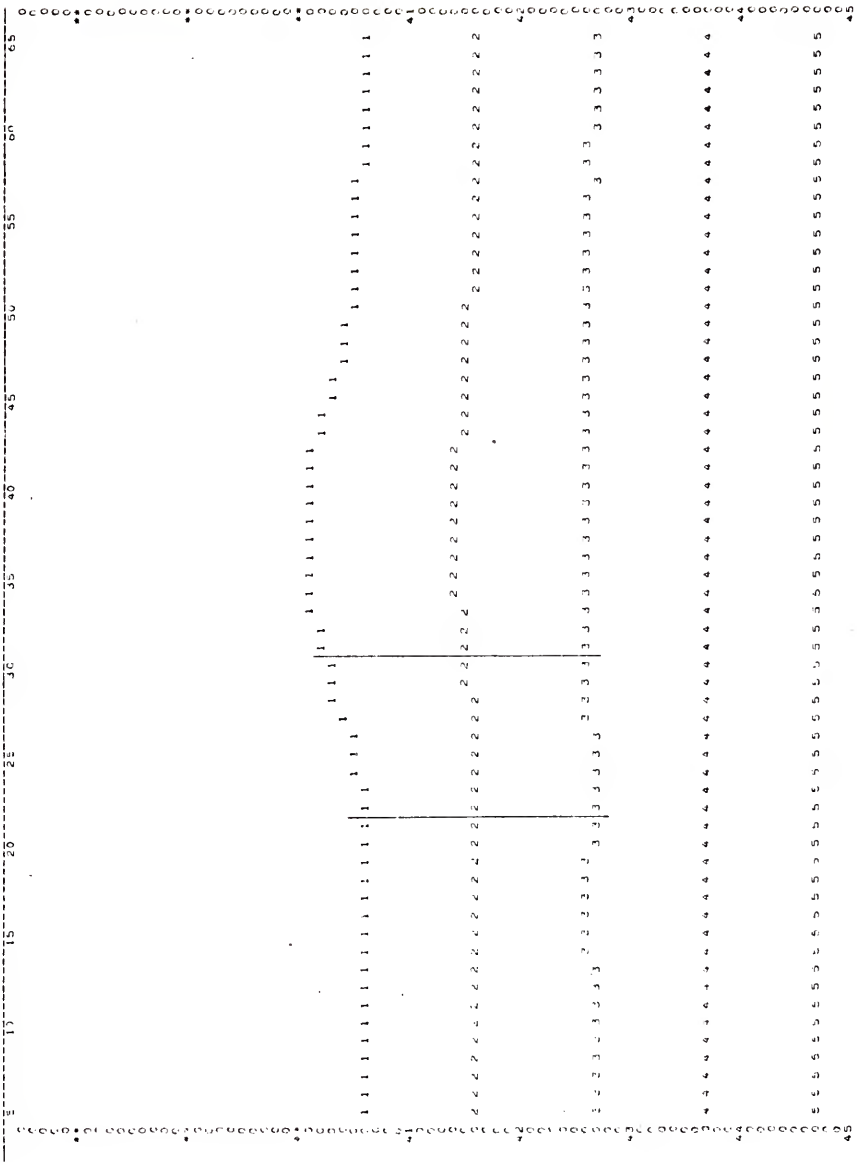

PROFILES FOR SUPERPOSITION NO 2 SCAN LINES 41 TO 45

```
SUPERIMPOSED JUPITER ARRAY NO   3

  0        10        20        30        40        50        60        70
  .         .         .         .         .         .         .         .
 1 ......................................................................  1
 2 ......................................................................  2
 3 ......................................................................  3
 4 ......................................................................  4
 5 ......................................................................  5
 6 ..............................222332322222............................  6
 7 ..........................2345666666666554322.........................  7
 8 .......................23557799AAAAAAAAA88654322......................  8
 9 .....................356799ABCCDDDDDDDDDDCB9865322....................  9
10 ...................34689ACCDEFFFFFFGGGGGGFFDCA87532................... 10
11 ................34579BCDFFGHHHHHHIIIIIIIIHHHGEDA86432................. 11
12 ................358ACDEEFHIIIJJJJJJJJJJJKJJJIHGEC98432................ 12
13 .............247AHDFFGHIJJKKLLLLLLLLLLLLLLLLLKJJGDC8632............... 13
14 ............3668BDEGHIJKLLLMNNNNNOOOOOUOOOUNNNMMKHGDA632.............. 14
15 ...........26ABEGHJKLMNNOOOPPPQQQQQQQQQQQQQQPPUNNMLHDA642............. 15
16 ..........364CFHJKMNNOOPPPQQRRRSSSSSSSSSSSSSSRRQPPNKHF8742............ 16
17 .........258EGHKLMOPPQQRSSTTTUUUUUVVVVVVVVUUTTTSSRONLIDA532........... 17
18 ........239EGJLMOPQRRSSTTUUUUUUVVVVVVVVVVVUUTTTSSRQPMKGU842........... 18
19 ........35CGJLMOPPQRSSTTTUUUUUUUUUUUUUUUUUTTSSRRQQPPNMIFA52........... 19
20 ........68CHKMMOOPPQRSSSSTTTTTTSTSSSSSSSSSSSSRRQQQQPNMJGC63........... 20
21 ........78DHKMMNOOPPQQRRRRRSRRRRRRRRRRRRRRRRRRRQQQQPONLID84........... 21
22 ........79FIKLMNNOOOPPQQRRRRRRRSSSSSSSSTTTTSSSSSRRRQPOMID953.......... 22
23 .......29DFIKLMNOOPPPPQQQRRRRSSSSSTTTTTTTTTTTSSSSRRQQPNKE9522......... 23
24 .......29CGJLMNNOPPQQQQQRRSSSSSSSSTTTTTTTTTSSSSSRRRQPONKE952.......... 24
25 .......29CGJLMMNOOPPQQQQQQRRRRRRRRRRRRRRRRRRRRRRQQQPPNLJD952.......... 25
26 .......29AGJKLMMMNOOPPPPPPPPPQQQQQQQQQQQQQQQQQQQQQQPUNLJE952.......... 26
27 .......28AEIJKLMMMNOOOOPPPQQQQQRRRSSSSSSSSSSSSSSSRRPPOLIC942.......... 27
28 ........78FHJKLMMNOPPQRRSSSTTTUUUVVVVVVVVWWVVVVVUTTROOKHB73........... 28
29 ........78EHJLMNPPQRSTTUVVVWXXXXXYYYYYYYYYYYYXXXVUTQOLIE963........... 29
30 ........58DHKMNPQRSTUVVWXXXYYZZZZZZZZZZZZZZZYXXXVUTQNKFD942........... 30
31 ........358FKMNPRSTUVVWWXXYYYYZZZZZZZZZYYYYXXWWVTTRQLIEC632........... 31
32 .........46FHKMOQRSTUUUVVVWWWWWWWWWWWWWWWWWWVUUTSRONJG8953............ 32
33 ..........683JKNPPQRSSTTTTTTUUUUUUVVVVVVVUUUTSSRQPOLME8732............ 33
34 ..........2TCFHKNNOPQRRSTTTTTTTTUUUUUUUUUUUTSSSQPONJG8542............. 34
35 ...........37BFIKLNOPQRSSSSSTTTUUUUUUUUUTTTSRRQPNLJF87432............. 35
36 ............37AFHJLNOPPQRRRSSTTTTTTTTTTTSSSRPOONKGEA7422.............. 36
37 .............36AEGIKLMNUOOPQQQRRRRRRRRQQQPPUNLKJGCA642................ 37
38 ..............258BEFHIJKLLMMNNNNNNNNNNNNNMLKJGED97642................. 38
39 ................347ACEEFGHIIIJJJJJJJJJJJIIHGD8985322.................. 39
40 ..................24689ABCDEEEEFFFFFFFFFEDCA965422.................... 40
41 ....................23456799ABBBCCCCCCBBA9765332...................... 41
42 .......................233456667777776655432.......................... 42
43 ............................233333333332.............................. 43
44 ...................................................................... 44
45 ...................................................................... 45
46 ...................................................................... 46
47 ...................................................................... 47
48 ...................................................................... 48
49 ...................................................................... 49
50 ...................................................................... 50
```

```
    SUPERPOSITION RECORD
IMAGE  TRIAL  HCENT  VCENT
  46     1     37     25
  47     1     40     26
  48     1     38     27
  49     1     34     28
   0     0      0      0
   0     0      0      0
   0     0      0      0
   0     0      0      0
   0     0      0      0
   0     0      0      0
   0     0      0      0
   0     0      0      0
   0     0      0      0
   0     0      0      0
   0     0      0      0
   0     0      0      0
   0     0      0      0
   0     0      0      0
   0     0      0      0
   0     0      0      0
   0     0      0      0
   0     0      0      0
   0     0      0      0
   0     0      0      0
   0     0      0      0
   0     0      0      0
   0     0      0      0
   0     0      0      0
   0     0      0      0
   0     0      0      0
   0     0      0      0
   0     0      0      0
   0     0      0      0
   0     0      0      0
   0     0      0      0
   0     0      0      0
   0     0      0      0
   0     0      0      0
   0     0      0      0
   0     0      0      0
   0     0      0      0
   0     0      0      0
   0     0      0      0
   0     0      0      0
   0     0      0      0
   0     0      0      0
   0     0      0      0
   0     0      0      0
   0     0      0      0
   0     0      0      0
```

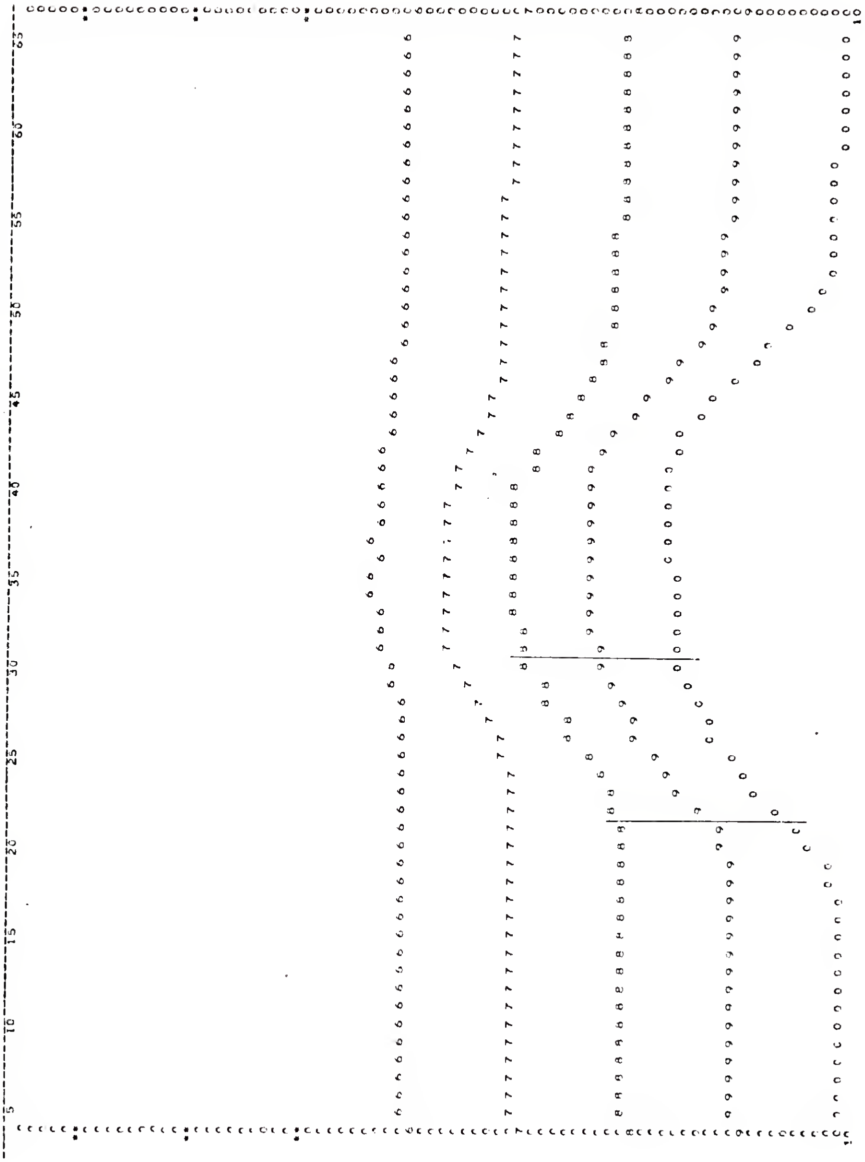
PROFILES FOR SUPERPOSITION NO 3 SCAN LINES 6 TO 10

PROFILES FOR SUPERPOSITION NO 3 SCAN LINES 41 TO 45

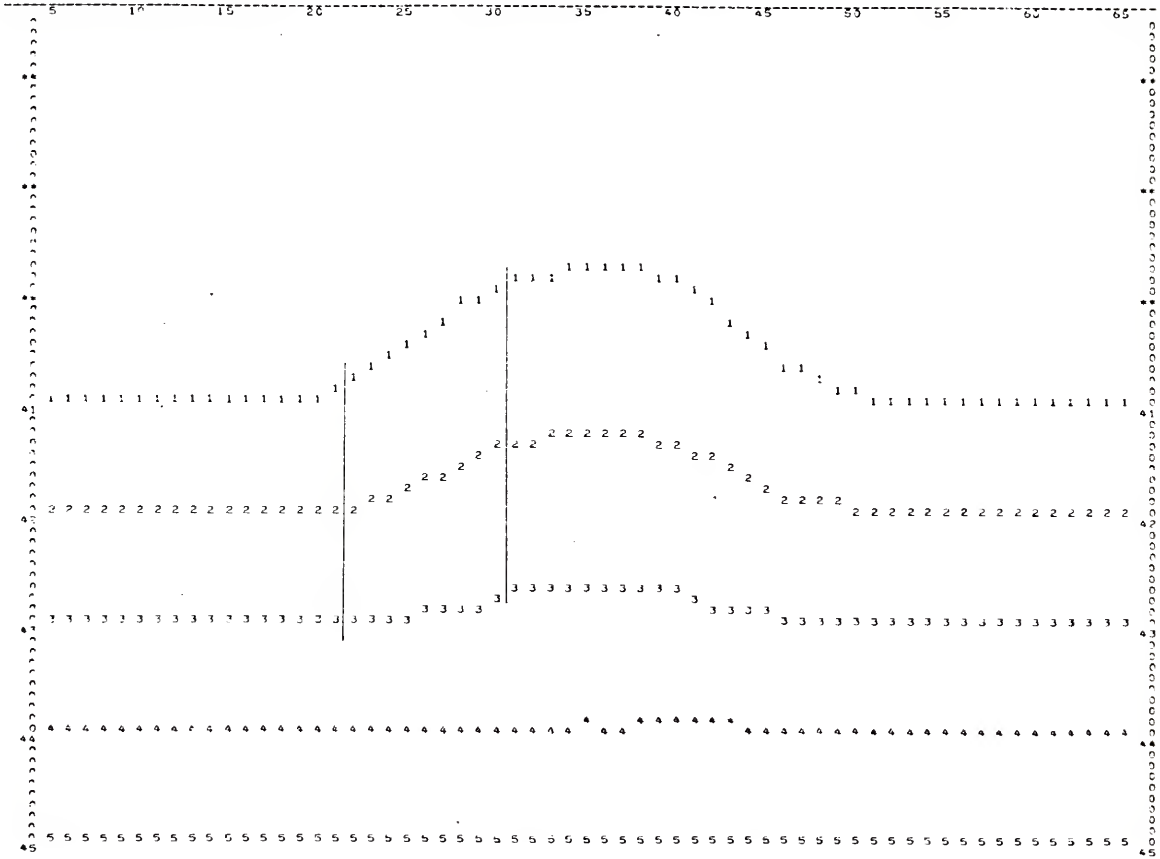

SUPERIMPOSED JUPITER ARRAY NO 4

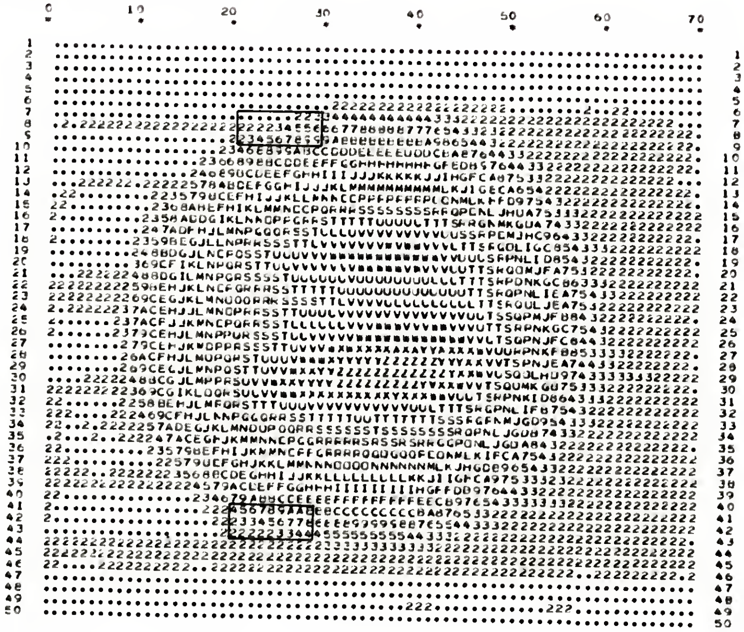

```
     SUPERPOSITION RECORD
IMAGE   TRIAL   HCENT   VCENT

  61      1       35      29
  62      1       34      29
  64      1       38      22
  66      1       37      30
  68      1       33      22
  69      1       34      27
  70      1       32      26
  71      1       36      25
   0      0        0       0
   0      0        0       0
   0      0        0       0
   0      0        0       0
   0      0        0       0
   0      0        0       0
   0      0        0       0
   0      0        0       0
   0      0        0       0
   0      0        0       0
   0      0        0       0
   0      0        0       0
   0      0        0       0
   0      0        0       0
   0      0        0       0
   0      0        0       0
   0      0        0       0
   0      0        0       0
   0      0        0       0
   0      0        0       0
   0      0        0       0
   0      0        0       0
   0      0        0       0
   0      0        0       0
   0      0        0       0
   0      0        0       0
   0      0        0       0
   0      0        0       0
   0      0        0       0
   0      0        0       0
   0      0        0       0
   0      0        0       0
   0      0        0       0
   0      0        0       0
   0      0        0       0
   0      0        0       0
   0      0        0       0
   0      0        0       0
   0      0        0       0
   0      0        0       0
   0      0        0       0
   0      0        0       0
```

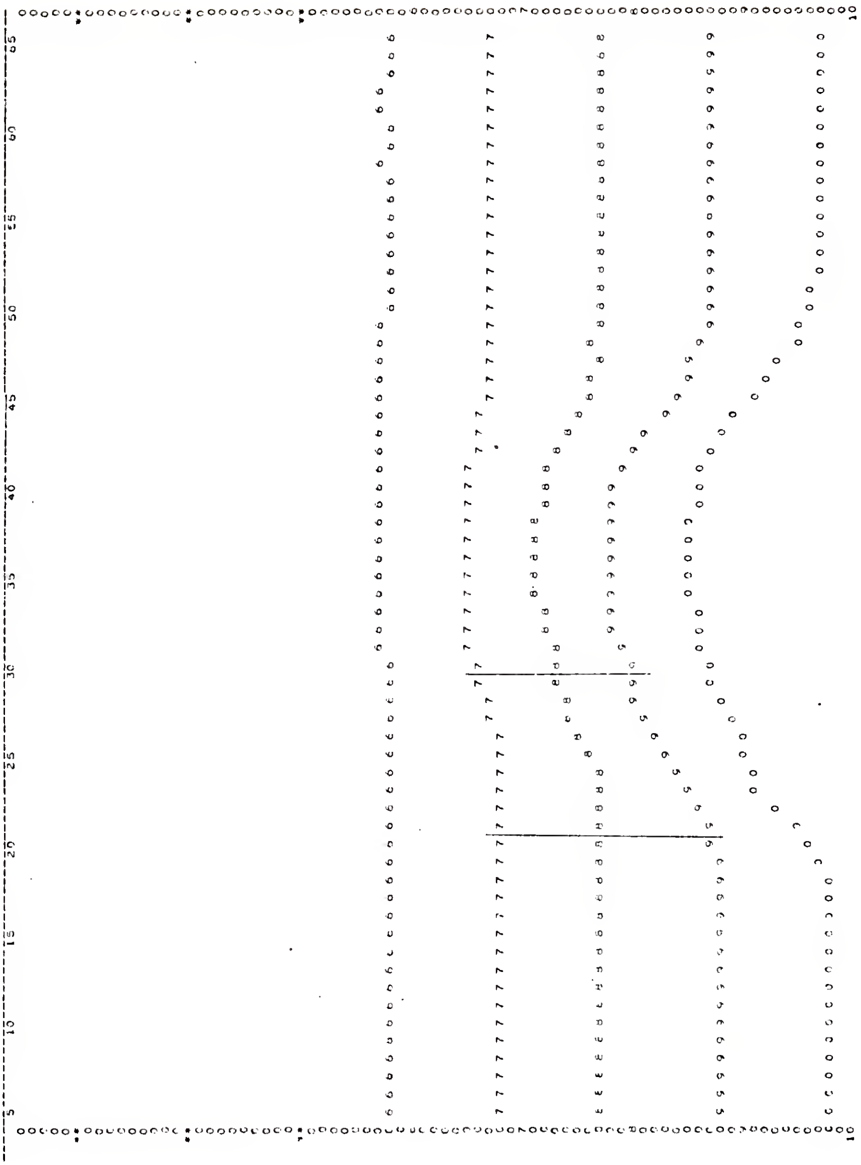

PROFILES FOR SUPERPOSITION NO 4 SCAN LINES 6 TO 10

PROFILES FOR SUPERPOSITION NO 4 SCAN LINES 41 TO 45

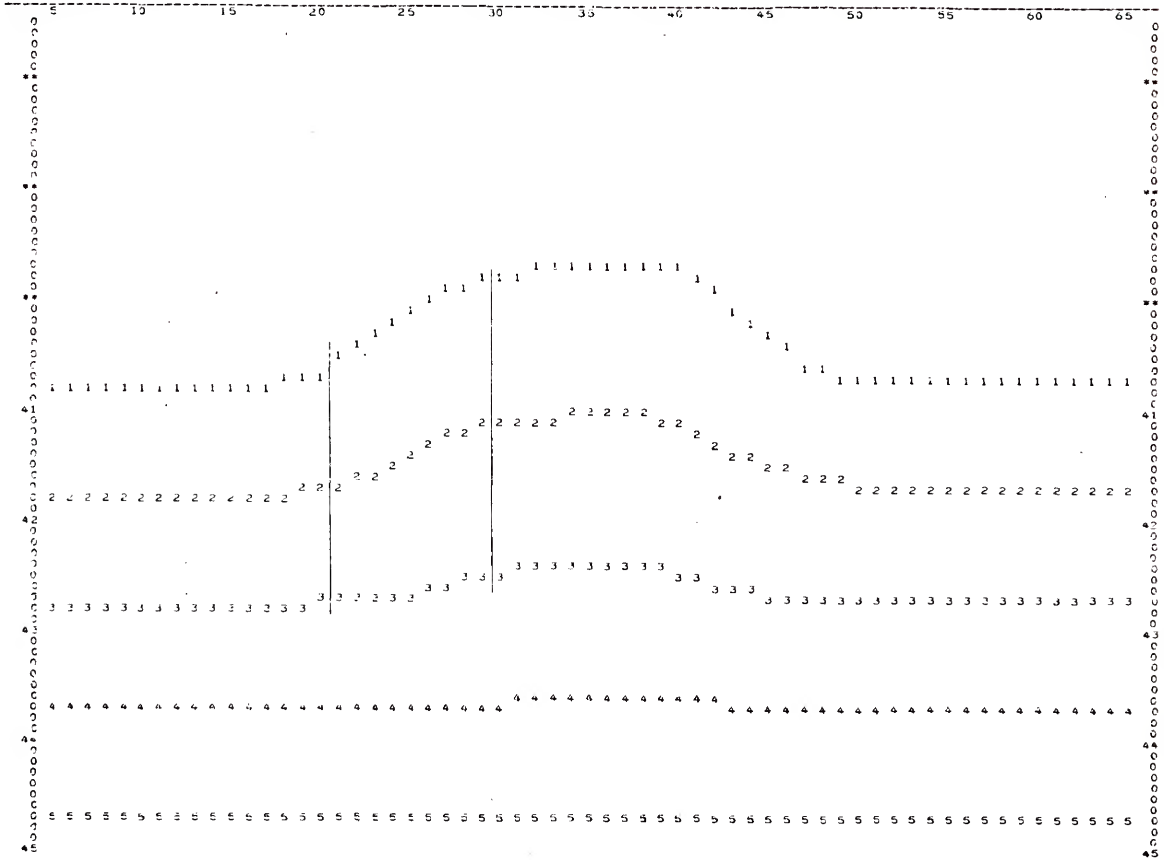

SUPERIMPOSED JUPITER ARRAY NO 5

```
   0         10        20        30        40        50        60        70
   .         .         .         .         .         .         .         .
 1  ......................................................................  1
 2  ......................................................................  2
 3  ......................................................................  3
 4  ......................................................................  4
 5  ......................................................................  5
 6  ......................................................................  6
 7  ...........................223333444444433222222......................  7
 8  ........................34566788999999987654322222....................  8
 9  .....................245789BBCDDEEFEFEEDDC998643222...................  9
10  ...................24689BCEEFGGHHHIIHHHHGFEECA864322222............... 10
11  ..................468BDEFGHIJJKKKKLLLKKKJJIGFDA754222................. 11
12  ................247ACFGHIJKLLMMMMNNNNNNNNMMLKJHFDA6422................ 12
13  ...............358BDFHIJKLMMNOOOPPPPPPPPPPOUMLKHFB84322............... 13
14  ..............369CFGIJKLMNOOPQQQRRRSSSSSRRRRQPONLJGC8532.............. 14
15  .............379DFHJKLMNOPPQRRRSSTTTTTTTTTTSSSRQPOMKGB8522............ 15
16  ............26ACFHJKLNOPQQRRSSTTTUUUUUVUUUUTTSRQUMJGC8422............. 16
17  ...........248CFHJKMNPPQRSSSTTUUVVVWVVVVWVVVVUTTSRQUMJGB632........... 17
18  ...........373FHKLNPQRRSTTJVVVWWWXXXXXXXXXWWVUUTSQPLJE8522............ 18
19  ...........59DGJMNPRSSTUVVWXXYYYYYYYYYYYYXXXWVVUTRQNLGB732............ 19
20  ..........373FJLNPQRSTUVWVXXXYYYYYYYYYYYXXXAWVVVVUTSQOMI0942.......... 20
21  .........249CHJLNOPRSSTUVVVVWWWWWXWXWWWWWWVVVUUTRQUMJFA522............ 21
22  .........25ADGJLNOOPPRRSTTTUTTUUUUUUVVWWWWWVVVUTSRQUNKGC6322.......... 22
23  .........25AEHJLNUPORSSTTTTTTTUJUUVVWXXXXXAWVVVUTSOPOKGD7422.......... 23
24  .........36BEHKLNPPRRSTTTTTTTJVVVWWWXAXXXXXWWVVVUTSRPOLHE742.......... 24
25  .........37CFHKMOPQPSTTTTTUUUVVVVWWXXXXXXXAWWVVVVUTTRPOLI07A2......... 25
26  .........37BFHKMNPQRSSTTUUUJVVWWWWXXXXXXXXXWWVVUUTRQOMID842........... 26
27  .........27BEHJMNOPQSSTTUUVVVWWWXXXXYYXXXXXXXWWVUTRQOMND742........... 27
28  .........26ADHKLNOPRSTUVWWWWXXXYYZZZZZZZYZYYYXXWVTSRPMHC632........... 28
29  ..........59CHKLNPQSTJVWWWXYYYZZZZZZZZZZZZZZYZYXWVUSQOKF8532.......... 29
30  .........248CGJLNORSTUVWWXXYZZZZZZZZZZZZZZZZYYYXXWVTRQMJE942.......... 30
31  ..........26AFIKMOPRSTUVVWWXXYYYYYYYZYYYYYYXXWWVUTRQNLGC732........... 31
32  ...........58CGIKMOPQRSTUUVWWWXXXXXXXXXXXWWWVUTTSRPNKID952............ 32
33  ...........36ADGIKMMNOQOSSTUUVVVVVWWWWWWVVVVUTSSSQPNLIFA622........... 33
34  ............36ADGIJLMNOPQRSSSTTTUUVVVVVVVUUTTTSRQUNLIFB632............ 34
35  .............47ADFHJKMNOPQQRRRSSSTTTTTTTTSSRQPUNMKIFA8422............. 35
36  .............246ACFHIKLMNNOQQQQQRRRRRRRRQPPUNMKJHE8642................ 36
37  ..............2469CEGIJKLLNNOOOPPPPPOOOONMMLJIGDA6322................. 37
38  ................358BDEGHIJKLLLMMMMNNNNMMMMLLJIGEC86322................ 38
39  .................2478ACEFFGHIJJJJKKKKKKKJJIIGECA7A32.................. 39
40  ...................3469ACDEFFGGHHHHHHHHHGFDCA75432.................... 40
41  .....................34578ABCDDDDEEEEEEDDCB9754222.................... 41
42  .......................23456788999AA99987643222....................... 42
43  ...........................23344444444444433222....................... 43
44  ...................................................................... 44
45  ...................................................................... 45
46  ...................................................................... 46
47  ...................................................................... 47
48  ...................................................................... 48
49  ...................................................................... 49
50  ...................................................................... 50
```

```
     SUPERPOSITION RECORD
IMAGE   TRIAL   HCENT   VCENT

  72      1      38      25
  73      1      35      25
  74      1      45      25
  75      1      36      26
  76      1      45      27
  77      1      43      27
  78      1      39      25
  79      1      41      29
  80      1      40      28
  81      1      38      27
   0      0       0       0
   0      0       0       0
   0      0       0       0
   0      0       0       0
   0      0       0       0
   0      0       0       0
   0      0       0       0
   0      0       0       0
   0      0       0       0
   0      0       0       0
   0      0       0       0
   0      0       0       0
   0      0       0       0
   0      0       0       0
   0      0       0       0
   0      0       0       0
   0      0       0       0
   0      0       0       0
   0      0       0       0
   0      0       0       0
   0      0       0       0
   0      0       0       0
   0      0       0       0
   0      0       0       0
   0      0       0       0
   0      0       0       0
   0      0       0       0
   0      0       0       0
   0      0       0       0
   0      0       0       0
   0      0       0       0
   0      0       0       0
   0      0       0       0
   0      0       0       0
   0      0       0       0
   0      0       0       0
   0      0       0       0
   0      0       0       0
   0      0       0       0
   0      0       0       0
```

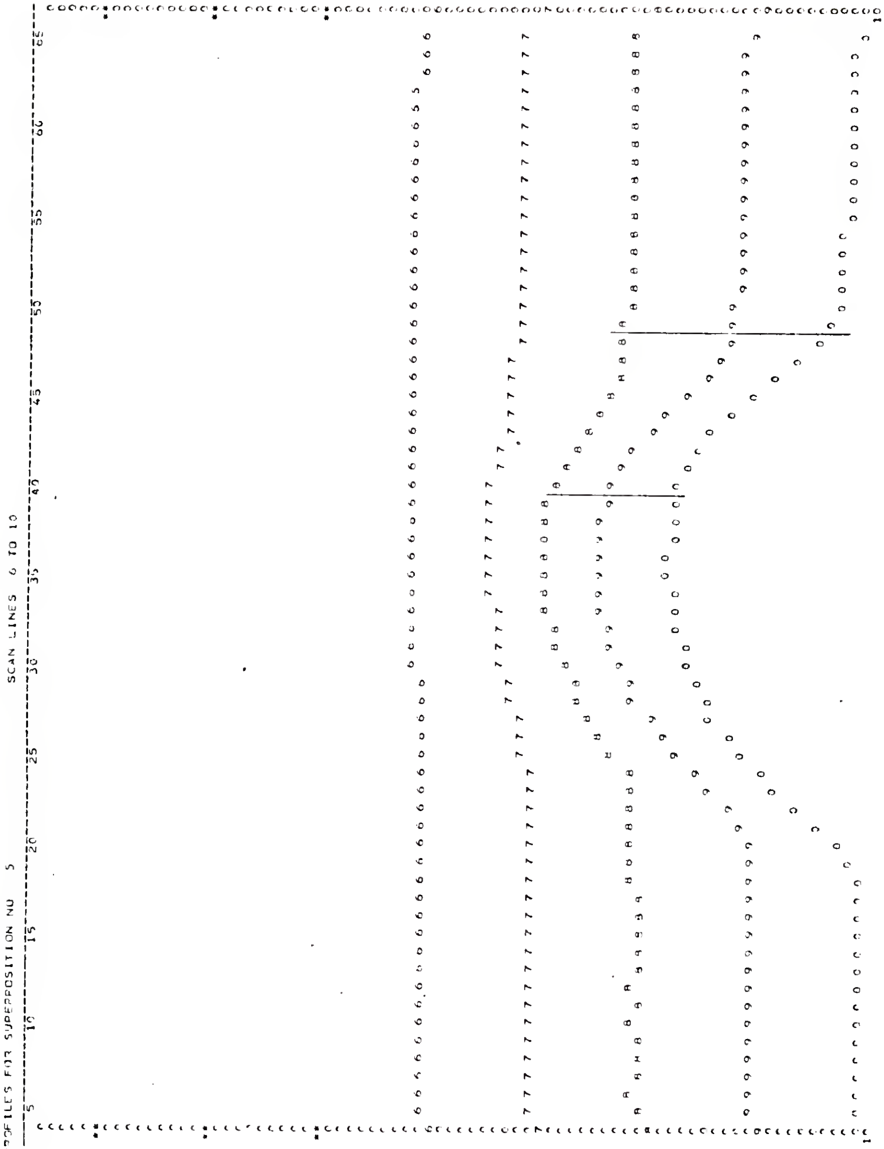

PROFILES FOR SUPERPOSITION NO 5 SCAN LINES 6 TO 10

PROFILES FOR SUPERPOSITION NO 5 SCAN LINES 36 TO 40

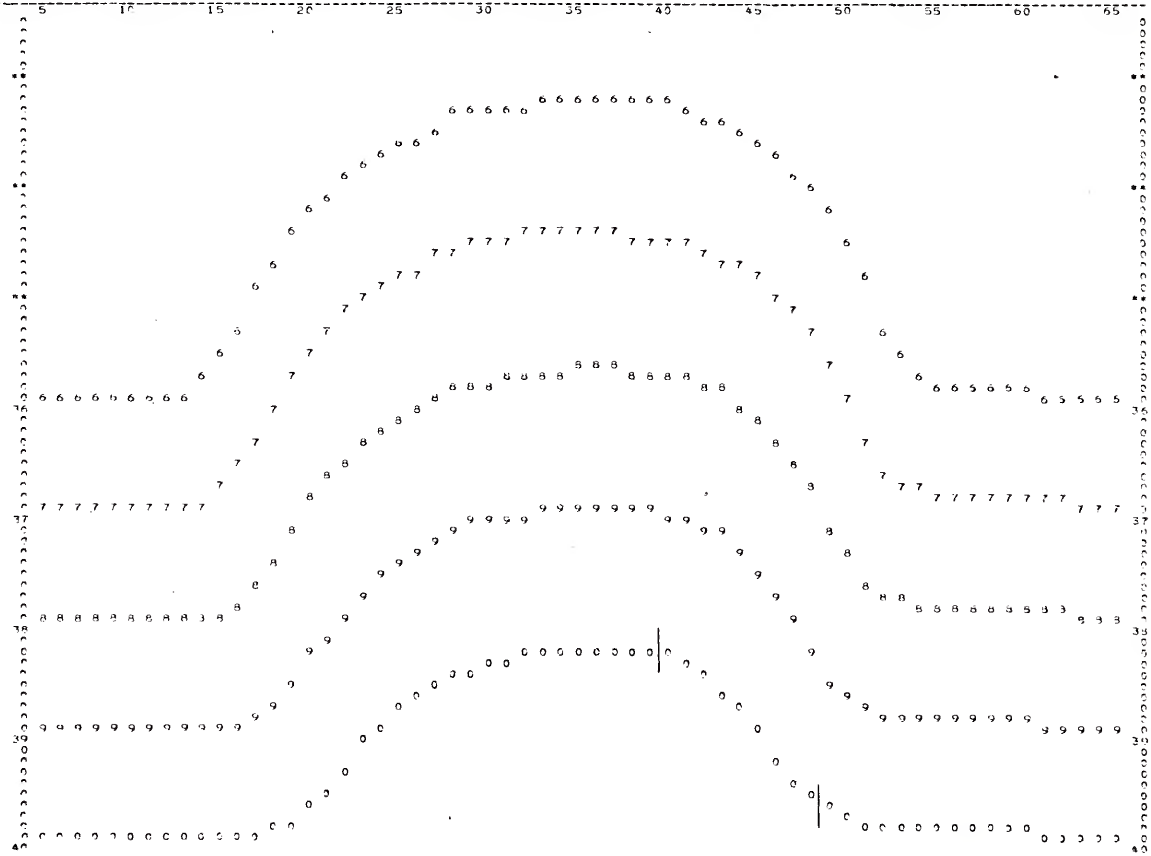

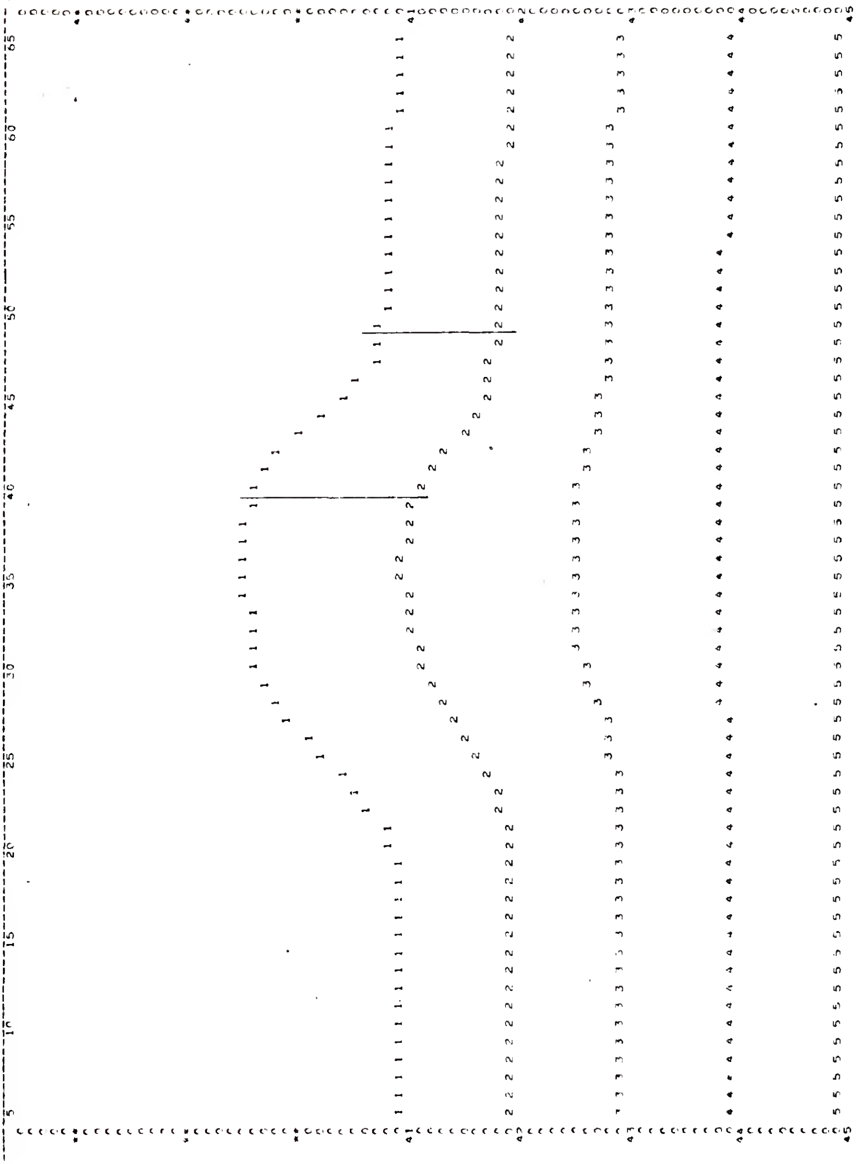

PROFILES FOR SUPERPOSITION NO 5 SCAN LINES 41 TO 45

```
SUPERIMPOSED JUPITER ARRAY NO    6

   0        10        20        30        40        50        60        70
   .         .         .         .         .         .         .         .
 1  ......................................................................   1
 2  ......................................................................   2
 3  ......................................................................   3
 4  ......................................................................   4
 5  ......................................................................   5
 6  .............................222333333333222..........................   6
 7  .........................2234556677777766554322.......................   7
 8  .......................3455799ABBCCCBBBA98765432......................   8
 9  ....................23468ABCEFFGGGGGFFEEDCBA8764322...................   9
10  ...................2469BDEGHIIIJJJJJIIIHGFFDCA9754322.................  10
11  .................2359CEGIJJKLMMMMMLLLKKJJIHHFEDA86532.................  11
12  ................257AEGIKLLNNOOOOOOONNNNMLLKJIHFEC97532................  12
13  ...............358CGIKLNOPPQQQQQQQQQQPUOONMLKKJHFC88532...............  13
14  .............2379EGJLNOPQQRRRRSSRSSSRRRQPPOONLKJHFEB8642..............  14
15  .............35AOHKNOPQQSSSSSSSTTTTTT7SSSRQQPOONLJIHEB8532............  15
16  ............258EIMNQRSTTUTUUUUUUUUUTTTTTSSROOPUNMKJGDA98322...........  16
17  ...........249BILOPRTUUVWWWWWWWWWWVWVVUUTSSROPONLLJGDB7432............  17
18  ...........26CFLOORSUVWXXXYXYYYYYYXXXXWWVVVUTSSROPNMKHFC96422.........  18
19  ...........48EHMOQSTUVWXYYYYYZZZZZZZZYYXXXWVVUTTRQONMJHEA8532.........  19
20  ...........4AFJNPRSUVVWWXYYYZYZZZZZZZZZYYYXXXVUTTSQPNLIGCA642.........  20
21  ..........268HKNPRSTUVVWWXXYYYZZZZZZZZZYZYYXXWWVUTRQOMKHE8743.........  21
22  ..........36CIKOQRSTUVVWWXXXXYYYYXYYZYYYXYXXWWVTTRRPNLIEB8532.........  22
23  ..........37DJLOQRRTUUWWWWXXXXXXXXXYXXXXWXWWVVVUSSRPNLIFC9542.........  23
24  ..........37DJLPQRSTUVWWXXXXXXXXXXXWWWWWWVVVUUUTSRQPNLJFC9642.........  24
25  .........237DILUQRSTUUVVVWWWWXWWXWWWWWWVVVVVUUUSSROONLJFD9642.........  25
26  ..........37DJLOQRSTUUUVVWWWWXWXWWWWWWWWVVUUUTSSSQQNMKIFC9632.........  26
27  ..........37CJLPQRSUUVVVWWWWWWWWWVWVVVVUUUUUUTSSQQPHMJIECB532.........  27
28  ..........26BHKPQRSUUVVWXXXYXXXXXWWWVVWUUUUUTSRRQPONLJHEB7532.........  28
29  ..........25AGJNPRSUVVVVXXXYYYYYXYXXXWWVUUUTSSRQQUONKIGDA742..........  29
30  ...........48DHMOORSTUVWXXXXXTYYVXXYXXXWVVUUTSSOPUNLKIGB8532..........  30
31  ...........37AEKMOORSTUUYWVWWXXXXXXXYXWWWVVUTTSRPUNLJGEA7532..........  31
32  ...........2480HJNOPQRSTTUUUVVVWWWWWWWWWVVVUTTSROONKIFC9642...........  32
33  ............2680HKMNPQRRSSSSTUUUVVUUVVUUUUUTSRQQONMJGEB7432...........  33
34  ............245BENJLNOPPQRRRSTTTTTTSTTTTTSSRRQQPONLKHEB9532...........  34
35  .............237AEHJLMNOOPQQRQQRRRSRRRRRRQQPUONMLIHEC96422............  35
36  ..............2579CFIKLMNOOOPPPPPQQQQQPPPOUNMMLJIGEB86432.............  36
37  ...............23698FGIKLMMNNNOOOOUOONNNNNMLKKIHFD8864322.............  37
38  ................2357ACEGIJKKLMMMMMMMMLLLLKJIHFEC985432................  38
39  ..................2468ACEGHIJJJKKKKKKKJJJIHGFECB865322................  39
40  ...................234579BCEFGGGHHHHHHHHGFEDCA8754322.................  40
41  .....................2345678ABCDDDDDEDDCCBA97644322...................  41
42  .......................223346677888888887765433222....................  42
43  ..........................222334445555544433222.......................  43
44  .............................222222222222222..........................  44
45  ......................................................................  45
46  ......................................................................  46
47  ......................................................................  47
48  ......................................................................  48
49  ......................................................................  49
50  ......................................................................  50
```

```
      SUPERPOSITION RECORD
  IMAGE   TRIAL   HCENT   VCENT

    94      1       34      27
    95      1       38      25
    96      1       34      27
    97      1       38      26
    98      1       36      25
    99      1       34      24
   100      1       36      25
   101      1       36      27
   102      1       34      27
   103      1       37      28
   104      1       33      27
     0      0        0       0
     0      0        0       0
     0      0        0       0
     0      0        0       0
     0      0        0       0
     0      0        0       0
     0      0        0       0
     0      0        0       0
     0      0        0       0
     0      0        0       0
     0      0        0       0
     0      0        0       0
     0      0        0       0
     0      0        0       0
     0      0        0       0
     0      0        0       0
     0      0        0       0
     0      0        0       0
     0      0        0       0
     0      0        0       0
     0      0        0       0
     0      0        0       0
     0      0        0       0
     0      0        0       0
     0      0        0       0
     0      0        0       0
     0      0        0       0
     0      0        0       0
     0      0        0       0
     0      0        0       0
     0      0        0       0
     0      0        0       0
     0      0        0       0
     0      0        0       0
     0      0        0       0
     0      0        0       0
     0      0        0       0
     0      0        0       0
     0      0        0       0
```

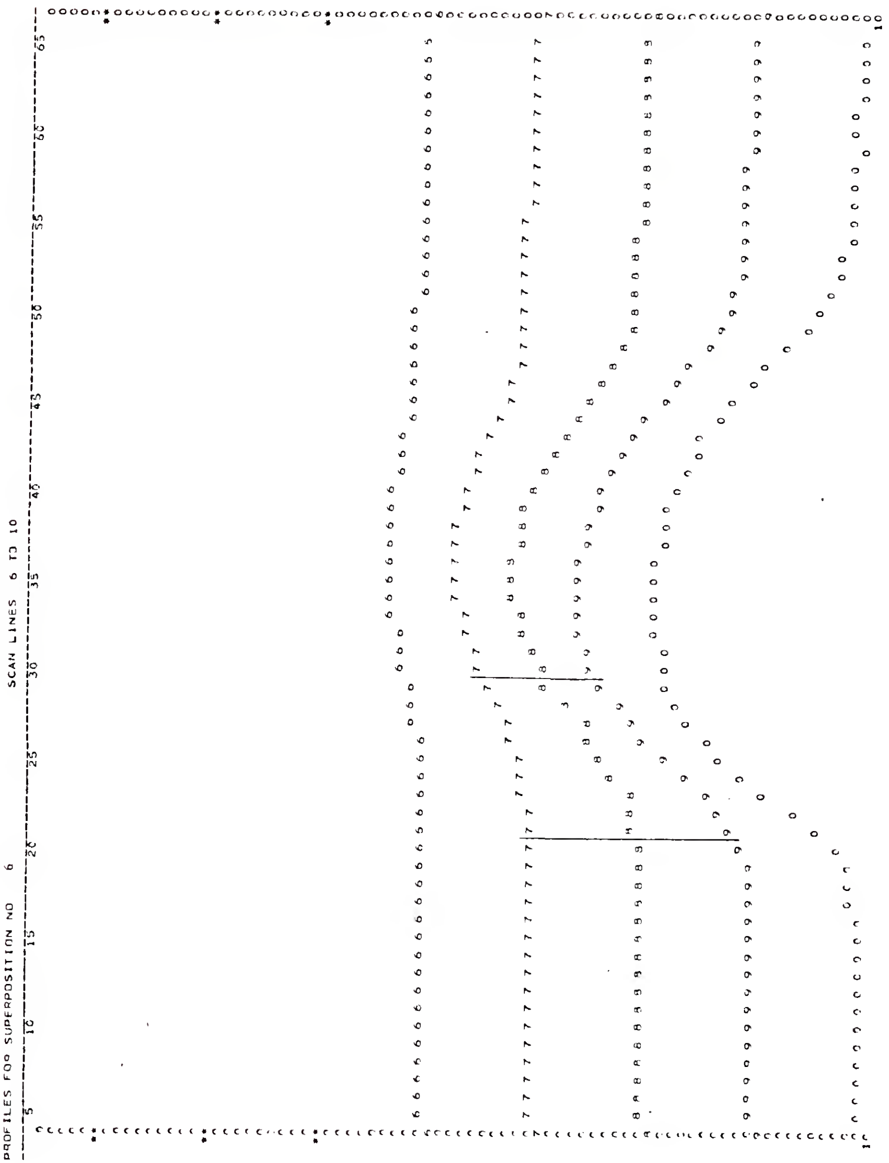

PROFILES FOR SUPERPOSITION NO 6 SCAN LINES 6 TO 10

PROFILES FOR SUPERPOSITION NO 6   SCAN LINES 41 TO 45

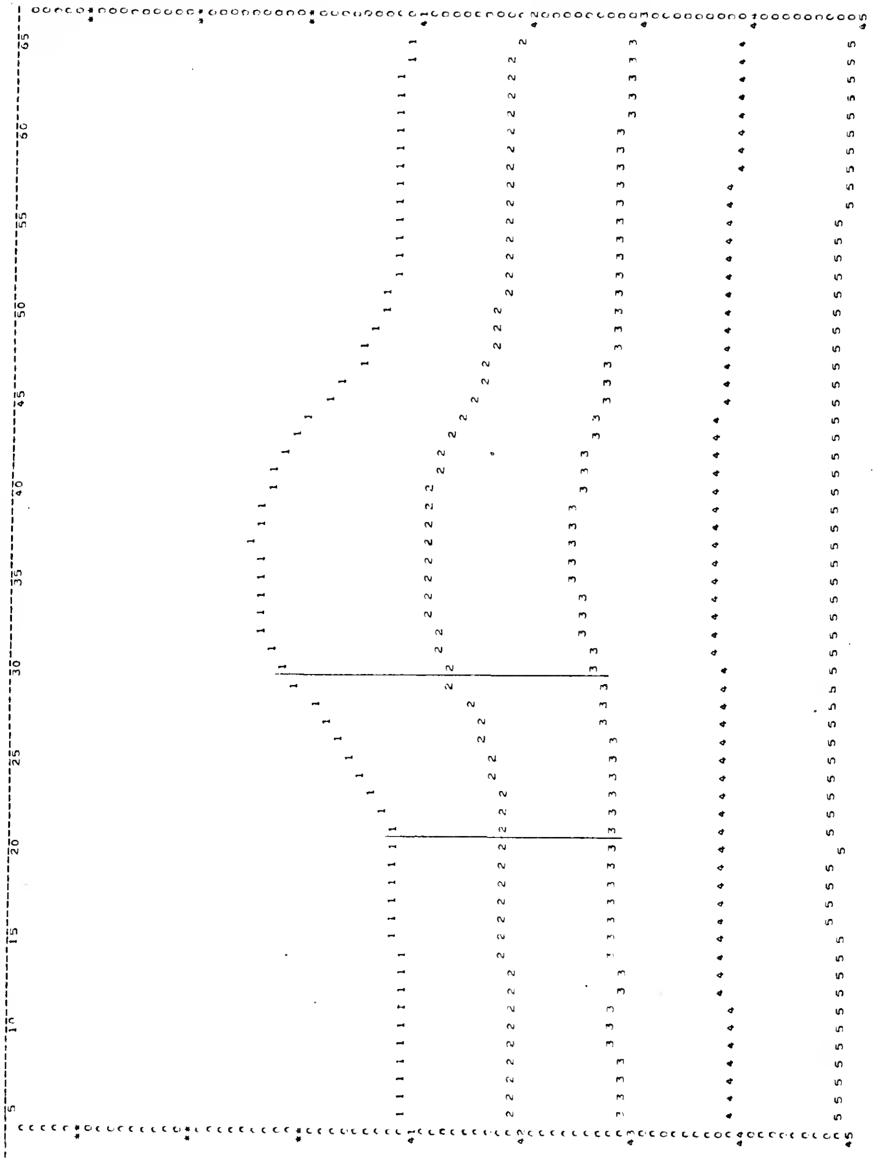

```
SUPERIMPOSED JUPITER ARRAY NO     7

    0         10        20        30        40        50        60        70          SUPERPOSITION RECORD
    .         .         .         .         .         .         .         .          IMAGE  TRIAL  HCENT  VCENT

 1  .......................................................................  1        117     1      38     26
 2  .......................................................................  2        118     1      39     25
 3  .......................................................................  3        119     1      38     27
 4  .......................................................................  4        120     1      42     24
 5  .......................................................................  5        121     1      43     25
 6  .......................................................................  6        122     1      37     25
 7  .............................2233334333222.............................  7        123     1      36     27
 8  .........................234567788888887654322.........................  8          0     0       0      0
 9  .......................3468AAABCDEDEEEECB987542........................  9          0     0       0      0
10  ....................2358ACDEFFGGHHHIHIIHGEDC98532......................  10         0     0       0      0
11  ...................358ACFFGHHHIJJJKKKKKKJJIGEC97432....................  11         0     0       0      0
12  .................2579BFFHMIJJKLMLMMMMMMMLLLKIHFB8632...................  12         0     0       0      0
13  ................36H9DEFHJJKLMMNNNNOOONNNNNNNMLJHDA632..................  13         0     0       0      0
14  ...............369CDGHJJKLMNOUPPPPPPPPPPPPPUONMKIFB632.................  14         0     0       0      0
15  ..............2698EGIIKMNNOPQQQQRRRRSRRRRRQRUUUNLIFA532................  15         0     0       0      0
16  .............358DFHJLMNOOPQQRRSSSTSTTTTTTTTSSRQPULKFV642...............  16         0     0       0      0
17  ............249DFHJLMNOPQRSSTTUUUUUVVWVVVUWUUUTRRPOJDA732..............  17         0     0       0      0
18  ............47BFHJLNOPRSTTUVUVVWXWXXXXXXXWXWWWVTSSPMGDV42..............  18         0     0       0      0
19  ...........369EHKLOPRSSSTVVWWWXXWYXAVYYXWXAWWWVTSRPNJF862..............  19         0     0       0      0
20  ...........583FJKMPQRRSUUVVWWWWWWWXXXXXWWWVVVUTTSRPNKHD8322............  20         0     0       0      0
21  ...........69CGJLNOPQRSTUUUUVVVVVVWWWWWVWVVVUUUTSRPULIF942.............  21         0     0       0      0
22  ..........378EHKLNOPQRRSTTTJUUVVVWWWWWWVVVVVUVUTSRQPNKG852.............  22         0     0       0      0
23  ..........388DHKLMNPQSSSTUUUVUVWVWWWWWWWWWWWVVVUUTRQNKHD53.............  23         0     0       0      0
24  ..........38CEHKLNPPQRSTTUUUWVWVWWWWWXWWWWVWWVWUUTSQNKID642............  24         0     0       0      0
25  ..........38CEHLMMOQRRSTUVVVVWWWVVWVWVWXWWVWWWVUUTTQOLIC63.............  25         0     0       0      0
26  ..........388EGKLNOPQRSTTUUVVVVVWWXXXXWWAWXWXWVVVUTROLICS32............  26         0     0       0      0
27  ..........388DGJLMUORSSTTTVVVVVWWWXXWXYAXYXXXXXWWVTSOLHA62.............  27         0     0       0      0
28  ..........26ACGJLNPRRSTUUVVWXXYYXXYYYYYYYYYYZYAWVUSONKF942.............  28         0     0       0      0
29  ...........69DFJLNOQRSTUVWWXXXYYYYZZZYZZZZYYAWWWVTRPLID732.............  29         0     0       0      0
30  ...........488FILMNORSSUUVXXXXXYYYYYYZZYYYYWWVUTSQPNJF862..............  30         0     0       0      0
31  ...........369DGJMNPRSTTUUVWWWXXXYYYYXWXWVUUTTSRQPMKGC842..............  31         0     0       0      0
32  ...........257AEHJLNPQQRSSSUUUUUUVVVUUUUSTSSSRQPPNLHDA532..............  32         0     0       0      0
33  ............358CFHILLMNPQRRRSSSSSTTTTTSTSSRRROPONLIE963................  33         0     0       0      0
34  .............359CDGIKLMNOPQQQRRRSSSSSSSSRRRQQPNLJIEA5322...............  34         0     0       0      0
35  ..............358BEGJKLMNOPPQRQRRQQQQQQPQQPUNMKIHEB632.................  35         0     0       0      0
36  ...............357BDFHIKLMMNNNNOOOOOODUOONNMLKIGCA63...................  36         0     0       0      0
37  ...............2346ACEFHIJJKLLMLMMNMMMMMLLKJIHFB8532...................  37         0     0       0      0
38  .................2368ACEEGHIIIIJKKKKKJKJJIIGFDA64322...................  38         0     0       0      0
39  ..................23557ABCDEFGGHHHHHHHHGFEDCA753222....................  39         0     0       0      0
40  ....................234578ABCDUDDEEEEEEDCA97543........................  40         0     0       0      0
41  ......................23345678899AAAAA9866532..........................  41         0     0       0      0
42  .........................2233344456554433222...........................  42         0     0       0      0
43  ...............................22222222................................  43         0     0       0      0
44  .......................................................................  44         0     0       0      0
45  .......................................................................  45         0     0       0      0
46  .......................................................................  46         0     0       0      0
47  .......................................................................  47         0     0       0      0
48  .......................................................................  48         0     0       0      0
49  .......................................................................  49         0     0       0      0
50  .......................................................................  50         0     0       0      0
```

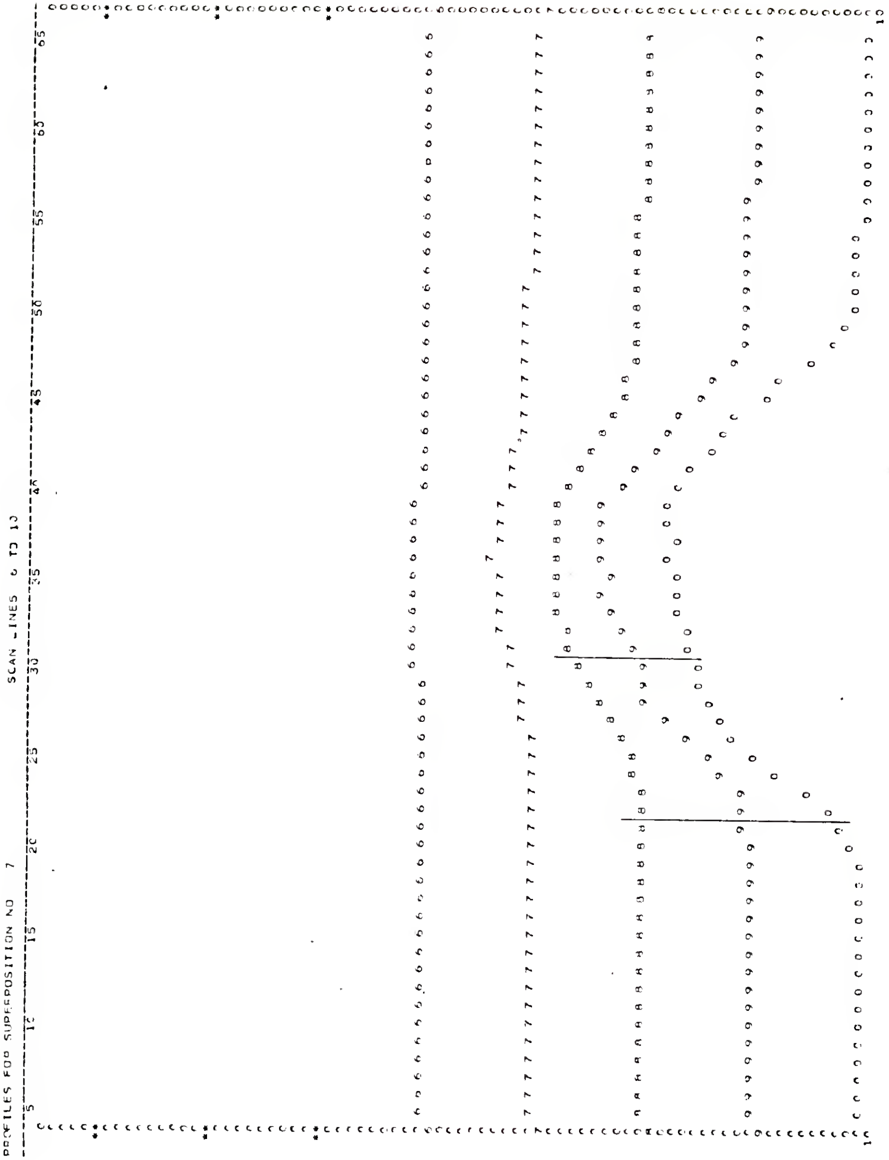
PROFILES FOR SUPERPOSITION NO 7
SCAN LINES 6 TO 10
5
10
15
20
25
30
35
40
45
50
55
60
65

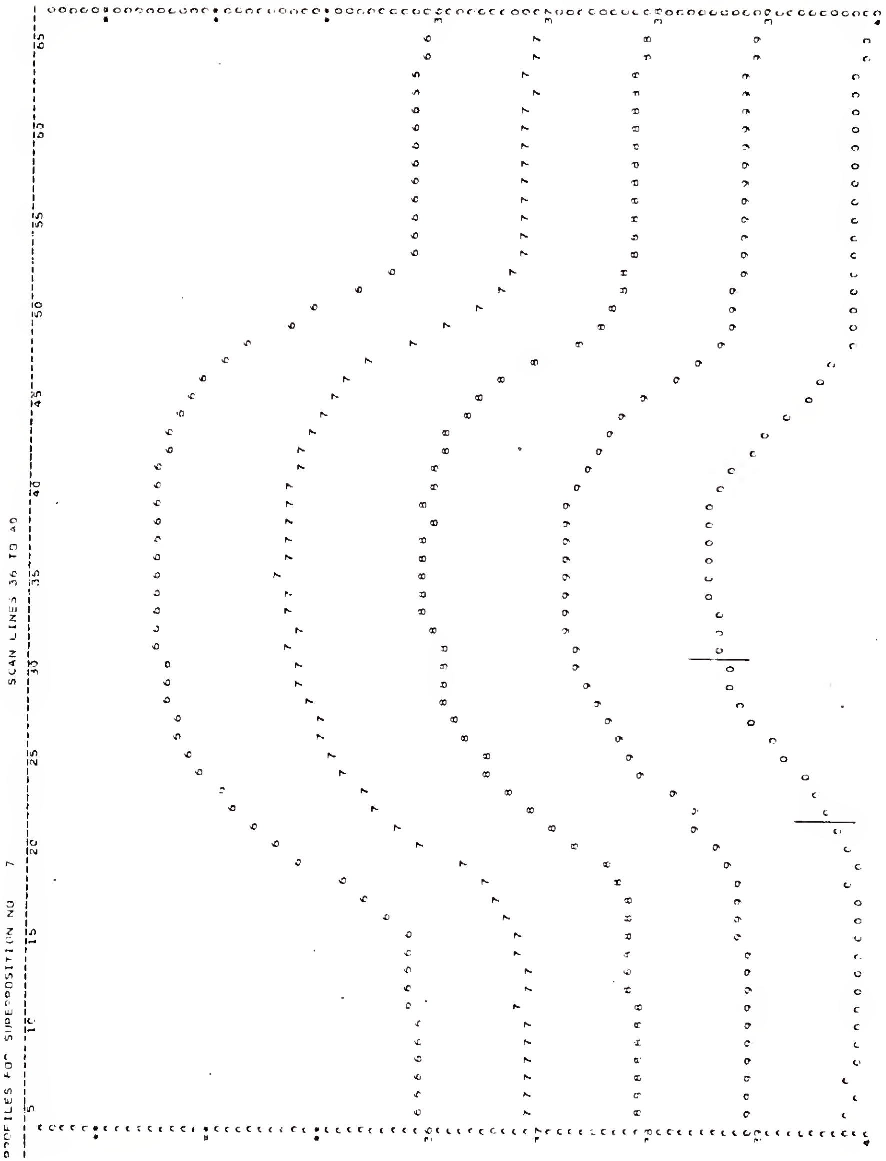

PROFILES FOR SUPERPOSITION NO 7   SCAN LINES 36 TO 40

PROFILES FOR SUPERPOSITION NO 7 SCAN LINES 41 TO 45

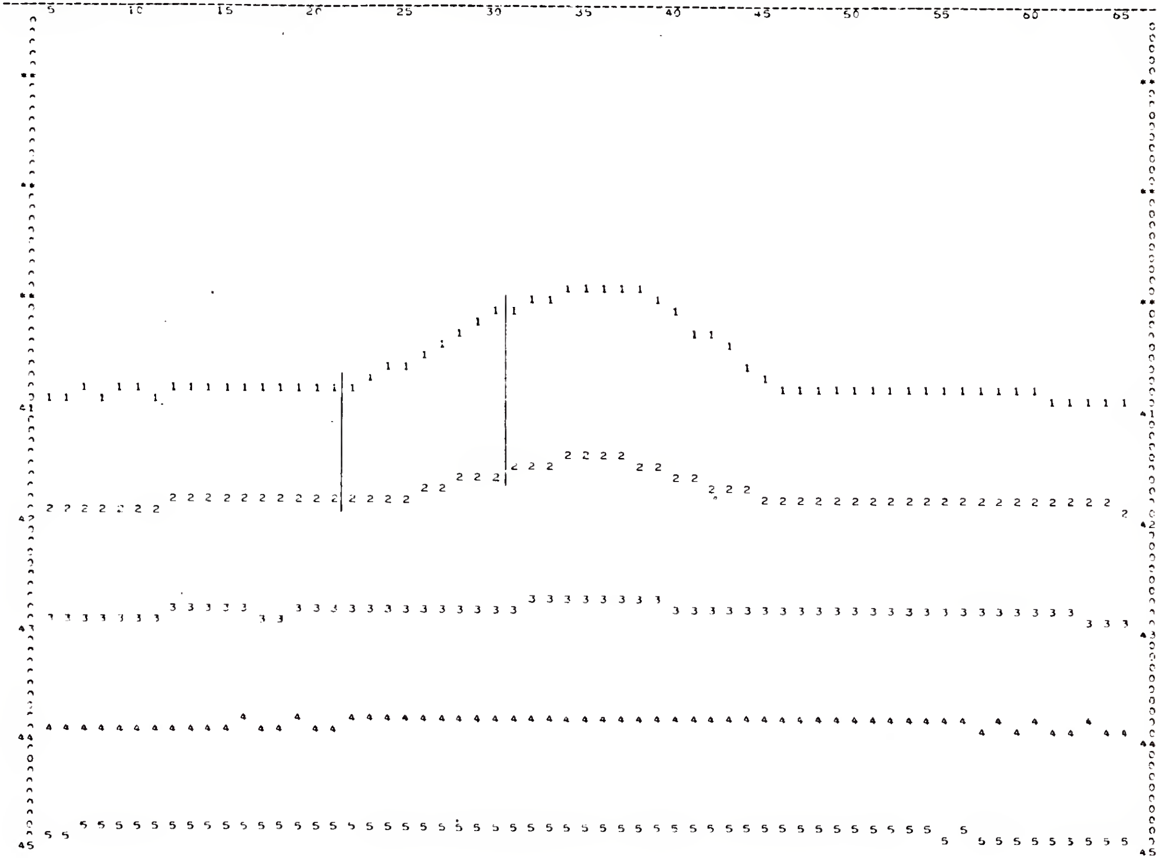

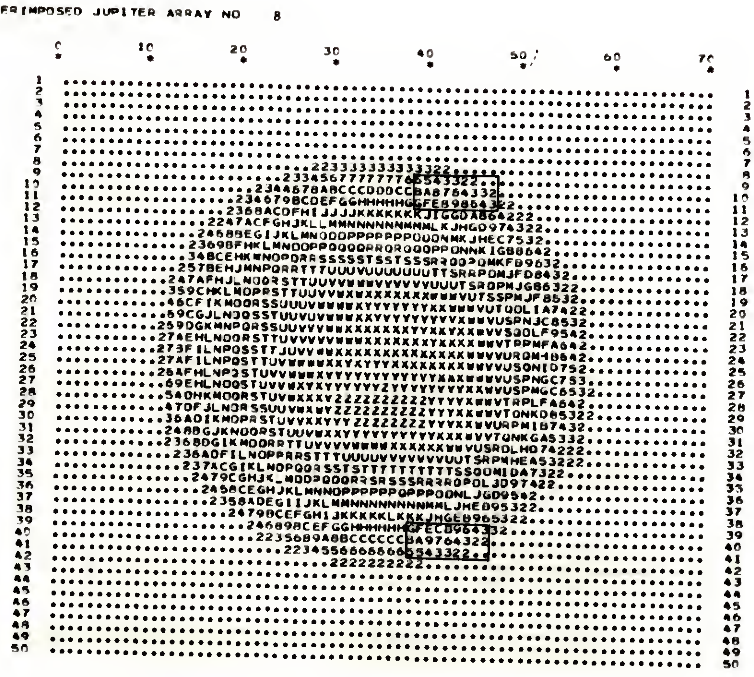

```
SUPERIMPOSED JUPITER ARRAY NO    8

  0        10        20        30        40        50        60        70
  *         *         *         *         *         *         *         *
 1 ...................................................................... 1
 2 ...................................................................... 2
 3 ...................................................................... 3
 4 ...................................................................... 4
 5 ...................................................................... 5
 6 ...................................................................... 6
 7 ...................................................................... 7
 8 ...........................223333333333322............................ 8
 9 ........................233456777777766543322......................... 9
10 .....................2344678ABCCCDDDCCBA8764332....................... 10
11 ...................234679BCDEFGGHHHHHGGFEB9864322..................... 11
12 ..................2368ACDFHIJJJJKKKKKKKJIGGDA864222................... 12
13 ................2247ACFGHJKLLMMNNNNNNNMMLKJHGD974322.................. 13
14 ...............24688EGIJKLMNOOOPPPPPPPOOONMKJHEC7532.................. 14
15 ..............23698FHKLMNOOPPQQQQRRQRQQQPPONNKIG88642................. 15
16 ..............348CEHKMNOPQRRSSSSSTSSTSSSRRQQPQMKFB9632................ 16
17 .............257BEHJMNPQRRTTTUUUVUUUUUUUTTSRRPOMJFD8432............... 17
18 ............247AFHJLNOORSTTUUVVWWVVVVVVVUUUTSRQPMJG86322.............. 18
19 ............359CHKLMOPPRSTTUUVVWXWXXXXXXWWWVUTSSPMJF8532.............. 19
20 ............46CFIKMOORSSUUUVWWWXYYYYYYYYXXWWWVUTQOLIA7422............. 20
21 ............69CGJLNOQSSTUUVUVWWWXXYYYYYYYYYXWWVUSPNJC8532............. 21
22 ...........259DGKMNPQRSSUUVVVWWXXXXXXXYYXXYXXWVVSQOLF9542............. 22
23 ...........27AEHLNOORSTTUVVVVVVWWWXXXXXXYXXXXWWVTRPMFA642............. 23
24 ...........273FILNPOSSTTJUVVWWXXXXXXXXXXXXXXWWVVUROMHB642............. 24
25 ...........27AFILNPQSTTUVWWWWXXYXYYYXXXXXXXXWWVVUSONID752............. 25
26 ...........26AFHLNPQSTUVVWWWXYYYYYYYYYYYYXXXWWWVUSPNGC753............. 26
27 ............69EHLNOQSTUVVWXYXYYYYYZYYYYYYYYYXXWVUSPMGC6532............ 27
28 ............5ADHKMOORSTUVWXXXYZZZZZZZZZYYYYVXWWVTRPLFA642............. 28
29 ............47DFJLNQRSSUUVWXWYZZZZZZZZZZYYYXXWWVTONKD85322............ 29
30 ............36ADIKMOPRSTUVVXXYYYZZZZZZZYYYVXXWVURPMIB7432............. 30
31 ............248BGJKNOQRSTUUVWXXYYYYYYYYYYXXXWVVTQNKGA5332............. 31
32 ............236BDGIKMOORRTTUVVVVVWWWWXXXXXXWWVUSRQLHD74222............ 32
33 .............236ADFILNOPPRRSTTTUUUUVVVVVVVVUUTSRPMHEA53222............ 33
34 ..............237ACGIKLNOPQQRSSTSTTTTTTTTTTTSSQOMIDA7322.............. 34
35 ...............2479CGHJKLMOOPQQQRRSRSSSRRRROPOLJD97422................ 35
36 ................2458CEGHJKLMNNOPPPPPPQPPPOONLJGD9542................. 36
37 .................2358ADEGIIJKLMMNNNNNNNNNNMMLJHED95322................ 37
38 ...................2479BCEFGHIJKKKKKLKKKJHGEB965322................... 38
39 .....................24689BCEFGGHHHHHHHGFECB964332.................... 39
40 ......................2235689ABBCCCCCCBA9764322....................... 40
41 .........................22345566666666543322......................... 41
42 ..............................2222222222.............................. 42
43 ...................................................................... 43
44 ...................................................................... 44
45 ...................................................................... 45
46 ...................................................................... 46
47 ...................................................................... 47
48 ...................................................................... 48
49 ...................................................................... 49
50 ...................................................................... 50
```

```
       SUPERPOSITION RECORD
IMAGE   TRIAL   HCENT   VCENT
 138      1      36      24
 139      1      34      23
 140      1      37      24
 141      1      35      24
 142      1      37      26
 143      1      34      25
 144      1      33      23
   0      0       0       0
   0      0       0       0
   0      0       0       0
   0      0       0       0
   0      0       0       0
   0      0       0       0
   0      0       0       0
   0      0       0       0
   0      0       0       0
   0      0       0       0
   0      0       0       0
   0      0       0       0
   0      0       0       0
   0      0       0       0
   0      0       0       0
   0      0       0       0
   0      0       0       0
   0      0       0       0
   0      0       0       0
   0      0       0       0
   0      0       0       0
   0      0       0       0
   0      0       0       0
   0      0       0       0
   0      0       0       0
   0      0       0       0
   0      0       0       0
   0      0       0       0
   0      0       0       0
   0      0       0       0
   0      0       0       0
   0      0       0       0
   0      0       0       0
   0      0       0       0
   0      0       0       0
   0      0       0       0
   0      0       0       0
   0      0       0       0
   0      0       0       0
   0      0       0       0
   0      0       0       0
   0      0       0       0
   0      0       0       0
```

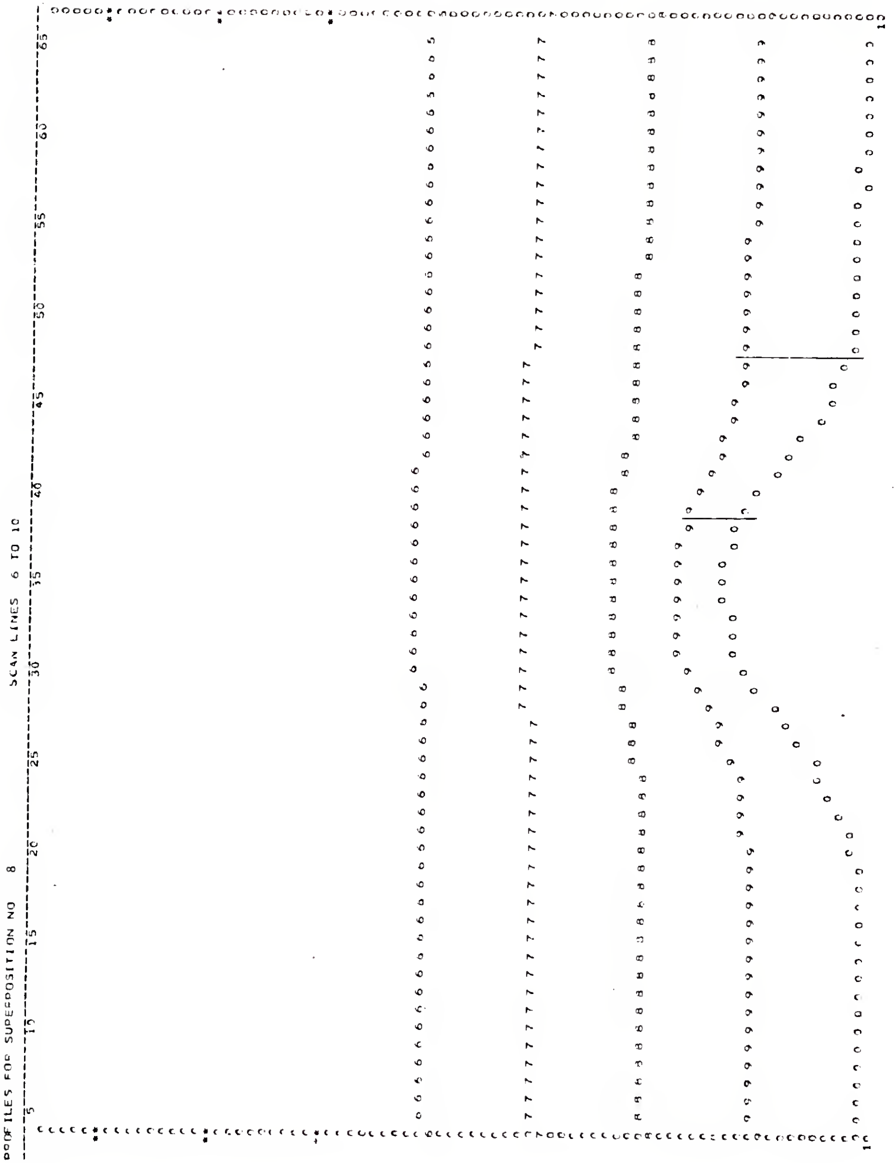

PROFILES FOR SUPERPOSITION NO 8 SCAN LINES 6 TO 10

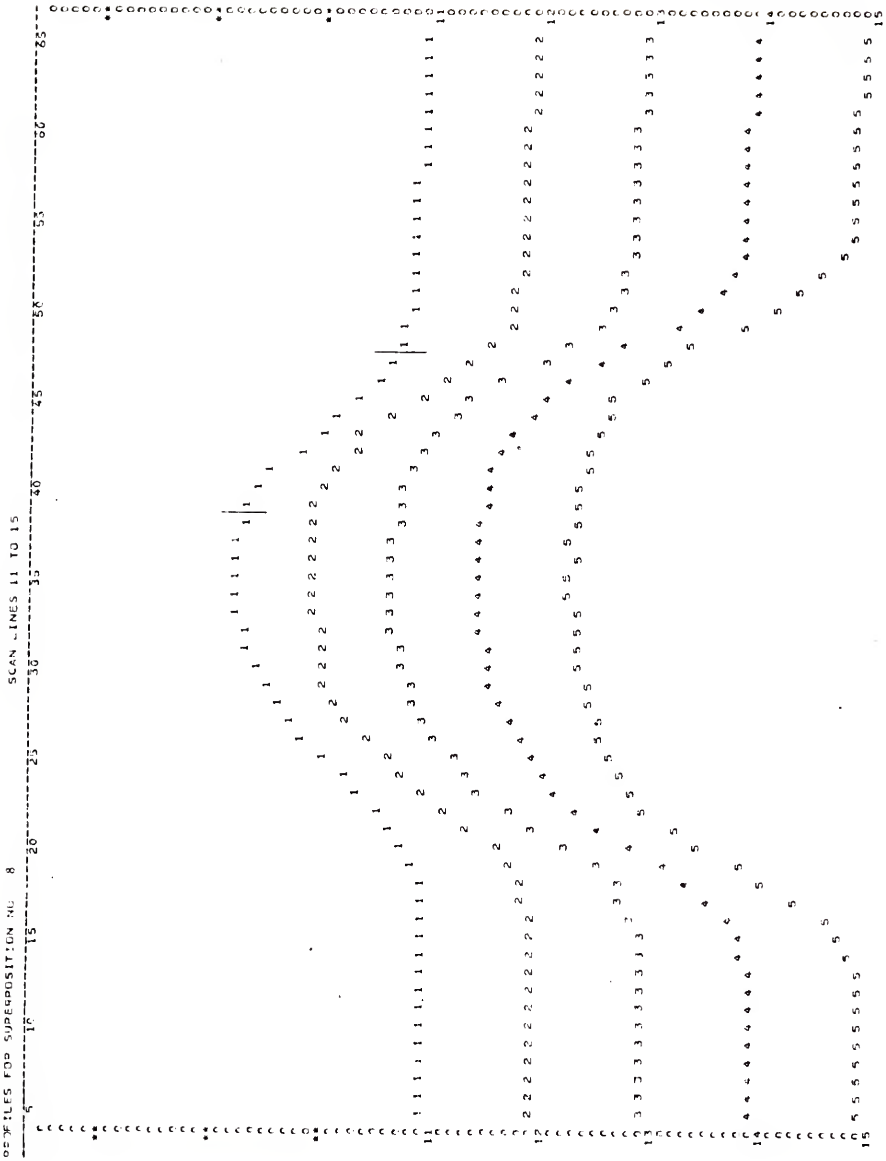
PROFILES FOR SUPERPOSITION NO 8
SCAN LINES 11 TO 15
5
10
15
20
25
30
35
40
45
50
55
60
65
11
12
13
14
15

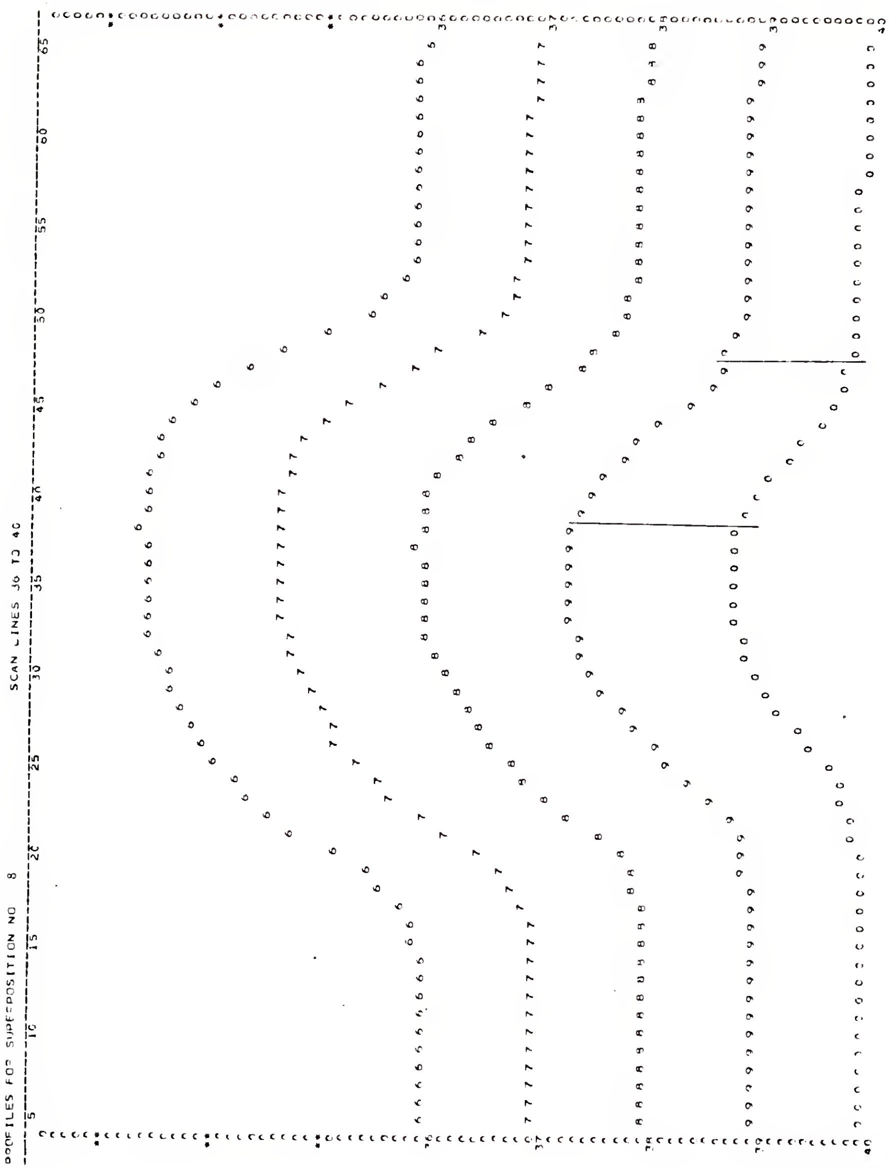

PROFILES FOR SUPERPOSITION NO 8 SCAN LINES 36 TO 40

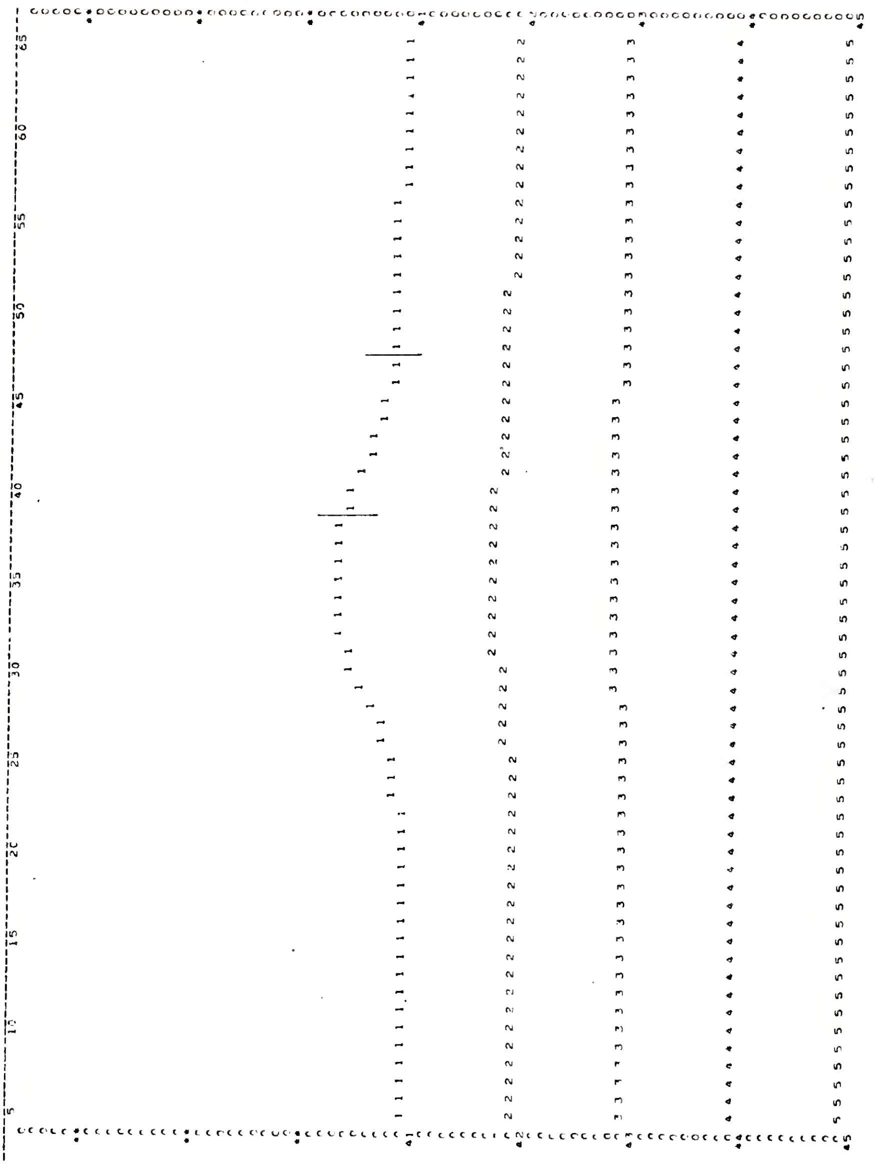

PROFILES FOR SUPERPOSITION NO 8 SCAN LINES 41 TO 45

BIBLIOGRAPHY

Andrew, B.H., MacLeod, J.M., Locke, J.L., Medd, W.J., and Purton, C.R. 1969, *Nature*, *223*, 598.

Angione, R.J. 1971, *A.J.*, *76*, 412.

Arp, H. 1971, *Ap. Letters*, *9*, 7.

Babcock, T.A., Ferguson, P.M., and James, T.H. 1974, *A.J.*, *79*, No. 1, 92.

Bahcall, J.N. and Hills, R.E. 1973, *Ap. J.*, *179*, 699.

Baldwin, J.A., Robinson, L.B., Wampler, E.J., and Burbidge, E.M. 1974, *Bull. Am. Astr. Soc.*, *6*, No. 4, Part 1, 431.

Barker, E.S. 1968, *Jourl. Op. Soc. Am.*, *58*, No. 10, 1378.

Barnes, R. 1966, *Ap. J.*, *146*, 1285.

Barnothy, J.M. and Barnothy, M.F. 1968, *Ap. Letters*, *2*, 21.

Bertaud, Ch., DuMortier, B., Veron, P., Wlerick, G., Adam, G., Bigay, J., Garnier, R., and Du Ruy, M. 1969, *A. and Ap.*, *3*, 436.

Bigg, E.K. 1964, *Nature*, *203*, 1008.

Biraud, F. 1971, *Nature*, *232*, 178.

Blake, G.M. 1970, *Ap. Letters*, *6*, 201.

Bolton, J.G., Clarke, M.E., and Ekers, R.D. 1965a, *Austral. J. Phy.*, *18*, 627.

Bolton, J.G., Clarke, M.E., Sandage, A.R., and Veron, P. 1965b, *Ap. J.*, *142*, 1289.

Bolton, J.G. and Ekers, J.A. 1966a, *Austral. J. Phys.*, *20*, 109.

Bolton, J.G. and Ekers, J.A. 1966b, *Austral. J. Phys.*, *19*, 713.

Bolton, J.G. and Kinman, T.D. 1966, *Ap. J.*, *145*, 951.

Bolton, J.G., Shimmins, A.J., and Merkelin, J. 1968, *Austral. J. Phys.*, *21*, 81.

Bond, H.E. 1971, Ap. J. (Letters), 167, L79.

Brandie, G.W. 1972, Ap. J., 77, 197.

Brandie, G.W. and Stull, M.A. 1971, Nature, 231, 149.

Browne, I.W.A. 1971, Nature, 231, 515.

Brun, A. 1957, Atlas des 139 Selected Areas du Mt. Wilson.

Burbidge, E.M. 1968, A.J., 73, 890.

Burbidge, E.M. and Burbidge, G.R. 1971, Ap. J., 163, L21.

Burbidge, E.M., Burbidge, G.R., Solomon, P.M., and Strittmatter, P.A. 1971, Ap. J., 170, 233.

Burbidge, E.M. and Strittmatter, P.A. 1972, Ap. J. (Letters), 174, L57.

Burbidge, E.M., Strittmatter, P.A., Smith, H.E., and Spinrad, H. 1972, Ap. J. (Letters), 178, L43.

Burbidge, G.R. and Hoyle, F. 1966. Scientific American, Dec., 305.

Campen, C.F., Cole, A.E., Condron, T.P., Ripley, W.S., Sissenwine, N., and Solomon, I. (Eds.) 1961, Handbook of Geophysics, Revised Edition. New York: The Macmillan Company.

Cannon, R.D., Penston, M.V., and Penston, M.J. 1968, Nature, 217, 340.

Carswell, R.F. and Strittmatter, P.A. 1973, Nature, 242, 394.

Cavaliere, A., Morrison, P., and Pacini, F. 1970, Ap. J. (Letters), 162, L133.

Chiu, B.C. and Morrison, P. 1973, Ap. J.,181, 295.

Colgate, S.A. 1969, Physics Today, 22, 27.

Craine, E.R. and Warner, J.W. 1973, Ap. J. (Letters), 179, L53.

Danielson, R.E. 1966, Ap. J., 143, 949.

Dent, W.A. 1965, Science, 148, 1458.

Dent, W.A. and Kojoian, G. 1972, A. J., 77, 819.

De Veny, J.B., Osborn, W.H., and Jones, K. 1971, Pub. A.S.P., 83, 611.

Diffley, J.A. 1968, A.J., 73, 762.

DuPuy, D., Schmitt, J., McClure, R., Van den Bergh, S., and Racine, R. 1969, Ap. J. (Letters), 156, L135.

Dyck, H.M., Kinman, T.D., and Lockwood, G.W. 1971, Nature, 234, 71.

Eastman Kodak Company 1973, Kodak Plates and Films for Scientific Photography, Publication P-315.

Eggen, O.J. 1972, Ap. J., 172, 639.

Ekers, J.A. (Ed.) 1969, Austral. J. Phys. Ap. Suppl., No. 7.

Elson, B.M. 1974, Aviation Week and Space Tech., Dec. 16, 61.

Folsom, G.H. 1970, Optical Variations of Quasars and Related Galaxies. Ph.D. Dissertation, University of Florida.

Folsom, G.H. and Smith, A.G. 1969, Pub. A.S.P., 81, 871.

Folsom, G.H., Smith, A.G., Hackney, R.L. 1970, Ap. Letters, 7, 15.

Folsom, G.H., Smith, A.G., Hackney, R.L., and Hackney, K.R. 1971, Nature, 230, No. 17, 199.

Goldreich, P. and Lynden-Bell, D. 1969, Ap. J., 156, 59.

Goldsmith, D.W. and Kinman, T.D. 1965, Ap. J., 142, 1693.

Goldsmith, S. 1972, Nature, 236, 122.

Greenstein, J.L. and Schmidt, M. 1964, Ap. J., 140, 1.

Gurney, R.W. and Mott, N.F. 1938, Proc. R. Soc. London, A, 164, 151.

Hackney, R.L. 1972a, Optical Behavior of Peculiar Extragalactic Radio Sources. Ph.D. Dissertation, University of Florida.

Hackney, R.L. 1972b, Private communication.

Hackney, R.L., Hackney, K.R., Folsom, G.H., Leacock, R.J., Scott, R.L., Smith, A.G. 1972a, Qtr. J. Fla. Acad. Sciences, 35, 19.

Hackney, R.L., Hackney, K.R., Smith, A.G., Folsom, G.H., Leacock, R.J., Scott, R.L., and Epstein, E.E. 1972b, Ap. Letters, 12, 147.

Hackney, K.R. 1973, Three Color Photographic Photometry of Active Quasi-Stellar Radio Sources. Ph.D. Dissertation, University of Florida.

Haro, G. and Luyten, W.J. 1962, Bol. Obs. Tonantzintla y Tacubaya, 3, 37 (No. 22).

Hoag, A.A. 1961, Pub. A.S.P., 73, 301.

Hoag, A.A. 1964, Sky and Telescope, 331.

Hoyle, F. and Fowler, W.A. 1967, Nature, 213, 373.

Hunter, J. and Lü, P.K. 1969, Nature, 223, 1045.

Johnson, H.L. and Sandage, A.R. 1955, Ap. J., 121, 616.

Kardashev, N.S. and Komberg, B.V. 1966, Astr. Circ. U.S.S.R., No. 357.

Kellerman, K.I., Clark, B.G., Jauncey, D.L., Cohen, M.H., Shaffer, D.B., Moffet, A.T., and Gulkis, S. 1970, Ap. J., 161, 803.

Kinman, T.D. 1967, Ap. J. (Letters), 148, L53.

Kinman, T.D. 1968, Science, 162, 1081.

Kinman, T.D., Bolton, J.G., Clarke, R.W., and Sandage, A.R. 1967, Ap. J., 147, 848.

Kinman, T.D., Lamla, E., Ciurla, T., Harlan, E., and Wirtanen, C.A. 1968, Ap. J., 152, 357.

Kinman, T.D., Wardle, J.F.C., Conklin, E.K., Andrew, B.H., Harvey, G.A., MacLeod, J.M., and Medd, W.J., 1974, A. J., 79, 349.

Kleinmann, D.E. and Low, F.J. 1970, Ap. J. (Letters), 159, L165.

Kraus, J.D., Scheer, D.J., Dixon, R.S., Fitch, L.T., and Andrew, B.H. 1968, Ap. J., 152, L35.

Latham, D.W. 1969, A.A.S. Photo Bull., 1, 3.

Low, F.J. 1970, Ap. J. (Letters), 159, L173.

Lü, P.K. 1972, A. J., 77, 829.

Lucchetti, S.C. and Usher, P.D. 1971, Nature, 232, 622.

MacLeod, J.M. and Andrew. B.H. 1968, Ap. Letters, 1, 243.

MacLeod, J.M., Andrew, B.H., Medd, W.J., and Olsen, E.T. 1971, Ap. Letters, 9, 19.

Matthews, T.A. and Sandage, A.R. 1963, Ap. J., 138, 30.

McCrea, W.H. 1966, Pub. A.S.P., 78, No. 460, 49.

McGimsey, B.Q. 1974, Optical Brightness and Polarization of Quasars and Related Objects. Ph.D. Dissertation, University of Florida.

McPeters, R. 1974, Private communication.

Medd, W.F., Andrew, B.H., Harvey, G.A., and Locke, F.L. 1972, Mem. R.A.S., 77, 109.

Miley, G.K. 1971, M.N.R.A.S., 152, No. 4, 477.

Miller, H.R., Clonts, S.L., and Folsom, G.H. 1975, A. J., 79, No. 12, 1352.

Miller, W.C. 1970, A.A.S. Photo Bull., 2, 15.

Milone, E.F. 1972, Pub. A.S.P., 84, 723.

Morrison, D. 1973, Physics Today, 26, 23.

Oke, J.B. 1967, Ap. J., 147, 901.

Oke, J.B. and Gunn, J.E. 1974, Ap. J., 189, L5.

Oke, J.B., Neugebauer, G., and Becklin, E.E. 1970, Ap. J., 159, 341.

Oke, J.B. and Sargent, W.L.W. 1968, Ap. J., 151, 807.

Olsen, E.T. 1969, Nature, 224, 1008.

Peach, J.V. 1969, Nature, 222, 439.

Penston, M.J., Penston, M.V., and Sandage, A. 1971, Pub. A.S.P., 83, 783.

Penston, M.W. and Wing, R.F. 1973, The Observatory, 93, No. 995, 149.

Pilcher, C.B. and McCord, T.B. 1971, Ap. J., 165, 195.

Pope, T.P. and Kirby, T.B. 1967, Jourl. Op. Soc. Am., 57, No. 7, 951.

Prasad, S.S. 1974, Private communication.

Purgathofer, A. 1969, *Lowell Obs. Bull. No. 147*, Vol. VII, No. 10, 98.

Racine, R. 1970, *Ap. J. (Letters)*, *159*, L99.

Rieke, G.H. 1972, *Ap. J. (Letters)*, *176*, L61.

Rieke, G.H. and Kinman, T.D. 1974, *Ap. J.*, *192*, L115.

Rodgers, A.W. 1971, *Nature*, *233*, 75.

Sandage, A. 1966a, *Ap. J.*, *145*, 1.

Sandage, A. 1966b, *Ap. J.*, *144*, 1234.

Sandage, A. 1966c, *Ap. J.*, *146*, 13.

Sandage, A. 1967, *Ap. J. (Letters)*, *150*, L177.

Sandage, A. 1970, *Ap. J.*, *162*, 841.

Sanitt, N. 1972, *New Scientist*, 494.

Schmitt, J.L. 1968, *Nature*, *218*, 663.

Scott, R.L. and Smith, A.G. 1974, *A. J.*, *79*, No. 5, 656.

Scott, R.L., Smith, A.G., Leacock, R.J., McGimsey, B.Q., Edwards, P.L., Hackney, K.R., Hackney, R.L., and Folsom, G.H. 1973, *Bull. Am. Astron. Soc.*, *5*, No. 4, Part 1, 396.

Searle, L. and Bolton, J.G. 1968, *Ap. J. (Letters)*, *154*, L101.

Semakin, N.K. 1955, *Var. Stars*, *10*, 283.

Setti, G. and Woltjer, L. 1973, *Annuals of the N.Y. Acad. of Sciences*, *224*, 8.

Shen, B.S.P., Usher, P.D., and Barrett, J.W. 1972, *Ap. J.*, *171*, 457.

Shimazaki, T. and Ogawa, T. 1974, *NOAA Technical Memorandum ERL OD-20*, 3.

Shimmins, A.J., Searle, L., Andrew, B.H., and Brandie, G.W. 1968, *Ap. Letters*, *1*, 167.

Smith, A.G. 1969, *The American Scientist*, *57*, 177.

Smith, A.G., Schrader, H.W., and Richardson, W.W. 1971, *Applied Optics*, *10*, 1597.

Smith, H.J. and Hoffleit, D. 1963, *Nature*, *198*, 650.

Stock, J. and Williams, A.D. 1966, Astronomical Techniques. Chicago: University of Chicago Press.

Stong, C.L. 1969, Scientific American, Aug., 125.

Strittmatter, P.A. and Burbidge, G.R. 1967, Ap. J., 147, 13.

Stull, M.A. 1970, Nature, 225, 832.

Stull, M.A. 1972, A. J., 77, 13.

Stull, M.A. and Carpenter, R.D. 1973, Ap. Letters, 13, 73.

Tan, A. 1974, "Some Studies of the Jovian Ionosphere," M.S. Thesis, University of Florida.

Terrell, J. 1964, Science, 145, 918.

Terrell, J. 1967, Ap. J., 147, No. 2, 827.

Tritton, K.P. and Selmes, R.A. 1971, M.N.R.A.S., 153, 453.

Vander Laan, H. 1966, Nature, 211, 1131.

Visvanathan, N. 1973, Ap. J., 185, 145.

Visvanathan, N. and Elliot, J.L. 1973, Ap. J., 179, 721.

Wampler, E.J., Robinson, L.B., Baldwin, J.A., Burbidge, E.M. 1973, Nature, 243, 336.

Weistrop, D. 1973, Nature, 241, 157.

Westerlund, B.E. and Wall, J.V. 1969, A. J., 74, 335.

Wills, B.J., Wills, D., and Douglas, J.N. 1973, A. J., 78, No. 7, 521.

Wills, D. and Bolton, J.G. 1969, Austral. J. Phys., 22, 775.

Wing, R.F. 1973, A. J., 78, No. 8, 684.

Wolf, M. 1916, Astr. Nach, 202, 415.

BIOGRAPHICAL SKETCH

Roger Leonard Scott was born on September 6, 1945, in Bowling Green, Kentucky. He was graduated from Bowling Green High School, June, 1963. As an undergraduate at Western Kentucky University he was a member of the Sigma Pi Sigma Physics Honor Society. He was graduated in August, 1967, with the degree of Bachelor of Science in Physics and Mathematics. In September of 1967 he entered graduate school at Western to begin work toward the Master of Science degree. He became an instructor in the Department of Physics and Astronomy in September of 1968, and received the Master of Science in Physics in August, 1970. In September, 1970, he enrolled in the Graduate School of the University of Florida to pursue studies in the Department of Physics and Astronomy leading to the degree of Doctor of Philosophy with a major in astronomy. In addition to Sigma Pi Sigma he is a member of Sigma Xi, the American Astronomical Society, the Astronomical Society of the Pacific, the American Association for the Advancement of Science, and the Southeastern Section of the American Physical Society.

I certify that I have read this study and that in my opinion it conforms to acceptable standards of scholarly presentation and is fully adequate, in scope and quality, as a dissertation for the degree of Doctor of Philosophy.

A. G. Smith

A. G. Smith, Chairman
Professor of Physics and Astronomy

I certify that I have read this study and that in my opinion it conforms to acceptable standards of scholarly presentation and is fully adequate, in scope and quality, as a dissertation for the degree of Doctor of Philosophy.

G. R. Lebo

G. R. Lebo
Assistant Professor of Astronomy

I certify that I have read this study and that in my opinion it conforms to acceptable standards of scholarly presentation and is fully adequate, in scope and quality, as a dissertation for the degree of Doctor of Philosophy.

C. N. Olsson

C. N. Olsson
Associate Professor of Physics
and Physical Sciences

I certify that I have read this study and that in my opinion it conforms to acceptable standards of scholarly presentation and is fully adequate, in scope and quality, as a dissertation for the degree of Doctor of Philosophy.

F. B. Wood

F. B. Wood
Professor of Astronomy

I certify that I have read this study and that in my opinion it conforms to acceptable standards of scholarly presentation and is fully adequate, in scope and quality, as a dissertation for the degree of Doctor of Philosophy.

T. L. Bailey

T. L. Bailey
Professor of Physics

This dissertation was submitted to the Graduate Faculty of the Department of Physics and Astronomy in the College of Arts and Sciences and to the Graduate Council, and was accepted as partial fulfillment of the requirements for the degree of Doctor of Philosophy.

March, 1975

Dean, Graduate School

1853

UNIVERSITY OF FLORIDA
3 1262 08666 412 4